GRANT TITLE: Tropical Disturbances in Relation to General Circulation Modeling

REPORT TYPE: Final Technical Report

PERIOD COVERED BY REPORT: May 1, 1979 to October 31, 1982

PRINCIPAL INVESTIGATOR: Mariano A. Estoque

GRANTEE INSTITUTION: Division of Meteorology and Physical Oceanography
Rosenstiel School of Marine and Atmospheric Science
University of Miami
Miami, Florida 33149

GRANT NO.: NSG-5342

(NASA-CR-169522) TROPICAL DISTURBANCES IN RELATION TO GENERAL CIRCULATION MODELING Final Technical Report, 1 May 1979 - 31 Oct. 1982 (Miami Univ.) 231 p HC A11/MF A01 CSCL 04B G3/47

N83-13711

Unclas 02007

PREFACE

This is the final technical report for NASA Grant No. NSG-5342 entitled "Tropical Disturbance in Relation to General Circulation Modeling". In general, the original objectives of the research were:

(1) to assess the realism of the simulations of the tropical atmosphere made with the Goddard Laboratory of Atmospheric Sciences general circulation model;

(2) to formulate improvements in the model equations on the basis of errors in the simulations.

This final technical report consists of the following parts:

Part I: Comparison Between Observed and Simulated Characteristics of Tropical Disturbances by M. A. Estoque and J. G. Jiing

Part II: African Disturbances in a General Circulation Model by M. A. Estoque, J. Shukla and J. G. Jiing

Part III: Further Studies of African Disturbances in the GLAS General Circulation Model by M. A. Estoque and J. Fernandez-Partagas

Part IV: Study of a Synoptic Disturbance Over Western Africa by J. Ngamini and M. A. Estoque.

Part I describes the initial results of the model evaluation for the tropical atmosphere. This evaluation showed the existence of tropical wave disturbances throughout the tropics. After this finding we decided to concentrate our efforts in a study of the characteristics of synoptic disturbances over Africa. Africa was chosen because the disturbances over this region have been studied more extensively, both observationally and theoretically, than in any part of the

tropics. The results of this study are described in Part II and Part III. Part II has been accepted for publication in Tellus. In order to supplement the existing observational studies for verifying the simulations, we conducted a synoptic case study of a selected African disturbance. The results of the case study are described by Part IV.

TABLE OF CONTENTS

* * * * * * * * * *

PART I

1

COMPARISON BETWEEN OBSERVED AND SIMULATED CHARACTERISTICS OF TROPICAL DISTURBANCES

1. Introduction

Since the advent of general circulation models, a considerable number of simulations of the global atmosphere has been made. These simulations provide a large amount of data which can be analyzed in order to evaluate the realism of the models. Generally the evaluations have compared observed and simulated geographical distributions of time averages of various meteorology variables as well as statistical properties of variations from the average. Most of the evaluations have been made especially for temperate latitudes; only a limited number has been done for the tropics. Three examples of the tropical evaluations are those which were done by Hayashi (1974), Tsay (1974) and Manabe et al. (1974). The former two are global studies of space-time spectra while the latter deals with seasonal variations of the tropical circulation. So far very little effort has been made to evaluate the realism of the simulations of synoptic scale disturbances in the tropics.

In the present report, we will present the results of an evaluation of the performance of the GLAS general circulation model in simulating the tropical atmosphere during the summer. These evaluations are concerned primarily with tropical disturbances.

2. Data and Analysis

Two sets of data, observed and simulated sets, were used in the study. The observed set consists of winds from the NCAR data collection and satellite data from the National Environmental Satellite Services (NESS). Wind components are available at grid points on the National Meteorological Center tropical Mercator projection at 00Z and 12Z. The values are based on an analysis of rawinsonde, satellite, and aircraft data at levels of 1000, 850, 700, 500, 300, 250 and 200 mb. Wind data for the three month period (June to August) of the year of 1977 were used.

The satellite data consist of radiation measurements in the infrared and visible regions of the spectrum which were then converted into energy units. These are available on magnetic tapes from the Satellite Data Services Division, NESS. The radiation values are given at grid points ($5^{o}x5^{o}$) at 00Z and 12Z for the same period as the wind data. The distributions of infrared and the visible radiation intensities are used in this study as a representation of the cloudiness.

The simulation data corresponds to a simulation of three summer months (June, July, and August of 1974) using the Goddard Laboratory of Atmospheric Sciences (GLAS) general circulation model. The general characteristics of this model have been described previously by Sommerville et al. (1974). Simulated values of the various meteorological variables are given at the surface and at nine levels of the atmosphere at 6 hourly intervals. The distances between grid points are 5^{o} longitudinally and 4^{o} latitudinally. The simulated data were interpolated vertically to obtain values at every 100 mb level. Since the observed data correspond to the year of 1977 while the model simulation is for 1974, direct comparisons of distributions for each synoptic time will be meaningless. Therefore, only comparisons of the statistical features of the tropical atmosphere which do not change significantly from year to year can be made.

For ease of comparison of our results with previous observational studies, (e.g. Wallace, 1971; Chang et al., 1970) we use methods of analysis which are similar to those used in those studies. The primary method used in the present study is the construction of the so-called Hovmöller diagram. The diagram depicts the variations of a quantity with respect to a space coordinate (abscissa is longitude) and to time (ordinate). With the aid of the diagram, one is able to see conveniently the existence of disturbances, their longitudinal scale, time scale, as well as speeds and directions of

propagation. In addition to Hovmöller diagrams, we have also constructed geographical distributions of variability relative to time average for different time scales of variation.

The results of the analysis are presented in the next 5 sections. In Sections3 and 4 we describe a comparison of the monthly mean wind patterns. These comparisons are useful in interpreting the discrepancies between the properties of the synoptic scale disturbances which are discussed in Sections 5 to 7.

3. Low-level Monthly-averaged Circulation Patterns

In order to assess the accuracy of the simulated wind patterns, we used the 900 mb level winds for comparison with the 1000 mb level NMC wind patterns. Figures 1-3 show the mean monthly NMC wind distribution at 1000 mb for June, July and August; wind vectors are plotted at every 5^0 latitudinally. The corresponding circulation patterns for the GLAS simulations at 900 mb are shown in Figures 4-6; no wind vectors are plotted in areas where the surface pressure is below 900 mb anytime during the period. It may be seen that the gross patterns of the global circulations in the tropics such as the oceanic trades and the monsoons (Indian and Africa) are reproduced by the simulations. However, there are many aspects of these patterns which appear to be unrealistic; theseare located in several areas. The first is the Southeastern Pacific Ocean just west of South America. In this area, the NMC wind pattern is characterized by an anticyclone which is centered at about 90^0W and 30^0S. The vortex is relatively weak in June; however, it increases in intensity with time and becomes quite strong in August. The corresponding GLAS simulations do not reproduce this feature correctly. It is interesting to note that, in the equatorward section of this area, the GLAS simulations show an irregular wind distribution. This is especially pronounced in August with the winds showing an apparent pattern of two-grid

length waves along the longitudinal direction west of Equador. Their existence is extremely surprising if one considers the fact that the wind vectors represent average values for an entire month. The second area of unrealistic simulation is the portion of South America east of the Andes Mountains in the vicinity of Argentina and Brazil. Here the NMC maps for all three months show southward flow. On the other hand, the GLAS maps show winds with northward components. The third area of discrepancy between the observation and simulation is Southwestern Africa and the Eastern Atlantic Ocean. The NMC wind distribution shows a well-defined clockwise circulation pattern with relatively strong northly winds in the interior of the continent and easterly flow over Angola and Southwest Africa. The GLAS wind distribution shows very little indication of this pattern. Instead it shows a strong southwesterly monsoon flow which penetrates deeply into the Sahara desert. The fourth area of unrealistic simulation is the Arabian Peninsula. Note the rather strong southerly jet over the center of the area which persists during the three months. The jet appears to be a northward extension of the Somali jet. The fifth area of discrepancy between NMC and GLAS maps is the equatorial section of the central Indian Ocean. Note that the NMC maps show mainly easterly flow south of the equator and westerly flow to the north. The GLAS winds, on the other hand, show a significant amount of cross-equatorial flow throughout most of the region between Africa and Sumatra. It is not clear whether this discrepancy is an error in the GLAS simulation. Surface winds as shown by a climatic atlas (Riehl, 1979) show considerable cross-equatorial flow over the Indian Ocean. The sixth area is the tropical western Carribean. Here, it may be seen that the North Atlantic trades in the NMC maps are much stronger and extend farther south than those of the GLAS simulations. It is also noticeable that the easterly trades are too weak or nonexistent over the central

Atlantic in the GLAS maps. Lastly, one may note an interesting vortex off the east coast of China south of Japan in the GLAS simulation for August. This vortex appears also in individual daily maps (not shown) of August. On the corresponding NMC maps, there is an indication of a cyclonic curvature in the flow pattern, but not a closed circulation.

4. Circulations at Upper Levels

In this section, we will discuss the evaluation of the simulations at 700 mb and at 200 mb. Figures 7-12 show the observed and simulated flow patterns at the 700 mb level. Some of the discrepancies which have already been noted in the preceeding section are also present at 700 mb. Two notable examples are the southern sections of South America and the South-western Pacific Ocean just west of South America. Note the two well-defined anticyclones on the NMC maps. On the GLAS maps the anticyclones are generally weak and ill-defined. Note also the two-grid length waves on the GLAS maps in the vicinity of Equador. This features also appear on the 100 mb maps (not shown). Another discrepancy which has been pointed out on the low-level maps and which is also present at 700 mb is that which concerns the strength and the extent of the trades over the Carribean and over the northern section of South America. Here, we see again that the NMC trades are stronger and extend farther south.

In addition to the common discrepancies mentioned above, one may note other areas of differences in the flow patterns. One of these is the southern section of Australia. The GLAS wind field shows a much stronger westerly component than that of the NMC wind field. Another area of discrepancy is a zonal band over Africa near 10°N latitude. Along this band, the GLAS maps show westerlies which are rather well developed in June and August. The NMC maps show generally easterlies in the same area.

At the 200 mb level, there is greater agreement between the NMC and the

GLAS wind fields. Therefore, it is sufficient to show only the maps for July (Figures 13 and 14). The only significant discrepancy between these two maps is concerned with the wind field near the equator over the Pacific Ocean. On the NMC map, the winds in this area are primarily easterlies. The GLAS map shows mostly westerlies with exception of a small area north of New Guinea.

5. Cloudiness and Precipitation

One of the important variables which is simulated by the GLAS model is precipitation. Unfortunately, no observational data which are comparable in resolution with the simulated precipitation is available. The sparsity of precipitation observation is especially true over oceanic areas. In order to assess the accuracy of the simulated precipitation, we will have to use infrared (IR) radiation data from satellite observations. It is well known that there is a very good correlation between the patterns of IR and rainfall. The particular characteristic of the IR data which is used is the percentage of days in a month when the outgoing energy of long wave radiation is less than 260 watts per square meter. Figures 15-17 show the distribution of the percentages for each of the three months (June, July, and August). In these figures we have shaded the areas with values greater than 30 percent. It may be seen that the distribution is rather similar to the expected large scale precipitation patterns. Thus one can see the following features:

(1) Belts of high precipitation over the tropical oceanic regions of the Atlantic and the Pacific associated with the Intertropical Convergent Zone.
(2) Areas of maximum precipitation over Central Africa and the Amazon region.
(3) Maximum precipitation over New Guinea and the oceanic regions to the southeast.

(4) High precipitation over the Western Pacific Ocean, Southeast Asia, and India.

(5) Deserts or minimum precipitation over North Africa, Arabia, and eastern Brazil.

The corresponding GLAS precipitation maps are shown in Figure 18 to 20. These maps are based on the simulated precipitation rate at 00Z. The evaluation of the realism of the GLAS rainfall should be considered as highly qualitative due to the approximate nature of the relationship between IR and rainfall. The primary results of the comparison show the following differences.

(1) The GLAS maps show an absence of the ITCZ band of precipitation over the eastern Pacific Ocean and the Atlantic Ocean.

(2) The GLAS maps show the rainfall over Africa to be displaced farther north relative to the IR rainfall pattern. The northward displacement indicates the occurrence of simulated rainfall over the southern half of the Sahara Desert. This erroneous rainfall might be related to the simulated strong southwesterly monsoon flow at 900 mb over this area; this flow is characterized by high moisture content.

(3) The GLAS maps show unrealistic rainfall over the Arabia-Northeastern Africa region. This condition is presumably associated with the incorrect wind simulation with strong southerly flow over this region.

(4) The simulated rainfall over the Amazon appears to be underestimated in areal extent and displaced northward.

(5) The GLAS maps show less area of rainfall over the Indian Ocean, including the Bay of Bengal.

(6) The GLAS rainfall over the Indonesian Maritime Continent and New Guinea appears to be displaced northward relative to the IR rainfall pattern. In addition, the GLAS maps do not have the tongue of rainfall maximum which extends

southeastward from New Guinea.

(7) The GLAS maps show minimum rainfall or the absence of rainfall off the east coast of China (July and August) while the IR pattern indicates relatively high precipitation.

(8) The GLAS maps show little or no precipitation over the north coast of the Bay of Guinea, west coast of India, west coast of Indochina, and many parts of Central America. It is noticeable that the 900 mb wind over these coastal areas are onshore. One may conclude, therefore, that the GLAS model appears to displace unrealistically the precipitation farther inland than commonly observed.

Since the parameterization of rainfall in the GLAS model is rather strongly dependent on the mixing ratio, it is interesting to compare the monthly averaged 700 mb specific humidity maps with the precipitation maps. The humidity distributions are shown in Figures 21 to 23. It is surprising to note that over most of the oceanic regions the humidity distributions show more resemblance to that of the IR brightness patterns. One can see clearly the indication of the ITCZ over the Pacific and the Atlantic Oceans. However, some of the features of the humidity patterns confirms many of the unrealistic aspects of the GLAS rainfall simulations. Note, for example, the high humidity over the Arabian Peninsula.

For further comparison, monthly mean GLAS surface temperature simulations are shown on Figure 24. One can see that over the Pacific and the Indian Oceans, the areas with temperature higher than 26°C are well correlated with the areas which have higher specific humidity on 700 mb. The monthly changes in the size of these areas are also well correlated. However, only the precipitation patterns over the Central and the Western Pacific Ocean show these correlations with the higher surface temperature.

6. Wave Activity in the Wind Field

The existence of westward travelling waves in the tropical troposphere is well known from previous studies during the past two decades. Waves with periods of 3 to 5 days and phase speeds of about 6° to 7° of longitudes per day have been found over the Pacific and the Atlantic Oceans. The maximum amplitude of the waves is observed to be at the 700 mb level. In this section, we will describe the results of an analysis to determine the existence of these types of waves in the GLAS simulations. The analyses were done with the aid of calculations of variances and the constructions of Hovmöller diagrams. In order to limit the spectral range in the calculation of variance, we considered variance only in the spectral band between periods of 3.3 days to 5.4 days. The geographical distribution of variance of the north-south wind component at 700 mb of the GLAS simulations is shown in Figure 25. The variance pattern is dominated primarily by two zonal belts of maxima. The first is centered slightly north of the equator; the second is located in the south temperate zone. The equatorial band is presumably associated with the observed easterly waves and similar tropical disturbances. The south temperate band must be due to extratropical waves in the westerlies of the southern hemisphere. The variances in the equatorial belt is not zonally uniform; there is a relative maximum in the western Pacific (northeast of New Guinea) and a relative minimum over the Indian Ocean between India and Africa. In order to assess the realism of the variance pattern in the GLAS simulations, we have calculated the corresponding variances of the NMC 700 mb north-south wind component. The results are shown in Figure 26. It may be seen that there are considerable differences between the GLAS and the NMC distributions. The most important features which are common to both are as follows:

(1) The zonal maximum at south temperate latitudes.

(2) The relative maximum northeast of New Guinea.

(3) The minimum between India and Africa.

Aside from these common features, the distributions are very different. The most important ones are:

(1) The absence of the equatorial maximum band in the NMC distribution. Instead, there is a maximum band over eastern Pacific north of the equator.

(2) The relatively large variances over extra-tropical latitudes in the northern hemisphere in the NMC map.

(3) The absence of maximum variance over west Carribean and the Gulf of Mexico in the GLAS map.

In order to examine further the properties of the pertubations, we constructed Hovmöller diagrams. These are diagrams showing the distribution in time and longitude at selected latitudes, i.e. longitude-time cross-sections. In these diagrams, except for precipitation, the local time means have been removed from the data so that only the pertubations will be seen. The Hovmöller diagrams for the north-south wind component in the GLAS simulations at three latitudes (22°N, 18°N, and 14°N) are shown in Figures 27, 28, and 29. It may be seen that there are indications of westward propagating disturbances; these are especially pronounced at 22°N and 18°N. It is interesting to note that many of the disturbances at 14°N appear to originate in Africa near 20°E longitude. This is the same general location of easterly wave generation which Burpee (1972) found previously. The periods are between 7 to 8 days on the average and the speed is about 8°/day, the wavelength is about 30° to 40° of longitudes. These wave parameters are not significantly different from the observed values. Note also that the wave patterns are less distinct between 40°E and 180°E longitude where the southwest monsoon

prevails during the three month periods. Looking at the diagrams for 22°N (Figure 27), we can see a feature in the disturbances which is somewhat different from those at other latitudes. This is the fact that waves at 22°N seem to originate farther east (near 100°E longitude). At 14°N (Figure 29) the patterns are rather disorganized. Nevertheless, one can still recognize the existence of westward propagating disturbances especially during the latter part of the period over the Atlantic Ocean and the Eastern Pacific Ocean. Over the same regions during the first half of the period, one can see indications of fast, eastward moving disturbances. These fast moving disturbances have not been observed in the actual atmosphere. In general, pertubations at 14°N, 10°N and 6°N (not shown) show rather higher frequency disturbances with periods about 3 to 4 days.

For comparison with the simulated disturbances described above, we present in Figures 30, 31 and 32, the Hovmöller charts based on the NMC wind data for latitudes 19.6°N, 14.8°N and 5°N. It may be seen that waves of the same phase speeds are found in Figures 30 and 31. The dominant period is about 5 days and the wavelength is about 35° of longitude. In Figure 31, which corresponds to the latitude closest to the equator, the waves are less distinct. The main difference between the GLAS diagrams and the NMC diagrams appears to be the fact that the NMC waves are better defined over the western Pacific Ocean. On the whole, however, one can say that the GLAS simulated waves are quite realistic in terms of the wave features depicted in these diagrams. This finding is rather surprising on the basis of the large differences in the GLAS and NMC variance maps shown in Figures 25 and 26.

7. Wave Activity in the Moisture Field

Easterly waves and similar disturbances in the tropics are characterized

by perturbations not only in the wind field but also in the moisture field. It is observed, for example, that the vicinity of wave troughs are generally characterized by clouds and precipitations as well as maximum in the mixing ratios. Thus, moisture parameters should exhibit similar features as those of the wind shown in the preceeding section. In order to verify this expectation, we have constructed the Hovmöller diagrams for the GLAS specific humidity at 700 mb and the rainfall rate. The diagrams for the specific humidity are shown in Figures 33 to 35 for latitudes 18°N, 14°N and 10°N. Looking at the diagram for 18°N, one sees waves which have similar propagation speeds as those in the corresponding diagrams for the v-component. In fact, one can easily identify some of the waves which are common to both these figures. Note, for example, the wave which develops near 10°W on the 50th day. Note also that many of the waves start near 20°E. Note also that there are no distinct wave disturbances between 40°E and 140°E. These features are common to both v-components and the specific humidity diagrams. In the case of the specific humidity diagram for 14°N, it suffices to say it has the same characteristics as that for 18°N. However, the corresponding diagram for 10°N is entirely different from the two just mentioned. Here, one can see that the patterns are relatively disorganized. Nevertheless, one can recognize a number of westward traveling waves especially over the Atlantic Ocean and the Eastern Pacific Ocean. During the first half of the period, the phase speeds are approximately the same as those at 14°N and 18°N. However, during the second half, the speeds appear to be less. In brief, one may conclude that the wave disturbances which are seen in the humidity field are generally consistent with those in the wind field.

The Hovmöller diagrams for rainfall are shown in Figures 36 to 38 for latitudes 18°N, 14°N, and 2°N. The most striking feature which is a common feature in these diagrams is the absence of a strong indication of the

existence of propagating disturbances. Instead, one can see that the rainfall patterns tend to be primarily stationary with the exception of those over the Eastern Pacific Ocean at 2°N. The rainfall in Figures 36 and 37 occur mainly in three general areas: Africa, Western Pacific Ocean, as well as the western Carribean-Central America region. These locations are consistent with the rainfall areas in the GLAS monthly average precipitation maps (Figures 21 to 23). The general lack travelling disturbances in the rainfall pattern is somewhat surprising because such disturbances are clearly indicated in the GLAS north-south wind component (v) and the humidity charts. A careful look at these charts and the rainfall charts indicates that the travelling waves in the humidity patterns produce rainfall mostly when they pass over certain favorable locations; i.e. those mentioned above. This tendency for occurrences in specific locations is not entirely unrealistic on the basis of observations. However, the tendency appears to be rather excessive in the GLAS simulations and needs further study.

Hovmöller diagrams for humidity and rainfall which may be used for comparison with the corresponding diagrams of the GLAS simulations described above and are not possible to construct due to the lack of observations. A reasonable substitute for observed humidity and rainfall is the IR radiation observations. The IR radiation Hovmöller charts are shown in Figures 39, 40 and 41, corresponding to latitudes 19°N, 14°N and 9°N. It is evident from these charts that there are westward moving disturbances with approximately the same speed as those in the GLAS specific humidity diagrams. The disturbances are rather well-defined in Figure 40 which corresponds to conditions at 14°N latitude. The indications of travelling waves are not as clear at 9°N latitude (Figure 41).

8. Concluding Comments

In the preceeding sections, we presented a comparison between the GLAS GCM-simulated and the observed properties of the tropical atmosphere. Monthly mean as well as synoptic scale properties were compared. We found a considerable number of differences. The differences which were found may be explained in terms of: (1) errors in the simulations or (2) errors in the observed distributions. The errors in the simulations are, in turn, due to errors of two types. These are (1) errors in physical assumptions in the model equations or (2) truncation errors associated with numerical integration. The errors in the observed distributions are primarily due to the sparsity of observational data. In regard to simulation errors of the first type, the most serious appears to be in the rainfall prediction. The deficiency of rainfall over the oceanic intertropical convergence zone and the tendency for rainfall patterns to be nonpropagating are most probably due to the inaccurate parameterization of rain formation. Since the simulated humidity patterns do propagate at the proper speeds, this parameterization error may be remedied rather easily. On the other hand, the occurrence of simulated rainfall over the desert areas (Arabia and North Africa) could be a more difficult error to correct. The source of this error may be associated with the specification of the boundary conditions at the earth surface. Concerning truncation errors in the simulation, the most obvious one is the two-grid length waves west of South America. The unrealistic downwind displacement of rainfall patterns over coastal regions might also be related to truncation errors. Some of the differences between the simulated and the observed patterns could be due entirely to errors in the observed patterns. An example of such a difference is that which occurs in the windfield at low levels over the central regions of the

Indian Ocean near the equator. As mentioned in a previous section, the observed (NMC) maps show very little equatorial crossing while the simulated ones show considerable crossing. Winds based on satellite observations and mean winds (Riehl, 1979) show considerable crossing.

We now turn our concluding comments to one of the more realistic features of the GLAS simulation. We refer to the simulation of easterly waves over Africa and the Atlantic Ocean. In this case, the model reproduces rather accurately the propagation speeds and the wavelengths of the disturbances. Moreover, the model simulates also the development of waves over Africa, an occurrence which has been shown by previous investigators. Still another interesting feature of the simulated waves is the indication that some of these waves are simply waves which originate farther from the east. This behavior has not been documented previously. However, the NMC Hovmöller charts appear to indicate that waves which are observed in Africa may develop in India and Southeast Asia. Further tests of the realism of the wave simulation involve comparisons of the simulated and the observed structure. In particular, one should assess the accuracy of the three-dimensional structure and its geographical variation. Preliminary indications at this time show that the simulated structure may be relatively unrealistic. For example, the amplitude of the temperature wave is excessive; in the upper troposphere, the amplitude is about three times that of the observed values. A report describing the results of the evaluation of the simulated structure is forthcoming.

In closing, one must reiterate the fact that the results of this comparative study must be considered as only preliminary due to the difference in years between the periods of the simulation and the observations and the inaccuracy of the observed distributions due to the sparsity of data. More

definitive conclusions concerning the realism of the GLAS general circulation model can be made by using simulations corresponding to the FGGE observational period, such as the ones being done by Dr. Rivas of the Modeling and Simulations Facility, Goddard Space Flight Center. The extensive observations during FGGE should provide a more accurate basis for the evaluation of GLAS GCM simulations of tropical disturbances.

References

Burpee, R.W., 1972: The origin and structure of easterly waves in the lower troposphere in North Africa. J. Atmos. Sci,, 29, 77-90.

Chang, C.P., Morris, V.F., and J.M. Wallace, 1970: A statistical study of easterly waves in the Western Pacific: July - Dec. 1964. J. Atmos. Sci., 27, 195-201.

Hayashi, Y., 1974: Spectral analysis of tropical disturbances appearing in a GFDL general circulation model. J. Atmos. Sci., 31, 180-218.

Manabe, S., Hahn, D.G. and L.J. Holloway, 1974: The seasonal variation of the tropical curculation as simulated by a global model of the atmosphere. J. Atmos. Sci., 31, 43-83.

Riehl, H., 1979: Climate and Weather in the Tropics. Academic Press, 611 pp. (see p. 13).

Sommerville, R.C.J., Stone, P.H., Halem, M., Hansen, J.E., Hogan, J.S., Druyan, L.M., Russel, G., Lacis, A., Quirk, W., and J. Tenenbaum, 1974: The GISS model of the global atmosphere. J. of Atmos. Sci., 31, 84-117.

Tsay, C-Y. 1974: Analysis of large-scale wave disturbances in the tropics simulated by an NCAR global circulation model. J. Atmos. Sci., 31, 330-339.

Wallace, J.M., 1971: Spectral studies of tropospheric wave disturbances in the tropical Western Pacific. Rev. Geophys. and Space Phys., 9, 557-612.

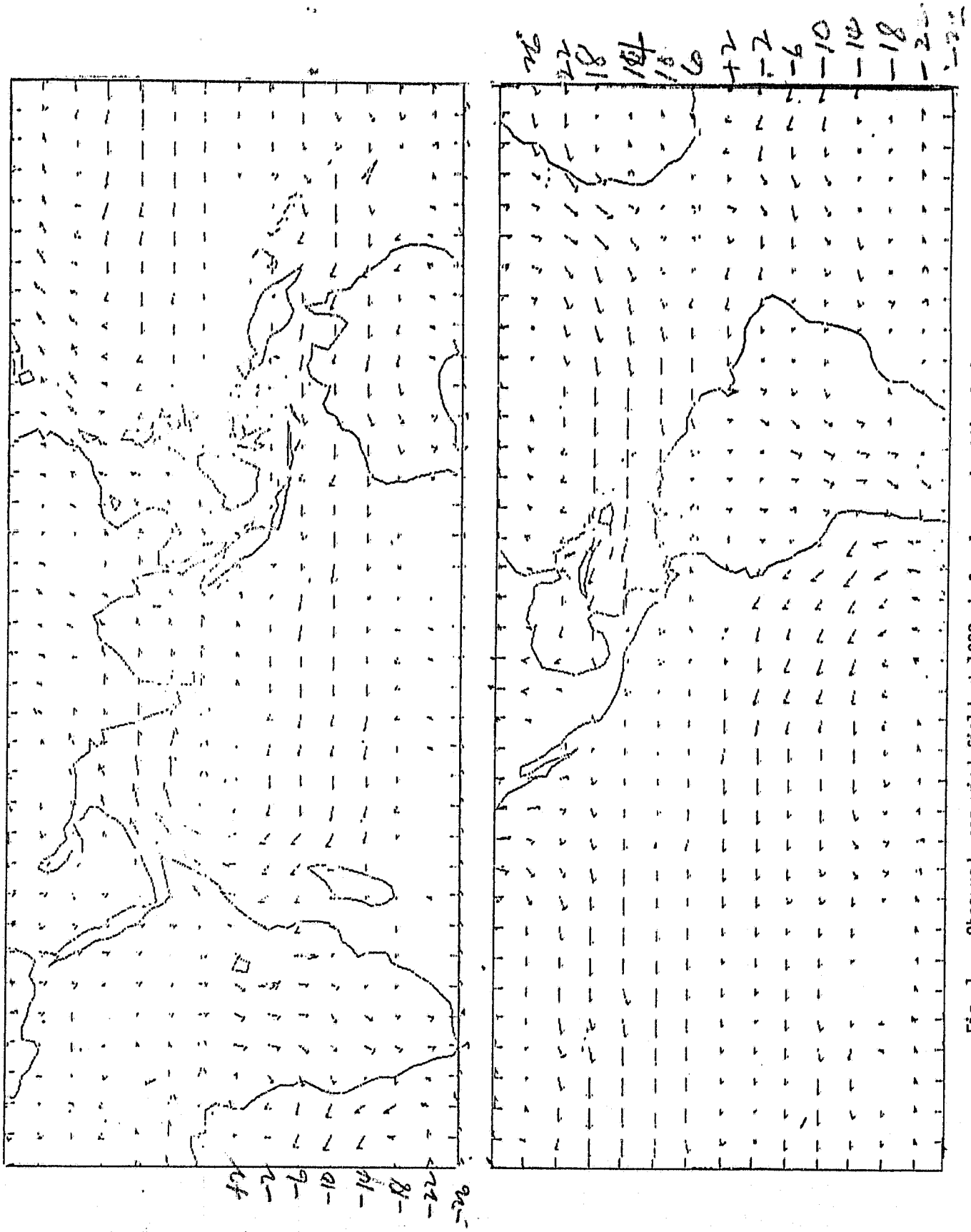

Fig. 1. Observed mean wind field at 1000 mb for June. Length of the arrow is proportional to wind speed. Maximum length is 7 ms^{-1}.

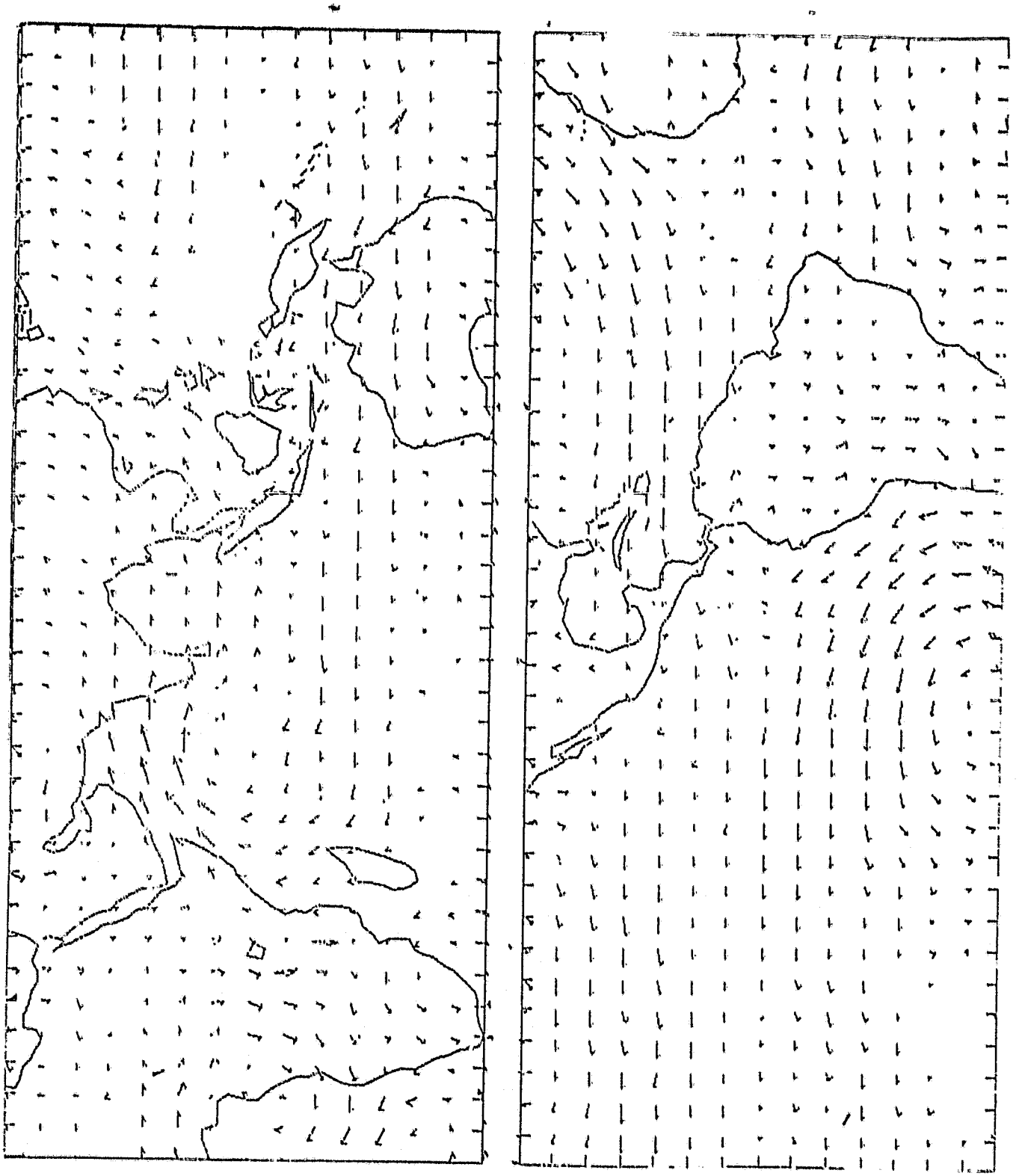

Fig. 2. Same as Fig. 1 except for July. Maximum arrow length is 8 ms^{-1}.

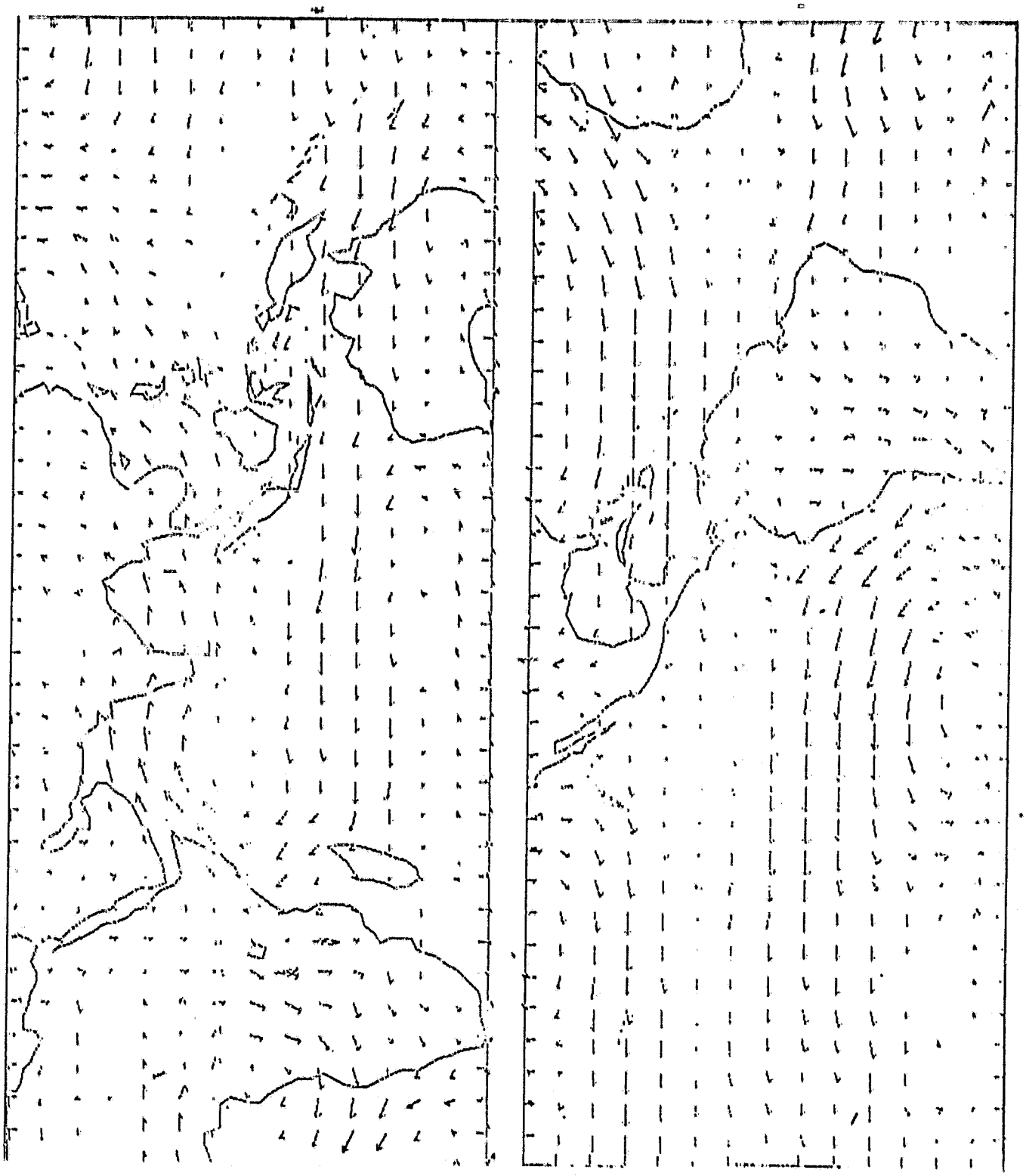

Fig. 3. Same As Fig. 1 except for August. Maximum arrow length is 6 ms^{-1}.

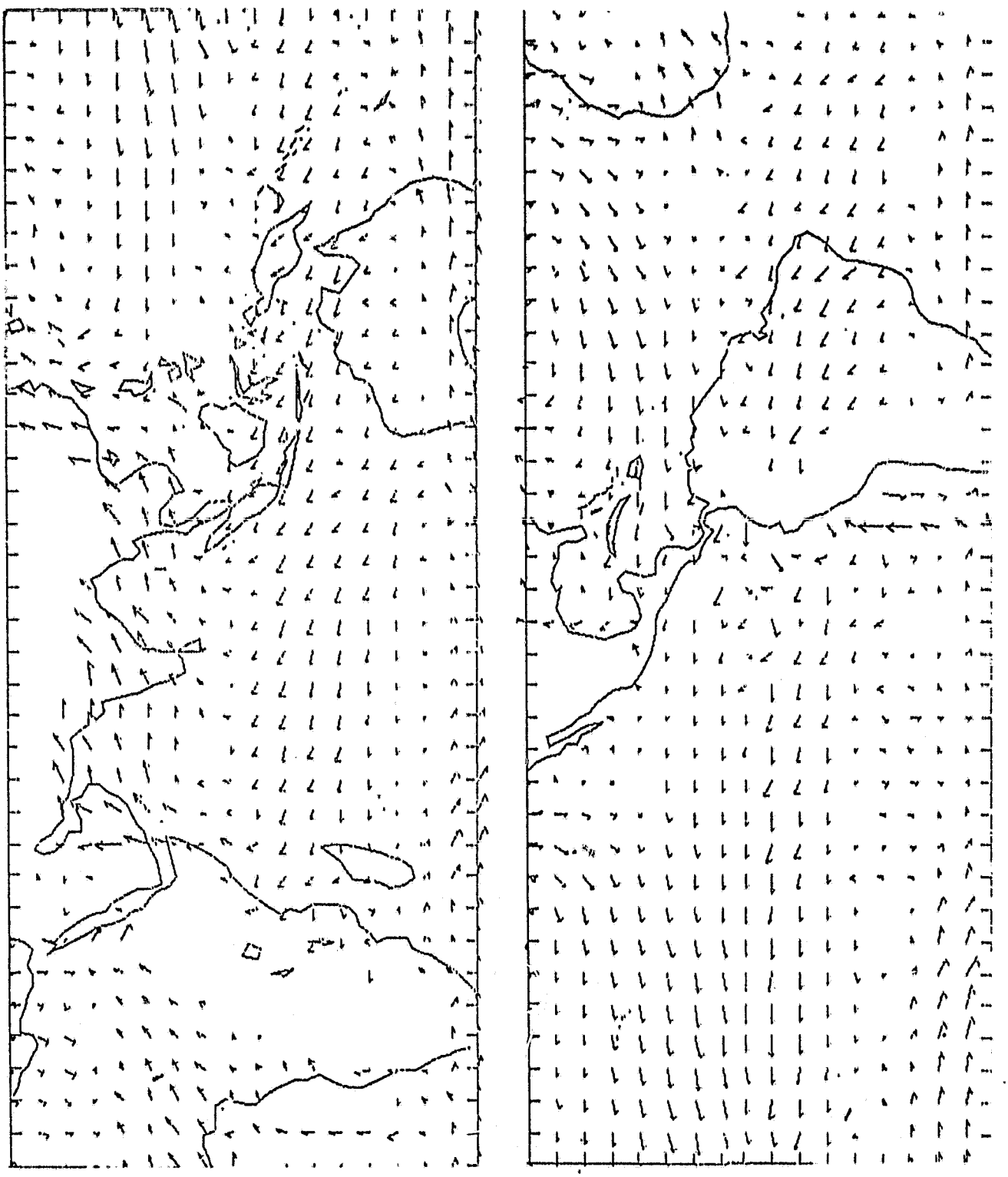

Fig. 4. Simulated mean wind field at 900 mb for June. Length of the arrow is proportional to wind speed. Maximum length if 6 ms^{-1}.

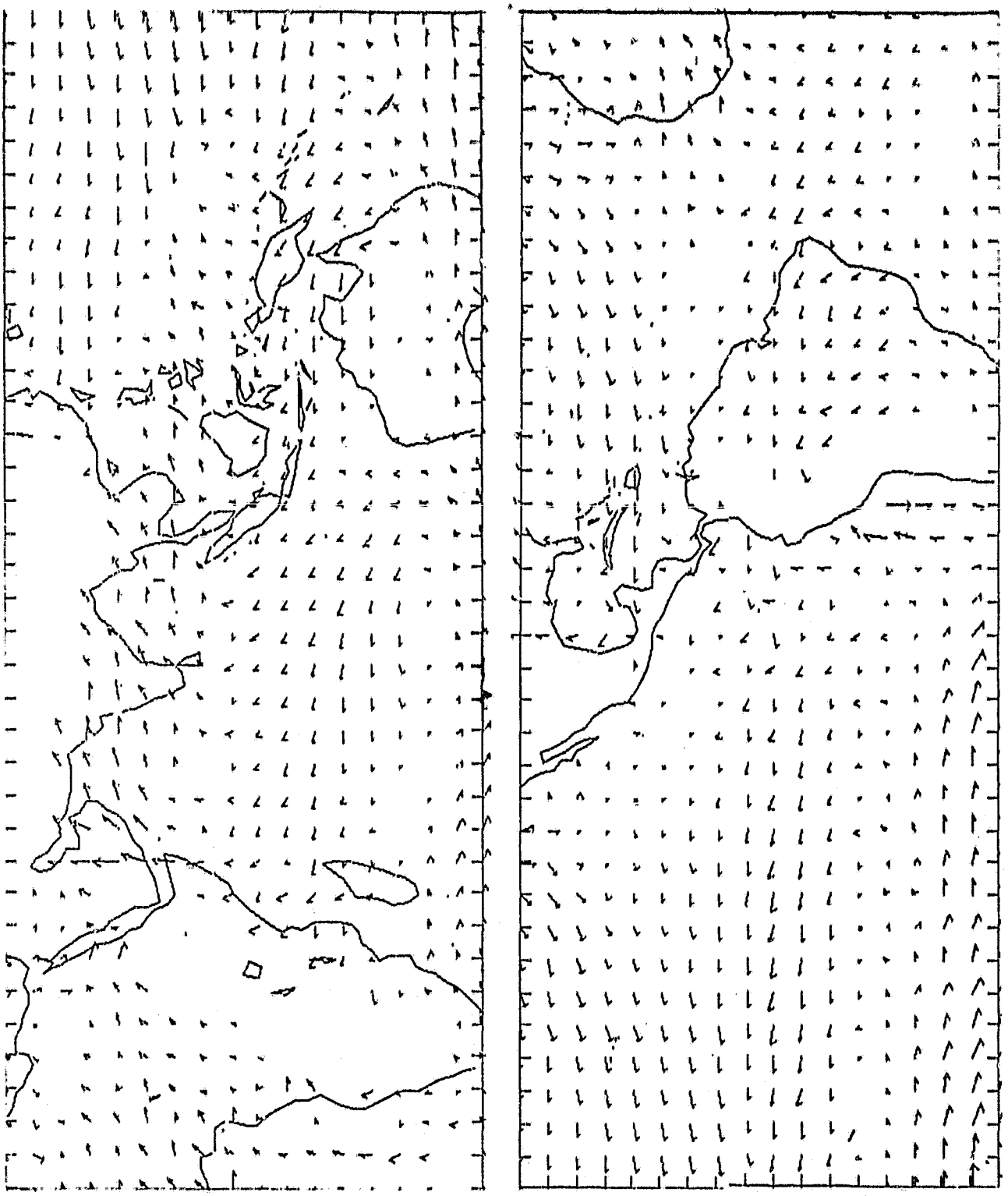

Fig. 5. Same as Fig. 4 except for July. Maximum arrow length is 7 ms^{-1}.

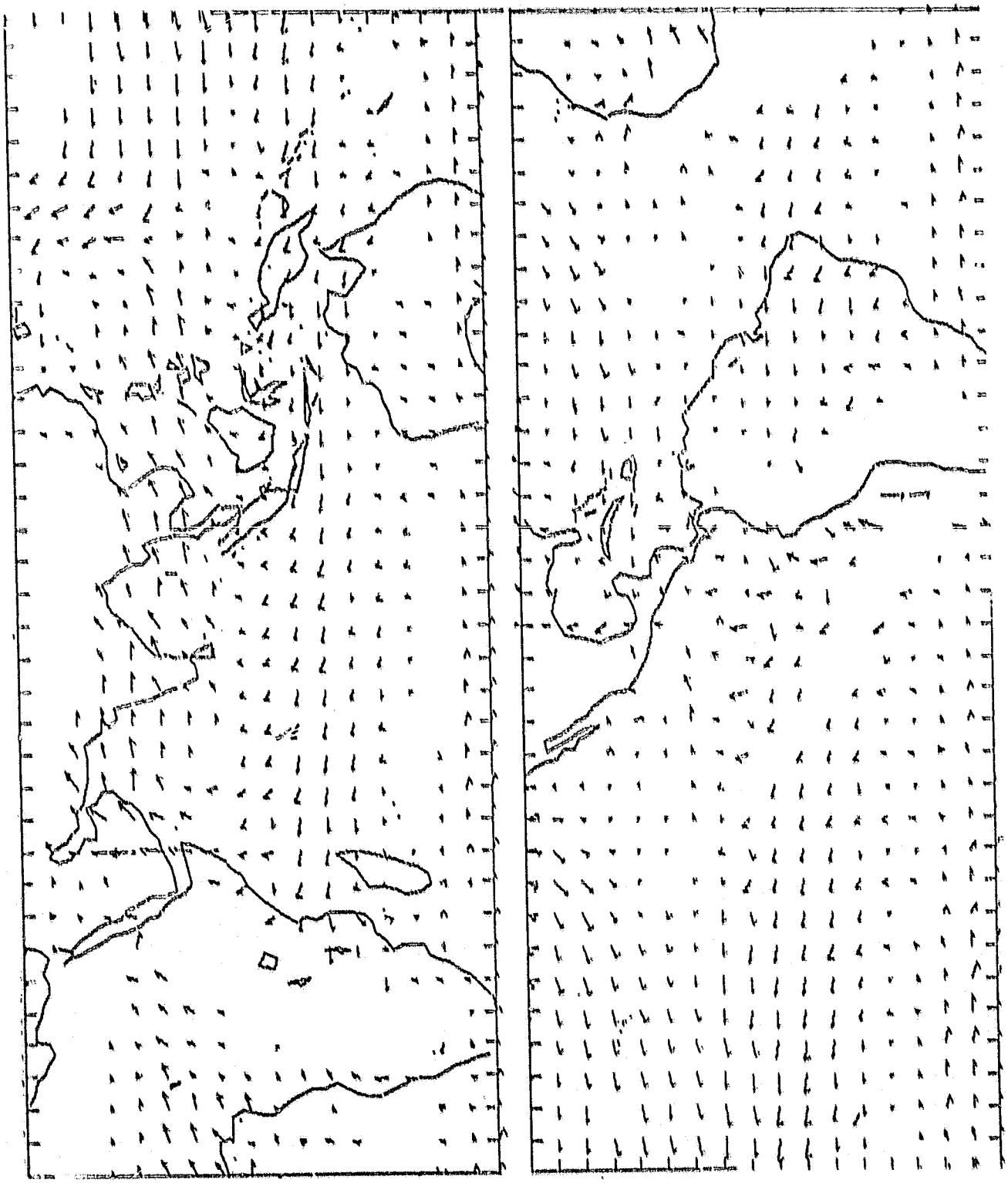

Fig. 6. Same as Fig. 4 except for August. Maximum arrow length is 7 ms^{-1}.

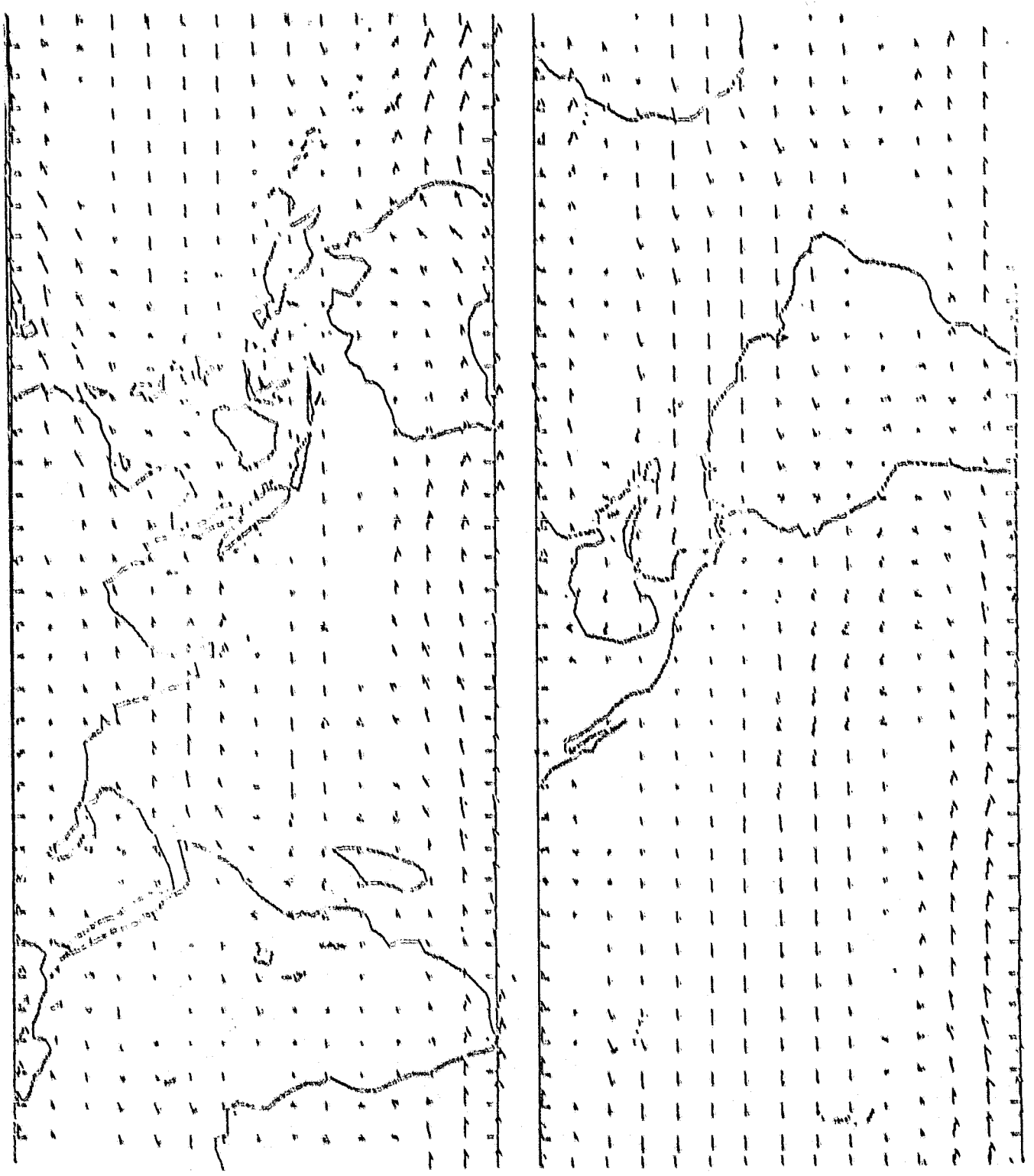

Fig. 7. Observed mean wind field at 700 mb for June. Maximum arrow length is 9 ms^{-1}.

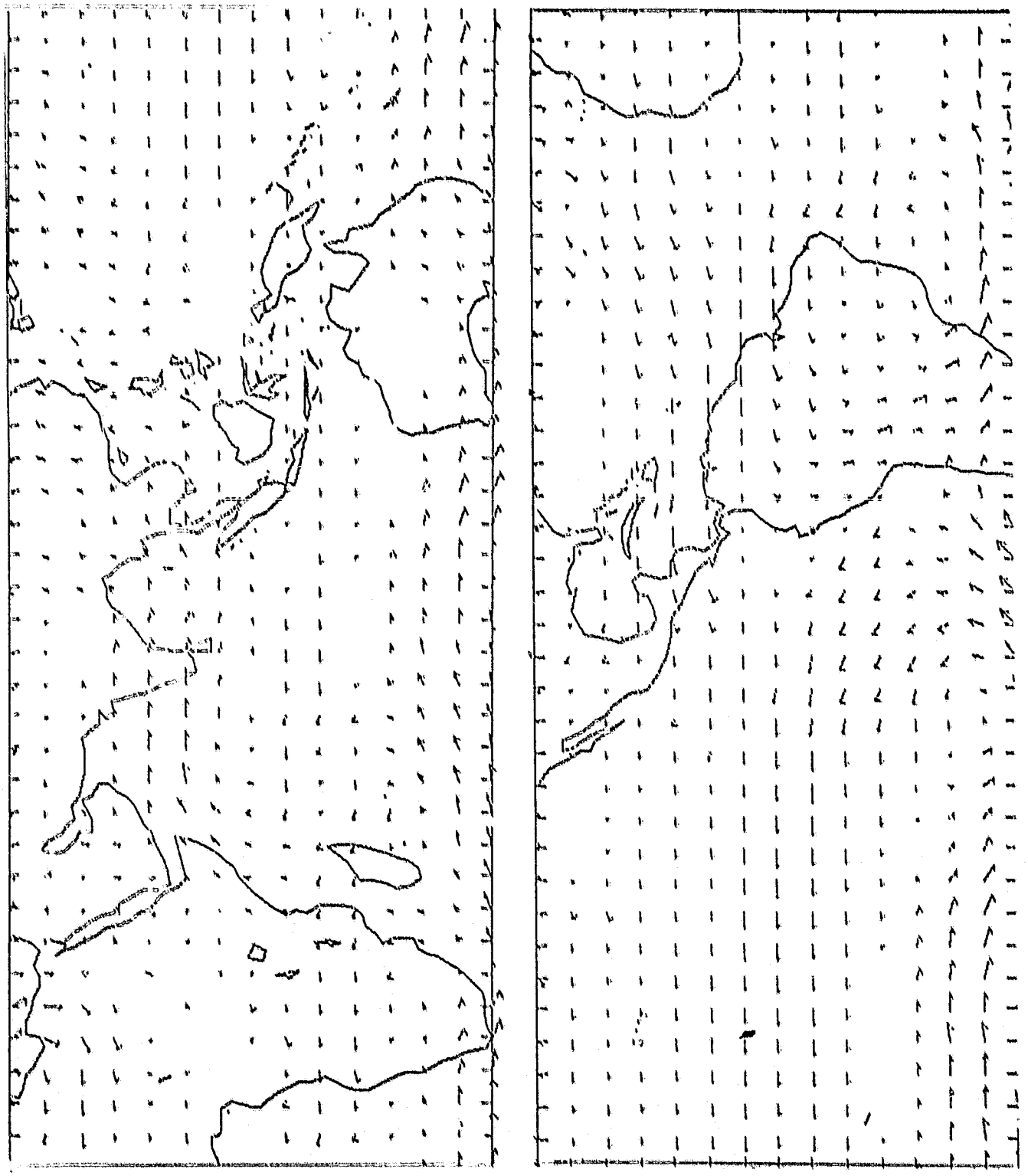

Fig. 8. Same as Fig. 7 except for July. Maximum arrow length is 9 ms^{-1}.

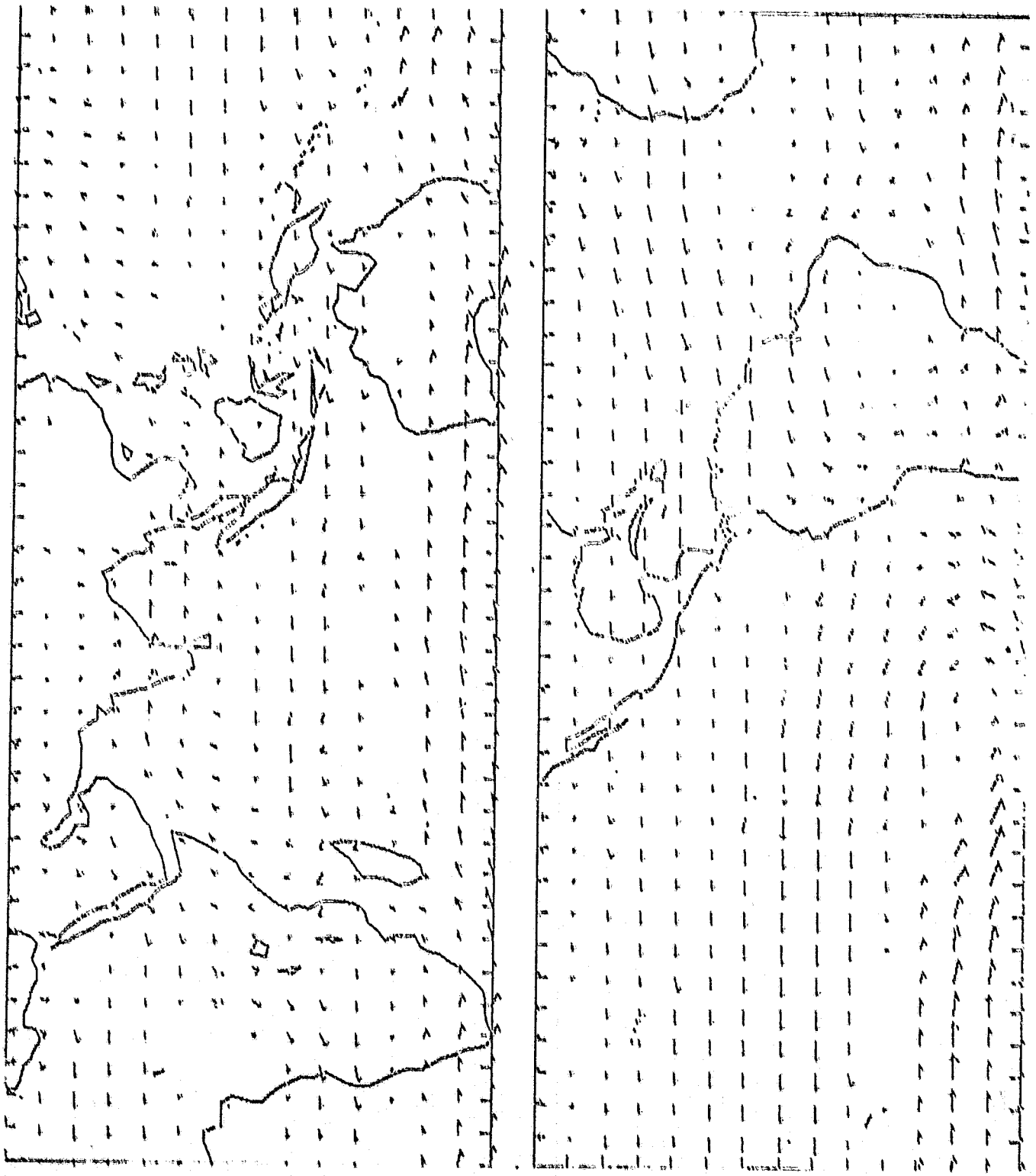

Fig. 9. Same as Fig. 7 except for August. Maximum arrow length is 9 ms^{-1}.

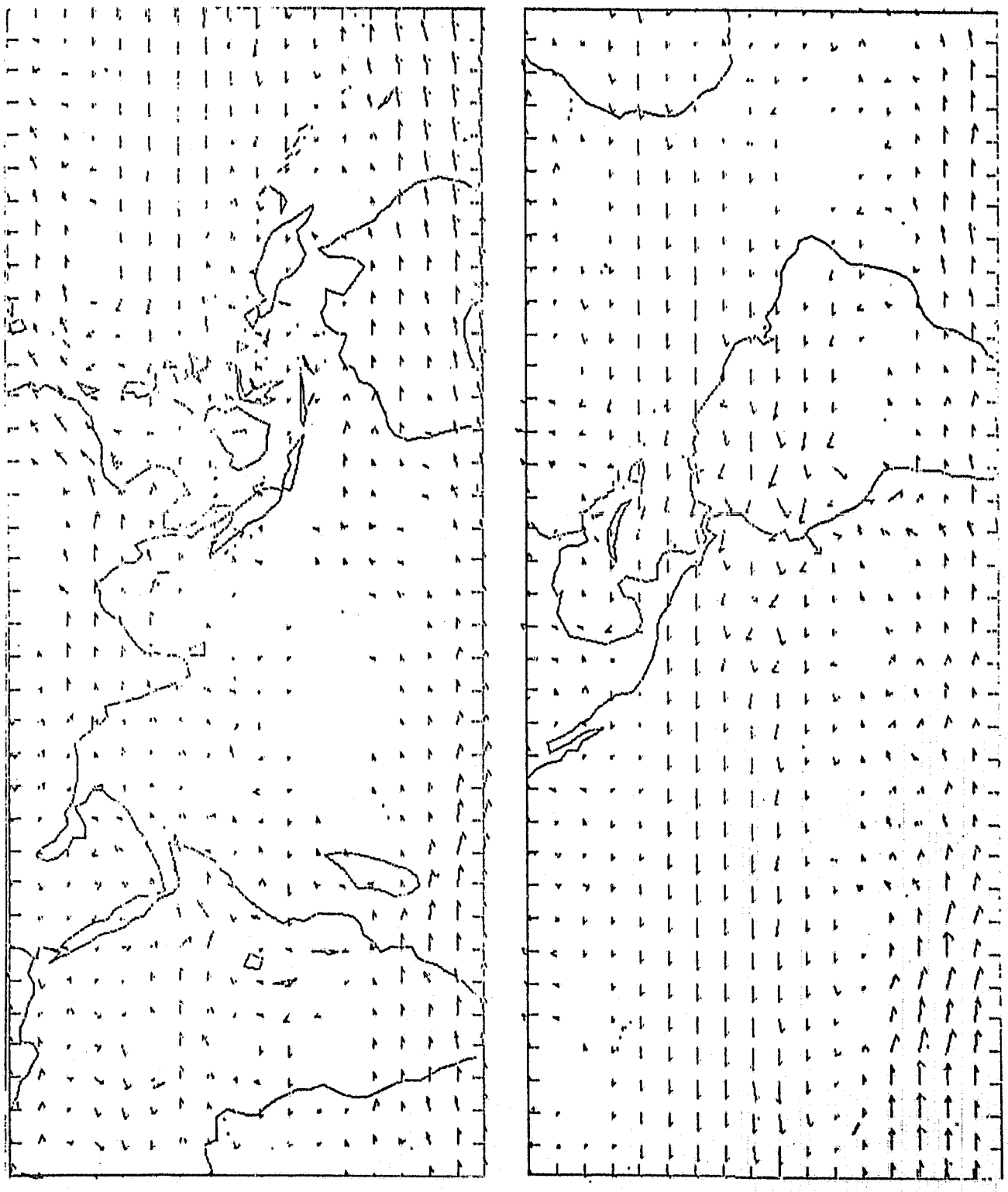

Fig. 10. Simulated mean wind field at 700 mb for June. Maximum arrow length is 9 ms^{-1}.

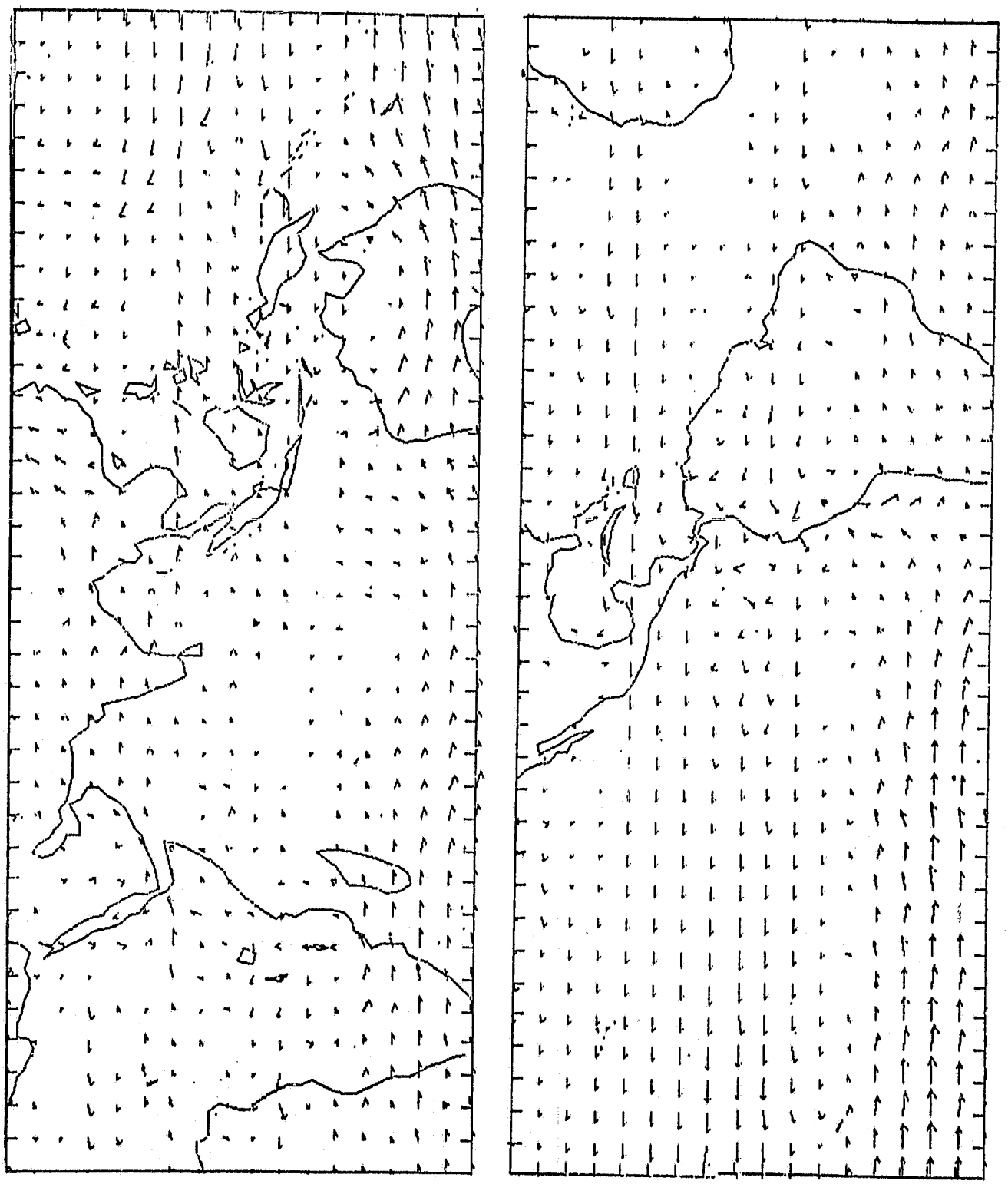

Fig. 11. Same as Fig. 10 except for July. Maximum arrow length is 10 ms^{-1}.

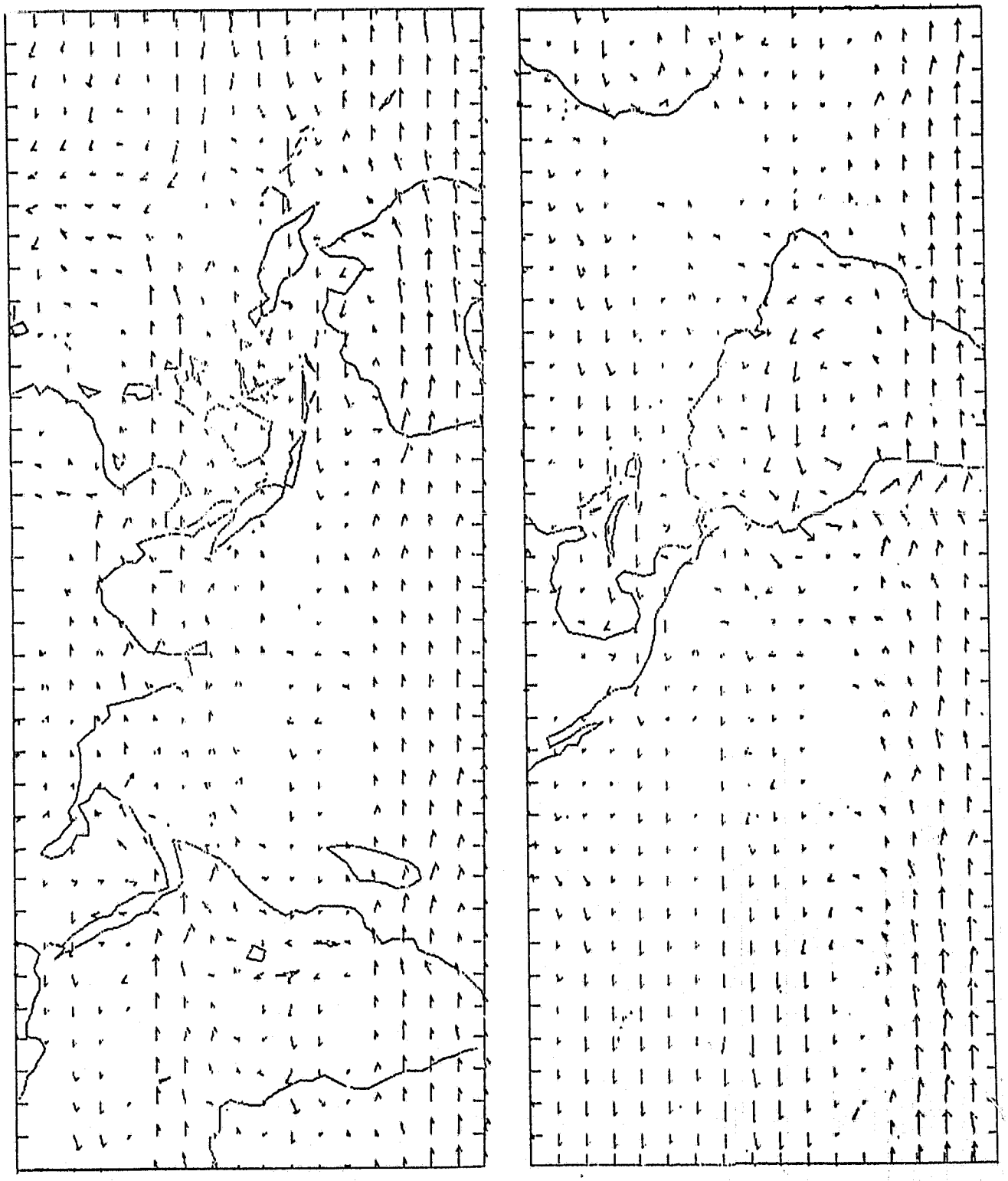

Fig. 12. Same as Fig. 10 except for August. Maximum arrow length is 8 ms^{-1}.

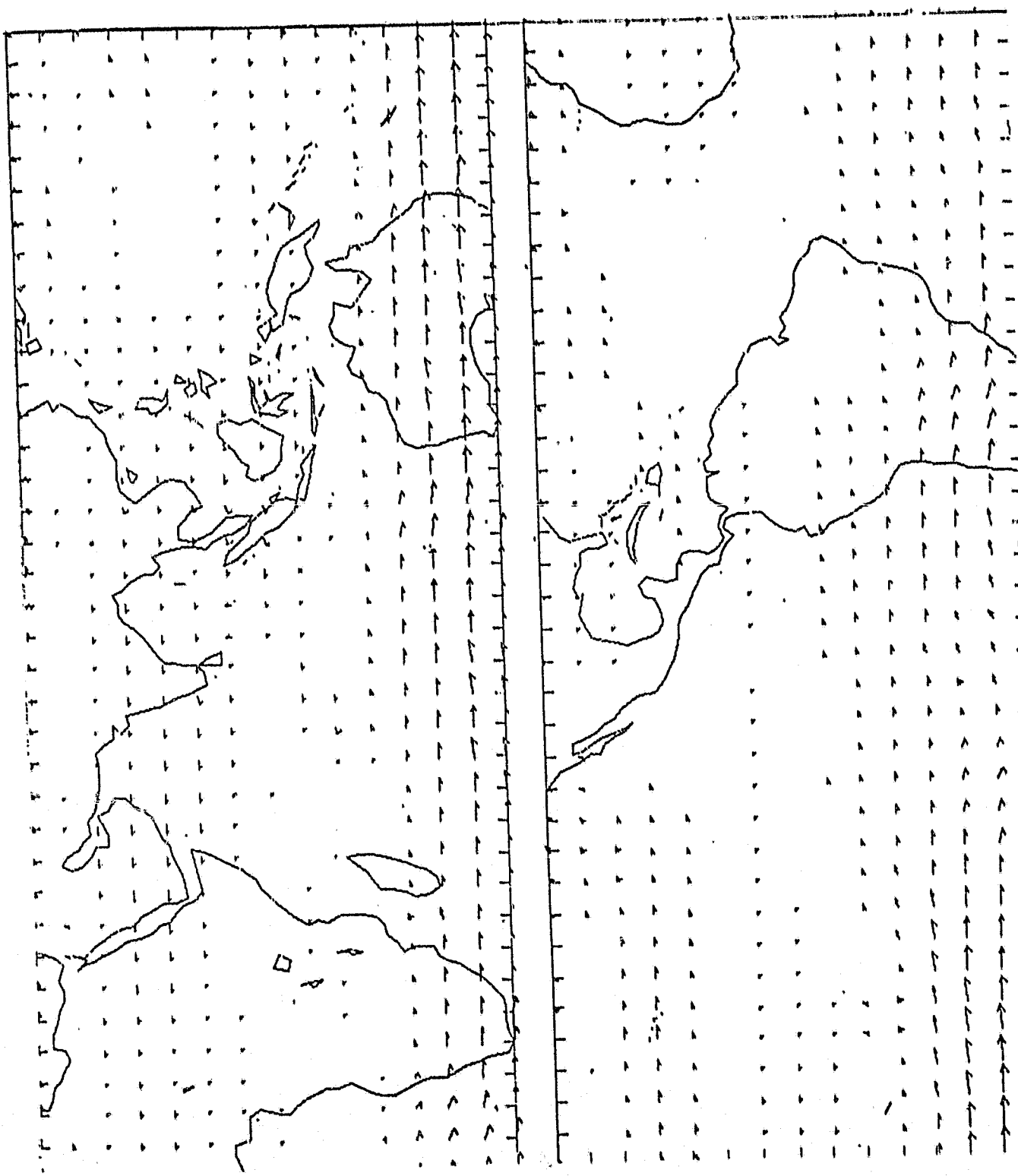

Fig. 13. Observed mean wind field at 200 mb for July. Maximum arrow length is 31 ms^{-1}.

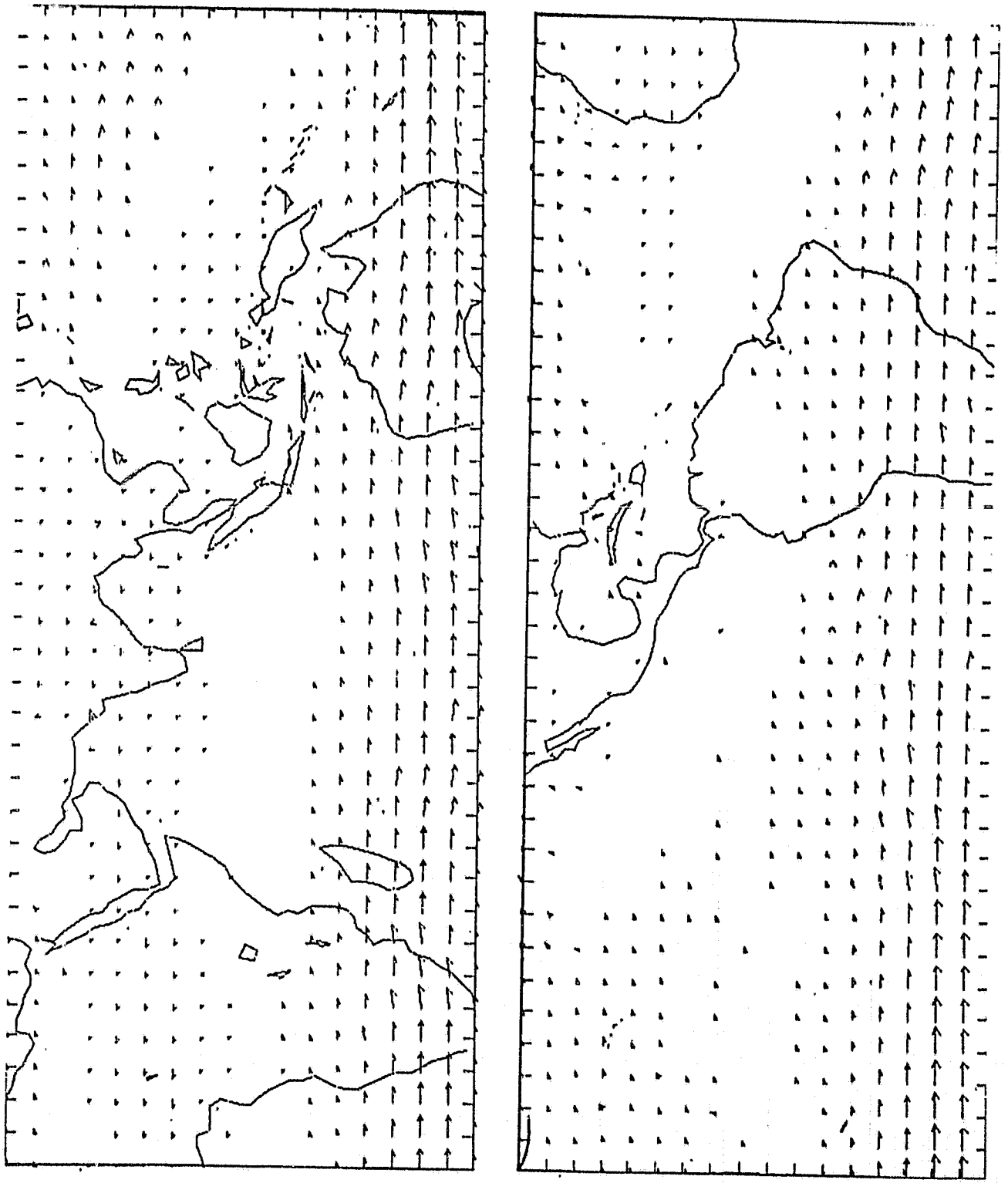

Fig. 14. Simulated mean wind field at 200 mb for July. Maximum arrow is 31 ms^{-1}.

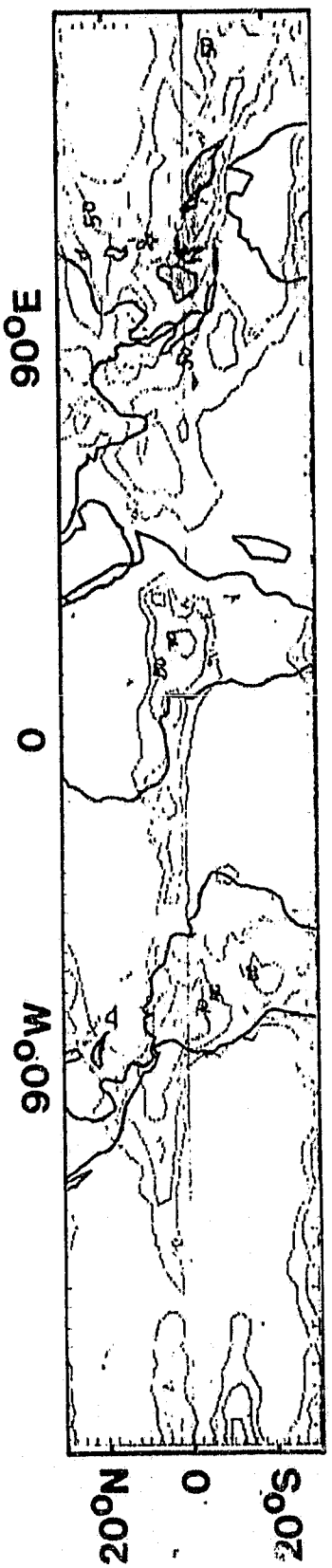

Fig. 15. Observed mean rainfall distribution inferred from satellite observations for June. Unit = arbitrary.

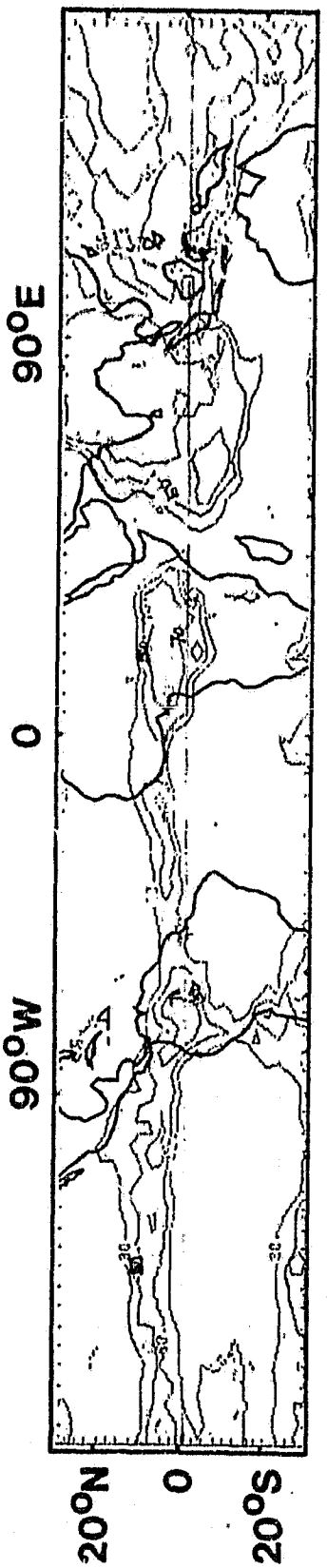

Fig. 16. Same as Fig. 15 except for July.

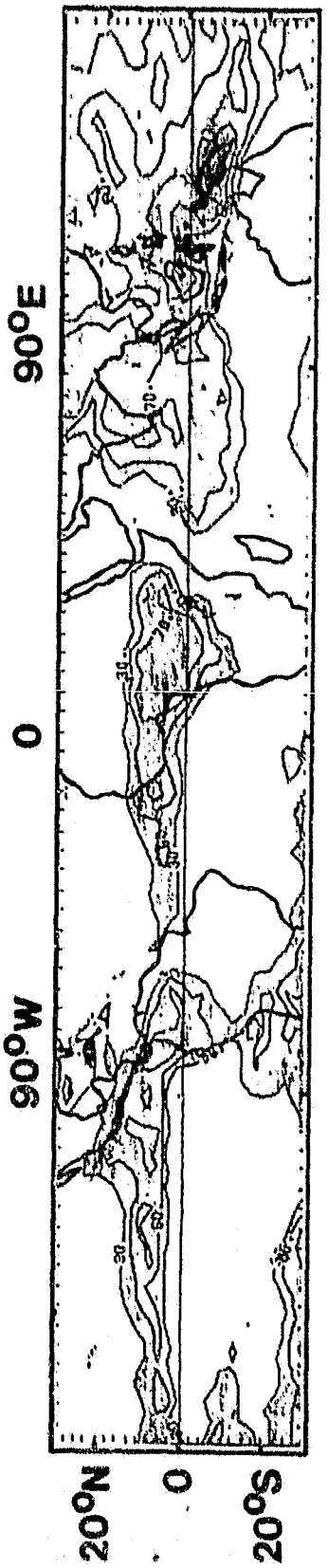

Fig. 17. Same as Fig. 15 except for August.

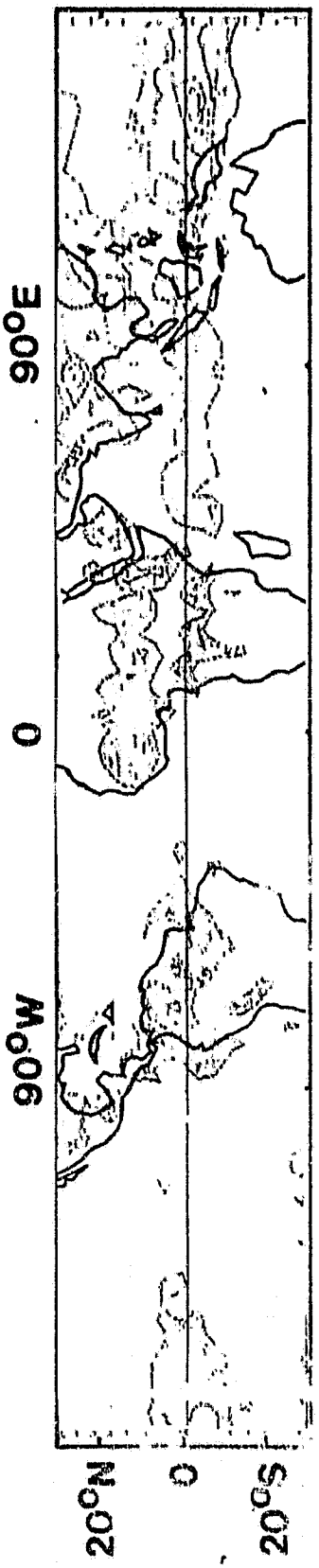

Fig. 18. Simulated mean rainfall rate distribution for June. Unit = arbitrary.

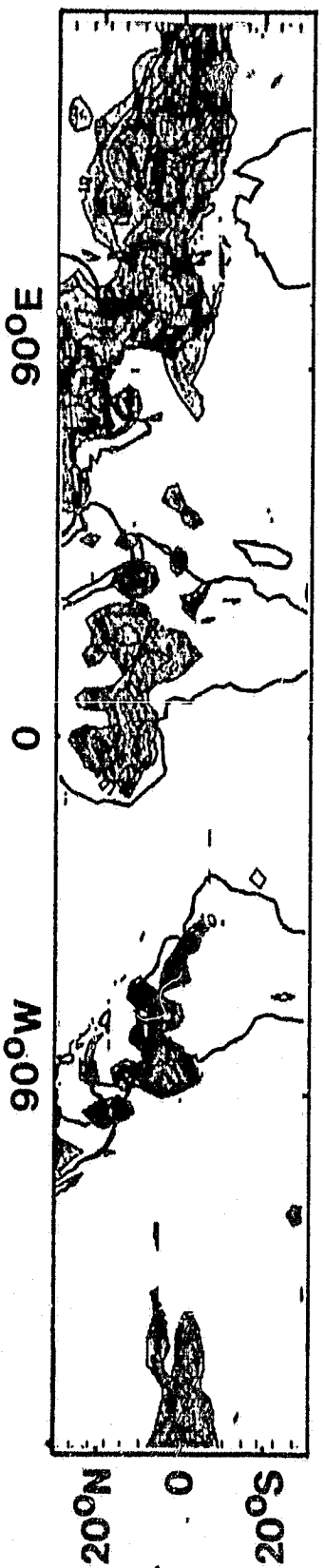

Fig. 19. Same as Fig. 18 except for July.

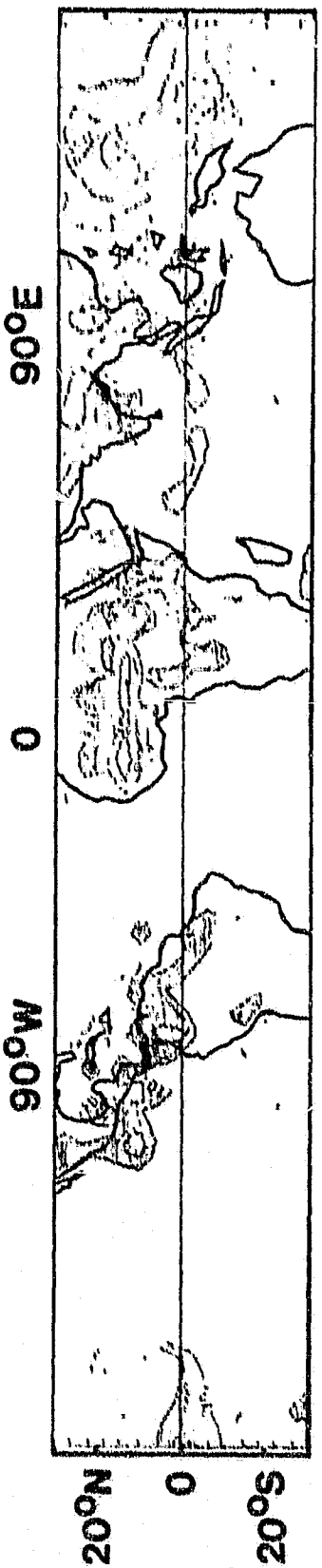

Fig. 20. Same as Fig. 18 except for August.

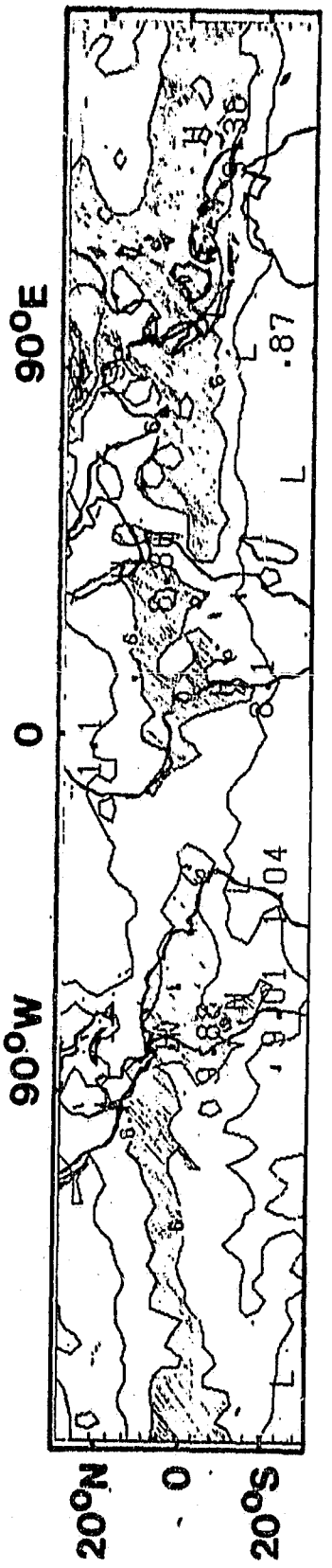

Fig. 21. Simulated mean specific humidity distribution at 700 mb for June.
Unit = $x10^{-3}$ g/kg.

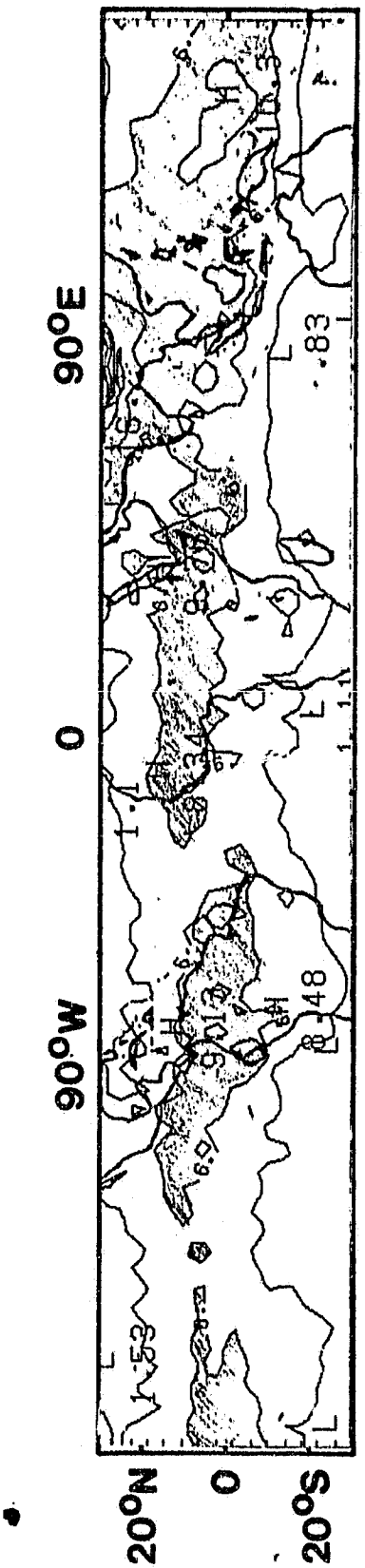

Fig. 22. Same as Fig. 21 except for July.

Fig. 23. Same as Fig. 21 except for August.

Fig. 24. Simulated mean surface temperature for (a) June, (b) July and (c) August. Unit = °C.

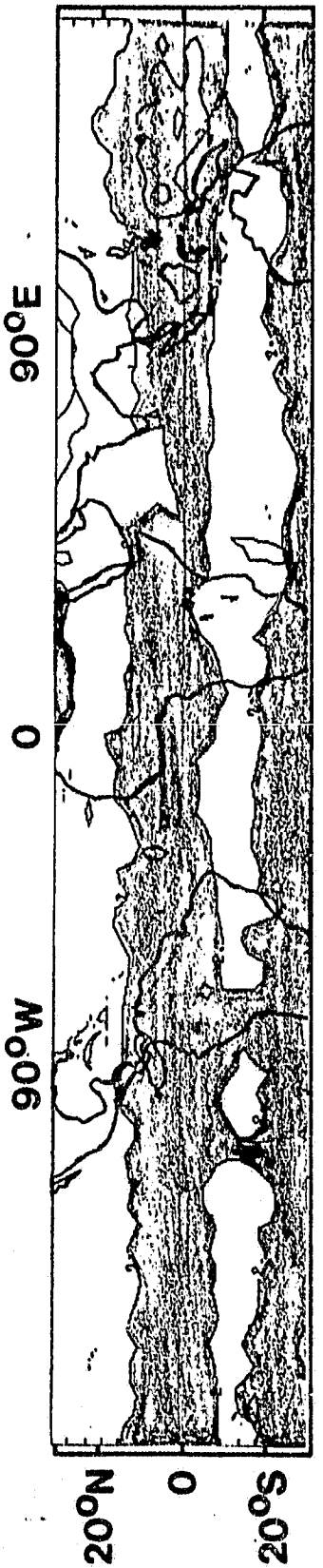

Fig. 25. Geographical distribution of variance between periods of 3.3 days and 5.4 days for 700 mb meridional wind. Unit = m^2s^{-2}.

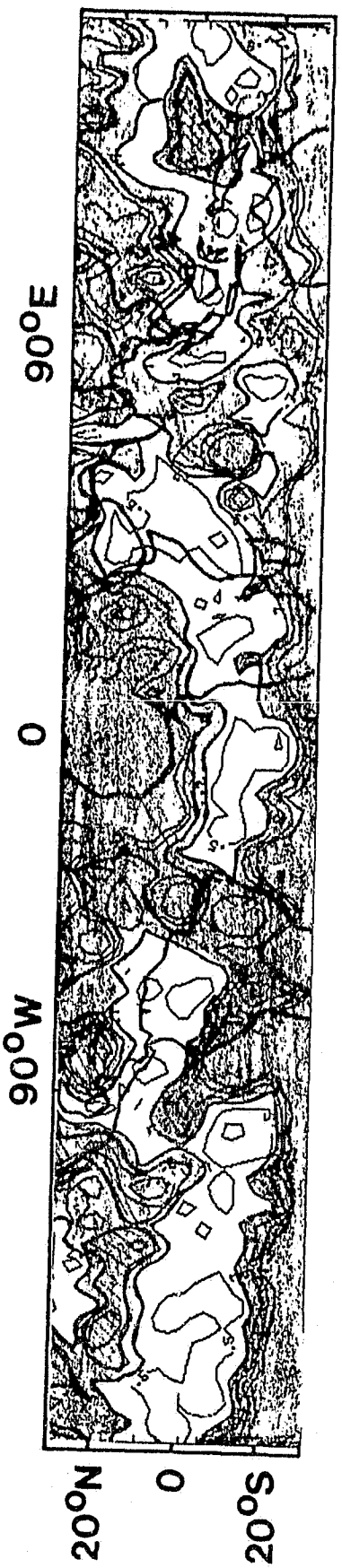

Fig. 26. Same as Fig. 25 except for observed wind.

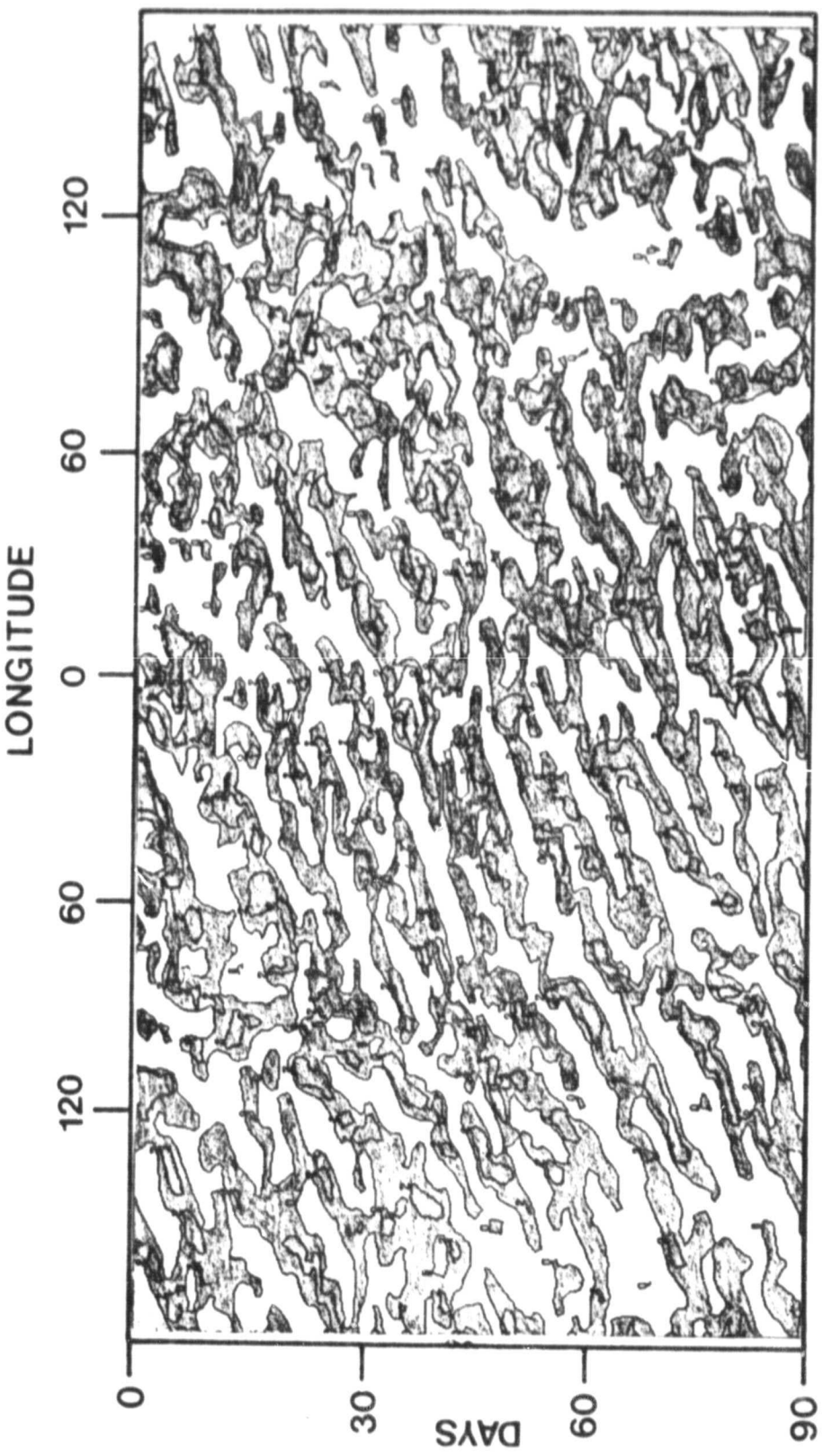

Fig. 27. Longitude-time section for simulated 700 mb north-south wind component. Local time means have been subtracted and positive values are shaded. Latitude corresponds to 22°N.

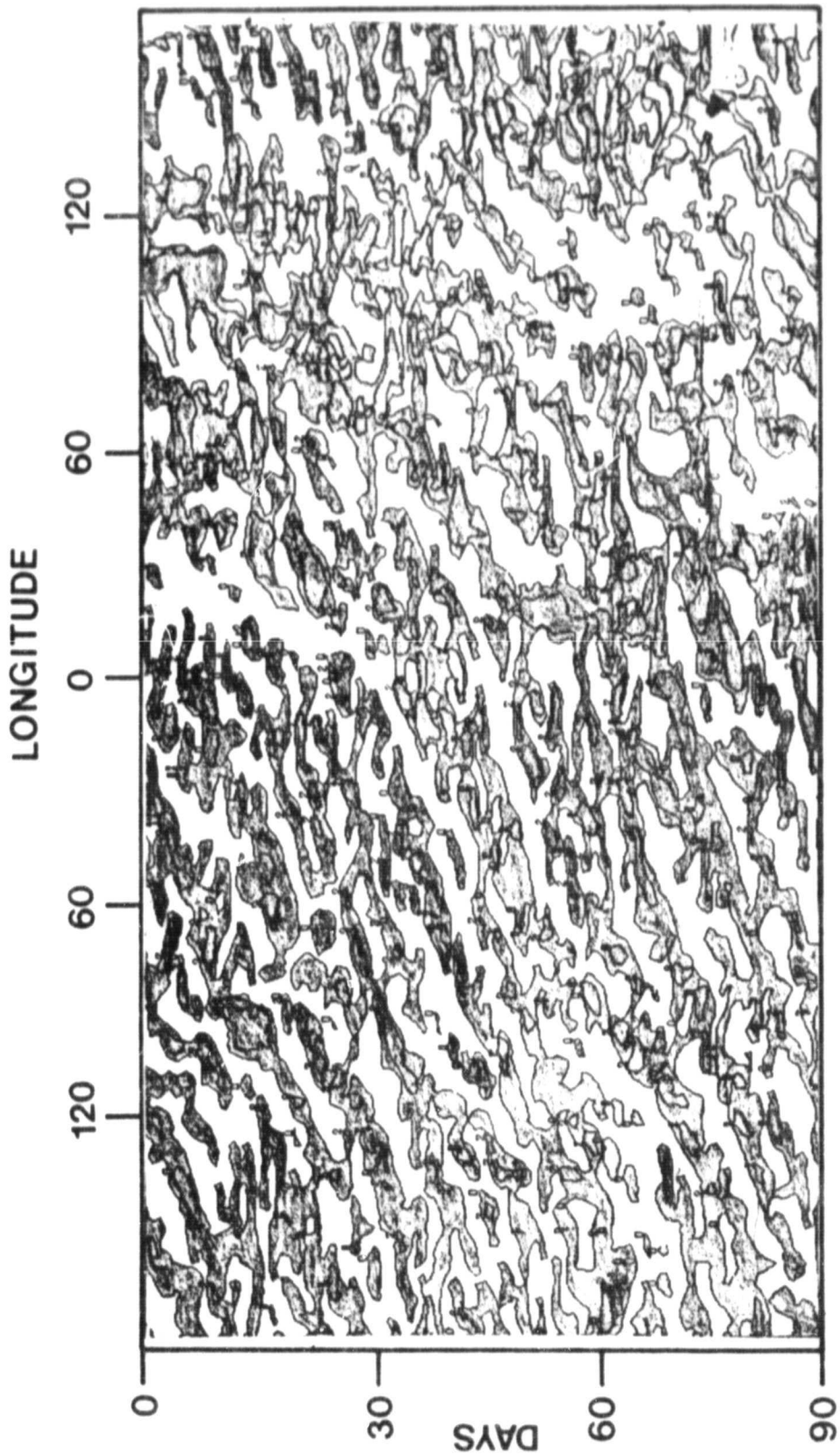

Fig. 28. Same as Fig. 27 except for 18°N.

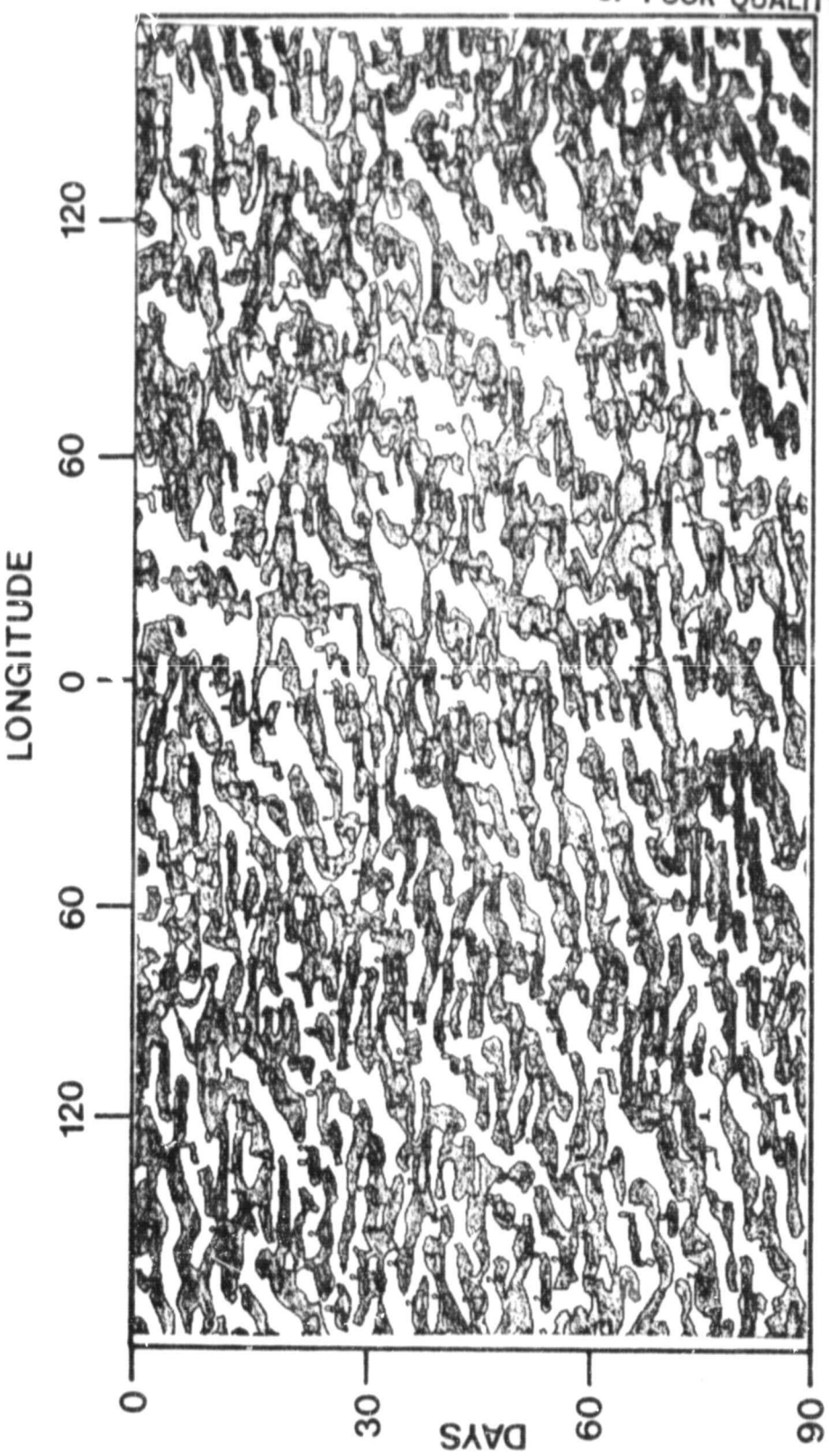

Fig. 29. Same as Fig. 27 except for 14°N.

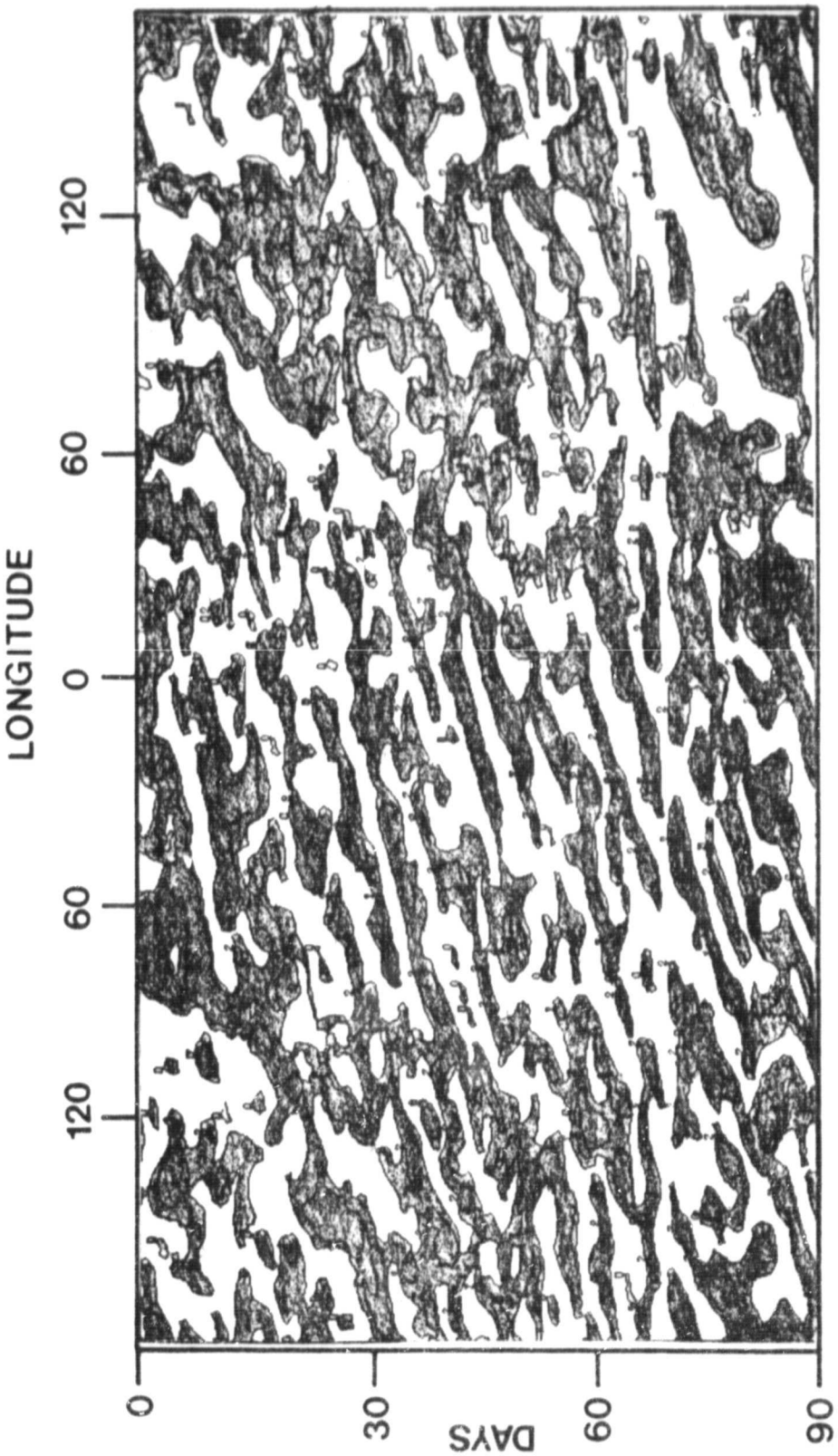

Fig. 30. Longitude-time section for observed 700 mb north-south wind component. Local time means have been subtracted and positive values are shaded. Latitude corresponds to 20°N.

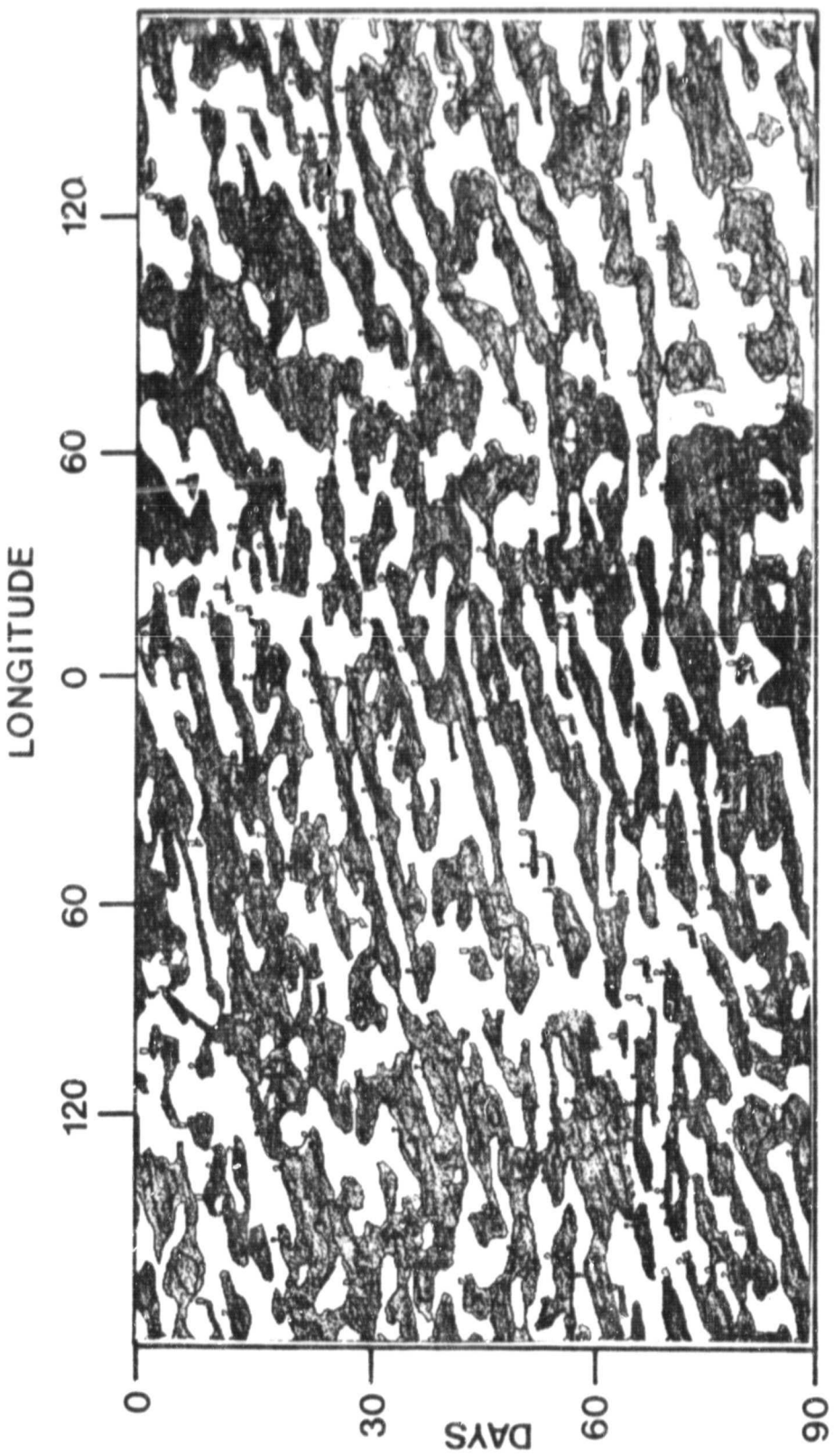

Fig. 31. Same as Fig. 30 except for 15°N.

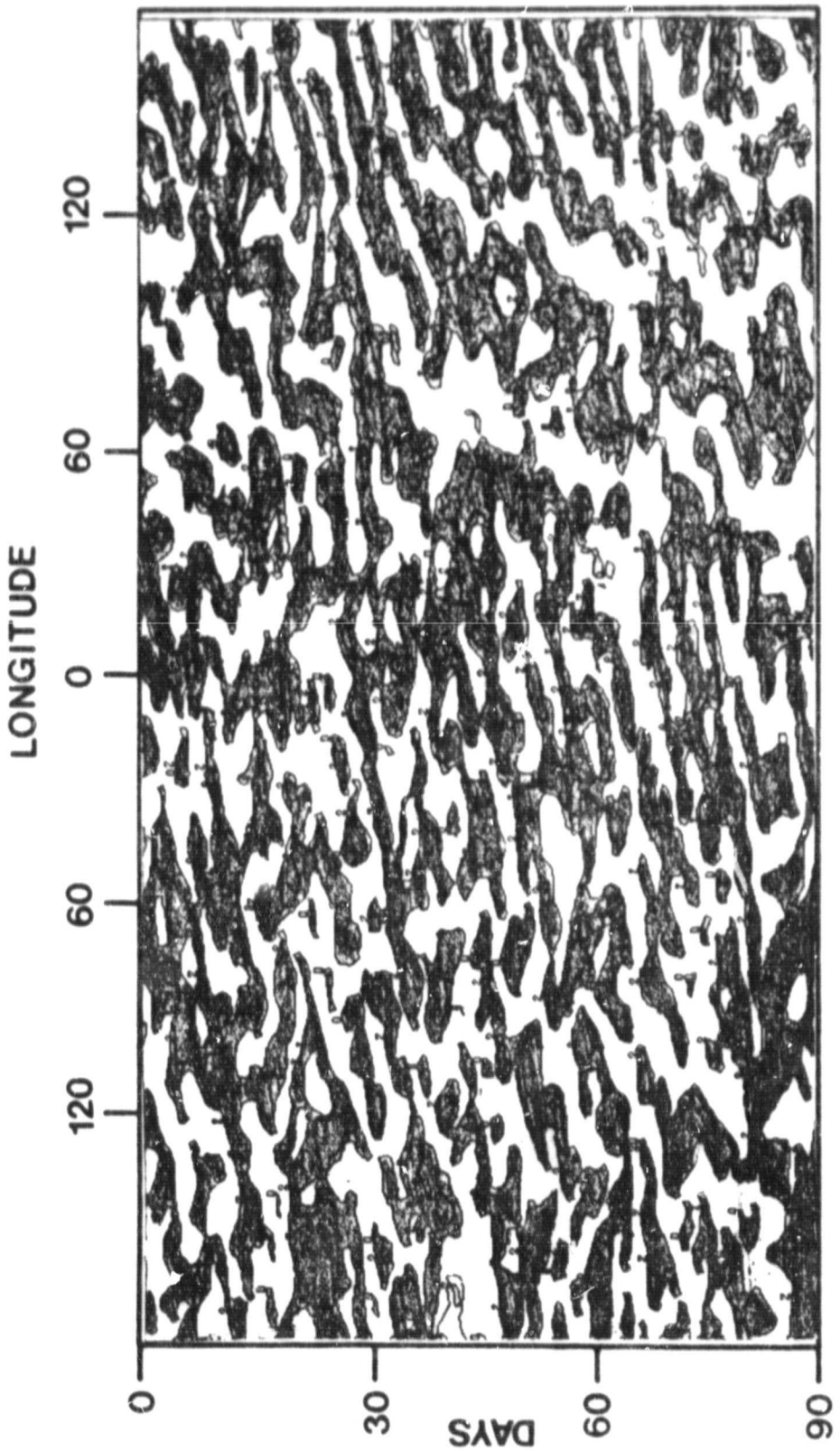

Fig. 32. Same as Fig. 30 except for 5°N.

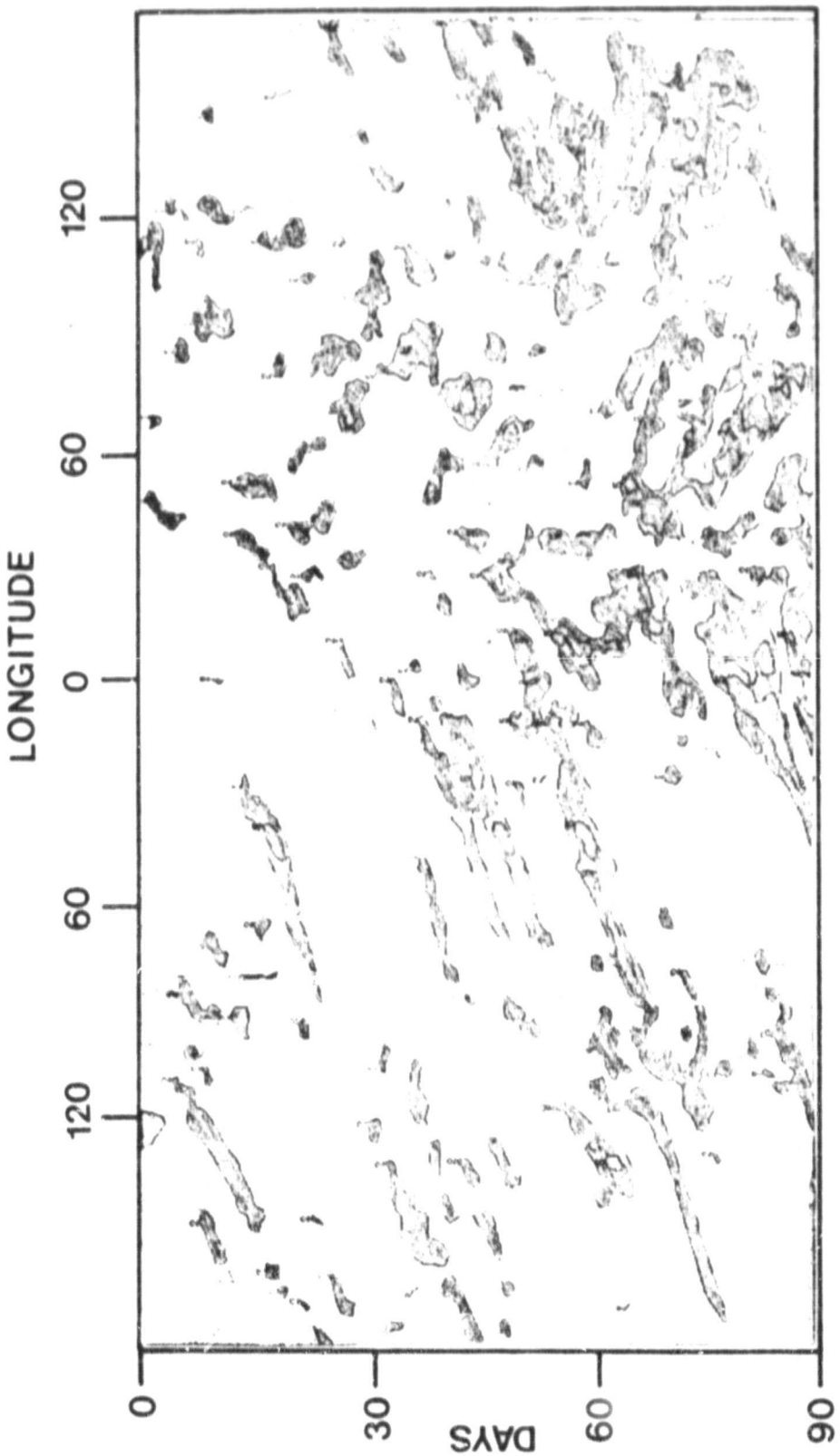

Fig. 33. Longitude-time section for simulated 700 mb specific humidity. Local time means have been subtracted and values greater than 2×10^{-3} g/kg are shaded. Latitude corresponds to 18°N.

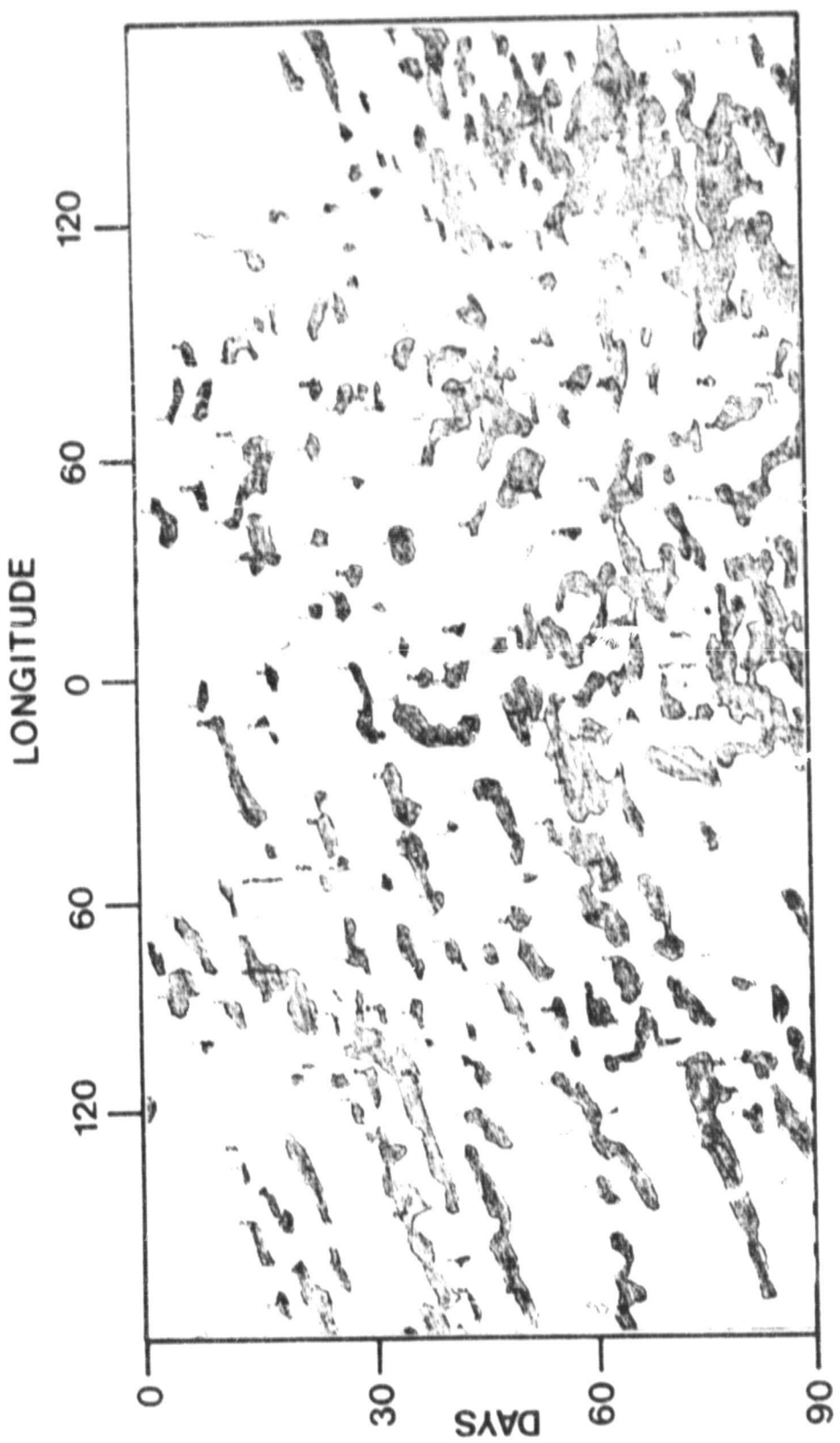

Fig. 34. Same as Fig. 33 except for 14°N.

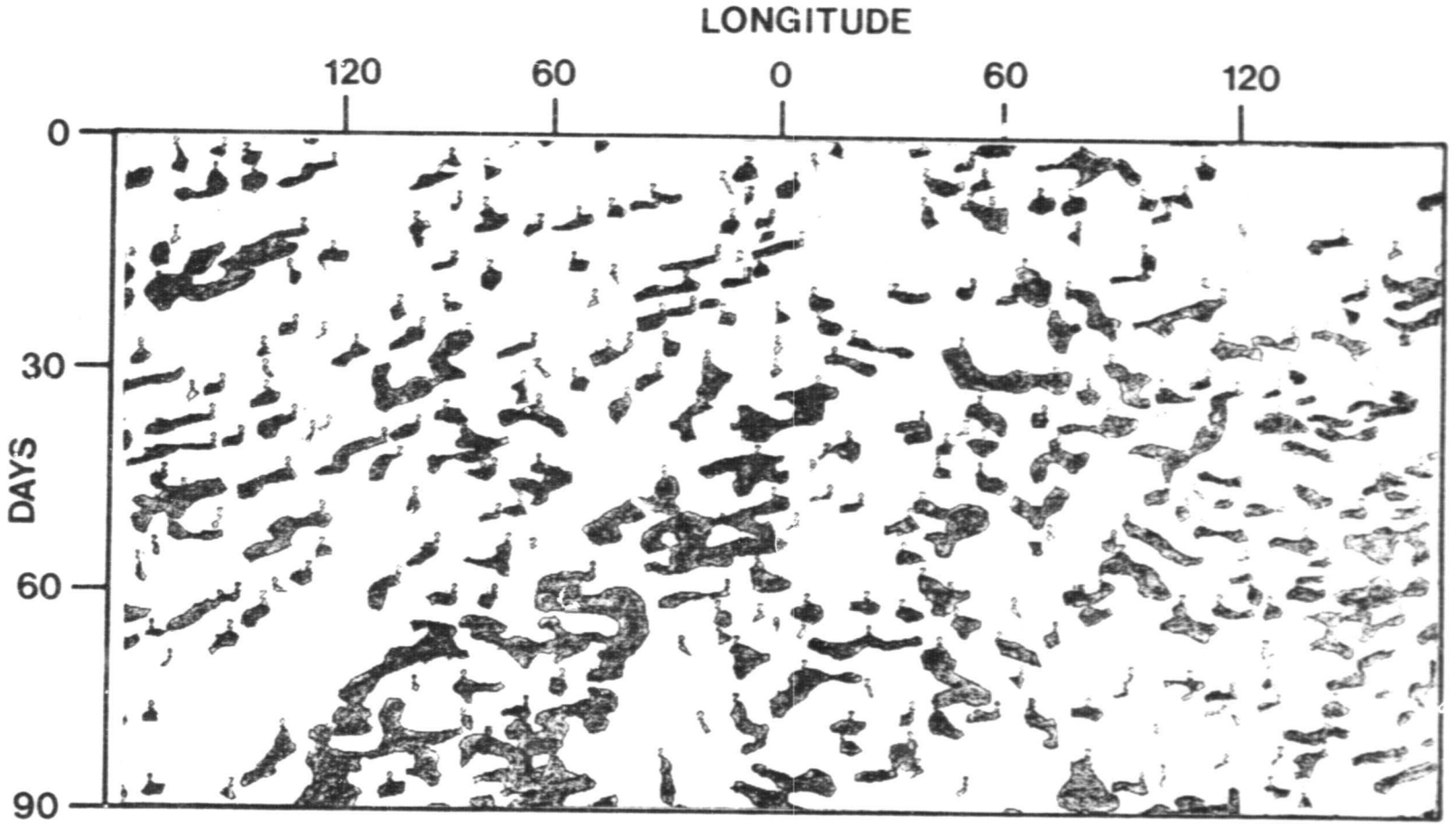

Fig. 35. Same as Fig. 33 except for 10°N.

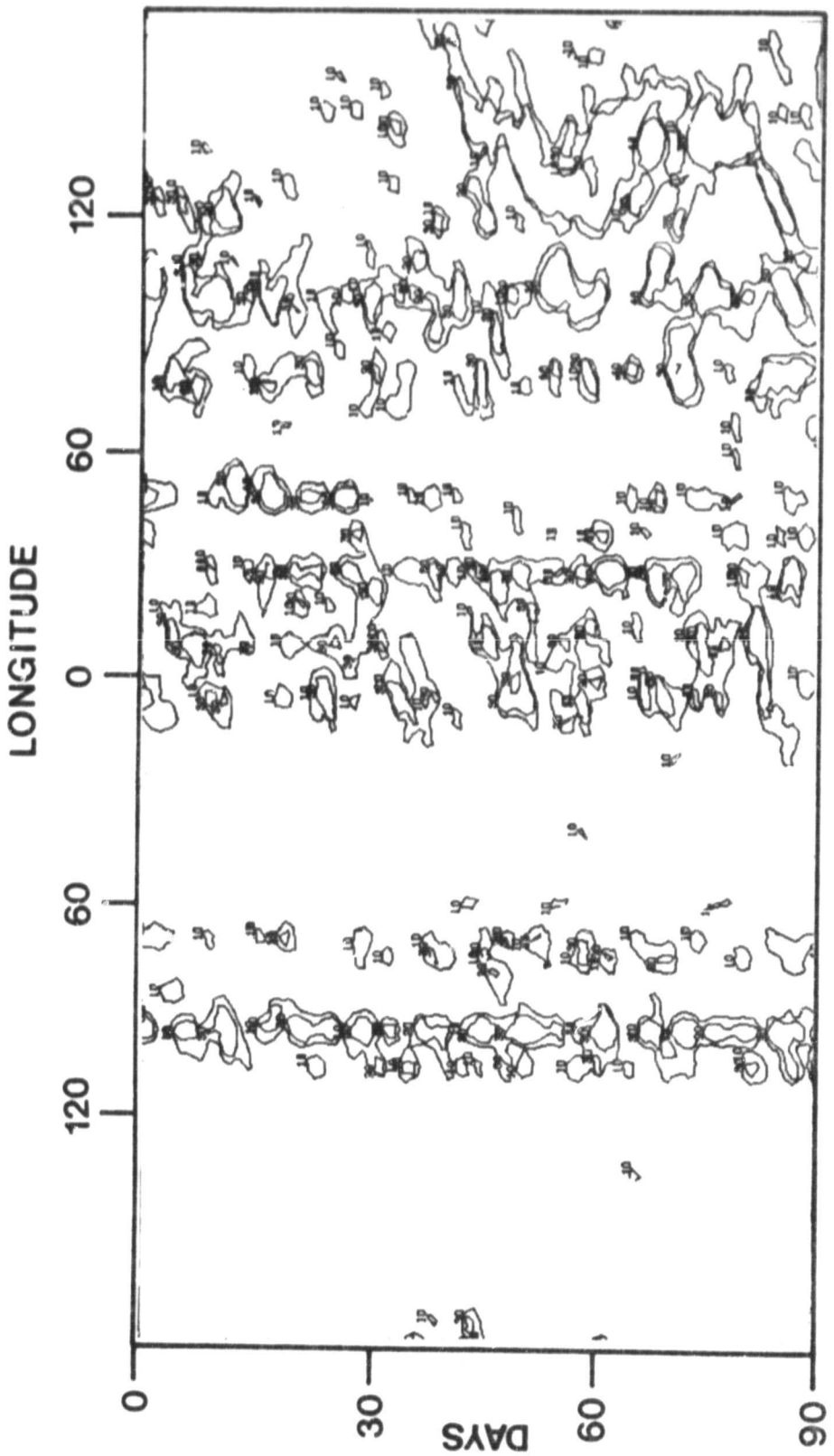

Fig. 36. Longitude-time section for simulated precipitation rate at 18°N. Unit - arbitrary.

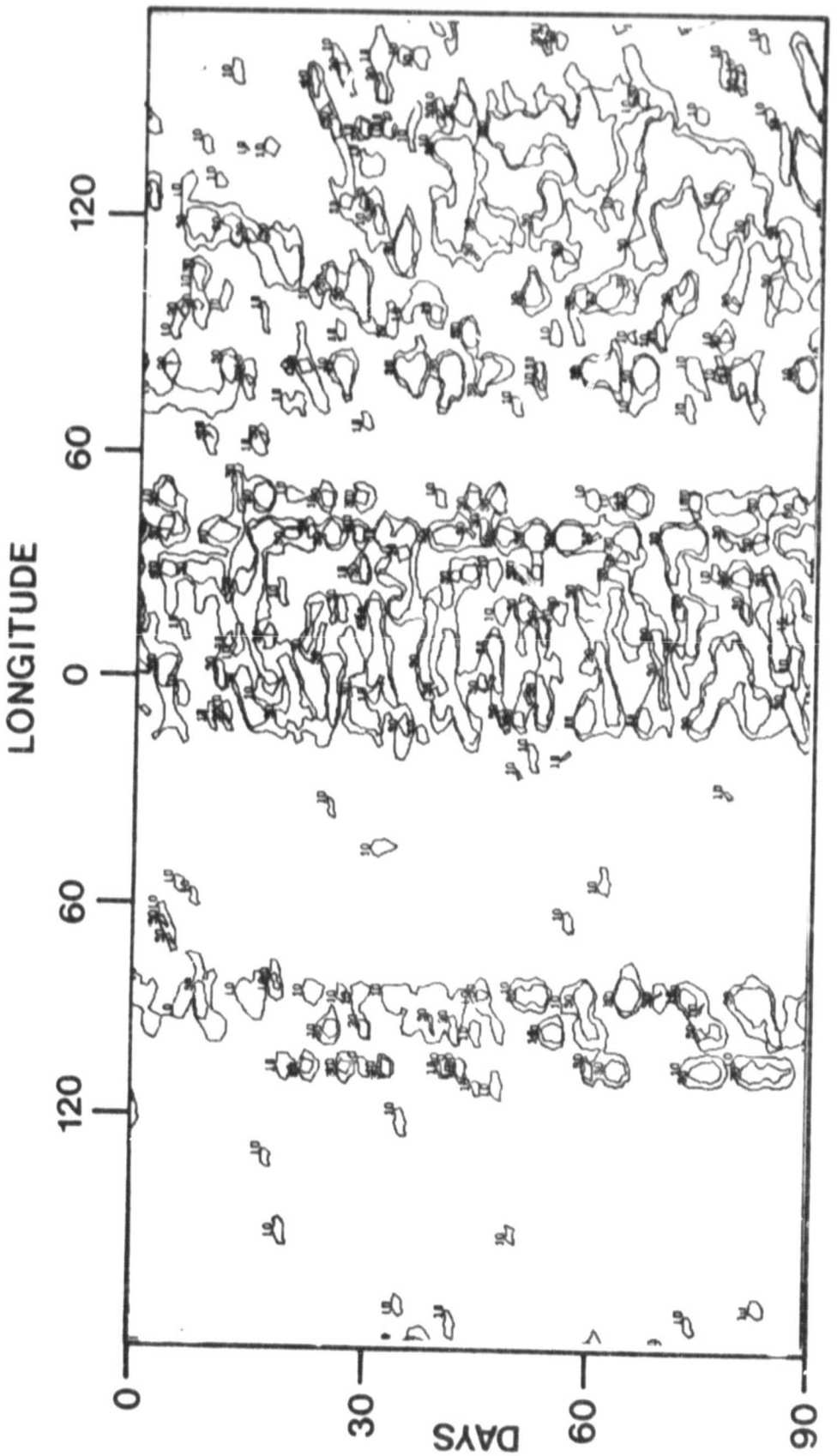

Fig. 37. Same as Fig. 36 except for 14°N.

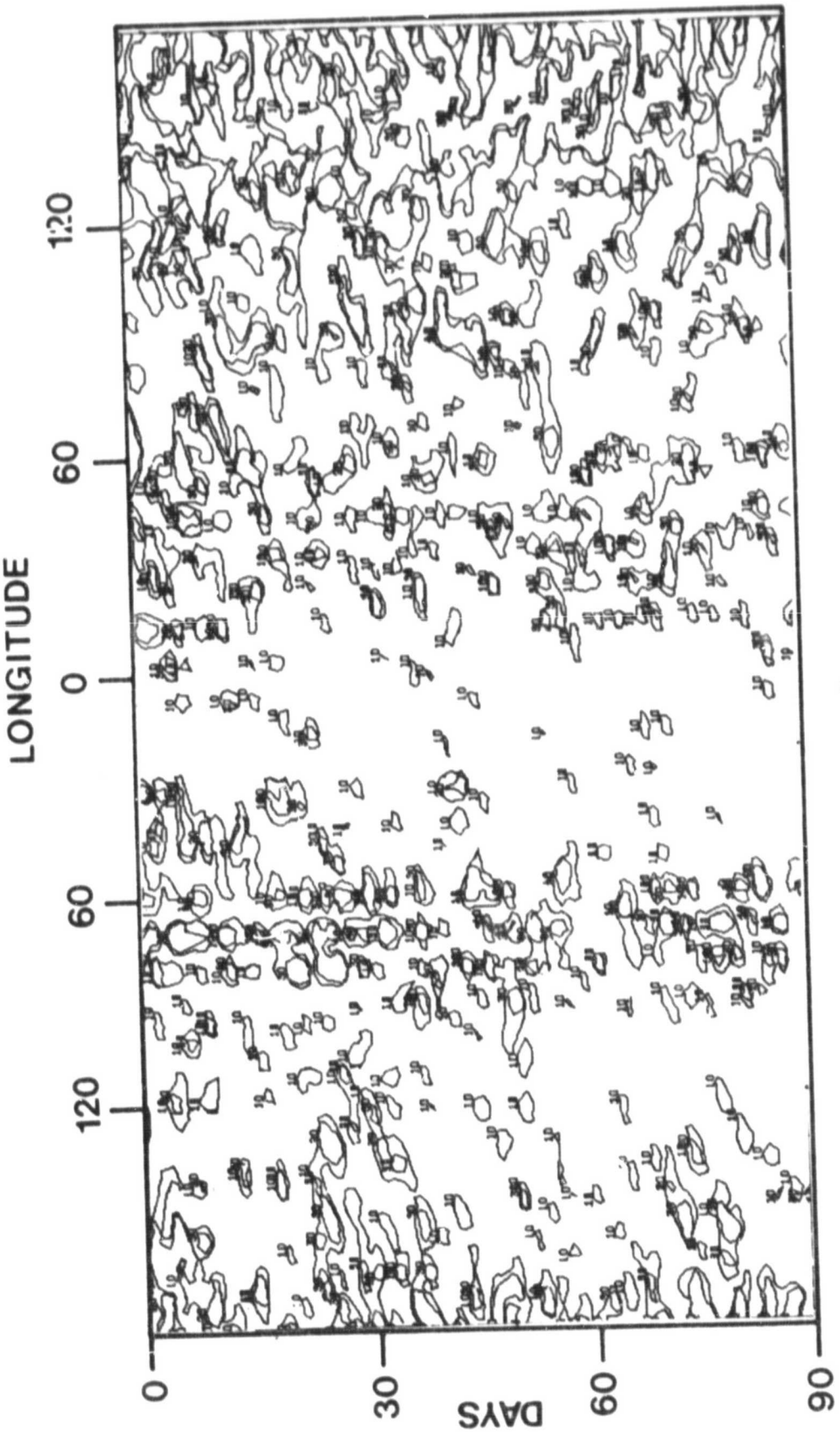

Fig. 38. Same as Fig. 36 except for 2°N.

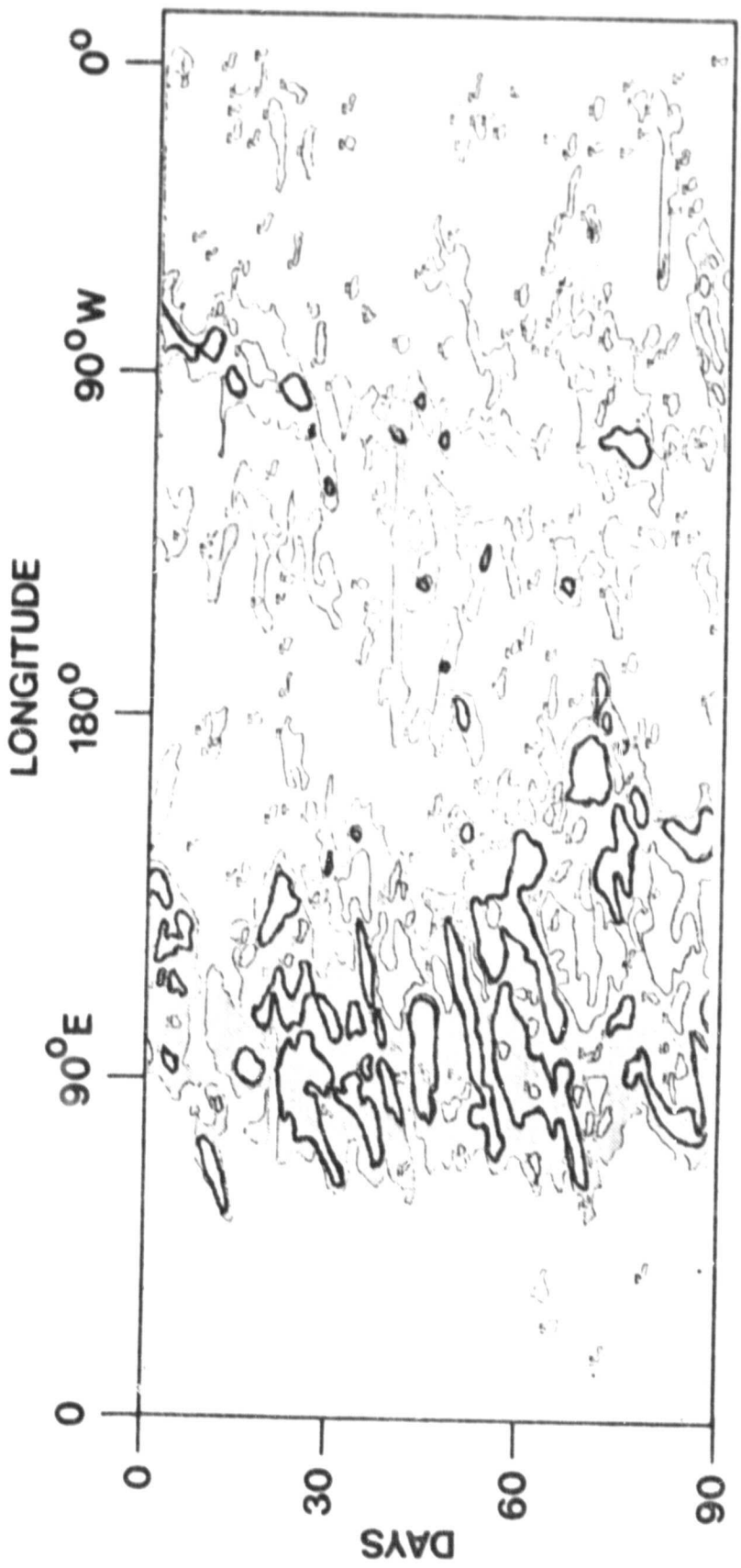

Fig. 39. Longitude-time section for observed rainfall inferred from IR observations at 19°N. Unit - arbitrary.

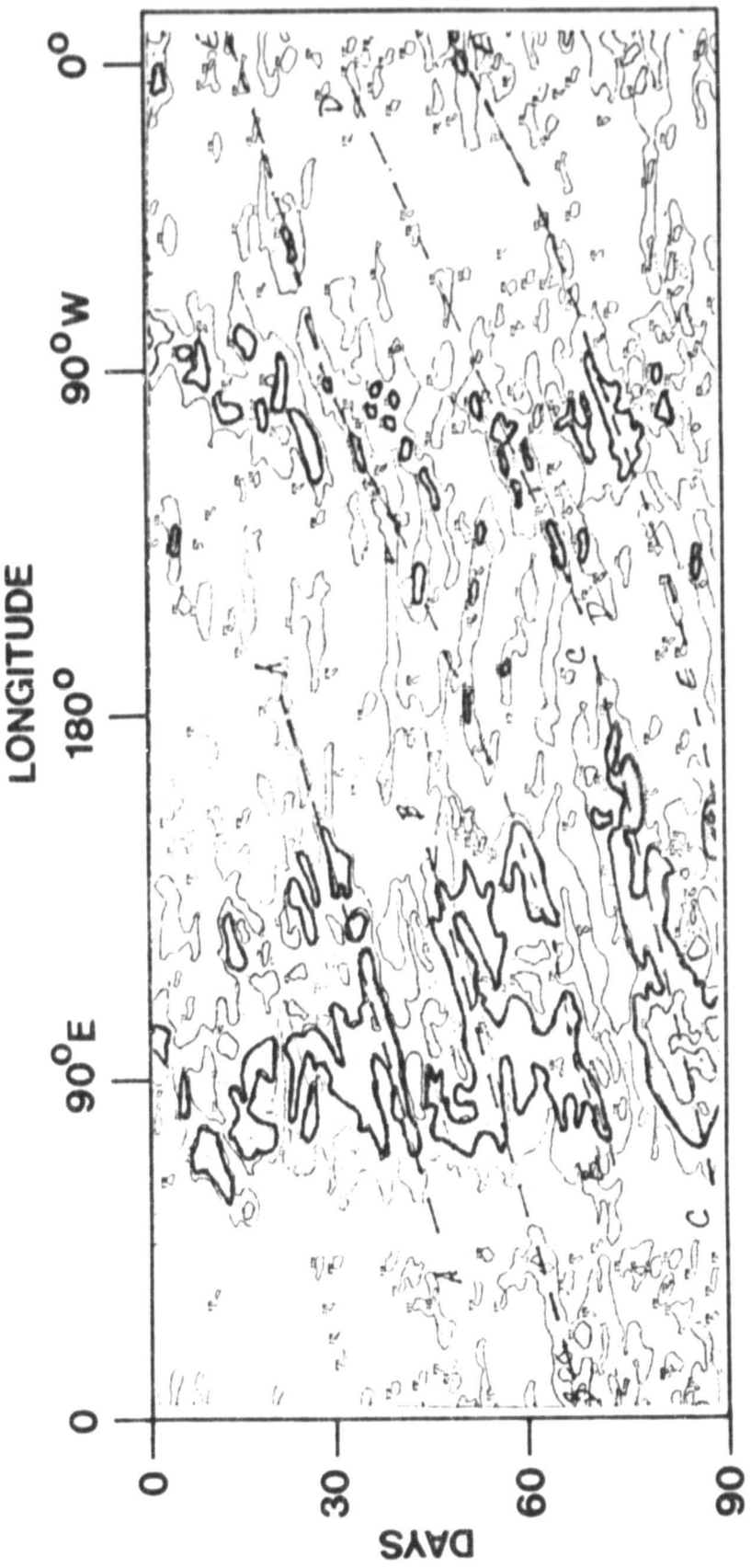

Fig. 40. Same as Fig. 39 except for 14°N.

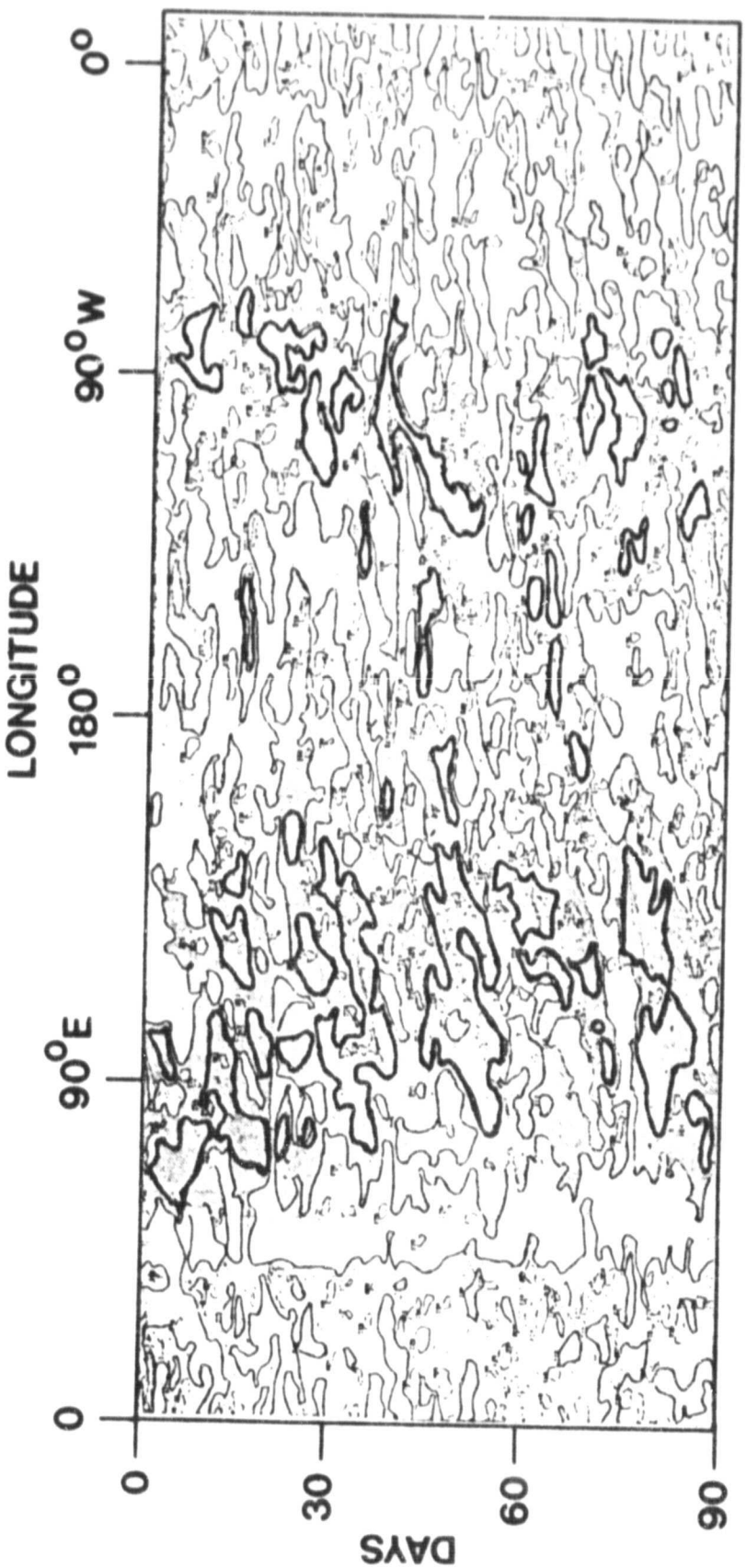

Fig. 41. Same as Fig. 39 except for 9°N.

PART II

AFRICAN WAVE DISTURBANCES IN A GENERAL CIRCULATION MODEL

AFRICAN WAVE DISTURBANCES IN A GENERAL CIRCULATION MODEL

by

M.A. Estoque, J. Shukla and J.G. Jiing

1. Introduction

The existence and the structure of synoptic scale disturbances over tropical North Africa have been studied observationally by numerous investigators, such as Carlson (1969a, 1969b), Burpee (1974), and Reed et al. (1977). The disturbances occur primarily during the summer season and travel westward, sometimes developing into tropical cyclones over the Western Atlantic. The observational studies indicate that the disturbances usually have wavelengths of about 2500 km and propagation speeds of approximately 7° longitude per day. During the early summer, the occurrence of disturbances is rather sporadic; they also tend to be weak in intensity. But later in the season, they occur more or less regularly at intervals of about 4 days. However, even during this part of the summer, there are periods of relative inactivity, presumably due to unfavorable conditions in the large scale flow patterns in which the disturbances develop. Observational data indicate that the waves are most intense near the 700 mb level where the perturbations in the meridional wind component attain magnitudes of about 5 m s^{-1}. Reed et al. (1977) found that there is a secondary maximum near the 200 mb level with wind perturbations whose magnitudes are somewhat less than those of 700 mb. It may be mentioned that the relatively large wind perturbations of 200 mb are not reproduced satisfactorily by the theoretical models of Rennick (1976) and Mass (1979). This is possibly due to the fact that the primary mechanism for perturbation development in these models is barotropic instability; this may not actually be the case in the real atmosphere.

Some of the characteristics of the wind field associated with these disturbances are shown in Fig. 1. This is a series of four 24-hourly streamline maps at the 10,000 ft. level (approximately 700 mb) based on a previous study by Carlson (1969a). Note the general westward movement of the disturbances. Note also the development of Disturbance, W-4, between 10°E and 15°E and the weakening of Disturbance W-1 as it approaches the western coast of Africa. According to Carlson (1969b), the disturbances usually achieve their greatest intensity in the area between 10°W and 20°W; thereafter, they tend to disintegrate and to become disorganized.

The problem concerning the place of origin of these disturbances has been considered by several investigators. In his analysis of 1968 synoptic data, Carlson (1969b) showed that almost one half of the observed disturbances appeared to originate east of 18°E and only a few were first observed west of 4°E. The frequency distribution of initial wave positions has a minor peak between 10°E and 12°E. Burpee (1972) indicated that the disturbances form in the region between 15°E and 30°E. He found no clear evidence of waves at locations farther east at Khartoum (32°E) and at Adem (45°E). Subsequently, Dean and La Seur (1974) found that some disturbances originate near Khartoum. The finding that disturbances may originate farther east appears to be supported by the investigations of Aspliden (1974) as well as by Albignat and Reed (1980). In particular, the work of Albignat and Reed (op. cit.) indicates that some disturbances may originate as far east as the southern tip of the Red Sea.

In regard to physical mechanisms which are responsible for the development of the disturbances, the observational study by Burpee (1972) as well as the theoretical studies by Rennick (1976) and by Mass (1979) suggest that barotropic instability is the major mechanism. However, on the basis of GATE observations, Norquist et al. (1976) found that baroclinic

instability appears to be more important than barotropic instability over Africa. This finding is in agreement with a theoretical study of the energetics of the disturbances by Walker and Roundtree (1977) who concluded that barotropic instability made only minor contributions to the energy budget. A somewhat different generating mechanism has been suggested by Carlson (1969b). He suggests that the mechanism is associated with an interaction of the convective processes with the mountainous terrain over Cameroon as well as over Sudan and Ethiopia. Based on the above studies, one may conclude, therefore, that there is still no complete agreement concerning the mechanism for the generation of African disturbances.

The problem concerning the behavior, structure and the development of African disturbances may be investigated theoretically by using model simulations of the general circulation of the atmosphere. In the present paper, we will describe the initial results of such an investigation using simulation data from the NASA Goddard Laboratory for Atmospheric Sciences (GLAS) general circulation model. The basic characteristics of the model has been described previously by Sommerville et al. (1974). Our preliminary results indicate that the model is able to simulate many of the important properties of African disturbances. It is, therefore, expected that further analysis of the simulation data will contribute to a solution of the problem mentioned at the beginning of this paragraph.

2. Data and analysis procedure

The simulated meteorological data which were available for our study are the horizontal wind components (u and v), temperature (T) and specific humidity (q). Values of these variables are given at nine levels of the

atmosphere and on a horizontal grid whose grid points are spaced 5° longitudinally and 4° latitudinally. The variables correspond to a simulation of the summer 1974 which is also the period of the GATE observational program. Since the raw simulation data were quite noisy, we applied a band pass filter in order to retain only the perturbations within the spectral band whose wave numbers range from 6 to 20 along a latitude circle. Over the tropics, this spectral band correspond to wavelengths from about 2,000 to 6,000 km. The filtering was done by computing the amplitudes of the Fourier components along the longitudinal direction which correspond to the above wave numbers. Additional smoothing of the data was done along the north-south direction by using a method described by Shapiro (1970).

3. Results

Some general ideas concerning the existence and the properties of the simulated disturbances may be seen in Figs. 2, 3 and 4. These are Hovmoeller diagrams for the perturbation in the meridional component of the wind (v') the temperature (T') and the specific humidity (q') for 18°N. The perturbations correspond to deviations from local time means computed to each grid point. The diagram for v' encompasses the whole globe and corresponds to the three-month period of June, July, and August 1974. The diagrams for T' and q' are only for the month of July 1974. Regions with positive deviations are shaded. It may be seen that the patterns of shaded and unshaded areas in the diagrams demonstrate the existence of disturbances in the wind, temperature, and the moisture fields. The slope of the patterns from the lower left hand corner to the upper right corner near the Greenwich meridian imply a westward propagation of about 6 to 7 degrees of longitude, per day. This speed is close to that observed for African disturbances. Note that there is a

general tendency for disturbances to develop over Central Africa (10°E) during the early part of July. The tendency is seen best in the Hovmoeller diagrams for v' and T'. However, later during the month, one can see evidences in the diagrams of disturbances which originate east of Africa.

More results relating development of disturbances over Africa are presented in Figs. 5. Figure 5 shows the root mean square (RMS) of the perturbation v component and the mean wind vectors for July 1974 at 700 mb. It may be seen that there is a region of maximum values of the root mean square perturbation near the Greenwich meridian and 8°N. This region of large RMS of v' extends both eastward and westward but with decreasing values. Since the diagram is constructed using bandpassed data, the RMS values reflect only the contributions of disturbances with wavelengths from 2,000 to 5,000 km. The pattern of the isopleths indicates that the disturbances tend to intensify in the vicinity of 10°E. It is interesting to note that Carlson (1969b) found a relative maximum in the frequency distribution of initial wave positions in the same region. A similar region of intensification, although somewhat displaced westward, was found by Albignat and Reed (1980) by analyzing GATE observations. The maximum value of the root mean square (4.5m s^{-1}) is almost the same as the amplitude of the meridional wind oscillation in the 0.2 to 0.4 cpd frequency band at 700 mb found by Albignat and Reed. In their analysis, Albignat and Reed also found a secondary maximum of wind oscillation amplitude just west of the Red Sea. Fig. 5 does not show a separate maximum in the same area, however, it may be noted that the region just southwest of the Red Sea is a region of large magnitudes of the root mean square v' relative to the regions located north and south. Fig. 5 also shows that disturbances tend to weaken west of the Greenwich meridian.

In order to illustrate the actual development of individual disturbances

in the model simulations, we present a series of five 24-hourly maps in Figs. 6 to 10. The maps are streamline maps based on the simulated 700 mb winds at gridpoints for the first 5 days of July 1974. Looking at the first map (12Z July 1, 1974), one can see two disturbances: a weak wave disturbance designated as A west of the West African Coast and a cyclonic vortex designated as B over West Africa near 10°N. In addition to these two synoptic features of the wind field, we also note a trough whose axis is oriented along the east-west direction, extending from Lake Chad to the Red Sea. During the next 24 hour period, Wave Disturbance A moves westward while the cyclonic vortex (B), intensifies and travels towards the west. At the same time, a cyclonic vortex (designated by C) forms at the western end of the east-west trough near Lake Chad (Fig. 7). The next two maps show further westward movement of the wave disturbance (A). In the meantime, the cyclonic vortex (B) moves to the coast while decreasing in intensity and becoming just a trough. The cyclone near Lake Chad (C) intensifies and moves slowly westward. Finally, on the last map (12Z July 5, 1974), we see a new synoptic feature -- a new cyclonic disturbance (D) which formed near the southern tip of the Red Sea. It is interesting to note that many features of the simulated 700 mb streamline maps resemble those of the observed streamline maps in Fig. 1.

In order to depict some of the important variations of the structure along the vertical direction, we have constructed Fig. 11. This diagram represents an east-west vertical section along 14°N latitude of the total wind and the temperature deviation at 12z July 5, 1974. The latitude, which has been selected, runs close to the centers of the cyclonic vortices (C and D in Fig. 10) over Western Africa and near the Red Sea. The picture, as a whole, shows a series of perturbations in the temperature and in the wind fields along the east-west direction. Maximum values of the temperature

perturbations of about 1.5°C are located near the 600 mb level. A secondary maximum appears close to the 300 mb level. The perturbations are small at 900 mb. Note that, in general, the troughs in the middle troposphere (near 30°W, 5°W, 35°E) are characterized by negative temperature deviations. The alternation of positive and negative temperature deviations at 600 mb along the east-west direction indicates an average horizontal wavelength of about 3500 km. Focusing our attention to the region (near 5°W) of the West African vortex (C), we see that this vortex is cold-cored near 600 mb. Above this cold core, the disturbance is warm-cored at the 300 mb level, i.e., the temperature variation at 300 mb is opposite in phase to that at 600 mb. This type of phase relationship seems to be characteristic of the entire region. There also appears to be a westward tilt with height of the patterns of isotherms. In regard to the wind field, one can see that the trough at 700 mb is overlaid by a weak ridge at 200 mb. This means that the southerly winds east of the 700 mb trough are overlaid by northerly winds at the 200 mb, i.e.,a 180° out of phase relationship in the v component at these two levels. An analogous phase relationship occurs west of the 700 mb trough. It is interesting to note that this vertical structure of the simulated disturbance is generally in agreement with that obtained by Reed et al. (op. cit.) from GATE observational data.

4. Concluding remarks

In this paper we presented the results of a synoptic analysis of computer model simulations of the atmosphere over Africa and vicinity for the month of July 1974. The simulations were made by integrating the GLAS general circulation model for an entire summer season. The primary object of the analysis was to determine the existence, behavior, and the

structure of synoptic scale disturbances over tropical Africa north of the equator. We found that the GLAS general circulation model is able to simulate rather realistically the African disturbances which have already been studied extensively using observations. Some of the important characteristics of the simulated disturbances are as follows:

(1) During the month of July 1974, the disturbances intensify primarily in the region just south of Lake Chad and dissipate near the western coast of Africa. There is some indication that this intensification represents further development of already existing disturbances which have moved westward from the Red Sea region and in other regions even farther east.

(2) The disturbances have an average propagation speed of about 6° of longitude per day; the average horizontal wavelength is about 3000 km.

(3) The disturbances have a maximum amplitude near 600 mb; there appears to be a secondary maximum near the 300 mb level. The amplitude of the disturbance at 900 mb is relatively small.

(4) The troughs at 700 mb are characterized by negative temperature deviations. The temperature variations at 300 mb are 180° out of phase relative to the variations at 700 mb. A similar out of phase relationship exists in the north-south wind component.

By and large, the above simulated characteristics are similar to those which have been found by previous analysis of observational data. In particular, the structure of the simulated disturbance is similar to that found by Reed et al. (op. cit.) over continental Africa. Hence, the energetics of the simulated and the observed disturbances may also be similar to each other, i.e., baroclinic processes must be more important than baroclinic processes. The agreement between simulated and observed disturbances is quite remarkable in spite of the fact that the simulated July mean flow pattern differs somewhat from corresponding observed mean July flows.

The main difference is in the existence of westerly 700 mb winds over Equatorial Africa in the simulated wind field (Fig. 5) while available mean July winds based on observations usually show easterlies in the same region. The agreement in the characteristics of the simulated and observed disturbances in spite of the lack of complete agreement in the corresponding 700 mb mean July wind field is difficult to understand; further investigations are needed in order to clarify the matter. At any rate, the present study has succeeded in showing perhaps for the first time, that African disturbances can be simulated quite realistically by a primitive equation general circulation model. This success might imply that models of this type would be able to predict these disturbances on an operational basis in the near future.

REFERENCES

Albignat, J. P. and R. J. Reed, 1980: The origin of African wave disturbances during Phase III of GATE. J. Atmos. Sci., 37, 1827-1839.

Aspliden, C. J., 1974: The low level windfield and associated perturbations over tropical Africa during northern summer. Preprints Int. Tropical Meteorology Meeting, Nairobi, Amer. Meteor. Soc., 218-223.

Burpee, R. W., 1972: The origin and structure of easterly waves in the lower troposphere of North Africa. J. Atmos. Sci., 29, 77-90.

_____, 1974: Characteristics of North African easterly waves during the summers of 1968 and 1969. J. Atmos. Sci., 31, 1556-1570.

Carlson, T. N., 1969a: Synoptic histories of three African disturbances that developed into Atlantic hurricanes. Mon. Wea. Rev., 97, 256-276.

_____, 1969b: Some remarks on African disturbances and their progress over the tropical Atlantic. Mon. Wea. Rev., 97, 716-726.

Dean, G. A. and N. E. LaSeur, 1974: The mean structure and the synoptic-scale variation of the African troposphere. Preprints Int. Tropical Meteorology Meeting, Nairobi, Amer. Meteor. Soc., 224-228.

Mass, C., 1979: A linear primitive equation model of African wave disturbances. J. Atmos. Sci., 36, 2075-2092.

Norquist, D. C., Recker, E. E. and R. J. Reed, 1977: The energetics of African wave disturbances as observed during Phase III of GATE. Mon. Wea. Rev., 105, 334-342.

Reed, R. J., Norquist, D. C. and E. E. Recker, 1977: The structure and properties of African wave disturbances as observed during Phase III of GATE. Mon. Wea. Rev., 105, 317-333.

Rennick, M. A., 1976: The generation of African waves. J. Atmos. Sci., 33, 1955-1969.

Shapiro, R., 1975: Linear filtering, Math comp., 29, 1094-1097.

Sommerville, R. C., Stone, P. H., Halem, M., Hansen, J. E., Hogan, J. S., Druyan, L. M., Russel, G., Lacis, A., Quirk, W., and J. Tenenbaum, 1974: The GISS model of the global atmosphere. J. Atmos. Sci., 31, 84-117.

Walker, J. and P. R. Rowntree, 1977: The effect of soil moisture on circulation and rainfall in a tropical model. Quart. J. Roy. Meteor. Soc., 103, 29-46.

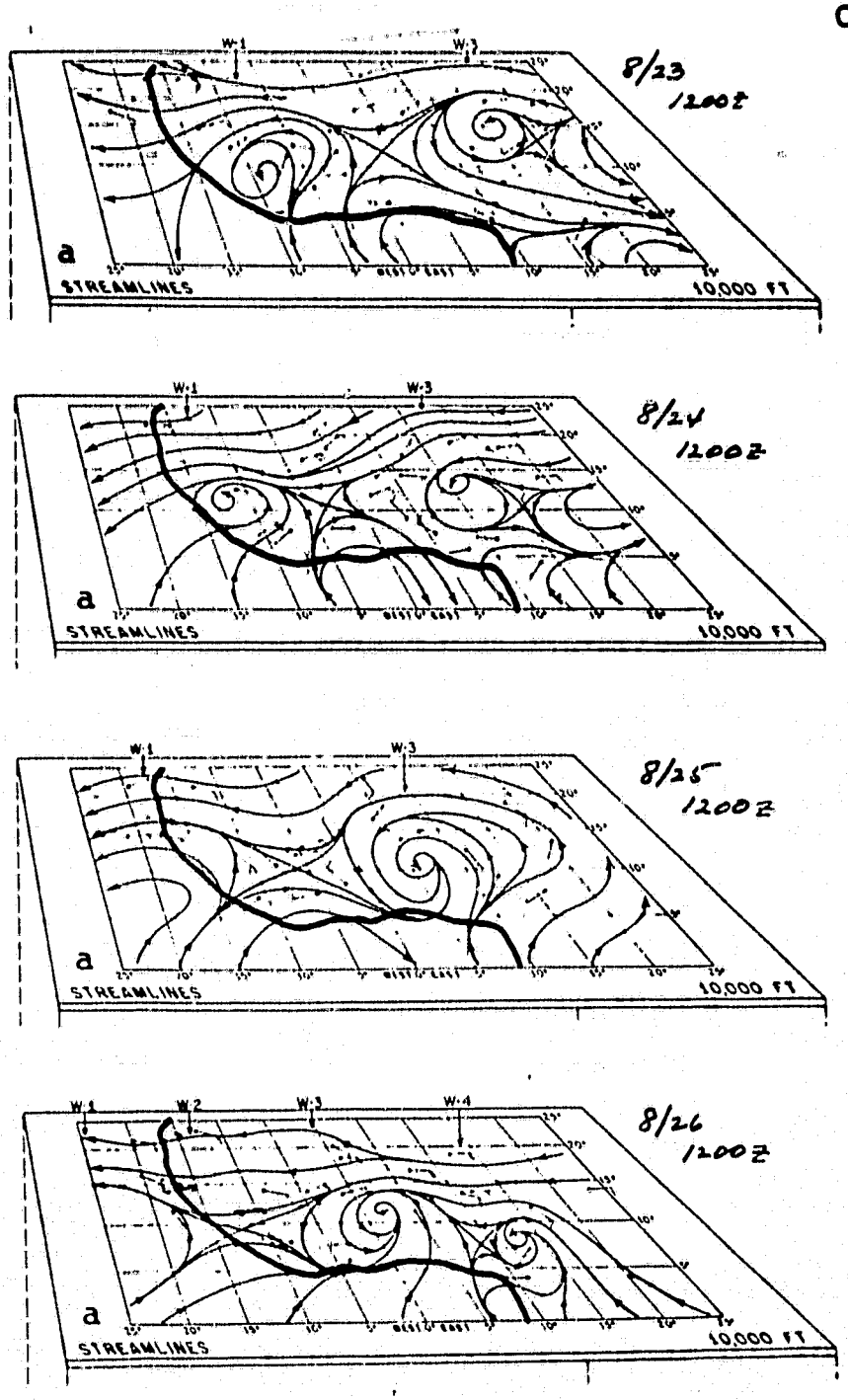

Fig. 1. Daily streamline maps at 10,000 ft. during the period, August 23-26, 1967 based on Carlson's (1969a) synoptic analysis.

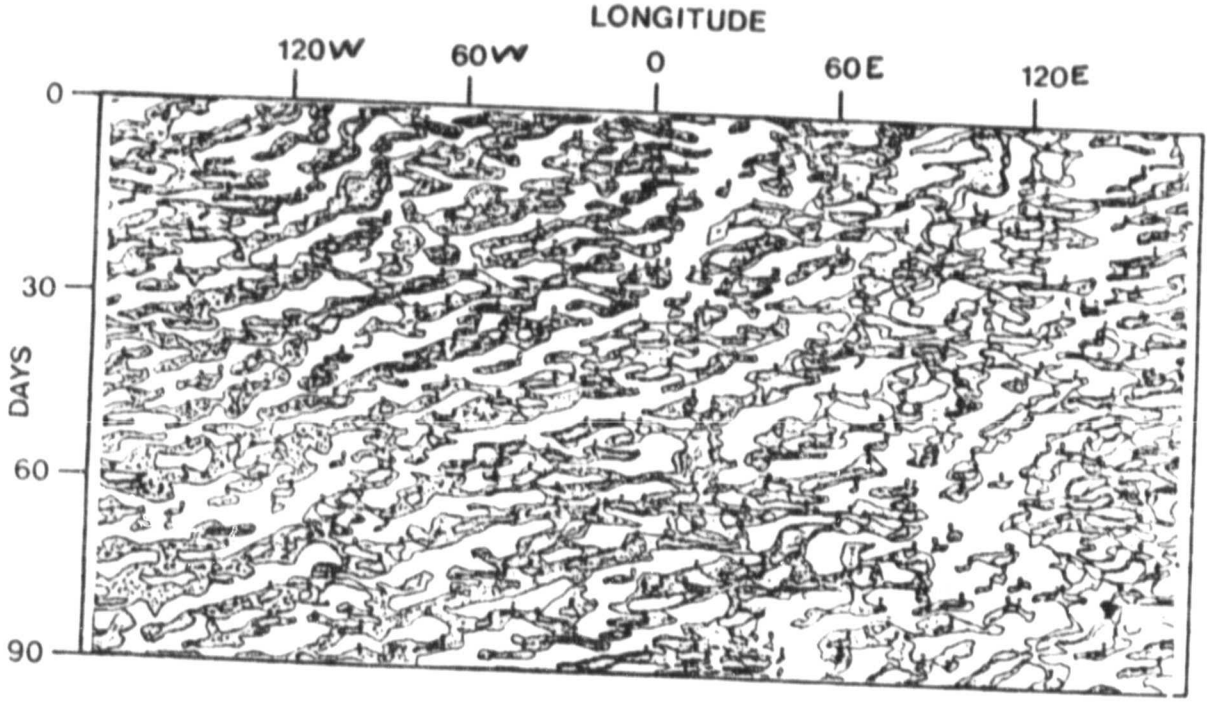

Fig. 2. Hovmoeller diagram for the perturbation north-south wind component along 18°N latitude during the period, June to August 1974, based on unfiltered simulation data. Areas with positive values are shaded.

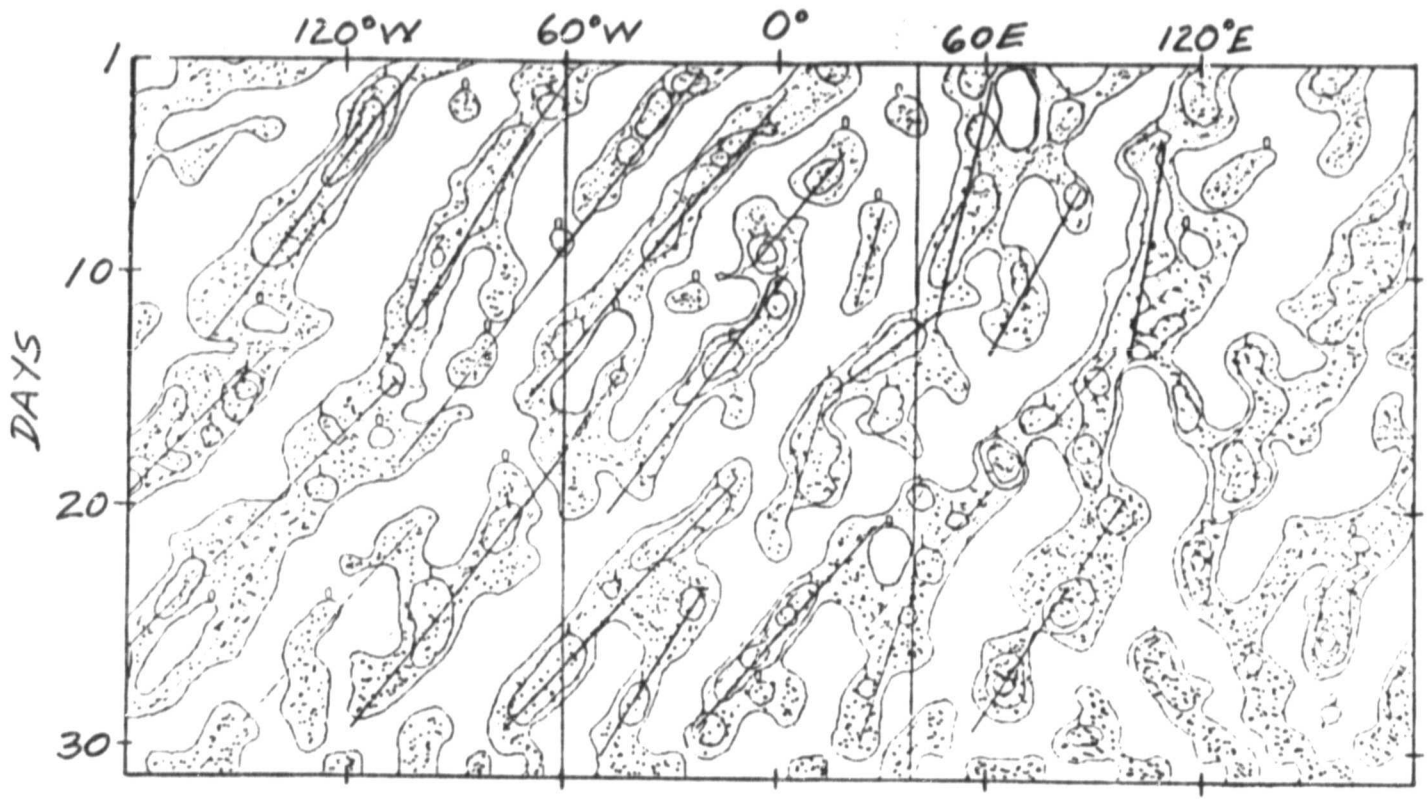

Fig. 3. Hovmoeller diagram for the temperature perturbation along 18°N latitude during the month of July 1974 based on filtered simulation data. Areas with positive values are shaded. Contour interval in the shaded areas is 1°C.

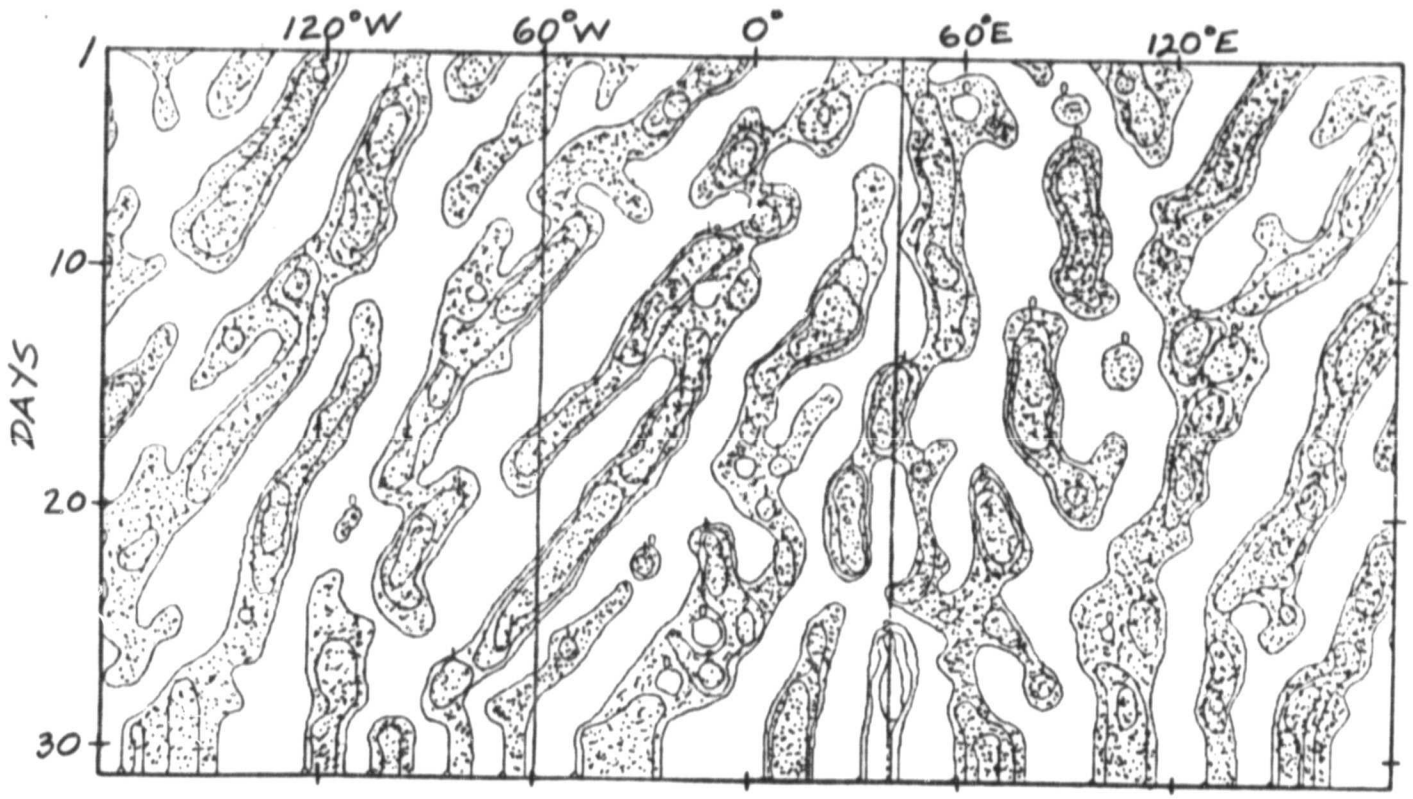

Fig. 4. Hovmoeller diagram for the specific humidity perturbation along 18°N latitude during the month of July 1974 based on filtered simulation data. Areas with positive values are shaded. Contour interval in the shaded areas is 1° grams per kilogram.

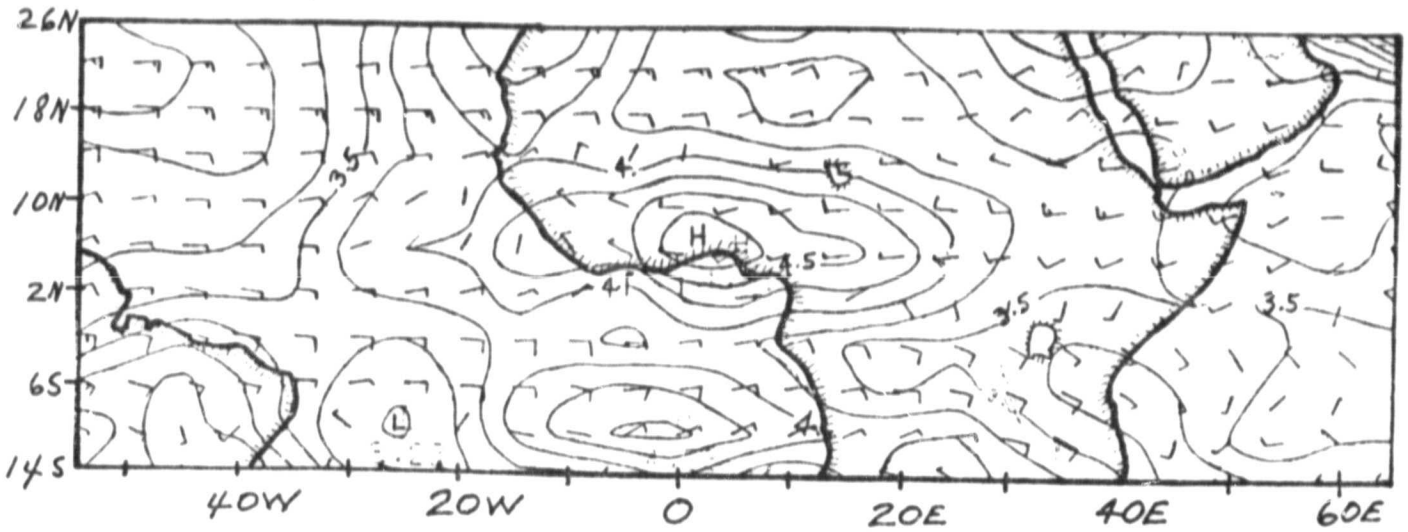

Fig. 5. Root mean square values of the perturbation in the meridional wind component and the mean wind at 750 mb for July 1974. The RMS values are in ms^{-1}; full barb for the wind vector corresponds to 5 ms^{-1}.

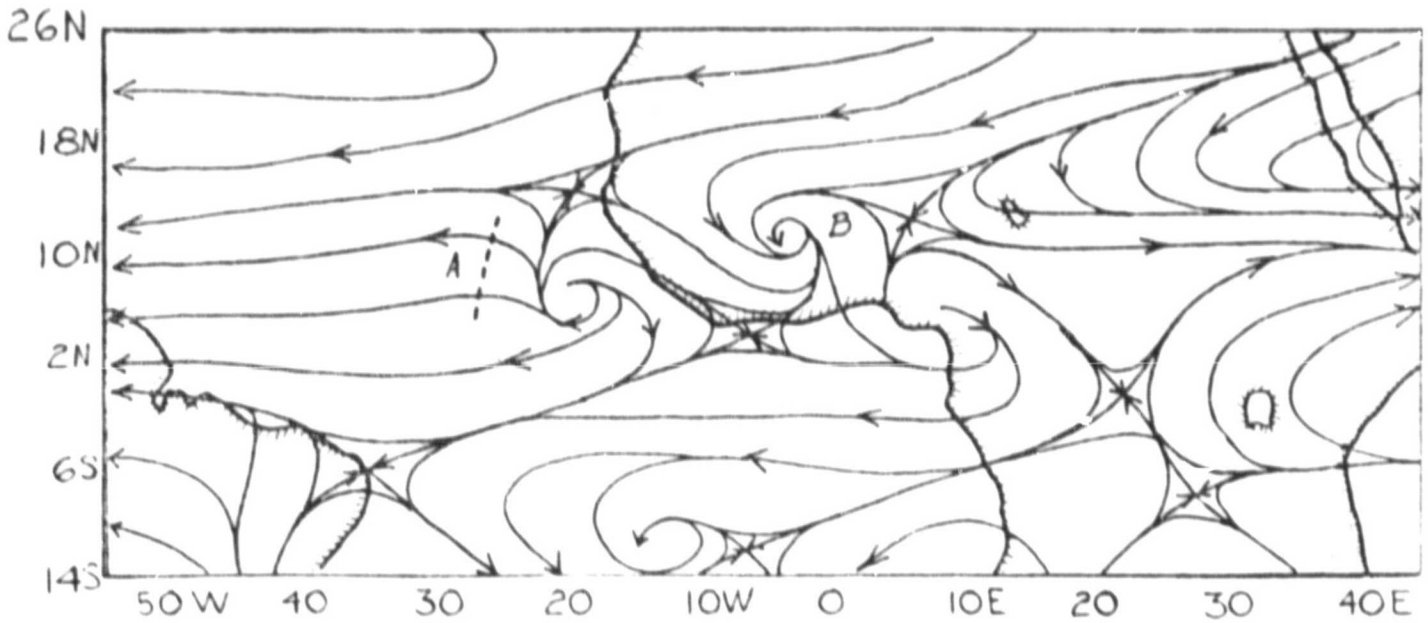

Fig. 6. Streamline map at 700 mb for 12Z July 1, 1974

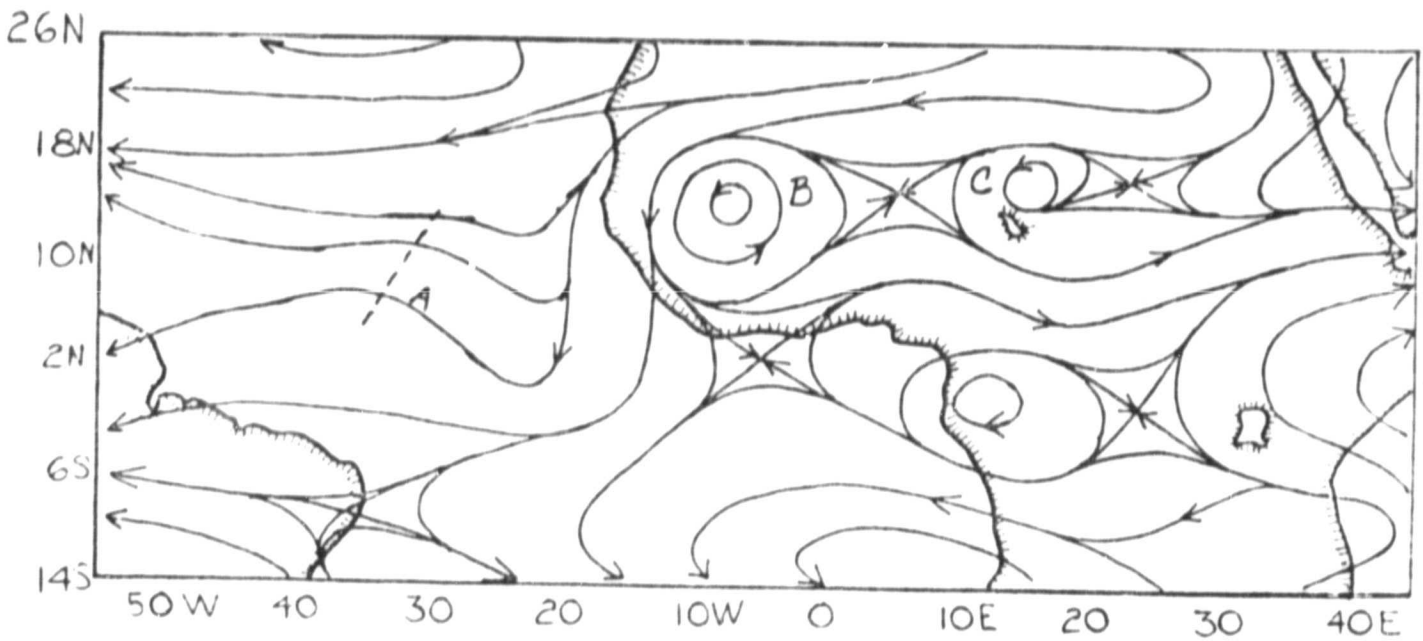

Fig. 7. Streamline map at 700 mb for 12Z July 2, 1974.

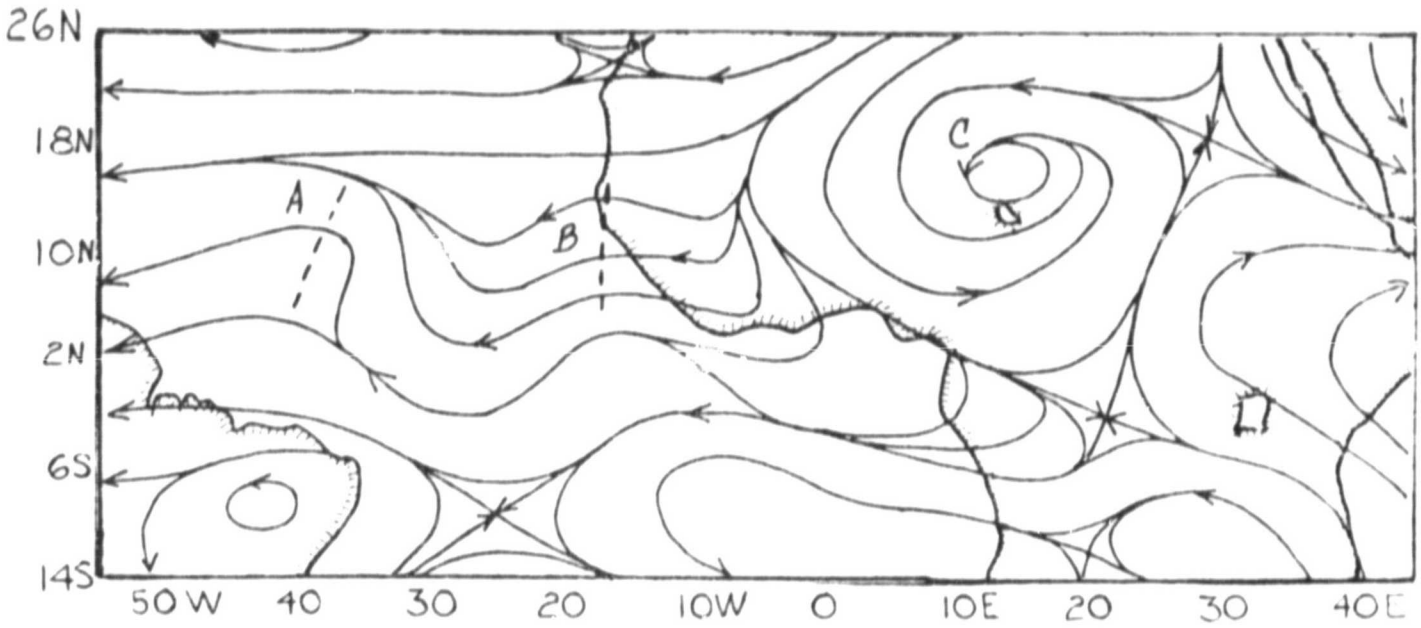

Fig. 8. Streamline map at 700 mb for 12Z July 3, 1974.

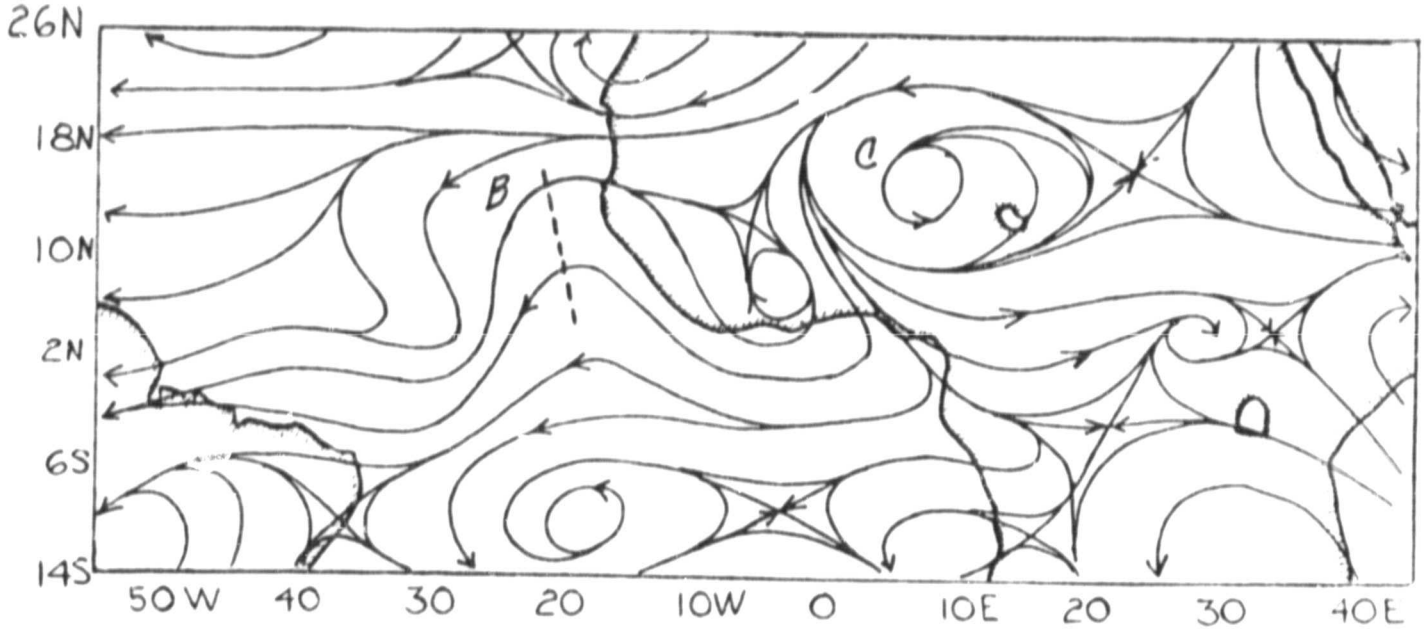

Fig. 9. Streamline map at 700 mb for 12Z July 4, 1974.

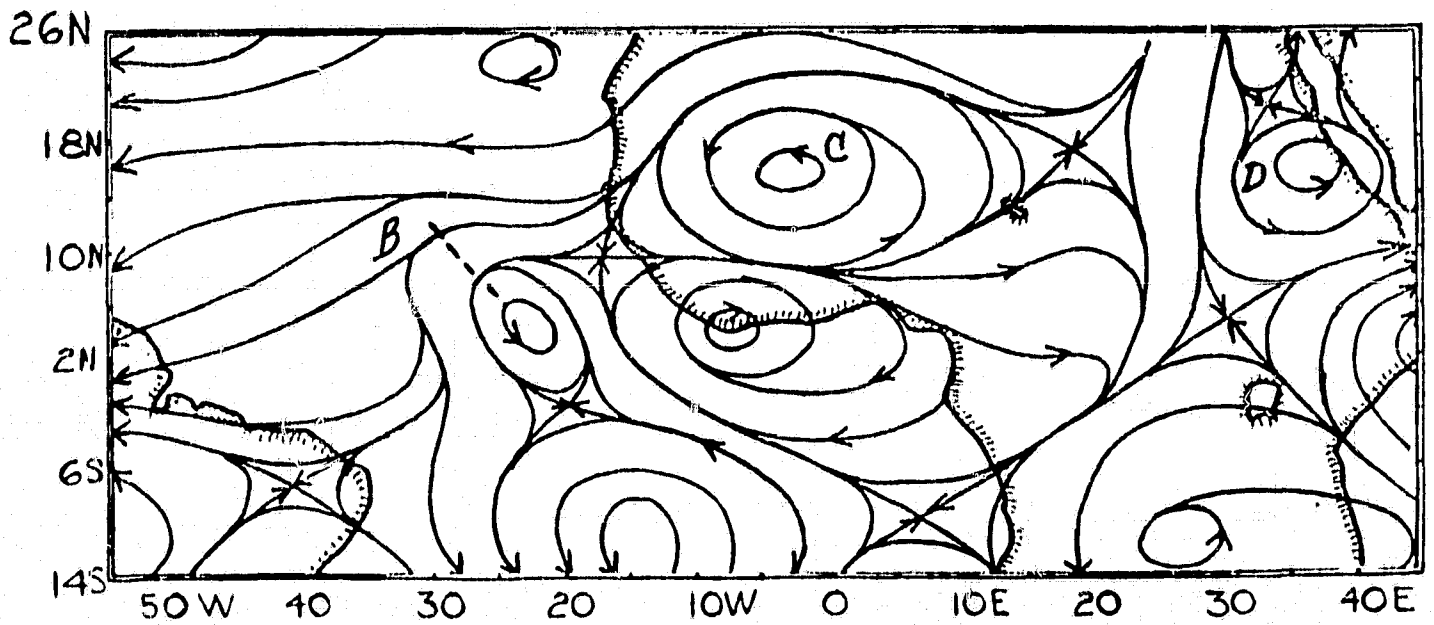

Fig. 10. Streamline map at 700 mb for 12Z July 5, 1974.

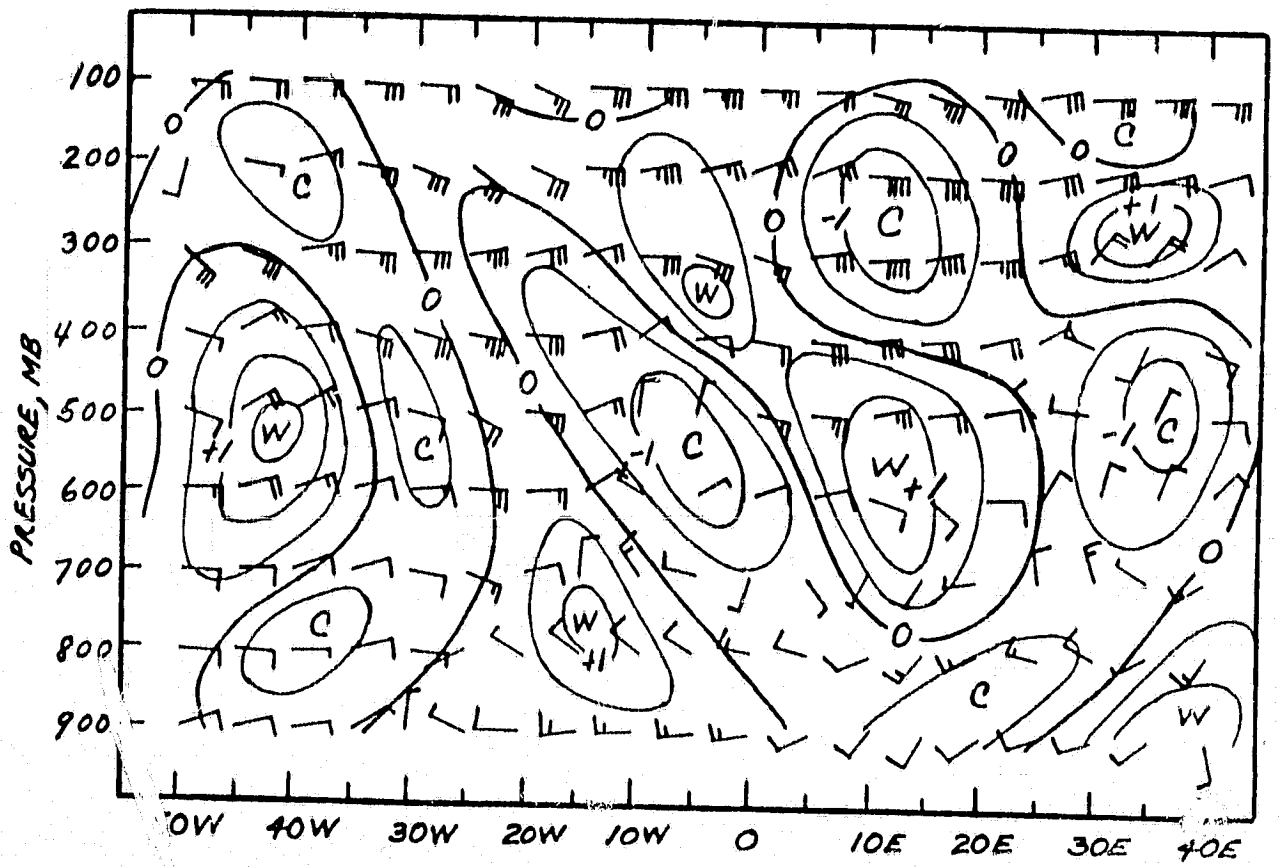

Fig. 11. Vertical cross-section along 14°N latitude for 12Z July 5, 1974. Isopleths represent isotherms of temperature deviations in °C; contour interval is 0.5°C. Wind barbs are total horizontal wind components; full barb is equal to X ms^{-1}.

PART III

FURTHER STUDIES OF AFRICAN DISTURBANCES IN THE GLAS GENERAL CIRCULATION MODEL

FURTHER STUDIES OF AFRICAN DISTURBANCES IN THE GLAS GENERAL CIRCULATION MODEL

1. Introduction

In Part II of this Final Report, we showed strong evidences of the existence of African wave-type disturbances in a simulation of the GLAS general circulation model. The simulation which was analyzed corresponds to the summer of 1974, more or less coinciding with the GATE observational field program. The preliminary analysis of the simulation indicated that the behavior and the structure of the disturbances are quite similar to those observed in the actual atmosphere. This part of the report describes the results of further analysis of the 1974 simulation as well as a similar simulation for the summer of 1979. It will be noted that the latter year corresponds to the FGGE observational period. Tha analysis which was done for both the 1974 and 1979 simulations involved not only the study of statistical properties of the disturbances for the month of July but also the synoptic investigation of selected disturbances. The analysis included the drawing of streamline maps and isotherms at 700 mb at 12 hourly intervals for the entire month of July for both years. The isolines of other parameters and the streamlines at other levels were also drawn for selected periods.

2. Statistical Properties of African Disturbances

In this section, we will describe some of the statistical properties of disturbances pertaining to their origin, intensity, propagation speed, and structure. An important aspect which relate to intensity and origin is the geographical distribution of the amplitude of the disturbances. In our study we have chosen the root mean square of the meridional perturbation wind component (v') of the disturbances, RMS (v'). It should be mentioned that the value of v' corresponds to the bandpassed simulation data, reflecting the contributions only of disturbances whose wavelengths are between 2000 km and 5000 km. Figs. 1 to 8 show the distribution of RMS (v') at various levels for July 1974 and July 1979. Looking at the RMS (v')

at 900 mb for July 1974 (Fig. 1), we see that the most significant feature of the RMS (v') relating to African disturbances is a pronounced maximum near the Sudan-Chad border. East of this maximum is a pronounced minimum over Northern Ethiopia. Between this minimum and the maximum is a region of strong gradient in the RMS (v'). Since the disturbances generally move westward, this must be a region where the disturbances intensify as they move towards West Africa. They attain their maximum intensity in the region of maximum RMS (v') over Eastern Chad. Thereafter, they decrease in intensity as they continue their westward movement. The corresponding distributions of RMS (v') at upper levels (800 mb,700 mb and 600 mb) for July 1974 are shown in Figs. 2, 3, and 4. Looking first at the RMS (v') for the 800 mb level, we see a region of maximum which is shifted slightly westward relative to the location of the 900 mb maximum. It is presumed that the 800 mb maximum is a mainfestation of the same disturbances which correspond to the 900 mb maximum. The RMS (v') distributions at the next two levels (700 mb and 600 mb) show similar maxima within the same general latitudes but displaced much farther toward the west. The greatest westward shift with height occurs between the 800mb and the 700mb levels. At both 700 mb and 600 mb levels the RMS (v') maxima are located over West Africa. It is interesting to note that Albignat and Reed (1980) found a maximum in the same general location and with about the same magnitudes. Their findings are based on an analysis of GATE observations. The RMS (v') maxima at the 700 mb and the 600 mb levels indicate that the simulated African disturbances at these levels tend to intensify east of the Greenwich meridian, primarily between 10^{o}E and 20^{o}E. They attain maximum intensity near the West African coast and then dissipate to the west over the Atlantic Ocean. This behavior of the simulated disturbances agrees with previous observational findings by Carlson (1969a).

The existence of RMS (v') maxima at all levels but at different locations is rather difficult to explain. Two possible explanations exist. First, the

RMS (v') maximum at 900 mb over East Sudan is due to disturbances which are not directly related to those which produce the RMS (v') maximum at 700mb over Western Africa. In essence, the 900 mb disturbances are surface heat lows which develop *in situ* and remain stationary while the 700 mb disturbances are a result of instability in the large-scale flow. Second, the RMS (v') maxima at all levels are manifestations of the same disturbances which move westward from the area of origin over Sudan across Africa towards the Atlantic Ocean. These disturbances develop initially as warm-cored disturbances over Sudan where they have large amplitudes at 900 mb but small ones at upper levels. As they move westward, the disturbances lose their warm-cored characteristics and gradually become cold-cored. The transformation from warm-cored to cold-cored characteristics occurs mainly in the general vicinity of Lake Chad. During the course of our study it was not possible to determine definitely which of these two explanations is the correct one. However, our experience based on looking at the daily maps of the simulation, appears to indicate that the second explanation may be the correct one.

The corresponding RMS (v') distributions for July 1979 are shown in Figs. 5 to 8. One can see that the distributions at 900 mb and 800 mb are somewhat similar to those for July 1974. For example, there are maximum values over Sudan but these are located slightly south of the corresponding July 1974 location. At about 600 mb the July 1979 distribution also has a maximum over Western Africa; it is located a little to the northwest of the July 1974 maximum. The most significant difference in the RMS (v') distributions between the two years occurs at the 700 mb level. Here, the July 1979 distribution shows a maximum over the Sudan-Ethiopian border while the corresponding 1974 location is near Nigeria in West Africa. It will be noted, however, that the region of large values of RMS (v') for July 1979 extends further westward into Central and West Africa. Another important difference

between the two distributions is the pronounced 1979 maximum over Northwestern Africa at 700 mb. In the 1974 distribution, the corresponding maximum is less pronounced, being located slightly west of the 1979 location, This maximum RMS (v') over Northwestern Africa may be related to extra tropical disturbances. Despite the above differences between the two distributions, there appears to be a common feature - - the existence of relatively large values of RMS (v') within a zonal belt bounded approximately by latitudes, 5^{o}N and 15^{o}N. The same is true with the diagrams presented by Albignat and Reed (1980). This common feature indicates the occurrence of disturbances during both years in the same latitudinal belt.

A somewhat different analyses concerning the occurrence of disturbances was done by examining the entire set of 12-hourly 700 mb maps for the purpose of determining the origin of individual disturbances. This was done by looking at the tracks of individual disturbances. Only those which could be tracked for at least two consecutive 12-hourly 700 mb maps were considered. The origin of the disturbances was specified as the starting point of their tracks. The points of origin of 23 individual disturbances (in this case, all closed cyclonic vortices) in July 1974 are shown in Fig. 9. The figure shows that the points of origin tend to cluster at three general locations. The clusters tend to lie within the latitudinal belt, 10^{o}N to 20^{o}N. One region is located just west of the Red Sea near the Sudan-Ethiopian border. A second region is located slightly northeast of Lake Chad. The third region is located over Western Africa in the vicinity of the Upper Volta. One may note that all three regions are in the vicinity of of mountains. Carlson (1969a) mentioned the possibility that the disturbances originate over mountainous terrain. It is interesting to find out whether these regions of origin are related with the distributions of the RMS (v') at 700 mb for July 1974 in Fig. 3. We had expected that there would be some relationship

between the areas of origin and the location of the maxima in the RMS (v'). Specifically, the areas of origin should tend to be located east of the RMS (v') maxima. This was surprisingly not the case. The implication is that the intensification of disturbances as inferred from the RMS (v') map is not necessarily close to the regions of origin. It may be noted that the points of origin are located generally along the east-west trough in the 700 mb mean streamlines whose axis extends from the middle of the Red Sea westward through Lake Chad.

The points of origin of 15 disturbances (7 cyclonic vortices and 8 open waves) in July 1979 are shown in Fig. 10. The points do not show as much clustering as those for July 1974. However, the points also tend to lie along a latitudinal belt between 10^{o}N and 20^{o}N, although somewhat south of the corresponding location for July 1979. Note also the tendency of the closed cyclonic vortices to originate over Eastern Africa near the trough of the mean 700 mb streamline field. The open waves, on the other hand, form over Western Africa in the region of the 700 mb easterlies.

We next present statistical characteristics of disturbances which relate to frequency of occurrence at 700 mb. The July 1974 maps, which consists of 57 12-hourly maps from July 1 to July 19, indicated that tropical disturbances are identifiable on the maps for a total of 108 times over Africa and 83 times over the Atlantic. The corresponding number of times for the July 1979 series of maps (60 12-hourly maps from July 1 to July 30) are 100 and 72, respectively. In other words, one can see about 3 tropical disturbances on each map on the average. The frequency of occurrence for the two categories,open wave or cyclonic vortex, is quite interesting. Examination of the 700 mb maps showed an overwhelming predominance of cyclnic vortices over open waves (97% vs. 3%) over Africa in 1974. On the other hand, there were more open waves than cyclonic vortices over Africa in 1979 (69% vs. 31%). Open waves were more predominant over vortices over the

Atlantic Ocean in both July 1974 (82% vs. 18%) and July 1979 (100% vs. 0%). This finding implies that cyclonic votrices over Africa tend to dissipate and become waves after reaching the Atlantic Ocean in agreement with the study of Carlson (1969a).

The statistical relationship between the thermal structure and the wind field of the disturbances at 700 mb has also been examined. For this purpose, we introduced four structural categories. The four categories are: (1) Cold-cored (minimum temperature coincide more or less with the wave trough or the center of the cyclone);(2) Warm-cored(maximum temperatures coincide more or less with the wave ridge or atmospheric center);(3) WTC (warm temperatures are west of the trough while cold temperatures are east of the trough); (4) CTW (cold temperatures are west of the trough while warm temperatures are east of the trough). If all disturbances of both years are considered, the breakdown in categories are as follows:

Category 1 (cold-cored) - 28%

Category 2 (warm-cored) - 17%

Category 3 (WTC - 43%

Category 4 (CTW) - 12%

It may be seen that 71% of the total number of cases are accounted for by category 1 and category 3. In other words, in 71% of the cases, the cold temperature is either in the trough or behind (east of the trough).The temperature structure corresponding to these two categories appear to agree with the composite structure based on observations presented by Burpee (1974) and Reed et al. (1977). With respect to differences in thermal structures between disturbances over Continental Africa and the Atlantic Ocean, we found that there were no significant differences;the breakdown of percentages over these two regions were quite similar. It appears, therefore, that there are no significant changes in thermal structrue as the disturbances cross the Western African coast. With respect to the breakdown of percentages for the

separate years of 1974 and 1979, we found that category 3 is more predominant in 1979 than in 1974 (53% vs. 35%).

In regard to the statistical aspect of the propagation speed of the disturbances, we made two separate investigations. The first investigation was concerned with the movements of a set of seven very well-defined disturbances while the second was concerned with the movements of all identifiable disturbances which occurred in both years. The set of well-defined disturbances consists of two cyclonic vortices in 1974 and five open waves in 1979. The speeds of the disturbances were computed during a 4-day period centered at the time of crossing of the West African coastline. The open waves were found to move at a mean speed (westward) of about 9^{o} longitude per day. On the other hand, the cyclonic vortices had a mean speed of approximately 7^{o} of longitude per day.

In doing the statistical analysis of all the disturbances for July 1974 and July 1979, we considered the speeds of open waves and vortices separately. We also differentiated between disturbances over the African Continent and the Atlantic Ocean. The results are shown in the table below:

	AFRICA		ATLANTIC	
	vortices	waves	vortices	waves
mean speed, degrees/day	4.0	5.6	6.5	6.4
number of disturbances	82	46	8	89

The number of disturbances refer to the number of cases used in computing the mean speed. It may be seen that, on the whole, the disturbances move faster over the Atlantic Ocean than over the African Continent. Note also that, over Africa, open waves move faster than vortices. Over the Atlantic, however, the speeds of movement are not significantly different. In the course of evaluating the mean speeds above, we noted that the individual speeds of motion which were computed from two successive 12-hourly intervals were rather irregular. There were some cases when the disturbances appeared to be stationary; a few cases were found to be moving

eastward. The irregularity of movement is probably due to the fact that the raw simulation data is inherently noisy and that the noise has not been entirely eliminated by the filtering. Lastly, we noted that the mean propagation speed for the set of seven well defined disturbances are larger than those indicated in the above table for all disturbances. We do not have an entirely satisfactory explanation for this discrepancy.

So far we have not mentioned anything about the 700 mb mean flow in Figs. 1 to 8 and the relationships between them and the statistical properties of the disturbances described above. For comparison with observations, the climatological 700 mb mean streamline map due to Van De Borgaard (1977) is shown in Fig. 11. In addition, the observed mean 700 mb wind field for the period August 23 to September 19, 1974, due to Albignat and Reed (1980) is shown in Fig. 12. It may be seen that the flow fields over Tropical Northern Africa are very similar, showing the customary easterlies. Turning back to the simulated 700 mb mean streamlines in Figs. 3 and 7, we see that the simulated 700 mb flow for July 1979 is similar to the observed ones in Figs 11 and 12. However, the simulated 700 mb flow pattern for July 1974 is very different from the corresponding observed as well as the simulated July 1979 flow patterns. The well-defined easterlies over the Tropical Africa region is absent in the July 1974 simulated flow pattern. Instead, this region is characterized by a more or less east-west trough in the northern sector and westerlies in most of the southern sections. This configuration of the 700 mb flow pattern is presumably the reason for the generation of cyclonic vortices instead of open waves in the simulation. The vortices developed in the vicinity of the mean 700 mb trough. It is surprising to note that, in spite of the great dissimilarity between the observed flow field in Fig. 12 and the 1974 mean 700 mb flow field, the patterns of the RMS (v') corresponding to these flow patterns are quite similar. On the other hand, even though the mean 700 mb flow field for 1979 is similat to the one in Fig. 12, the corresponding RMS (v') distributions

are not as similar to one another. An interesting, although not an unexpected finding from the above results, is that differences in the 700 mb mean flow are associated with corresponding differences in types (vortex vs open wave) of synoptic disturbances. A possible application of this finding is the possible long-range (range of a few months) prediction of the type and the frequency of African disturbances on the basis of a 4-month integration of a general circulation model with initial conditions specified during the month of May preceding the summer season.

3. Synoptic Properties of Simulated Disturbances

In this section we discuss the distributions of various meteorological variables associated with disturbances during selected periods. In order to illustrate the space and time variations of the motion field, we present three successive 12-hourly streamline maps for the period, 12 Z July 18, 1979 to 12 Z July 19, 1979 (Figs. 13 to 18). Focusing our attention on the 700 mb maps first, we see two troughs. One trough is located just west of the West African coast (labeled A) while the other trough is in the vicinity of Lake Chad (labeled B). Both troughs move westward at a speed of approximately 8 degrees of longitude per day. At lower levels, it may be seen that trough A is reflected as an open trough in the streamline field. On the other hand, trough B is reflected as a closed vortex at both lower levels. The difference in the low-level synoptic flow patterns are presumably due mainly to the fact that the low-level large scale basic flows are correspondingly different. We also note that the low-level vortices corresponding to trough B at 700mb are displaced to the north of the vorticity center associated with trough B. The existence of vortices at levels below 700mb and their positions north of the 700 mb vorticity maximum are confirmed by the analysis of observational data. See, for example, Fig. 3 of the article by Reed et al. (1977) based on GATE observations. Next, we look at the simulated velocity

distributions above the 700 mb level. It may be seen that, directly aboye the 700 mb region of maximum vorticity, at upper levels (300 mb and 100mb) there is anticyclonic circulation towards the north. Toward the south, however, there is cyclonic circulation. In other words, the center of maximum vorticity tends to tilt southward with height above 700 mb. The same general behavior is also seen in Fig. 3 of Reed et al. (1977) and in Part IV.

The wind distributions discussed above correspond to disturbances which are characterized by open waves at 700 mb. The corresponding distributions for which the 700 mb disturbances is a closed vortex are presented in Figs. 19 and 20. These maps correspond to 12 Z of July 4, 1974. Looking at the 700 mb streamline map, we see that there is a cyclonic vortex located just to the northwest of Lake Chad. Just as in the case of the upper wave described in the preceding paragraph, there is a closed vortex at 900 mb to the north of the 700 mb center of maximum vorticity. Also at upper levels (300 mb and 100 mb), we see a cyclonic circulation towards the south. It may be concluded, therefore, that for both 1979 and 1974 cases, there is an overall tendency for centers of maximum vorticity to tilt towards the south with height. This tendency is in general agreement with deductions from the thermal wind equation over this section of Africa.

The temperature distributions at the 700 mb level for two different cases (12Z July 18, 1979 and 12 Z July 4, 1974) are shown in Figs. 21 and 22. In these maps, the temperatures correspond to deviations of the actual temperature from the local time average for a monthly period. It may be seen that, in the 1979 map, the minimum temperatures are located generally behind (east)of the trough lines. In the 1974 map, however, the minimum temperatures are located in the trough lines and near the center of cyclonic vortices. The observational results of Reed et al. 1977) for GATE shows that the mininum temperature at 850 mb is also located east of the trough line (see Fig. 7c of their paper). In Part IV of this report, the

observations at 700 mb during FGGE indicate similar results. Somewhat different observational results were obtained by Carlson (1969b). His analysis of radiosonde soundings indicates that the troughs are cold-cored at 700 mb. On the basis of these observations, one can conclude that there is observational verification of both types (minimum temperature in and east of trough lines) of the simulated temperature structures at 700 mb shown in Figs. 21 and 22.

In order to describe the simulated distributions of specific humidity at the 700 mb level, we show three consecutive 12-hourly maps in Figs. 23 to 25. The isolines of specific humidity on these maps represent deviations from the local monthly means. Looking at the wave just west of the West African coast, we see a maximum in the specific humidity behind the trough. It may be noted that this location is the same as that of the minimum temperatures for many of the simulations at 700 mb. The existence of both maximum humidity and minimum temperatures behind the trough may be an indication of rising motions also in the same location. Rising motions tend to produce adiabatic cooling and also increase in humidity due to vertical advection of more moist air from lower layers. Turning our attention next to the trough in the vicinity of Lake Chad, we see that the maximum in specific humidity is also generally located behind the trough line. However, there is also a humidity maximum ahead of the trough; this maximum is centered near the Greenwich meridian and 2^{o}N. This maximum persists throughout the 24-hour period. On the last map of the period (Fig. 25), we see that this maximum has joined the other maximum behind the trough at its northern portion. The end result is an elongated distribution of maximum moisture which extends from a region ahead of the trough at southern latitudes through the trough line at intermediate latitudes and finally behind the trough at northern

latitudes. The observational results at 850 mb by Reed et al. (1977) in Fig. 7 of their paper shows also maximum moisture behind the trough, particularly at the northern portion of the trough. It is interesting to note also in the same figure that, the minimum in the temperature field coincides with the maximum in the humidity field. The existence of a maximum humidity behind the trough in the observations generally confirms the simulated humidity structure at 700 mb. The maximum humidity at the southern portion of the simulated trough over the continent in the vicinity of the African bulge lacks definite verification at this time. However, the humidity diagram of Reed et al. (1977) indicates a tendency for the moisture maximum to elongate from northeast to southwest; this is the same orientation in the two simulated troughs in Fig. 25.

A variable which is closely related to the specific humidity is the rainfall. In Figs. 26-28, we present the simulated rainfall patterns corresponding to the map times, 12 Z July 18, 00 Z July 19 and 12 Z July 19. The isophets in these diagrams are based on grid point values which were obtained by smoothing the original grid point values by means of a 3-point running average in space. By and large, the rainfall patterns which are associated with the 700 mb trough over continental Africa resemble the specific humidity distributions at 700 mb. These are characterized by a tendency to have maximum rainfall near the trough axis, somewhat west of the corresponding maximum in the specific humidity deviations. The rainfall pattern associated with the 700 mb trough over the ocean west of Africa is quite different. Here, we see that the rainfall maximum occurs ahead of the trough; this location is also different from the location of the specific humidity maximum. Whether this condition is the general rule over the oceans has not been ascertained. At present, we do not have an explanation why there is a difference in the relative location of rainfall between the oceanic and the

continental troughs. With regard to observational verification of the simulated rainfall, there appears to be some vagueness. Rainfall distributions deduced by Reed et al. (1977) from GATE observations show a maximum ahead of the 700 mb troughs. On the other hand Burpee (1974) study shows a tendency for the maximum rainfall to occur over the 700 mb trough; Carlson's (1969a) analysis of cloud observations appears to confirm this tendency. At any rate, it is probably correct to say that although the simulations are able to predict rainfall associated with troughs, the predicted locations of occurrence may not be very accurate. This is due to the fact that an important producer of rainfall for African disturbances are squall lines. The scale of such squall lines are not adequately resolved by the computational grid and the cumulus convection parameterization may not be sufficiently accurate.

An attempt has been made to determine the vertical motion field in the lower half of the troposphere with the aid of the kinematic method. For this purpose we integrated the divergence field in the layer, 900 to 600 mb. The result of this integration is shown in Fig. 29. The isopleths in this diagram are in units of $10^{-6}s^{-1}$ and the corresponding isopleths in terms of vertical velocity may be obtained by multiplying the divergence values by the thickness of the layer (approximately 3 km). In general, one can see that the upward motions occur behind the troughs. This condition is clearly seen for the trough off the west coast of Africa. On the other hand, the vertical motions associated with the trough over continental Africa is quite more complicated. Upward motions occur behind the northern sections of this trough and also ahead of the southern portions of the trough. Fig. 7 of the article by Reed et al. (1977) shows upward motions ahead of the trough and downward motions behind the trough, more or less the opposite condition for the simulated troughs. However, in Burpee's (1975) compositing of GATE observational data, there is some evidence in favor

of the simulated vertical velocity structure. His results show that the upper level cloud amount and the ascending motions at 925 mb are large behind the composited trough. Another evidence which favors the simulated vertical motion field is the occurrence of the main cloud mass behind the trough in the satellite picture shown in Part IV. The conflicting ideas concerning the vertical velocity structures is not surprising in view of the fact that the vertical velocity is a quantity which is very difficult to compute. It is hoped that better observations in the future would clarify the relationship between the 700 mb trough and the vertical motion field.

Finally, we present diagrams showing the surface pressure distributions associated with these African disturbances. In order to highlight the pressure variations, we show the fields of the deviations of surface pressure from the local monthly means. Figs. 30 - 32 show these deviations and the accompanying 700 mb streamline maps. We show three 24-hourly maps so that the evolution of the pressure field can be depicted during a longer period of time. It is apparent from the figures that the 700 mb troughs are generally associated with either closed lows or troughs in the pressure deviation fields. Note that there is a pressure trough directly underneath the 700 mb trough over continental Africa. Within the next 48 hours, this pressure trough develops into a closed low directly below the 700 mb trough. The pressure deviations which are associated with the 700 mb disturbances are generally a few millibars in magnitudes. Similar pressure fluctuations with about the same magnitudes were found from observations by Carlson (1969a). He also noted some tendency for the minimum pressure deviation to precede the accompanying 700 mb trough. This appears to be the case for the trough off the west coast of Africa on 12 Z July 18, 1979. Further confirmation of the simulated surface pressures is presented by Part IV on the basis of FGGE observations. A comparison between the characteristics of the simulated pressure distributions and those deduced from the FGGE observations shows a high degree of

similarity. One can conclude, therefore, that African disturbances are characterized by recognizable surface pressure deviation patterns which move westward together with the associated upper level perturbations. Hence it should be possible to diagnose the existence of such disturbances by a careful analysis of the surface pressure deviations.

4. Summary and Conclusions

In this Part III of the Final Technical Report, we have described the results of an intensive analysis of the behavior and the structure of the simulated African disturbances. We have shown that the characteristics of the simulated disturbances in the following aspects:

(1) the location of the regions of development and the places of origin;

(2) the three-dimensional structure of the wind field;

(3) the horizontal structure of the moisture and temperature perturbations at 700 mb;

(4) the distribution of the surface pressure perturbations;

(5) the speed in the westward propagation;

(6) the tendency for disturbances to dissipate after reaching the Atlantic Ocean.

The similarity in the other variables, such as vertical velocity and rainfall, has been difficult to verify. This is primarily due to the fact that these variables are inherently difficult to observe. In the case of precipitation, the model may have some difficulty in simulating rainfall because much of it occurs in the subgrid scale. However, there is no clear evidence that this difficulty is definitely apparent in the simulated rainfall distributions. Lastly, it is interesting to note the significant differences in the mean flow and the type of disturbances between the two years. In spite of the large differences

in the mean flows, however, the geographical latitudes of the points of origin of disturbances as well we the regions of development are only slightly different. This has been a surprising result.

REFERENCES

Albignat, J. P. and R. J. Reed, 1980: The origin of African wave disturbances during Phase III of GATE. Mon. Wea. Rev., 108, 1827-1839.

Burpee, R. W., 1974: Characteristics of North African easterly waves during the summer of 1968 and 1969. J. Atmos. Sci., 31, 1556-1570.

Carlson, T. N., 1969a: Some remarks on African disturbances and their progress over the tropical Atlantic. Mon. Wea. Rev., 97, 716-726.

Reed, R. J., 1969b: Synoptic histories of three African disturbances that developed into Atlantic hurricanes. Mon. Wea. Rev., 97, 256-276.

_____, 1975: Some features of synoptic-scale waves based on a compositing analysis of GATE data. Mon. Wea. Rev., 103, 921-925.

_____,D. C. Norquist and E. E. Recker, 1977: The structure and properties of African wave disturbances as observed during Phase III of GATE. Mon. Wea. Rev., 105, 317-333.

Van de Boogaard, H., 1977: The Mean Circulation of the Tropical and Stubtopical Atmosphere - July. NCAR/TN-118+STR NCAR TECHNICAL NOTE.

Fig. 1. Root mean square (RMS v') distribution of the meridional component (ms^{-1}) associated with synoptic disturbances and the mean streamlines at 900 mb for July 1974. Contour interval: 0.25.

Fig. 2. Same as Fig. 1 except at 800 mb.

Fig. 3. Same as Fig. 1 except at 700 mb.

Fig. 4. Same as Fig. 1 except at 600 mb.

Fig. 5. Root mean square (RMS v') distribution of the meridional component (ms^{-1}) associated with synoptic disturbances and the mean streamlines at 900 mb for July 1979. Contour interval: 0.25.

Fig. 6. Same as Fig. 5 except at 800 mb.

Fig. 7. Same as Fig. 5 except at 700 mb.

Fig. 8. Same as Fig. 5 except at 600 mb.

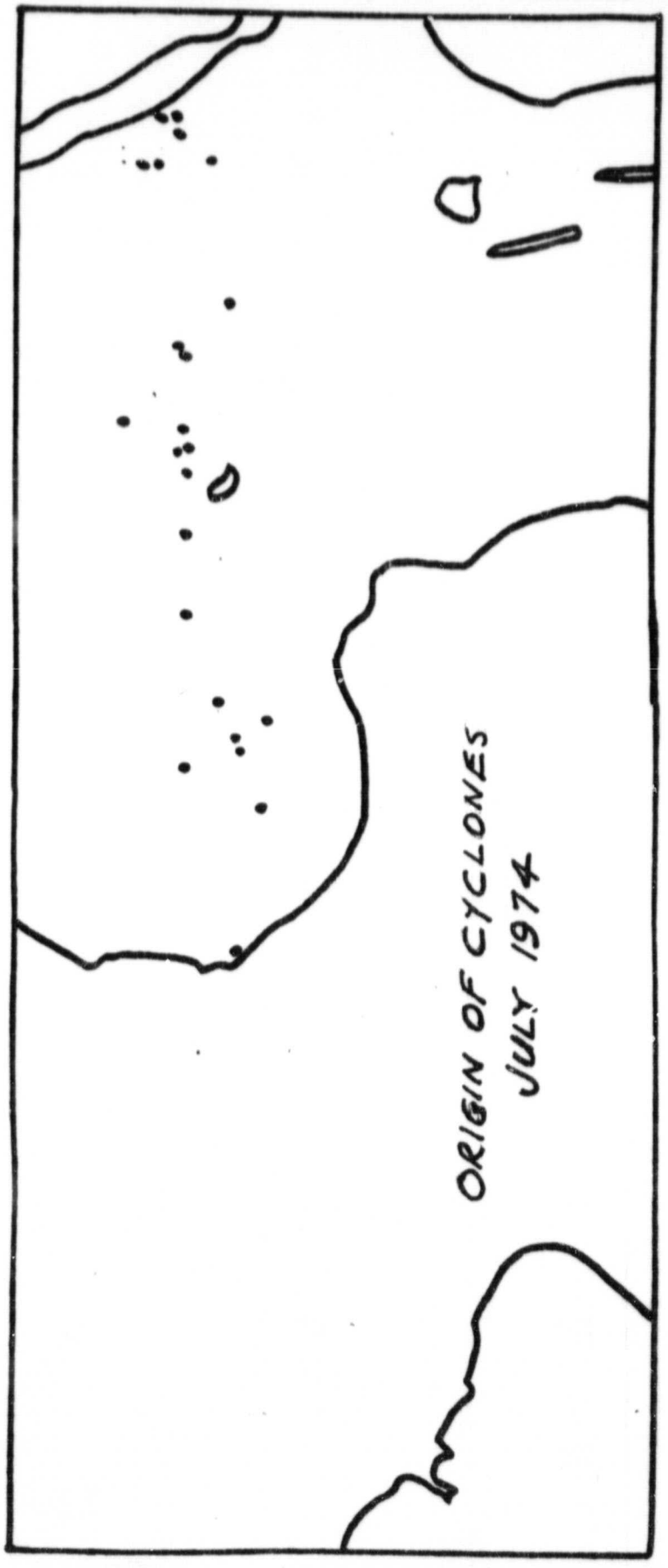

Fig. 9. Geographical locations of the origin of synoptic disturbances for July 1974.

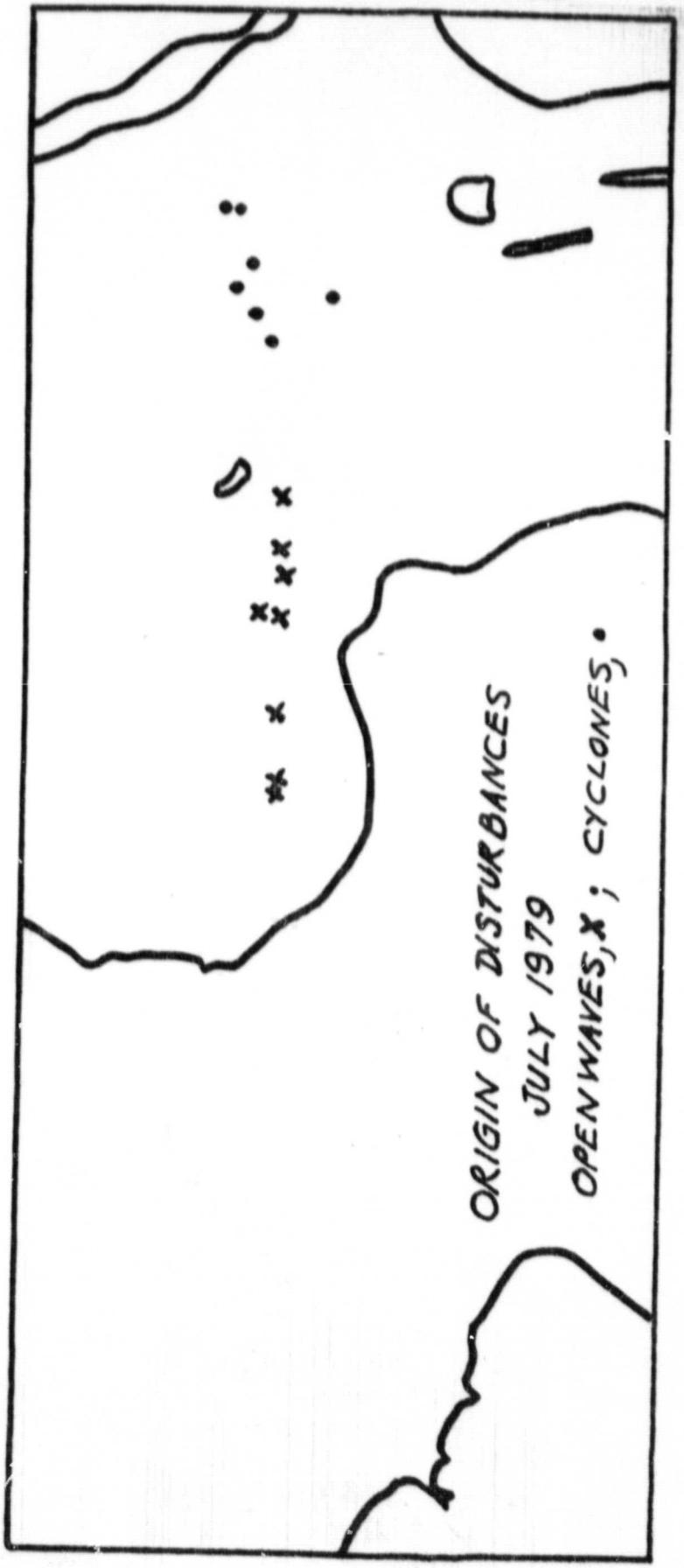

Fig. 10. Geographical locations of the origin of synoptic disturbances for July 1979.

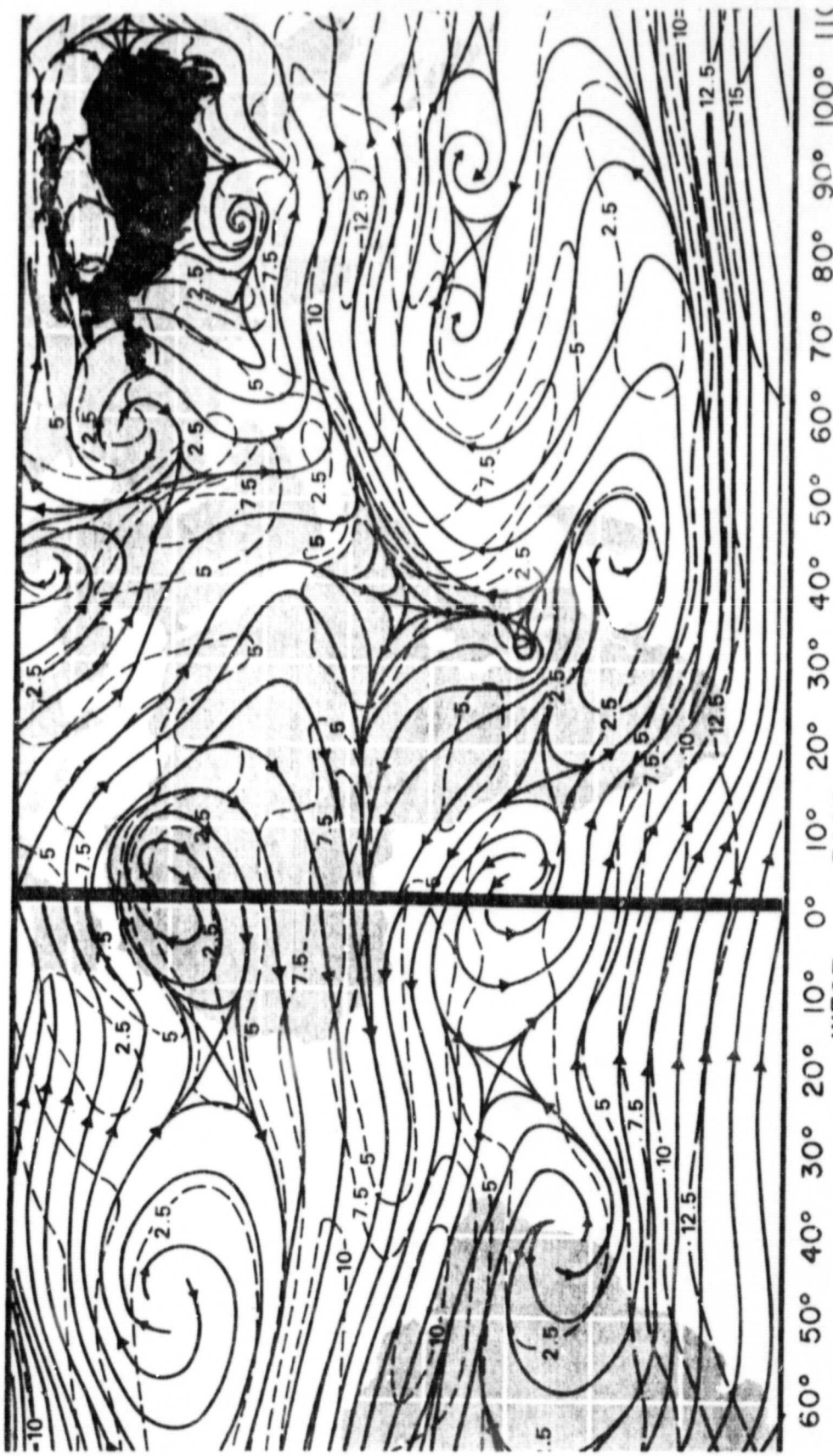

Fig. 11. Mean wind field for July at 700 mb after Van de Boogaard (1977).

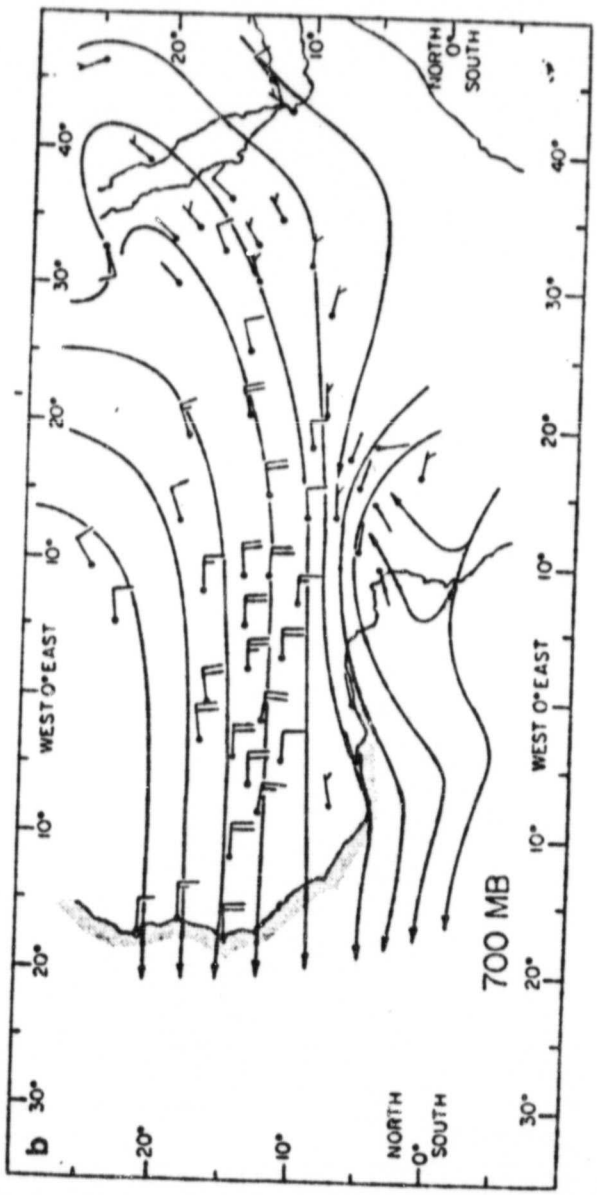

Fig. 12. Mean wind field for Phase III of GATE at 700 mb after Reed et al. (1977).

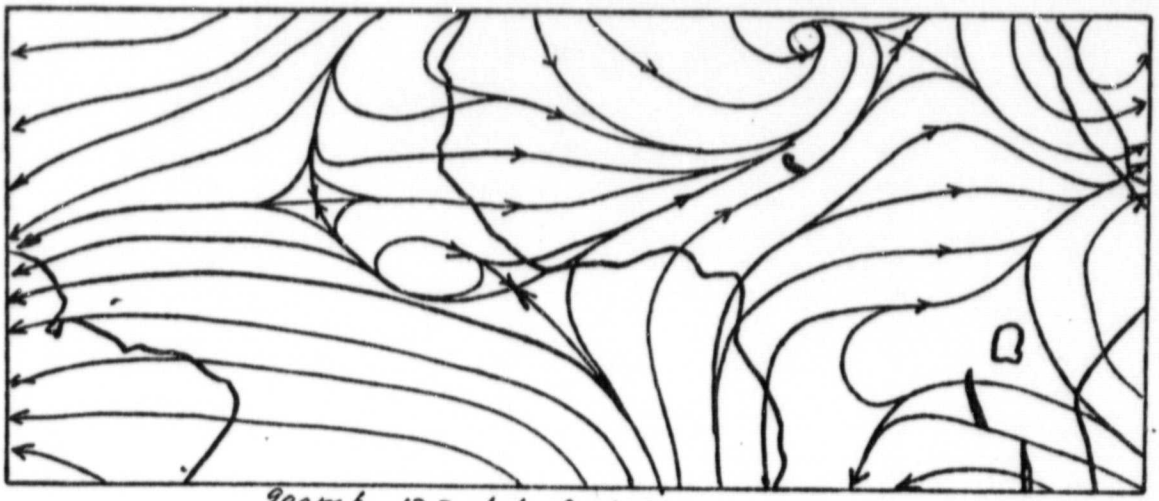

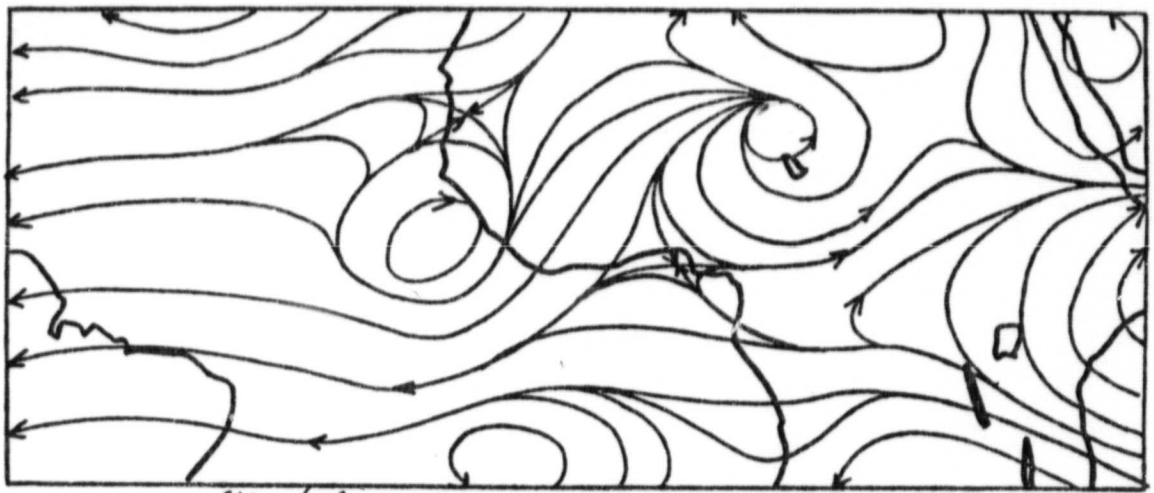

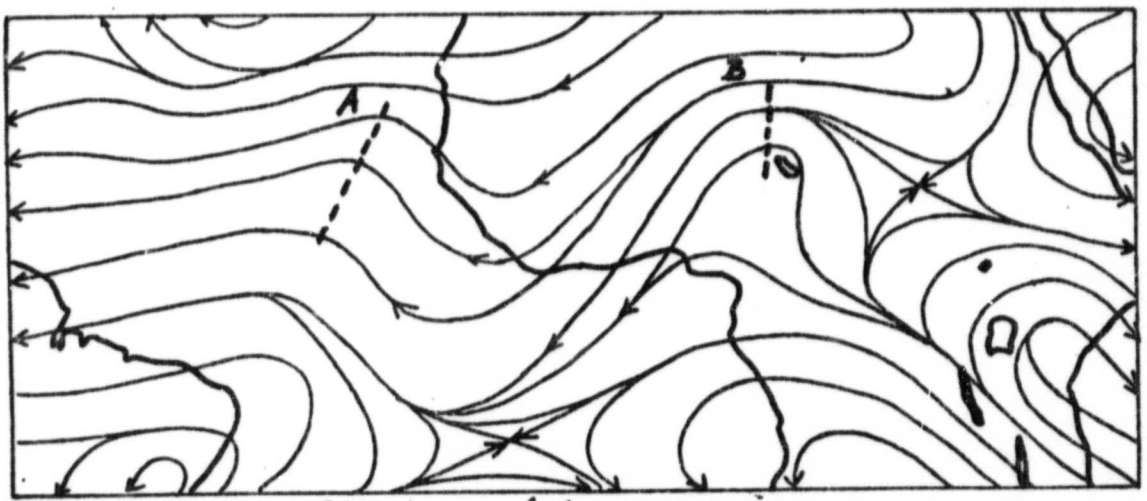

Fig. 13. Streamline maps for 12 Z July,18,1979:Top,900 mb; middle, 800 mb; Bottom, 700 mb.

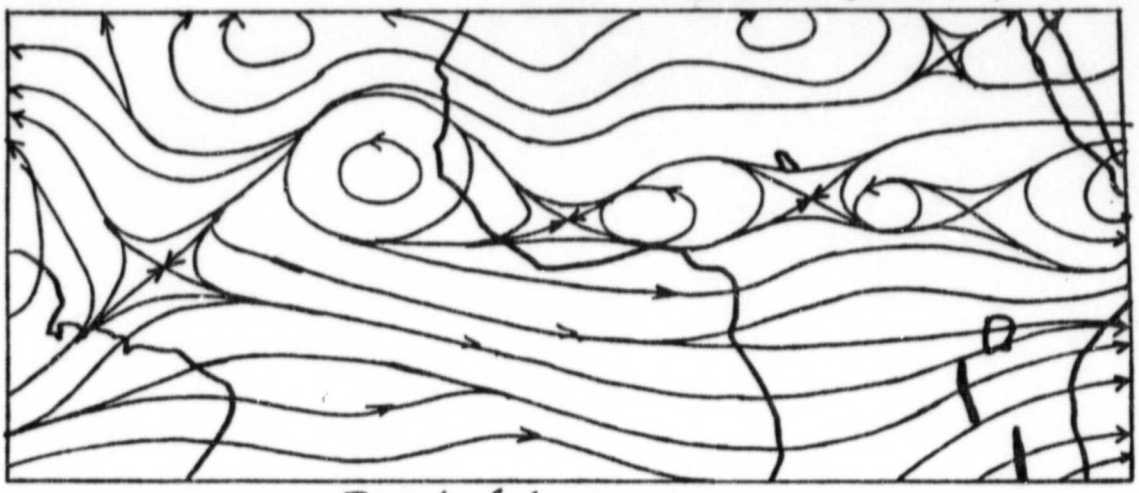

500mb, July 18, 1979

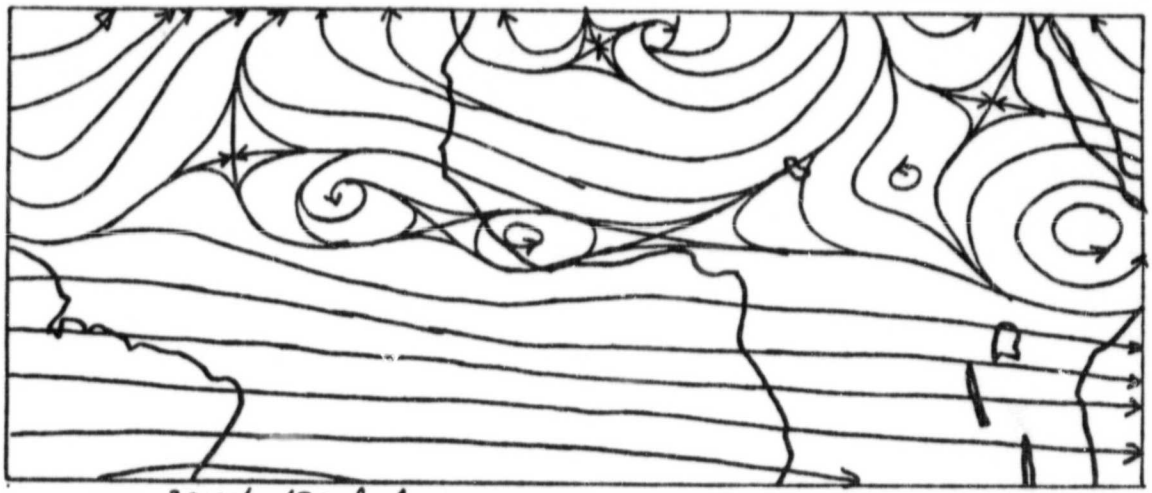

300mb, 12Z July 18, 1979

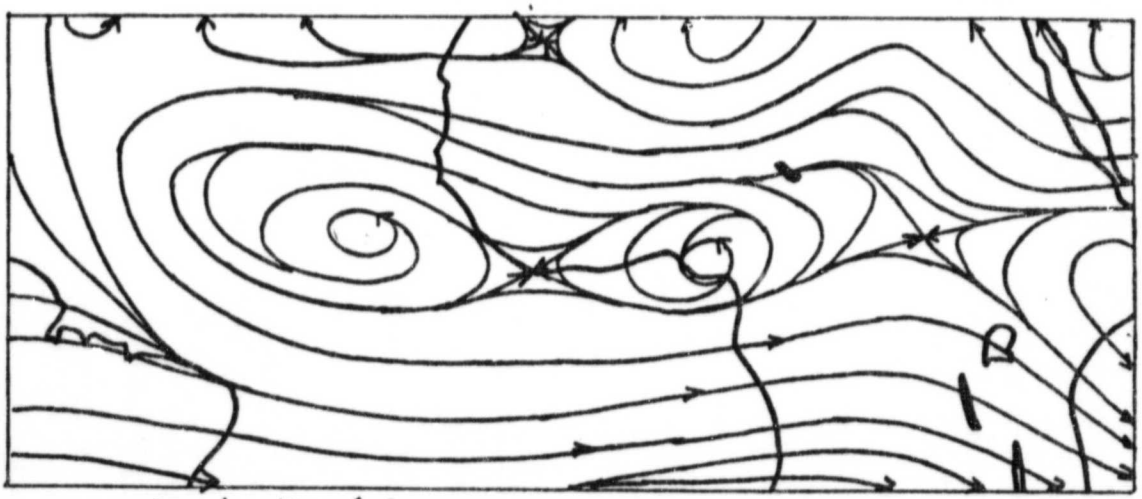

100mb, 12Z July 18, 1979

Fig. 14. Streamline maps for 12 Z July 18, 1979: Top, 500 mb; Middle, 300 mb; Bottom, 100 mb.

900mb, 00Z July 19, 1979

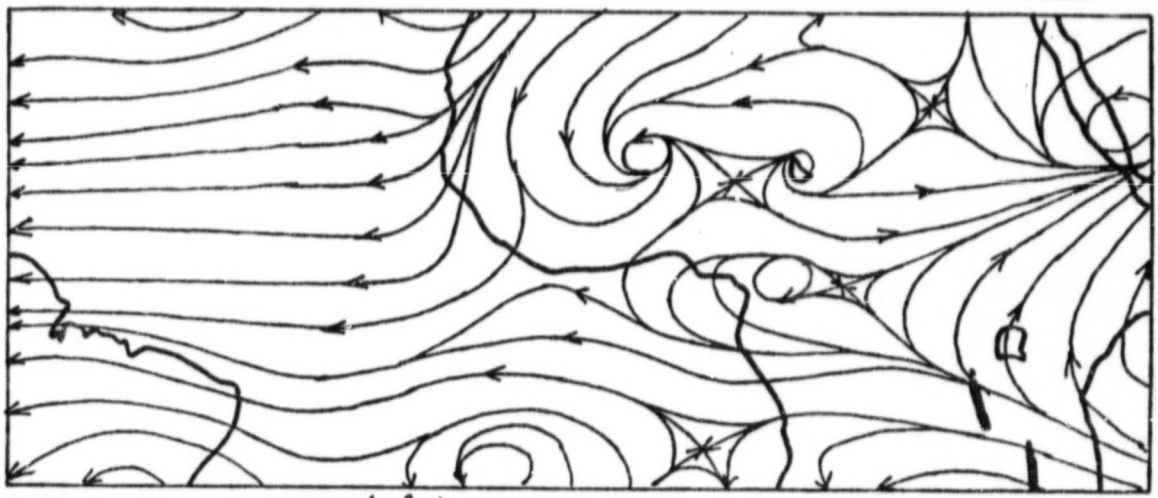

800 mb July 19, 1979, 00Z

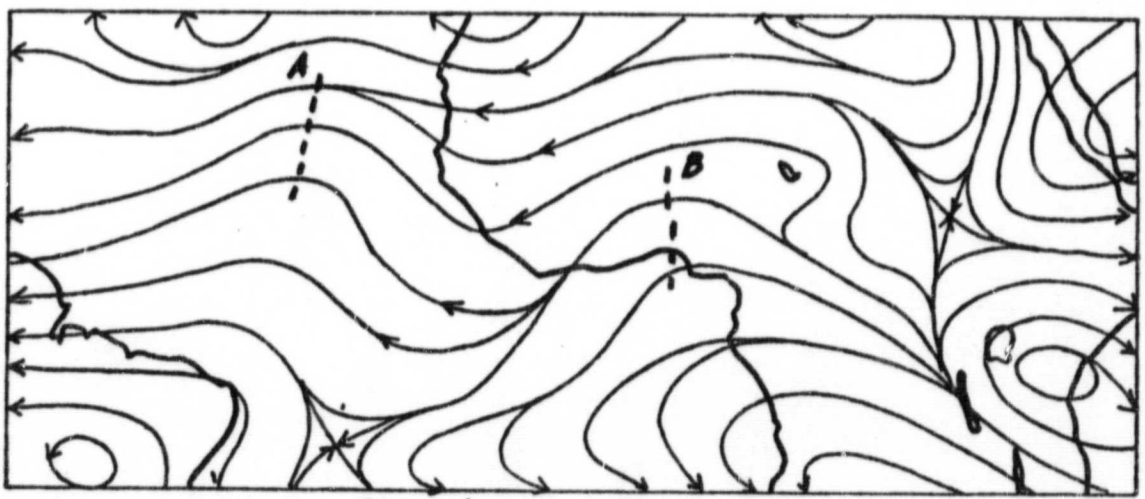

700mb, 00Z July 19, 1979

Fig. 15. Same as Fig. 13 except for 00 Z July 19, 1979.

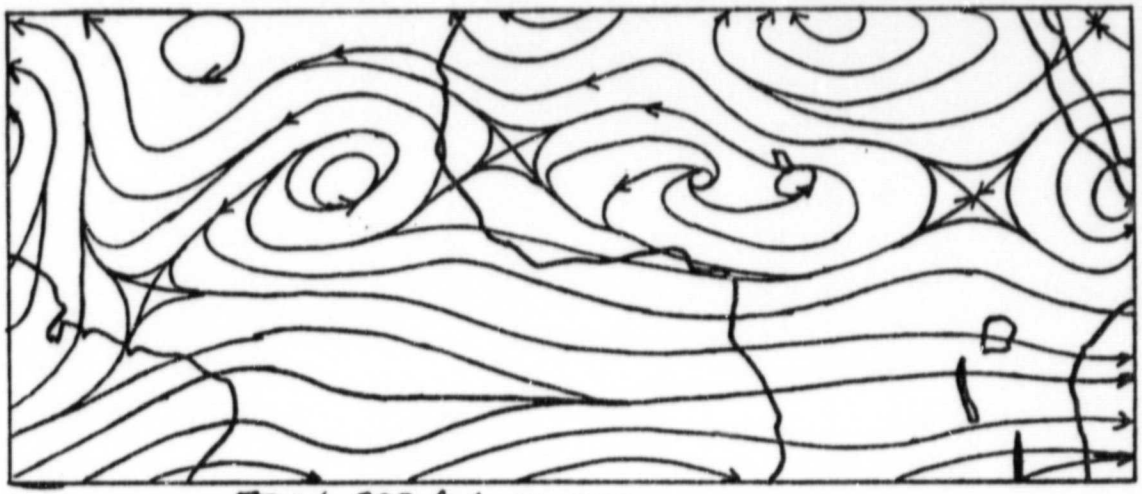

500mb, 00Z July 19, 1979

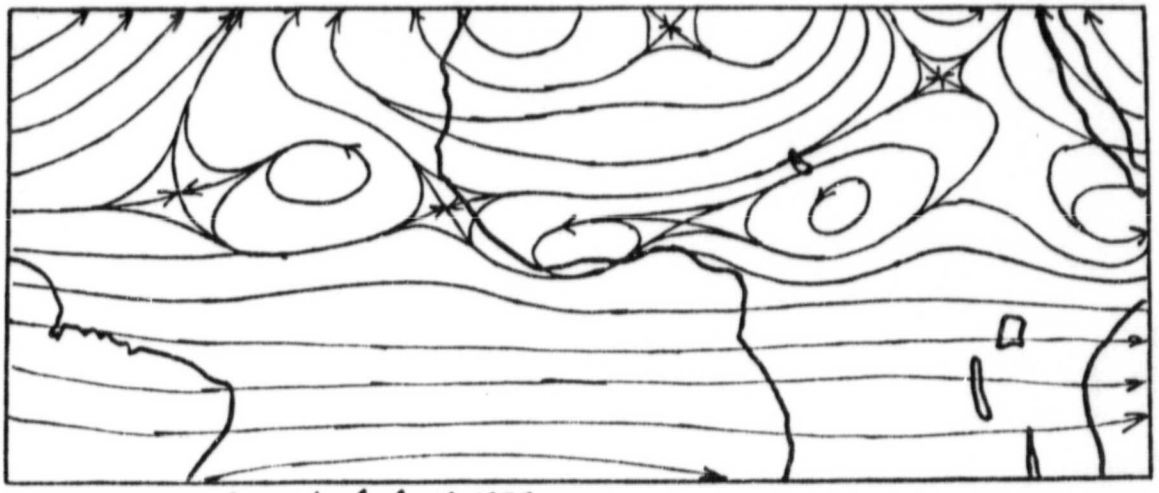

300mb, July 19, 1979, 00Z

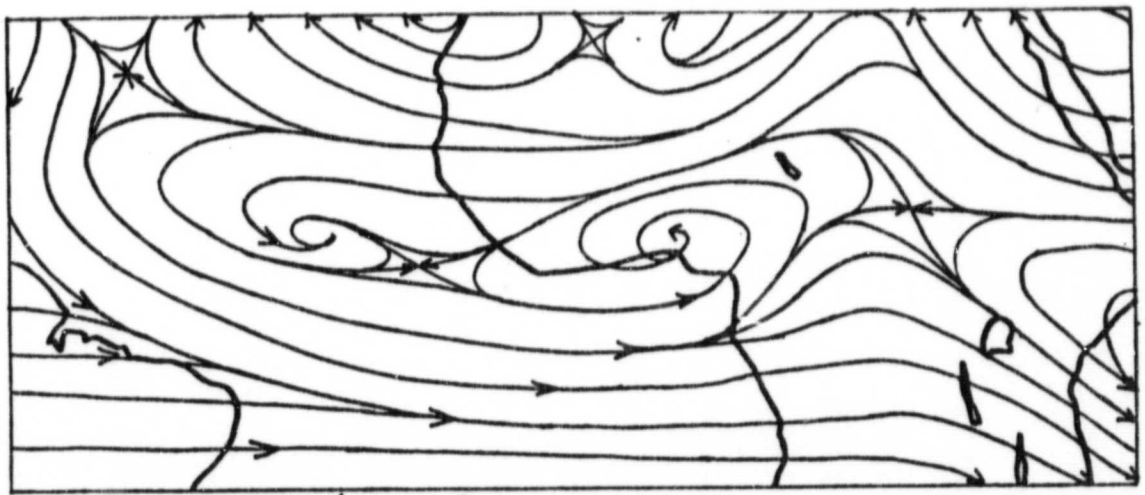

100mb, 00Z July 19, 1979

Fig. 16. Same as Fig. 14 except for 00 Z July 19, 1979

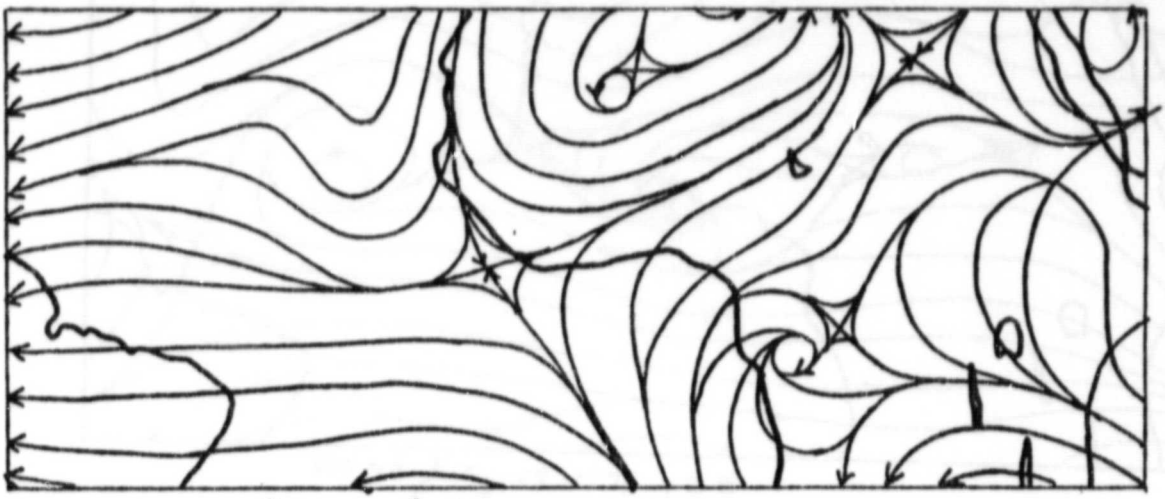

900 mb July 19, 1979, 12Z

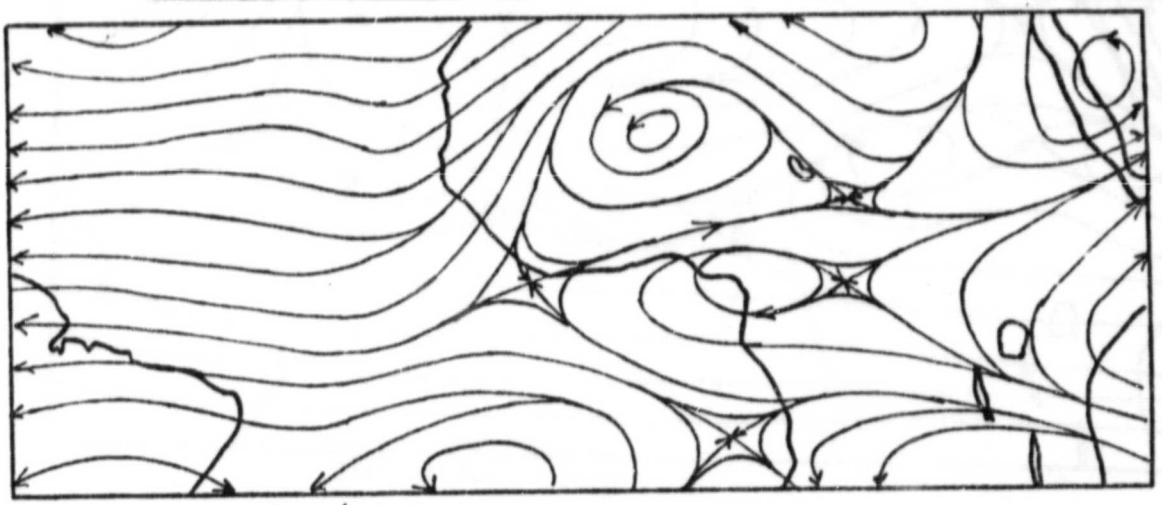

800 mb July 19, 1979, 12Z

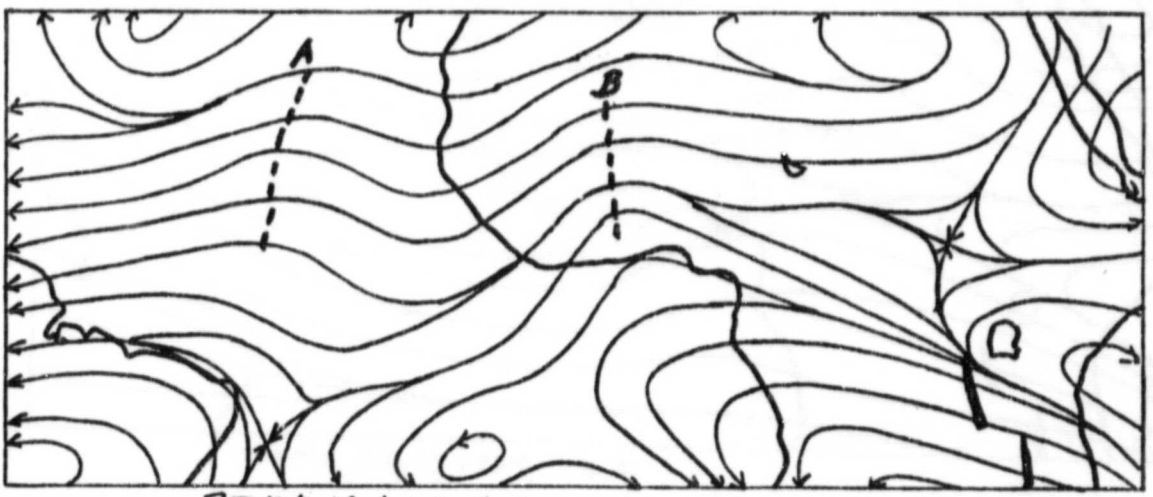

700 mb, July 19, 1979, 12Z

Fig. 17. Same as Fig. 13 except for 12 Z July 19, 1979.

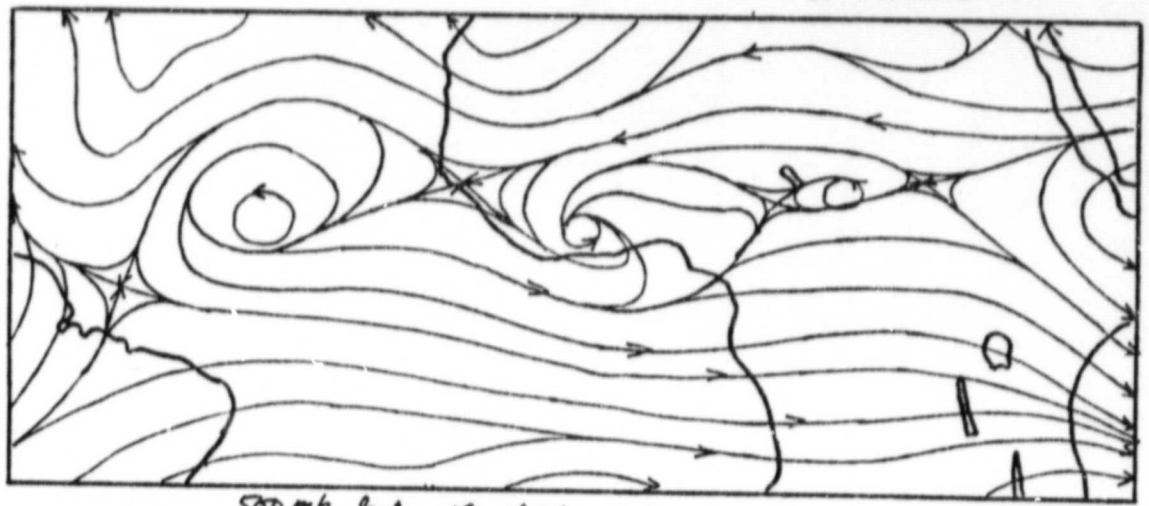

500 mb July 19, 1979, 12 Z

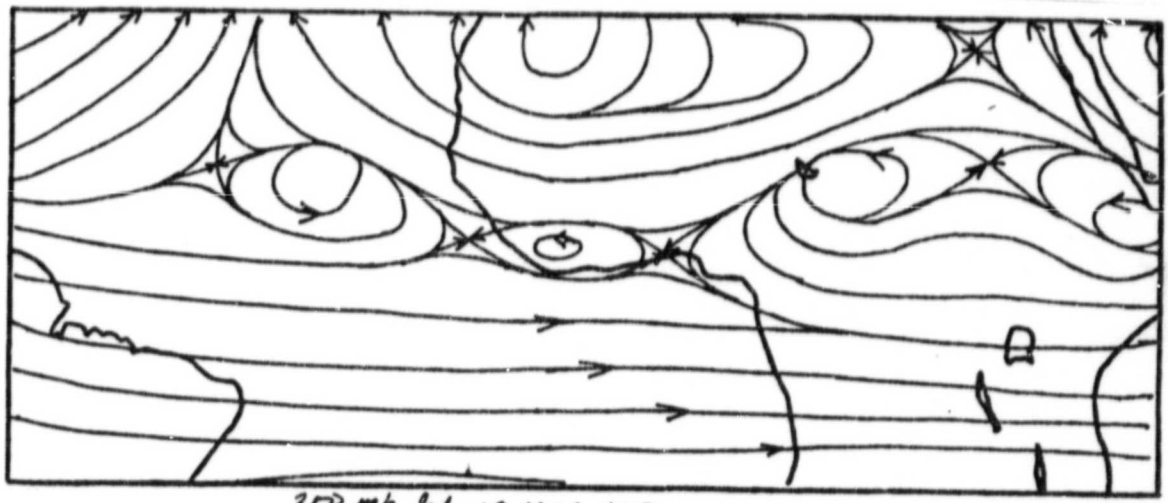

300 mb July 19, 1979, 12 Z

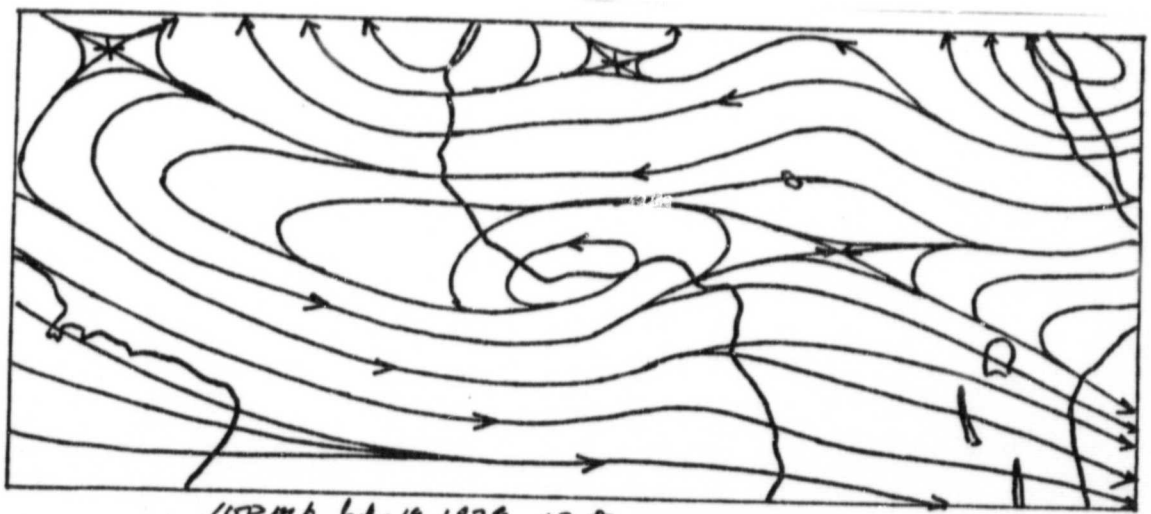

100 mb July 19, 1979, 12 Z

Fig. 18. Same as Fig. 14 except for 12 Z July 19, 1979.

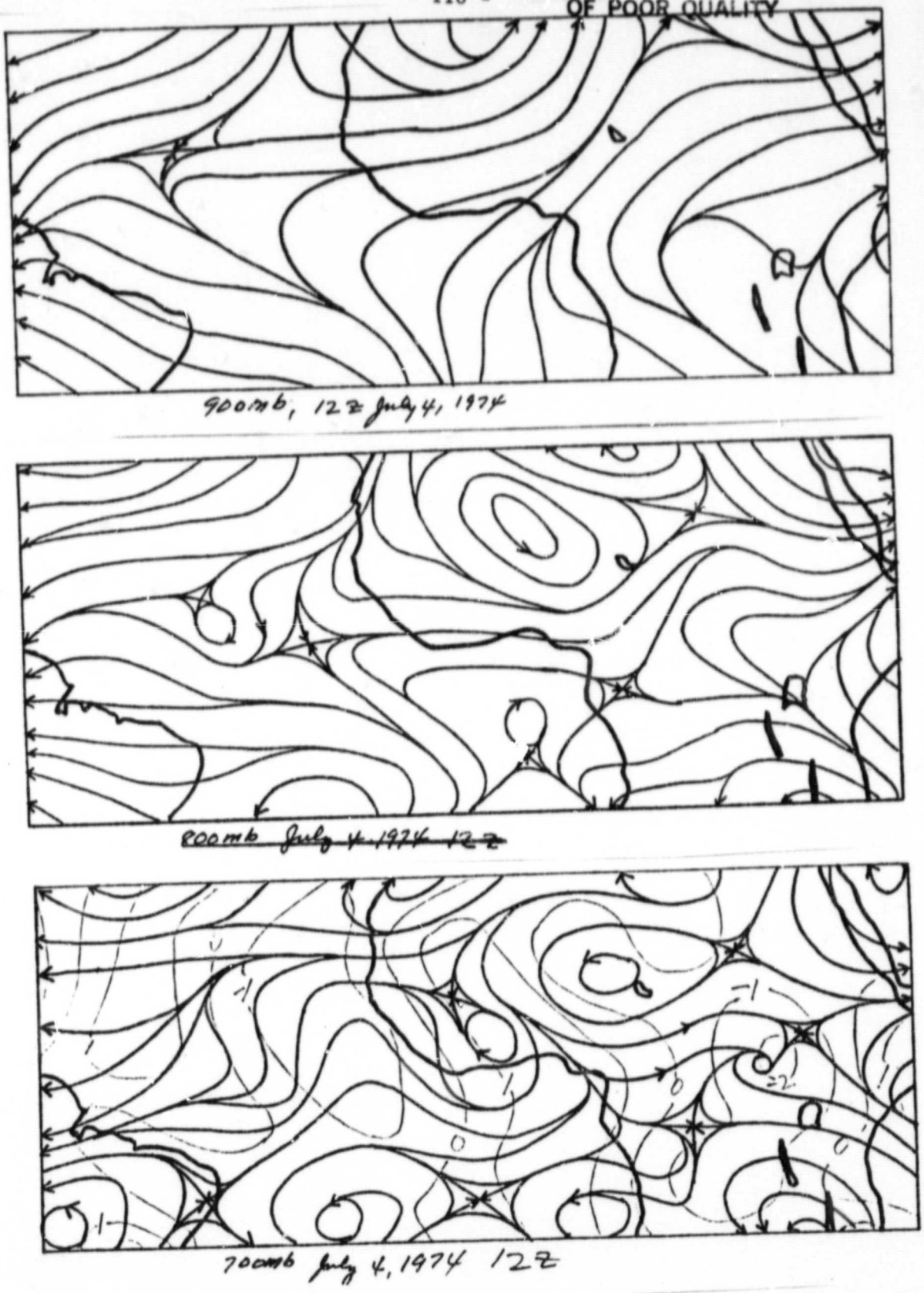

Fig. 19. Same as Fig. 13 except for 12 Z July 4, 1974.

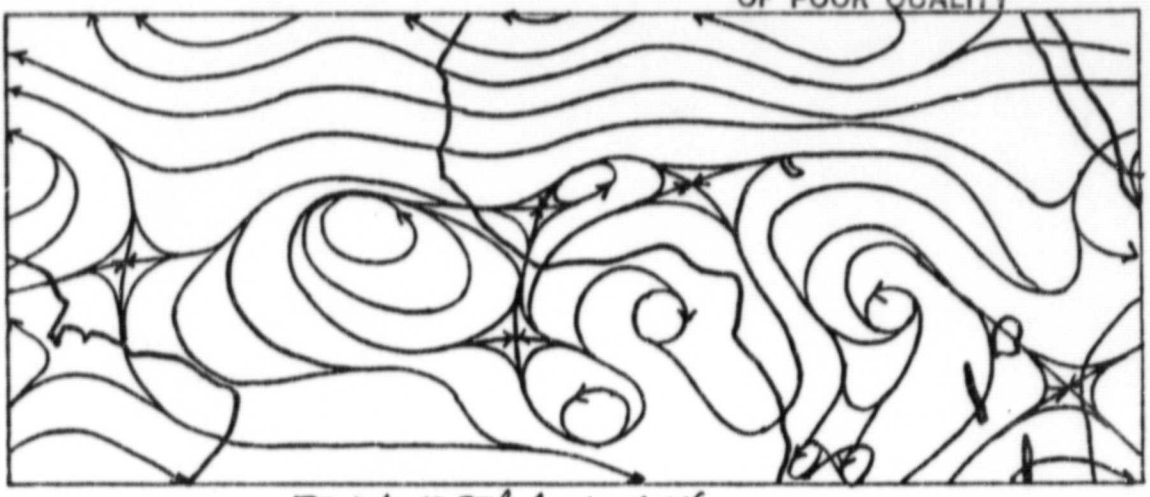

500 mb, 12Z July 4, 1974

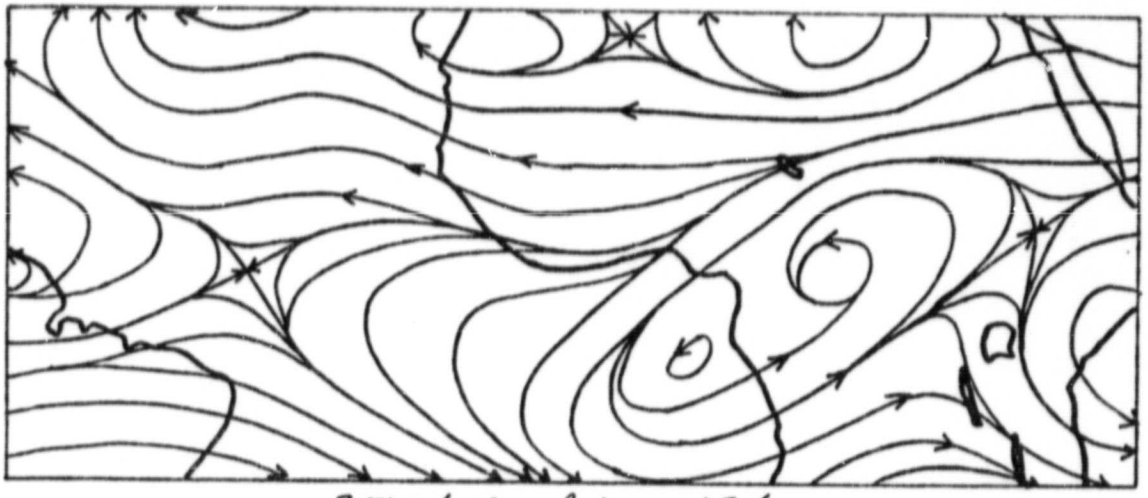

300 mb, 12Z July 4, 1974

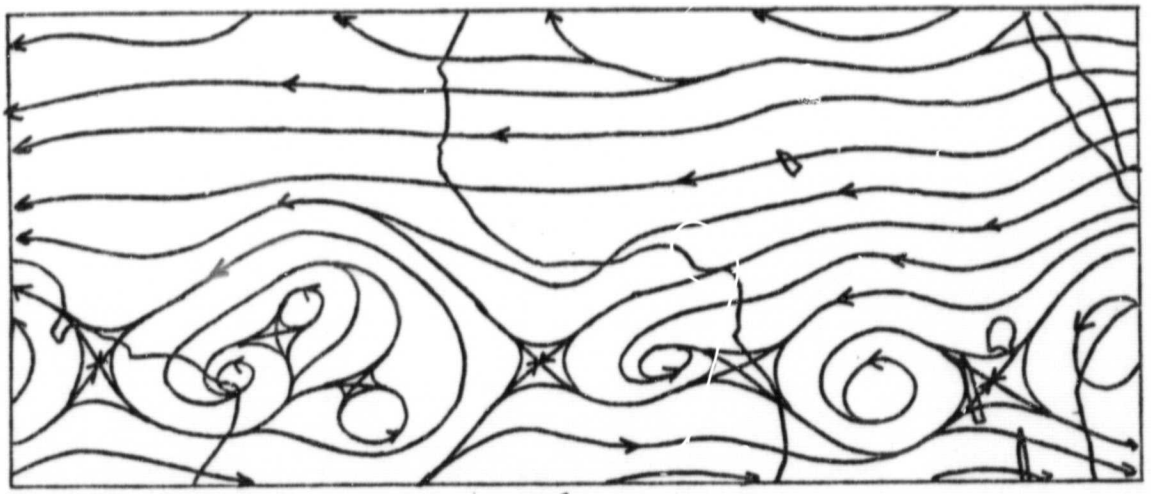

100 mb, 12Z July 4, 1974

Fig. 20. Same as Fig. 14 except for 12 Z July 4, 1974.

Fig. 21. Distribution of temperature deviations from local monthly means and the streamlines at 700 mb for 12 Z July 18, 1979. Contour interval: 1°C.

Fig. 22. Same as Fig. 21 except for 12 Z July 4, 1974.

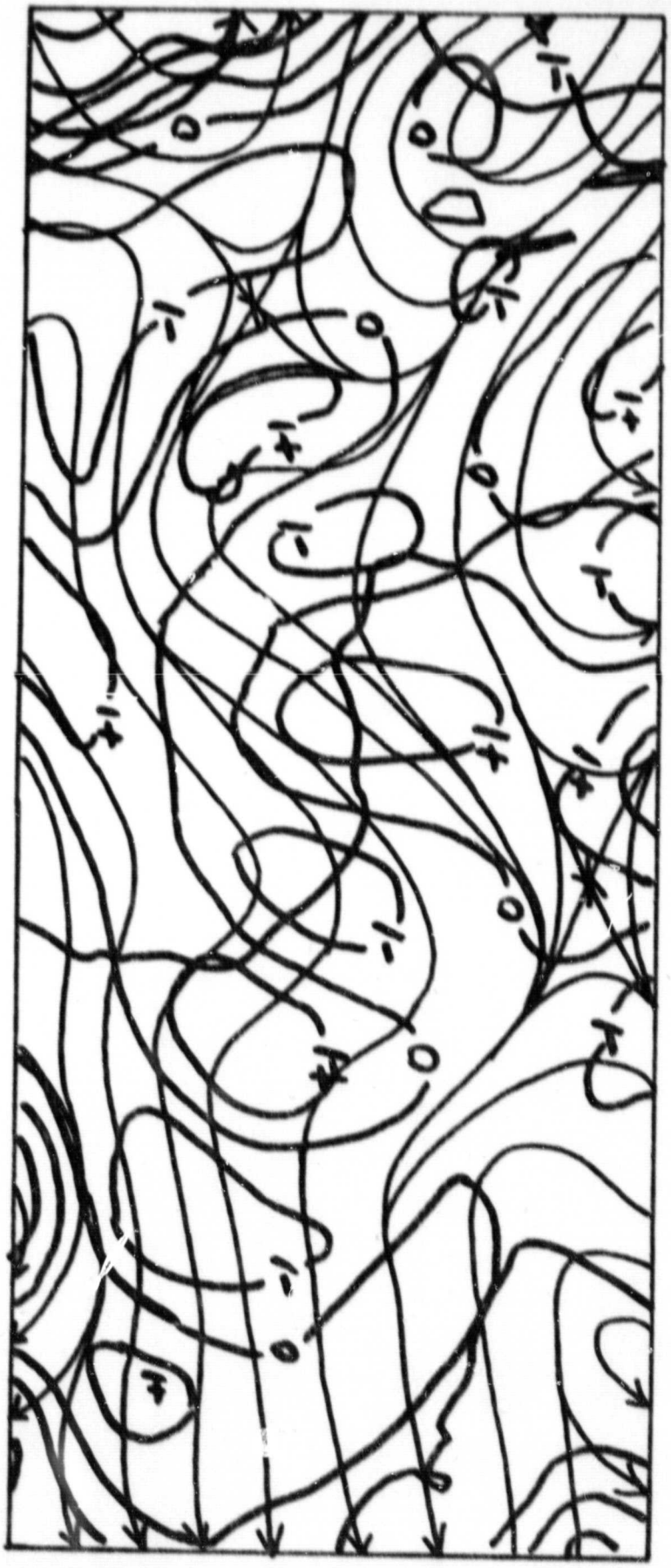

Fig. 23. Distribution of specific humidity deviations from local monthly means and the streamlines at 700 mb for 12 Z July 18, 1979. Contour interval: 1 gm/kg.

Fig. 24. Same as Fig. 23 except for 00 Z July 19, 1979.

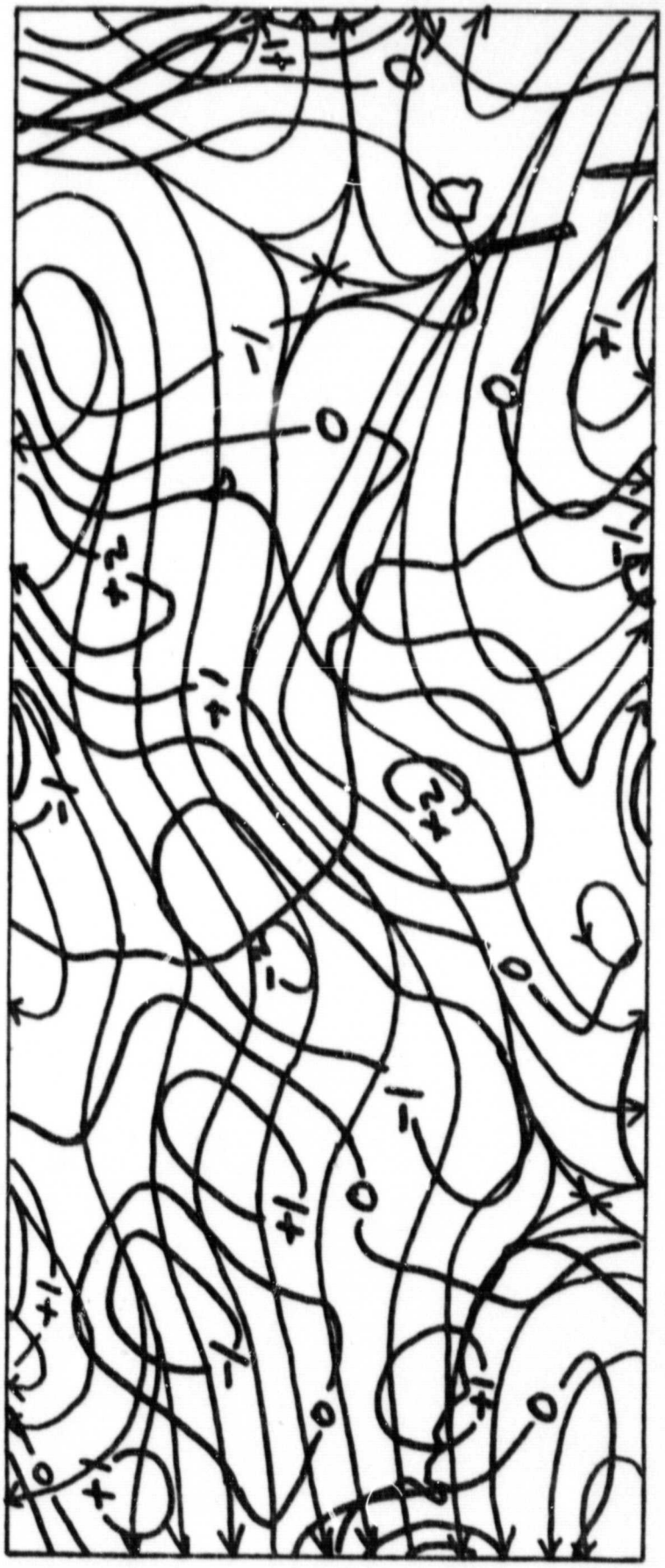

Fig. 25. Same as Fig. 23 except for 12 Z July 19, 1979.

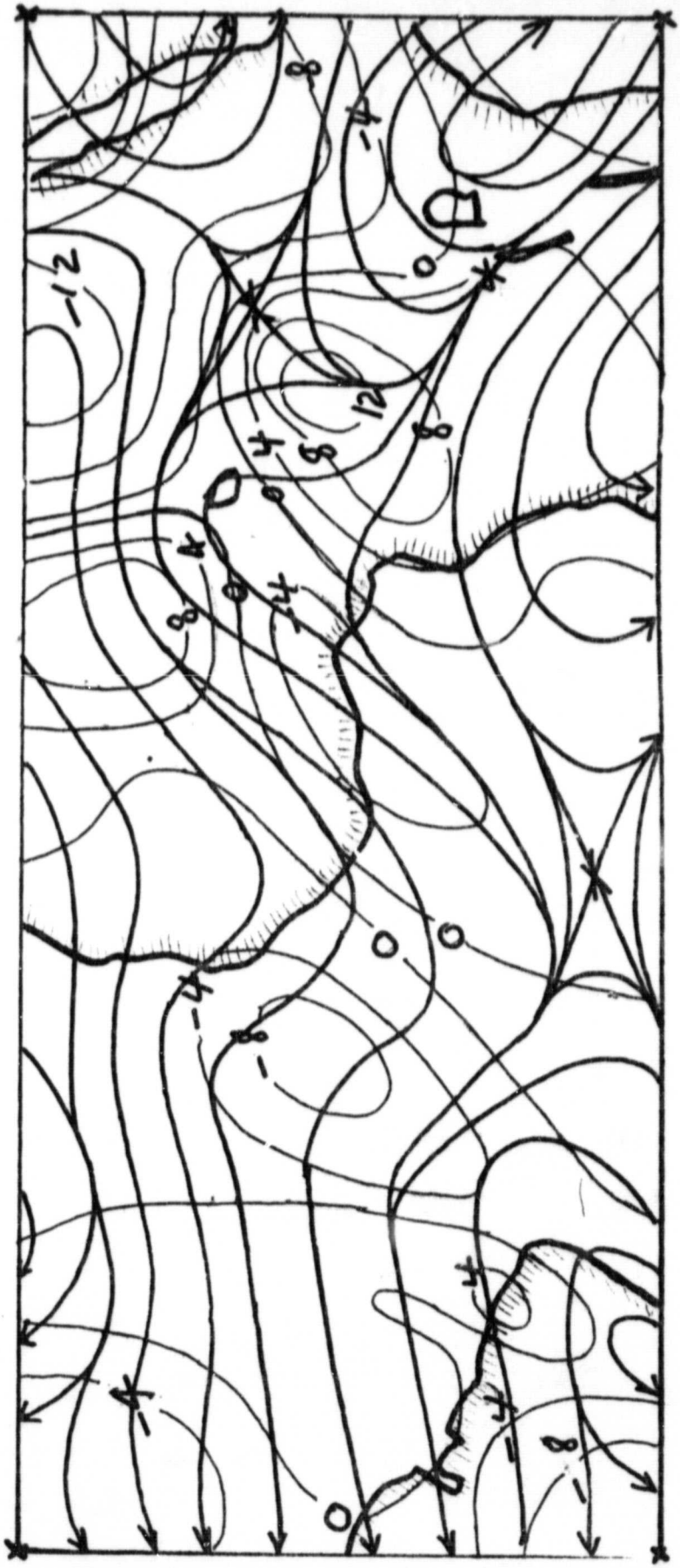

Fig. 26. Distribution of the vertically-integrated divergence from 900 to 600 mb and the 700 mb streamlines for 12 Z July 18, 1979. Contour intervals: 4 x 10^{-6} s^{-1}.

Fig. 27. Rainfall rate and the 700 mb streamlines for 12 Z July 18, 1979.
Units:xxxx cm s^{-1}.

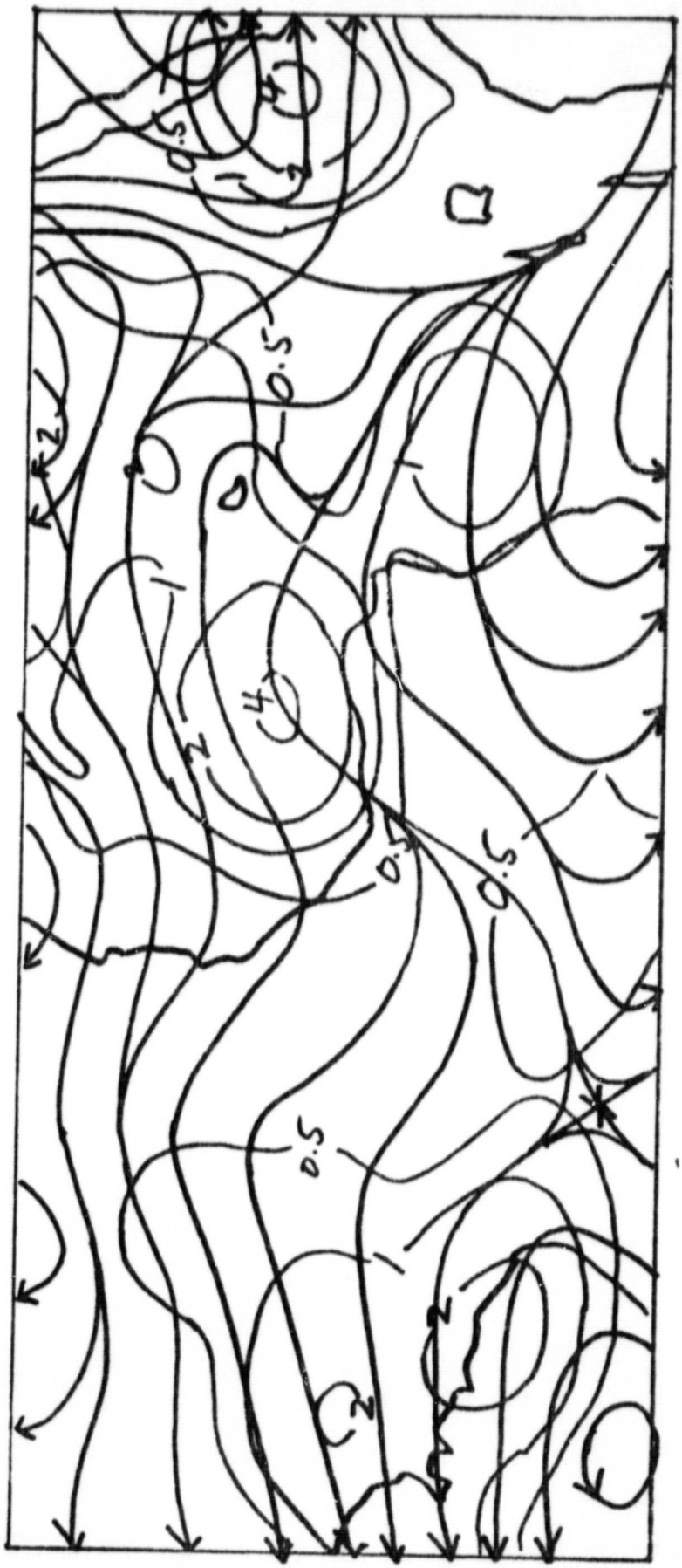

Fig. 28. Same as Fig. 27 but for 00 Z July 19, 1979.

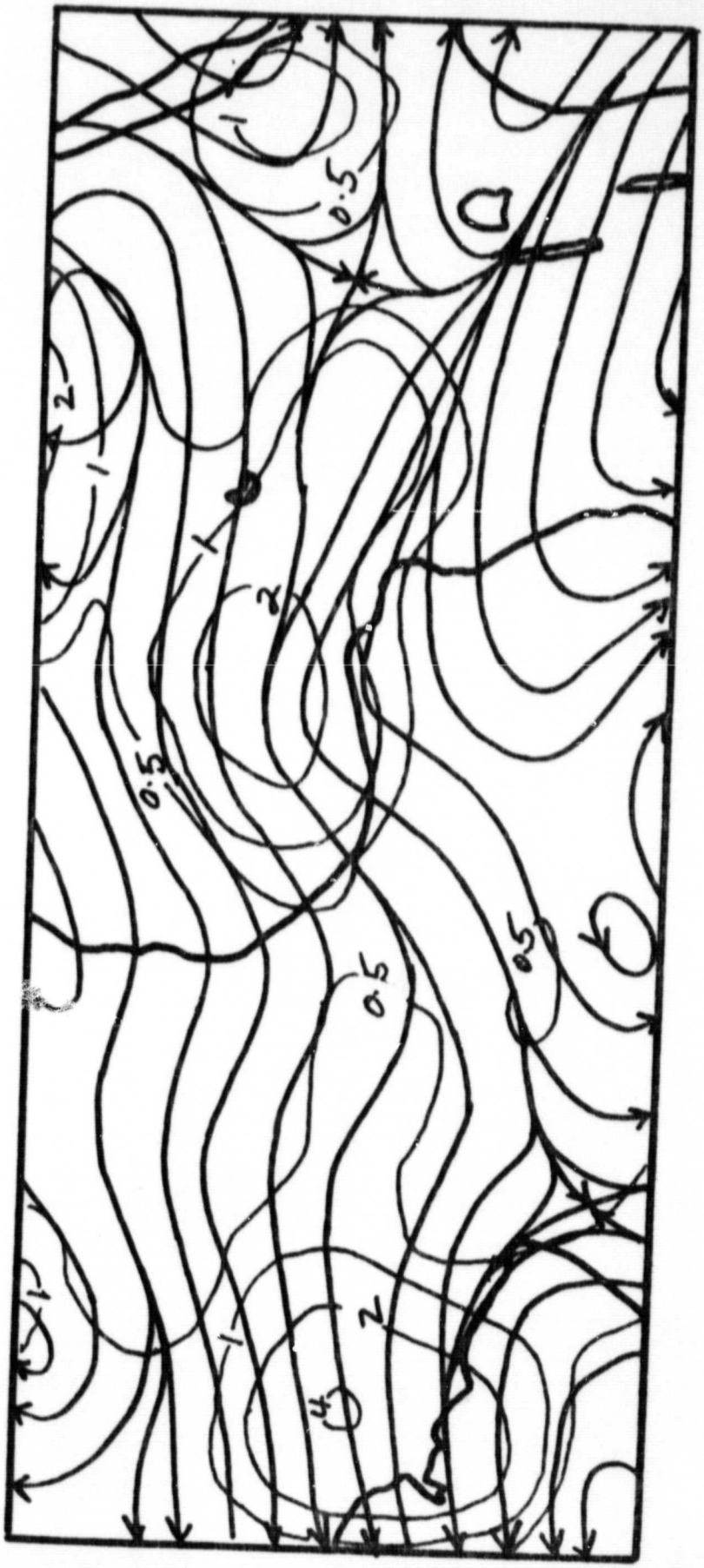

Fig. 29. Same as Fig. 27 but for 12 Z July 19, 1979.

Fig. 30. Distribution of surface pressure deviations from local monthly means and the streamlines at 700 mb for 12 Z July 18, 1979. Units:mb.

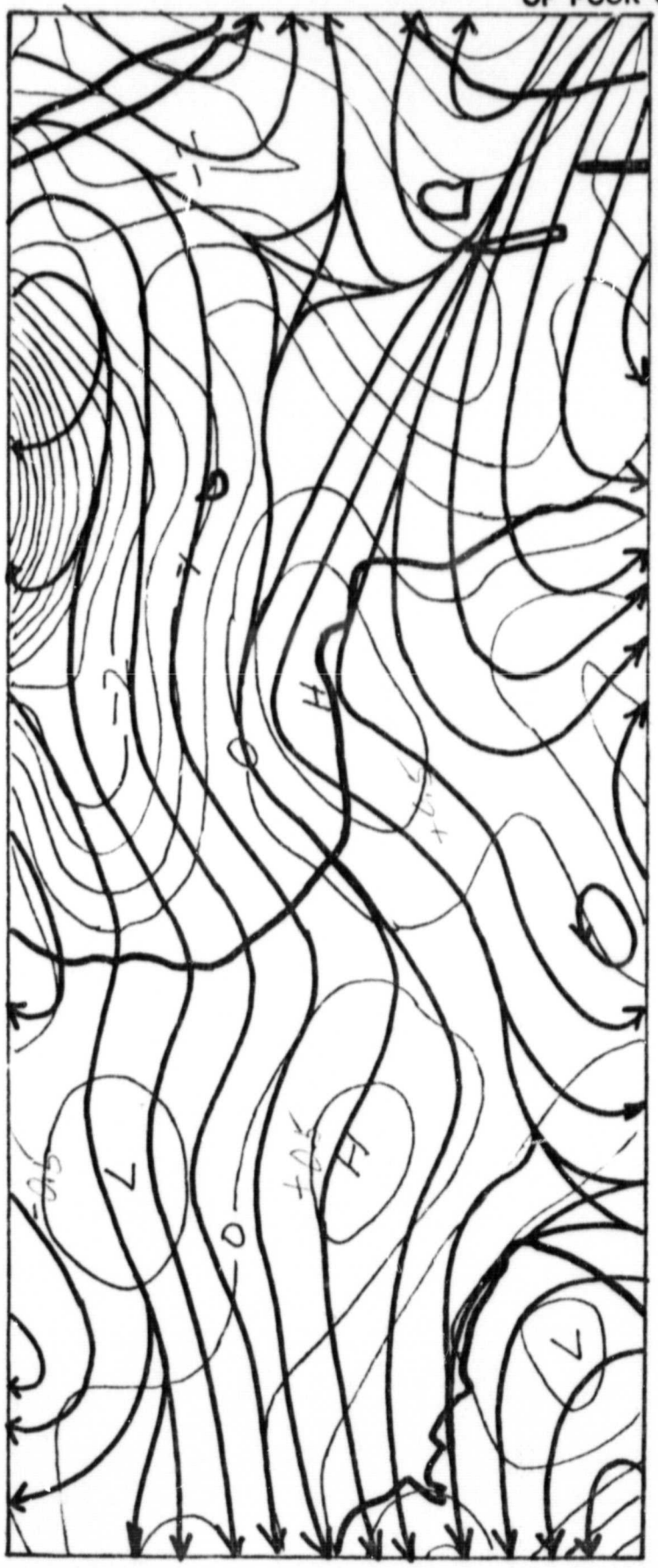

Fig. 31. Same as Fig. 30 except for 12 Z July 19, 1979.

Fig. 32. Same as Fig. 30 except for 12 Z July 19, 1979.

PART IV

CASE STUDY OF A SYNOPTIC DISTURBANCE OVER WESTERN AFRICA IN JULY 1979

A CASE STUDY OF A SYNOPTIC DISTURBANCE OVER WESTERN AFRICA IN JULY 1979

1. INTRODUCTION

The existence of westward propagating synoptic-scale wave disturbances over the tropical west Africa has been recognized for some time. Dunn (1940) found that a chain of isallobaric centers at sea level, initiated in the Cape Verde region and probably related to these disturbances, moved across the Caribbean from east to west in the hurricane season. Hamilton and Archbold (1945) described the passage of these disturbances in Nigeria. Working with conventional synoptic data, pilot reports and careful observation of the state of the sky they deduced that the disturbances have the characteristics of the tropical squall line, consisting of a row of cumulonimbus clouds forming at the edge of a broad downdraft region. Eldridge (1957) described the movement of these disturbances over Ghana and their importance in the local weather by investigating the percentage of the rainfall which could be attributed to the disturbances at four stations in Ghana.

The first comprehensive examination of these disturbances was carried out by Carlson (1969a,b) who made daily synoptic analyses between the longitudes 20E and 20W. He determined that there were many wavelike disturbances which formed east of the Greenwich meridian and propagated westward far to the south of the surface convergence zone (ITCZ) in the southern Sahara. He also determined that the surface pressure trough intensifed beneath the upper wave. Okulaja (1970) determined that an easterly wave model incorporating the 700mb trough

(and ridge) as integral feature(s) of the flow describes best the majority of significant weather zones and puts on a firmer basis the existence of westward moving lines of thunderstorms frequently traversing the heart of west Africa during the rainy season. Burpee (1972,1974) used spectral and compositing techniques and determined that the typical source region for the African disturbances was located between 15 and 30 degrees east. His study also revealed that in the region of large north-south temperature gradient between the hot Sahara and the relatively cool equatorial Africa there is a mid-tropospheric easterly wind maximum. This wind maximum shows large vertical and horizontal wind shear during the summer months. Payne and McGarry (1977) determined that wave-related convective activity was most intense at and ahead of the 700mb trough axis and most suppressed at and ahead of the ridge axis. Reed, Norquist and Recker (1977), using a compositing method found that the disturbance is most intense at 600mb, being cold core below and warm core above. Houze (1977) inferred from the evolution of squall line radar echoes that discrete convective cores, which he called line elements, form on the leading edge or even well ahead of the existing line and dissipate to the rear. In their study of a monsoon cyclone over west Africa, Pedgley and Krishnamurti (1976) calculated the meridional gradient of potential vorticity and concluded that the necessary condition for the existence of the combined barotropic-baroclinic instability was satisfied by the data. The African disturbances have been studied extensively in most recent years by Fortune (1979) who used time-lapse satellite imagery, Albignat and Reed (1980) who used spectrum and cross-spectrum analyses and Krishnamurti et al. (1980) who used a numerical method to predict the

African wave at the 700mb level.

The purpose of this study is to determine the characteristics of synoptic scale surface pressure disturbances over west Africa and the relationship between these disturbances and disturbances in the other meteorological variables such as wind, temperature, humidity, cloudiness and rainfall. The availability of the data of the West African Monsoon EXperiment (WAMEX) in July and August 1979 during FGGE gives an opportunity to make a case study of a west African disturbance which we hope will provide a better understanding of these disturbances. The disturbance chosen is the one on 16 to 19 July 1979 which after a preliminary investigation of several WAMEX disturbances was found to be a typical case. The existence of this wave disturbance has been indicated in a previous study by Frank and Clark (1980).

2. DATA AND ANALYSIS

The observational data for this study consist of 6-hourly surface meteorological observations and 12-hourly rawinsonde and pilot balloon data for the period 10 to 25 July 1979 from the FGGE data set. The surface and upper air stations used in this study are shown in fig. 1. In addition to the surface and upper air observations we also have the METEOSAT satellite pictures at 11:55 GMT for the period of study.

To analyze the pressure patterns we had to eliminate the relatively high frequency (time) variations from the 6-hourly raw surface station pressure applying a filter of the type suggested by Shapiro (1970). The particular filter which is used effectively eliminates variations whose periods are two days and smaller. In order to minimize the effect of systematic instrumental errors as well as

effects associated with local topography, we did the analysis on the perturbations from the time mean of the observed pressure for each station. Plotting these time series for selected stations we were able to choose the pressure disturbance of 16 to 19 of July 1979 which showed a good definition and movement as a pressure trough in fig. 2 . We then analyzed the 6-hourly maps of the deviations and the 6 hour changes in these deviations. The 24 hour changes in the raw pressure data were also calculated and analyzed.

In order to eliminate the diurnal and topographic effects in the temperature and dew point depression we calculated the 24 hour change in these quantities. We then analyzed the 6-hourly maps of cloud amount (eighth of total sky), present and past weather, the 24 hour change in temperature and dew point depression and the 24 hour precipitation for the period 16 to 19 July 1979. In the wind field we drew the streamlines every 6 hours for the same period.

Using rawinsonde and pilot wind data we drew the streamline maps at 2000 feet, 850mb and 700mb for this period. Since pilot balloons do not go very high and the region is not well covered by rawinsonde stations, the streamline analysis at upper levels (above 700mb) is only based on rawinsonde data and might not be very reliable. We also analysed time sections for DAKAR, BAMAKO, NIAMEY and ABIDJAN and space cross-sections for 16, 17, 18 and 19 July 1979 around 14 N.

3. GENERAL ASPECTS

Fig.2 shows selected stations around 14N from 3E to 17W for which pressure deviations are plotted. It can be seen that the amplitude of the disturbances on the pressure field increases as we move westward,

especially in the case of the wave that went through DAKAR on July 18, 1979. The other disturbances are of secondary importance since their associated pressure troughs are small compared to that of the 18th at DAKAR or have even been smoothed out in the pressure deviation analysis procedure.

Fig. 3a is a wind time section for the DAKAR station for the period of study (10 - 25 July 1979). We have 5 wave passages on this time section: the first one on the 11th, the second one on the 15th, the third one on the 18th, the fourth one on the 20th and the last one on the 23rd. Although preliminary analysis would place the position of the third trough between 00z and 12z on the 18th the trough is placed about 12 hours later for the sake of continuity of the wave motion which is supported by upper air winds at nearby stations (see Fig. 27b,c).

Fig. 4a is a wind time section for the BAMAKO station. All the waves we noticed at DAKAR can be traced back to BAMAKO. At this station the wave passages are on the 10th, 14th, 17th, 19th and 22nd of July. Wind reports for BAMAKO are not as complete as those for DAKAR; this makes it difficult to locate the waves accurately at this station.

Fig.5a is a wind time section for the NIAMEY station. We have only 3 of the 5 waves that have been identified at DAKAR and BAMAKO. The first wave that went through DAKAR on the 11th and BAMAKO on the 10th cannot be seen here because NIAMEY is further to the east of both stations. The disturbance at BAMAKO on the 19th and DAKAR on the 20th is not found at NIAMEY either; this suggests that this disturbance formed somewhere between NIAMEY and BAMAKO.

Fig. 6a is a wind time section for the ABIDJAN station. Only 3 wave passages can be identified on this time section, the waves that

went through DAKAR on 15 and 20 July did not affect ABIDJAN. Comparing this time section with those for DAKAR, BAMAKO and NIAMEY we can see that the winds are significantly weaker at ABIDJAN than at the other stations, particularly at low and mid tropospheric levels. This indicates that there is a wind decrease over western Africa as we move southward toward the coast. This difference in wind speed and the fact that some disturbances that affect NIAMEY, BAMAKO and DAKAR are not identified at ABIDJAN is in agreement with the findings of previous investigators (Burpee, 1974 et al.) of African disturbances who determined that these disturbances are more intense around 10 - 20N than along the coast.

In order to investigate the structure of these waves as they go through DAKAR, BAMAKO, NIAMEY and ABIDJAN, deviations from the mean temperature have been calculated at each mandatory sounding level, plotted and analyzed. To eliminate the diurnal effect only the 12z temperature reports have been considered. Means are obtained for each station from the 12z temperature at each level and the deviations from these means are calculated and analyzed in the form of temperature deviation time sections (Fig. 3b,4b,5b,6b). We can see on these figures that, in general, the wave disturbances are neither of warm nor cold core type; the wave troughs (shown by heavy dashed lines in the figures) are in the positions where the temperature deviation changes from warm to the west of the trough to cold to the east or vice versa. In some cases, the wave disturbances appear to have some change in temperature structure from one station to another. For instance, the 16 - 19 July disturbance shows a similar temperature structure (warm west of the trough and cold east of the trough) at NIAMEY,BAMAKO and DAKAR and the

opposite at ABIDJAN. This striking result is also obtained by Estoque et al. (1982) using a general circulation model. The basic characteristics of the model has been described previously by Sommerville et al. (1974). Using this model, the general circulation for the summer of 1974 and 1979 were simulated using initial conditions based on real data. The simulated variables at grid points were analyzed as if they were real synoptic data. Fig.7a,b show examples of the wind and temperature fields at 700mb. These figures show the location of two 700mb model waves over Africa at 24hr interval; one of the waves is moving off the continent and has a temperature structure similar to the one observed at NIAMEY, BAMAKO and DAKAR for the 16 - 19 July disturbance. The other wave, over central Africa, initially shows colder temperature to the west of the wave axis and warmer temperature to the east (Fig.7a). This thermal distribution reverses for the northern part of the wave in 24hr but remains unchanged for the southern part. Thus, the model wave for central Africa in Fig. 7b shows a structure similar to that of the 16 - 19 July wave disturbance not only for DAKAR, BAMAKO and NIAMEY but also for ABIDJAN.

4 THE 16 - 19 JULY 1979 WAVE DISTURBANCE

a. Satellite observations

The disturbance of the 16-19 July can be seen on METEOSAT satellite pictures (visible channel) taken daily at 11:55 GMT (Fig. 8a-e). On the 15th the system is to the east of our area of study between 9-12N and 15-20E and shows few signs of convective activity. This is the first day we can surely identify the system on the satellite picture. The satellite picture for the 16th shows that the system

becomes more convective as it moves westward; the convection is centered near latitude 10N and longitude 9E. On the 17th the system shows a well defined convective area centered near latitude 10N and longitude 3E. On the 18th, the ITCZ moves northward as the wave approaches the African coast; the disturbance is now centered around 11N and 7W and the convection associated with it has diminished considerably. On the 19th the disturbance (cloud mass) is centered around 12N and 15W, the ITCZ convection covers from 4N to 12N and 12W to 20W.

b. Surface observations

Figures 9 to 21 show the surface analyses at 6 hour intervals from the 16th at 00z to the 19th at 00z, when the region of study is affected by the most important disturbance of the period July 10 - 25. The area of study here is smaller than that shown in fig. 1 because there are very few data points between 15E and 30E. Every figure is a composite of 10 different analyses indicated by letters a to j. When an analysis is missing the portion of the figure where the analysis should be placed is left blank and the indicative letter is skipped.

Analysis a) is for the pressure deviation from the mean. This analysis is drawn at intervals of .25mb. In this analysis a negative quantity is shown by dashed lines and a positive and zero quantities are shown by solid lines. On this analysis the pressure trough associated with the wave disturbance is located where the pressure deviation is the most negative. This pressure trough appears to move slowly toward the west in the beginning of the period; then at a faster rate, reaching the Atlantic ocean by July 18 at 12z.

Analysis b) is the surface streamline analysis. In addition to

the streamlines (solid lines), heavy dashed lines are shown to represent either an east- west convergence zone or the leading edge a of wind regime (i.e thunderstorm outflow) associated with the disturbance. The streamline analysis starts to show some change in the southwest monsoon flow by the 16th at 12z. 6 hours later the leading edge of the disturbance is shown by the boundary between the monsoon flow and the easterly flow associated with the disturbance. This leading edge appears to represent the outer limit of the outflow from convective activity having tropical squall line character. This leading edge moves westward until it dissipates by the 18th at 6z. The dissipation is related to a drastic decrease of the convection over land. This decrease of convection over land seems to coincide with an increase of ITCZ convection over waters off the African coast as suggested by a satellite picture (Fig. 8d).

Analysis c) and d) are for the present and past weather respectively, plotted in the form of standard weather symbols. These analyses show that the passage of the 16 - 19 July disturbance is associated with an area of thunderstorms and rainfall, which appears to propagate westward with the disturbance, however superimposed on this trend there are weather areas of localized character, particularly near the Gulf of Guinea. Note that the weather area associated with the 16 - 19 wave disturbance is located to the east of the leading edge shown in analysis b).

Analysis e) is for the cloud amount in eighths of total sky; only isopleths for 6/8 and 8/8 cloud coverage are drawn. As expected there is a close correspondence between the wave disturbance passage and the maximum cloud coverage. It is found that, in general, the maximum cloud

coverage closely trails the leading edge of the disturbance.

Analysis f) is for the 24hr precipitation (inches) preceding the time of observation. Since the rainfall is reported once every 24hr it is not possible to have a time distribution of the actual precipitation amount reported by each station. This makes it difficult to determine the precipitation occurrence with respect to the wave passage. Furthermore, the convective character of the tropical rainfall may show strong horizontal variability in the 24hr precipitation (i.e neighboring stations can get several inches in heavy thunderstorms or little or no precipitation if they are not directly affected by nearby thunderstorms). This analysis does not show a well defined rainfall pattern moving with the disturbance, however it does show that the very heavy precipitation (about 2 inches) near 0E on the 17th at 6z (Fig. 14f) is indeed related to the disturbance passage.

Analyses g) and h) are for the 24hr temperature and dew point depression change respectively. These analyses are drawn at two degree intervals. Both temperature and dew point depression show negative changes after the passage of the wave. The zero line of these changes roughly corresponds to the position of the wave disturbance. The decrease in temperature is probably due to the combined effect of increasing cloudiness found in analysis e) and the precipitation associated with the disturbance. The decrease in dew point depression shows that there is a large moisture increase to the east of the wave trough.

Analysis i) is for the 24hr pressure change drawn at 1mb intervals and analysis j) is for the 6hr change in pressure deviation drawn at .2mb intervals. The 24hr pressure change shows falling

pressures as the disturbance approaches a station and rising pressures as it moves away from the station. This pattern can be seen more clearly in the 6hr pressure change analysis : the disturbance passage corresponds to the zero line; increasing pressures is found to the east of this line and decreasing pressure is found to the west.

c. Upper air analysis

Figures 22 to 28 show upper air streamline analyses at 12 hour intervals from 16 July at 00z to 19 July at 00z. Every figure is made of 6 different streamlines analyses(a to f). As in the surface case a blank space is shown when an analysis is missing and the corresponding letter is skipped. These 6 analyses show the streamlines at 2000 feet, 850, 700, 500, 300 and 200mb. The 2000 ft streamlines are initialy dominated by the southwest monsoon flow (Fig. 22a, 23a). This flow is then perturbed by easterlies associated with organized convective outflow of the wave disturbance (Fig.25a, 26a). The southerly flow is gradually restablished as the wave approaches the west African coast with diminishing convection (Fig.27a, 28a). To the west of the wave, the 850mb flow is mostly from a northwesterly direction (Fig.23b, 24b) and the wave is associated with an easterly flow having a marked cyclonic curvature (Fig. 24b). The wave has a large enough amplitude to show sometimes a cyclonic vortex (Fig. 25b, 26b). Figures 27b and 28b show the existence of a second wave trailing the 16 - 19 July wave disturbance. Note that the wave axis at 850 mb is located some distance to the east of the leading edge of the convective outflow at 2000 feet, implying an eastward tilt of the wave axis with height. The 700mb flow is mainly easterly, the wave is well developed at that level and can be

tracked from the vicinity of 8E on the 16th to the west of DAKAR on th 19th (Fig. 23c, 28c). The wave can still be identified at 500mb (se for instance figure 25d-27d) but there is not enough evidence of it a higher levels. At 200mb there is an anticyclonic condition correspondin closely to the position of the wave at lower level. This anticyclonic condition, represented by either a ridge or a close vortex propagate westward with the wave disturbance (Fig. 23f-26f), and appears to b related to the heavy convection in the disturbance.

In addition to the streamline maps presented, the vertical structure of the 16 - 19 July wave disturbance can be examined by space cross-sections (Fig.29a to g). These vertical sections are oriented east - west around 14N from 15E to 20W. Wind, temperature in degree centigrade and humidity (dew point depression) data from the surface to 100mb for DAKAR, BAMAKO, OUAGADOUGOU, NIAMEY and BILMA (wind only) are shown in these sections and the temperature (solid lines) and dew point depression (dashed lines) are analyzed; a schematic location of the wave disturbance is indicated by heavy dashed lines. Judging from the dew point depression distribution the air is dryer some distance west of the wave and moisture increases eastward toward the wave axis, reaching near saturation or saturation in the vicinity and to the east of this axis (see Fig. 28b to f). The temperature analysis shows that at middle level (800 to 500mb) the air is warmer west of the wave axis and colder to the east. The wave axis appears then to be in the transition zone from warmer to colder air, which is in agreement with the thermal structure found in the time section for the 16 - 19 July wave disturbance.

5. SUMMARY AND CONCLUSION

The FGGE data over west Africa have enabled us to select a wave disturbance for detailed study in July 1979. The disturbance selected is the 16 - 19 July wave disturbance which is found to be the most salient African disturbance over the 10 - 25 July FGGE intensive observational period. Using surface observations of the meteorological variables (wind, pressure, temperature, dew point depression, clouds, present and past weather and rainfall) as well as upper air information (wind, temperature, dew point depression), the four dimensional structure of this wave disturbance is described. This description is comparatively speaking a rather comprehensive case study of a tropical disturbance at the synoptic scale. To the authors knowledge, no individual African disturbance has been documented as thoroughly as the 16 - 19 July 1979 wave disturbance in the refereed meteorological literature. The description of previous individual African disturbances is shown to deal primarily with selected aspects of the disturbance. For instance, Fortune (1980) used primarily satellite imagery and a multiple level streamline analysis for studying a September 1974 disturbance, but did not include a detailed surface analysis. Carlson (1969a) studied a series of African disturbances using satellite pictures, surface pressure and streamline analysis from the surface to 700mb; however he did not include analyses above that level and did not use temperature or dew point in his analysis. Okulaja (1970) presented a very comprehensive upper air analysis for a July 1960 disturbance but did not include a surface analysis of the meteorological quantities.

Based on satellite pictures, the 16 - 19 July disturbance is first identified with reasonable confidence over the region east of Lake

Chad on 15 July. It enters the eastern boundary (about 8E) of our area of detailed study on the 16th. The 16 - 19 July wave disturbance is found to move westward from about 8E to the DAKAR area (18W) in about 3 days; therefore, the wave motion is about 9 degrees per day which is somewhat faster than normal. As expected the wave passage is associated with a minimum in the pressure field suggested by the pressure deviation and pressure changes with time. The surface wind field shows that the perturbation introduced by the wave in the monsoon southerly flow is primarily in the form of easterlies associated with organized thunderstorm outflow (squall line type). Cooling and a moisture increase in the vicinity and to the east of the wave is indicated by the changes in the surface temperature and dew point depression respectively. Maximum cloudiness and precipitation are also found near and to the east of the wave. Surface and upper air analyses of the wave show an eastward tilt of the wave axis with height at low levels. This is in agreement with observational (Burpee, 1972, 1974) and theoretical (Simmons, 1977 and Mass, 1979) studies of African waves. Surface and 2000 ft analyses suggest that most of the active convection associated with the 16 - 19 July 1979 wave disturbance is located west of the 700mb trough position. This agrees with the work by Aspliden et al. (1976), Payne and McGarry (1977) who showed that the most intense convection in African waves (squall lines) occurs to the west of the 700mb trough.

The upper air analysis of the wave shows dry air some distance west of the disturbance with increasing moisture to near saturation or saturation in the vicinity and to the east of the wave. This moisture distribution agrees with the results obtained by Burpee (1974) and by Reed et al. (1977) (Fig. 30a,32a) and Carlson (1969b) who found a cloud

cover maximum (percentage) to the east of the 700mb wave position (Fig. 31). The wave axis appears to be located, particularly at mid-levels, in the transition zone, from warmer temperatures to the west and colder temperatures to the east, except for ABIDJAN where the opposite has been observed. This shows that the 16 - 19 July wave does not appear to be a pure warm core or a pure cold core disturbance at these levels. The observed temperature distribution is in agreement with a composite wave model for DAKAR by Burpee (1974) which shows warmer temperatures to the west of the composite wave and colder temperatures to the east ; however, the 16 - 19 July wave differs in structure from a model by Reed,Norquist and Recker (1977) which suggest a cold core wave structure at mid-level (Fig. 32b) and from theoretical models by Rennick (1976) and Mass (1979) which suggest a cold core structure at low and mid-levels (Fig. 33,34).

The temperature and moisture distribution of the 16 - 19 July wave disturbance suggests a kinetic energy consuming synoptic scale vertical motion field (warm air sinking and cold air rising) for at least the mid-atmospheric levels and even part of the low levels. This indicates that the synoptic circulation associated with the wave does not appear to provide energy for the wave maintenance. Therefore the wave energy most be extracted from instabilities of the basic flow (i.e barotropic and (or) baroclinic instability) and (or) from diabatic heating introduced by an active convective scale. The probable presence of barotropic instability in the basic mid-tropospheric flow in which the 16 - 19 July wave is embedded is suggested by an observed north south wind shear near the 700mb level; the observed vertical wind shear implies some baroclinic conditions. The general role of barotropic and

baroclinic instability in the generation and maintenance of African wave was first suggested by Burpee (1972) and has been comfirmed theoretically in recent years by Rennick (1976) and Mass (1979). Furthermore, Mass (1979) showed that the enhancement of convection produces an increase in the vertical extend of the wave disturbances under the environmental thermodynamic instability condition frequently encontered over non desertic west Africa in summer. Thus the effect of deep convection is to intensify the synoptic scale disturbances in which the convection is embedded. The presence of active convection associated with the 16 - 19 July wave during most of its journey over west Africa is supported by METEOSAT satellite pictures, the present and past weather and the rainfall observations from surface stations.

REFERENCES

Albignat, J. D., and R. J. Reed, 1980: The origin of African wave disturbances during phase III of GATE. Mon. Wea. Rev., 108, 1927-1932.

Aspliden, C. I., Y. Tourre and J. B. Sabine, 1976: Some climatological aspects of west African disturbance lines during GATE. Mon. Wea. Rev., 104, 1029-1035.

Burpee, R. W., 1972: The origin and structure of easterly waves in the lower troposphere of north Africa. J. Atmos. Sci., 29, 77-90.

------, 1974: Characteristics of north Africa easterly waves during the summer of 1968 and 1969. J. Atmos. Sci., 31, 1556-1570.

Carlson, T. N., 1969a: Synoptic histories of three African disturbances that developed into Atlantic hurricanes. Mon. Wea. Rev., 97, 256-276.

------, 1969b: Some remarks on African disturbances and their progress over the tropical Atlantic. Mon. Wea. Rev., 97, 716-726.

Dunn, G. E., 1940: Cyclogenesis in the tropical Atlantic. Bull. Amer. Meteor. Soc., 21, 215-229.

Eldridge, R. H., 1957: A synoptic study of west African disturbance lines. J. Roy. Meteor. Soc., 83, 303- 314.

Estoque, M. A., J. Shukla and J. G. Jiing, 1982: African disturbances in a general circulation model. (unpublished manuscript)

Fortune, M., 1979: Properties of African squall lines inferred from time lapse satellite imagery. Mon. Wea. Rev., 108, 153-168.

Frank, N. L., and G. Clark, 1980: Atlantic tropical systems of 1979. Mon. Wea. Rev., 108, 966-972.

Hamilton, R. A., and J. W. Archbold, 1945: Meteorology of Nigeria and adjacent territory. Quart. J. Roy. Meteor. Soc., 71, 231-264

Houze, R. A. Jr., 1977: Structure and dynamics of a tropical squall-line system. Mon. Wea. Rev., 105, 1540-1567.

Krishnamurti, T. N., R. J. Pasch and P. Ardanuy, 1980: Prediction of African waves and specification of squall lines. Tellus, 32, 215-231.

Mass C., 1979: A linear primitive equation model of African wave disturbances. J. Atmos. Sci., 36, 2075-2091.

Okulaja, F. O., 1970: Synoptic flow perturbations over west Africa. Tellus, 22, 663-680

Payne, S. W., and M. M. McGarry, 1977: The relationship of satellite inferred convective activity to easterly wave over west Africa and the adjacent ocean during phase III of GATE. Mon. Wea. Rev., 105, 413-420.

Pedgley, D. E., and T. N. Krishnamurti, 1976: Structure and behavior of a monsoon cyclone over west Africa. Mon. Wea. Rev., 105, 149 - 167

Reed, R. J., D. C. Norquist and E. E. Recker, 1977: The structure and properties of African wave disturbances as observed during phase

III of GATE. Mon. Wea. Rev., 105, 317-333.

Rennick, M. A., 1976: The generation of African waves. J. Atmos. Sci., 33, 1955- 1969.

Shapiro, R., 1970: Smoothing, filtering and boundary effects. Geophys. and Space phys., 8, 359 - 387

Simmons, A. J., 1977: A note on the instability of the African easterly jet. J. Atmos. Sci., 34, 1670 - 1674

Sommerville, R. C., P. H. Stone, M. Halem, J. E. Hansen, J. S. Hogan, L. M. Druyan, G. Russel, A. Lacis, W. Quirk, and J. Tennbaum, 1974: The GISS model of the global atmosphere. J. Atmos. Sci., 31, 84-117.

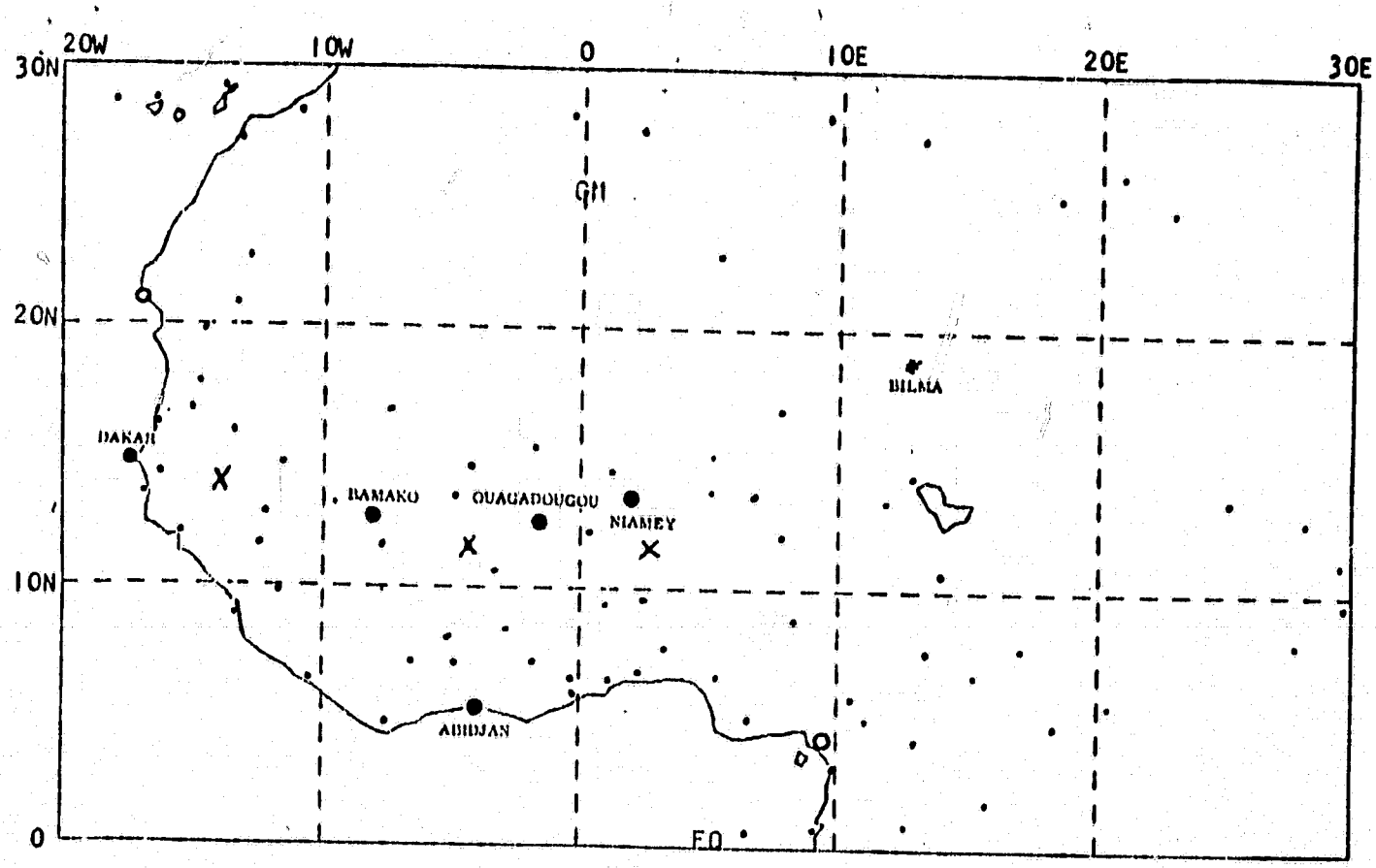

Fig. 1. The area of study and reporting stations.

- ● upper air station used in this study
- o upper air station not used
- • surface station
- * pilot wind station used in the cross-section
- × surface station used in Fig. 2.

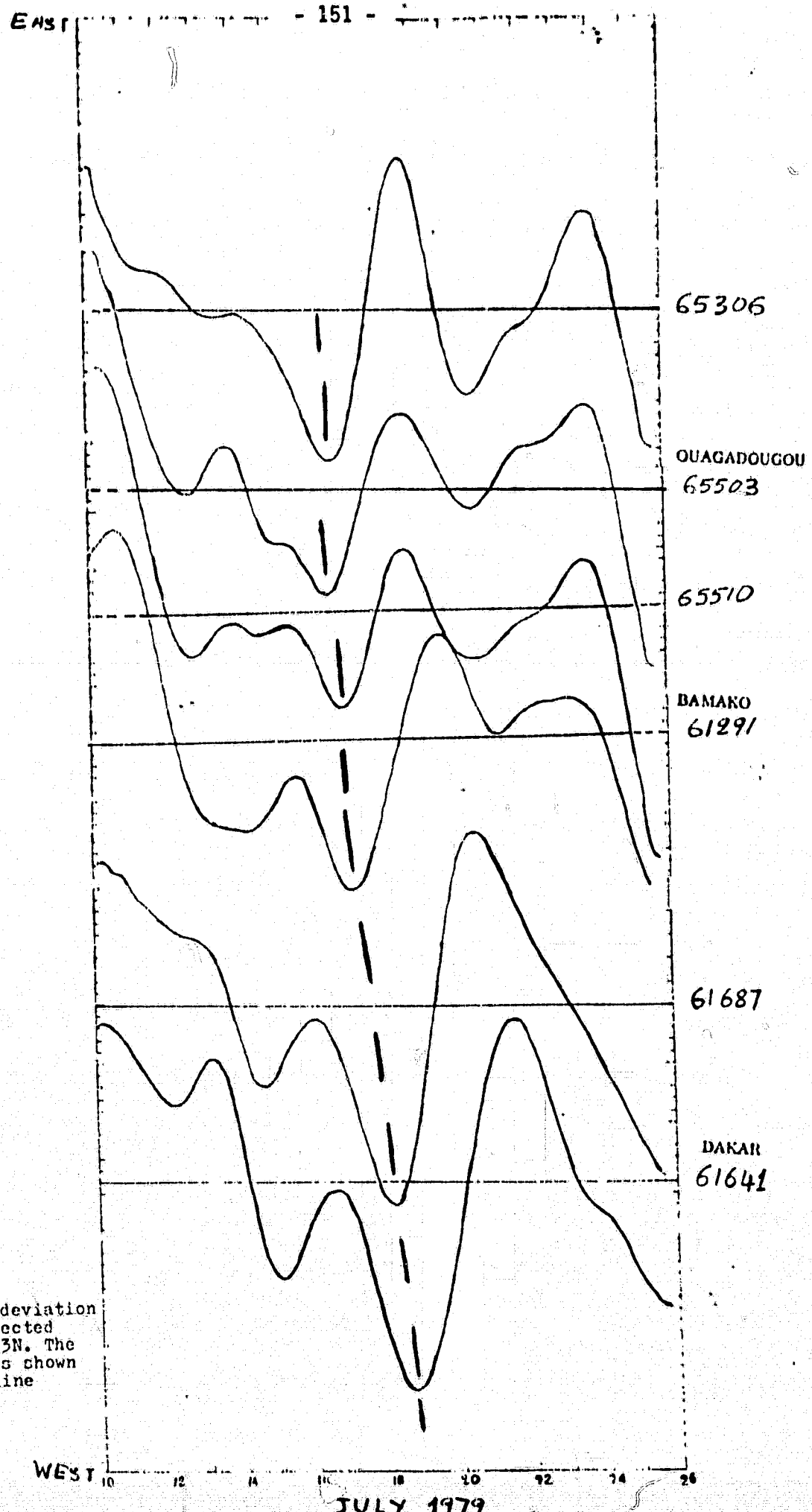

Fig. 2. Surface pressure deviation from mean for selected stations around 13N. The 16-19 July wave is shown in heavy dashed line

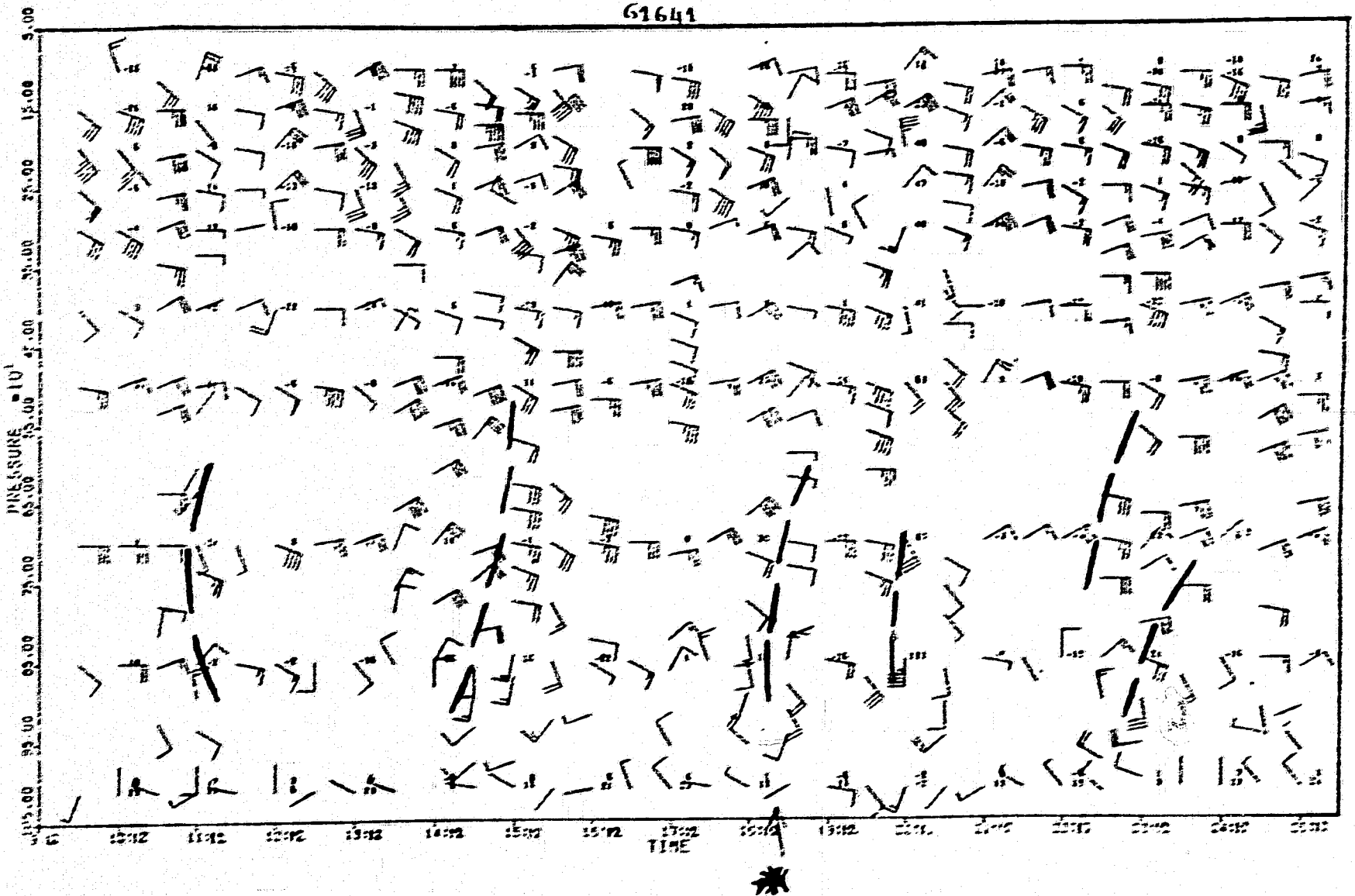

Fig. 3a. Wind time section for the DAKAR station: heavy dashed lines represente wave passages, the 16-19 wave is indicated by ✱

ORIGINAL PAGE IS
OF POOR QUALITY

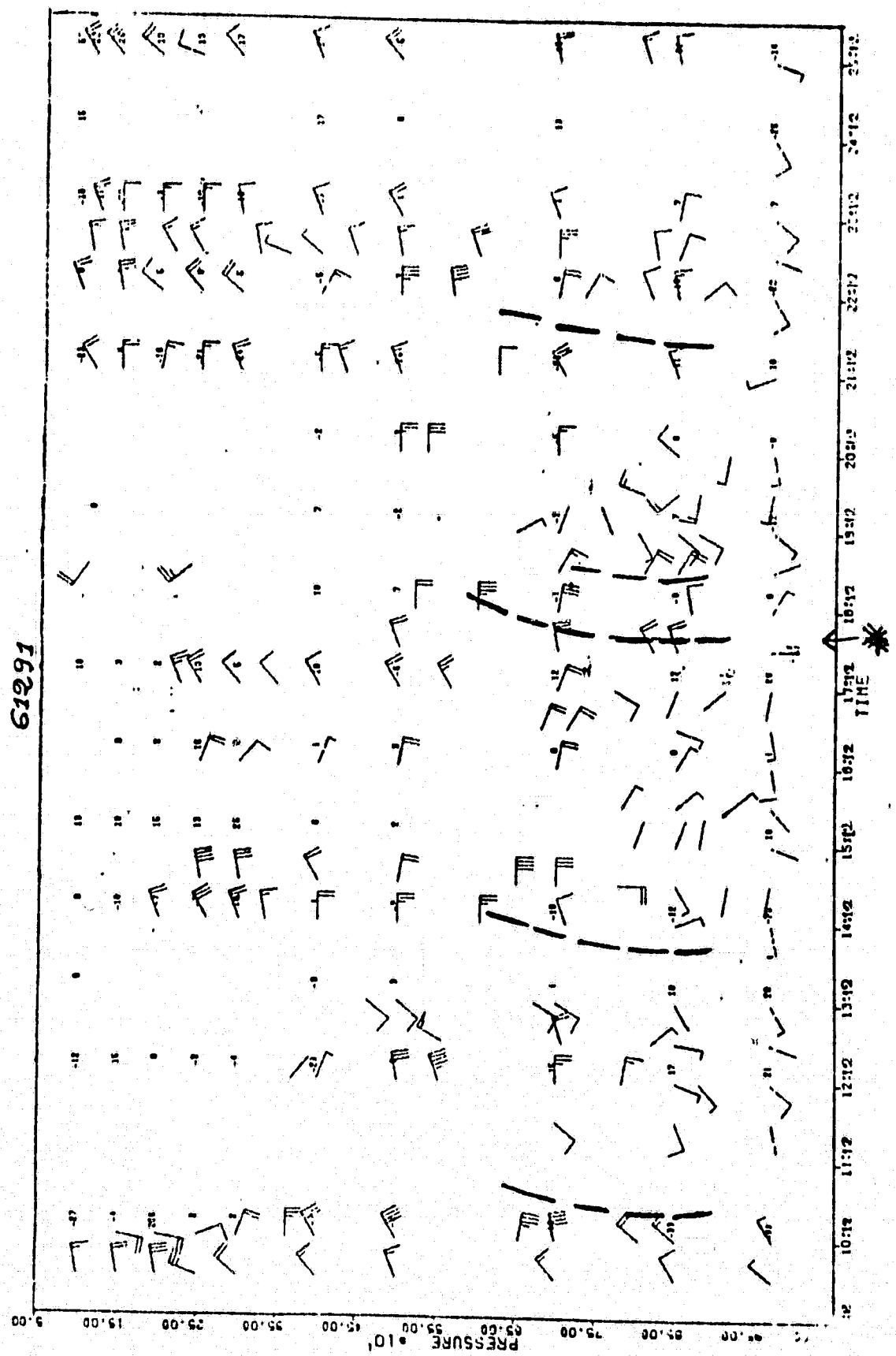

Fig. 4a. Same as Fig.3a. except for BAMAKO station

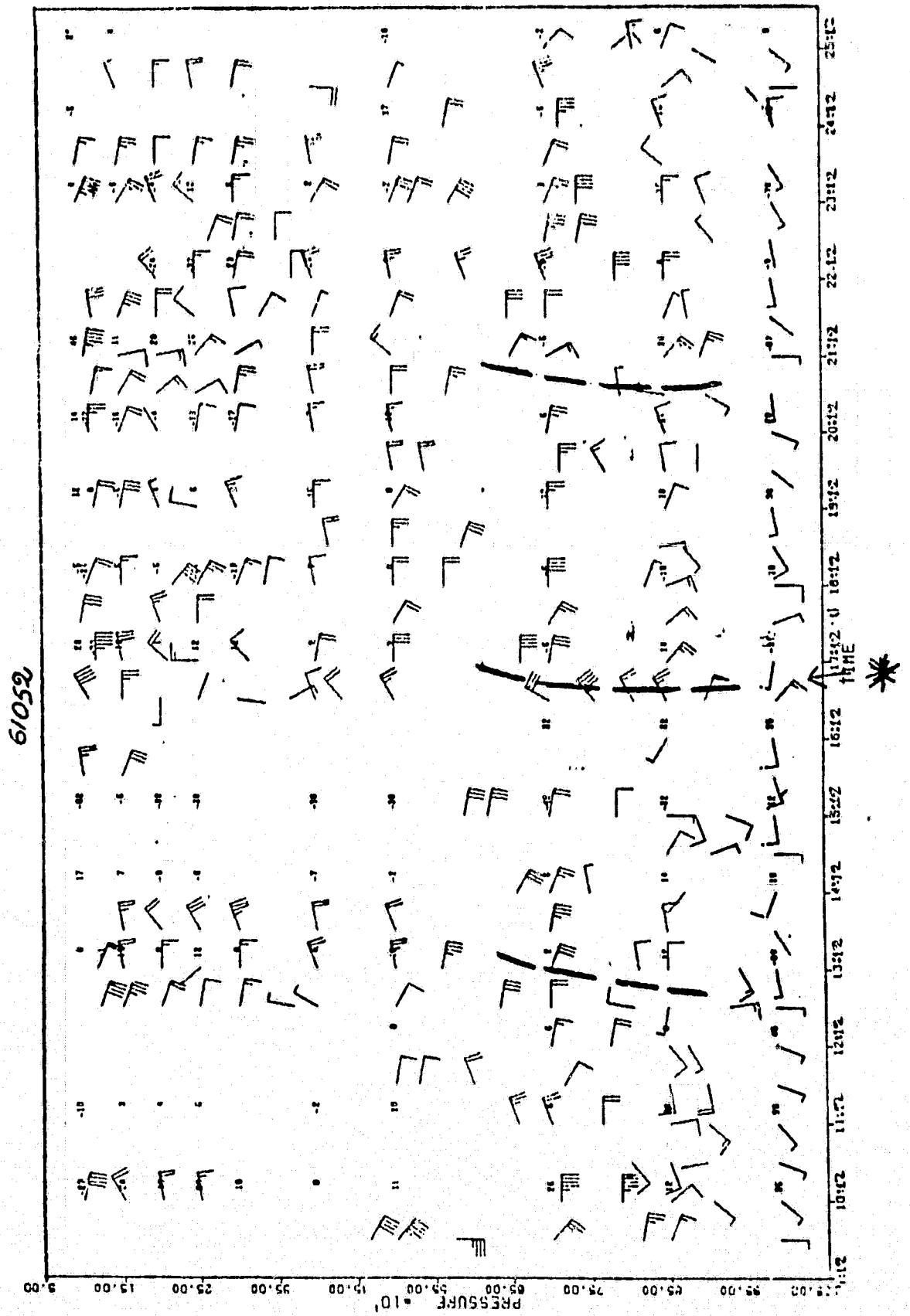

Fig. 5a. Same as Fig. 3a. except for NIAMEY station

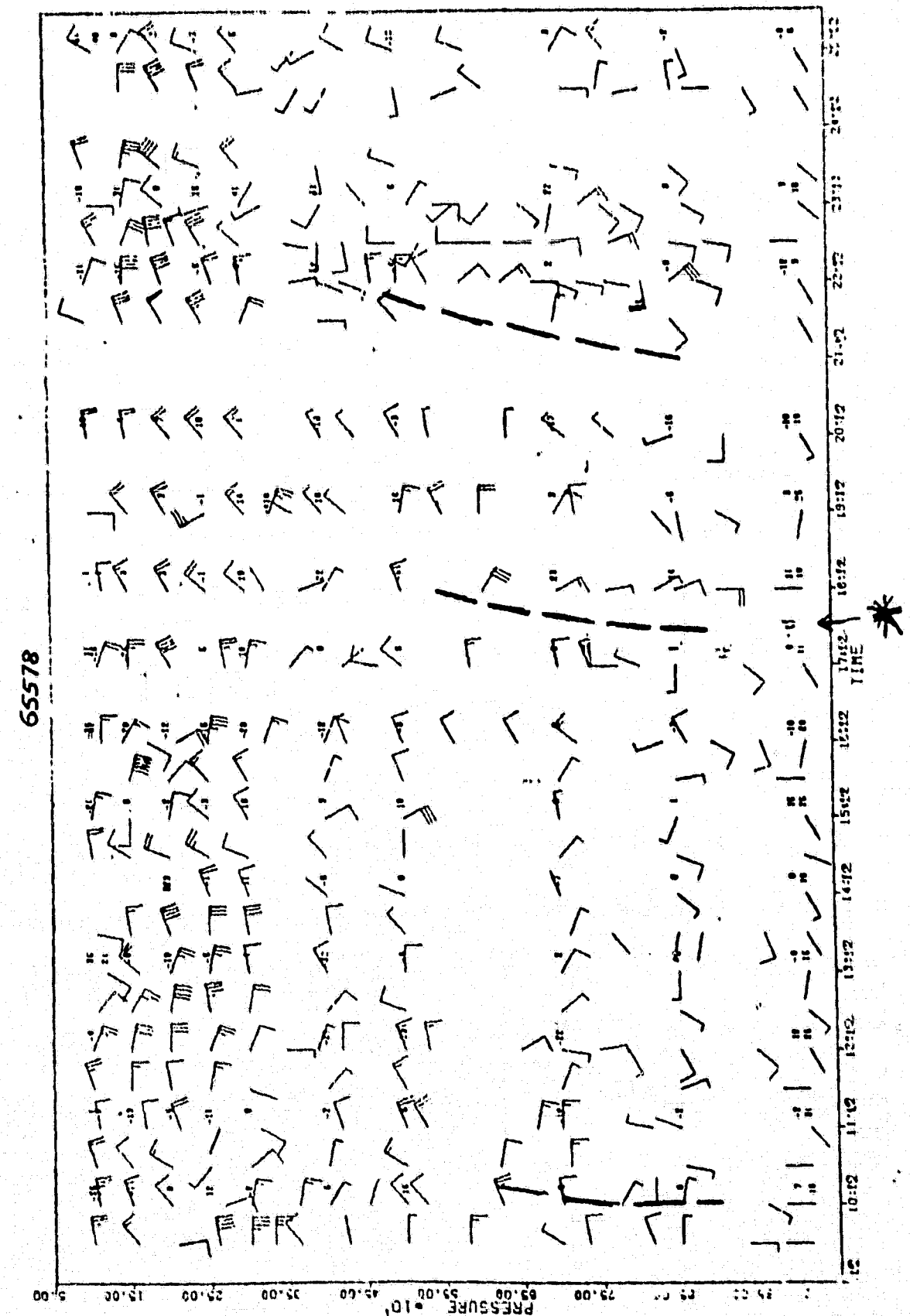

Fig. 6a. Same as Fig. 5a. except for ABIDJAN station

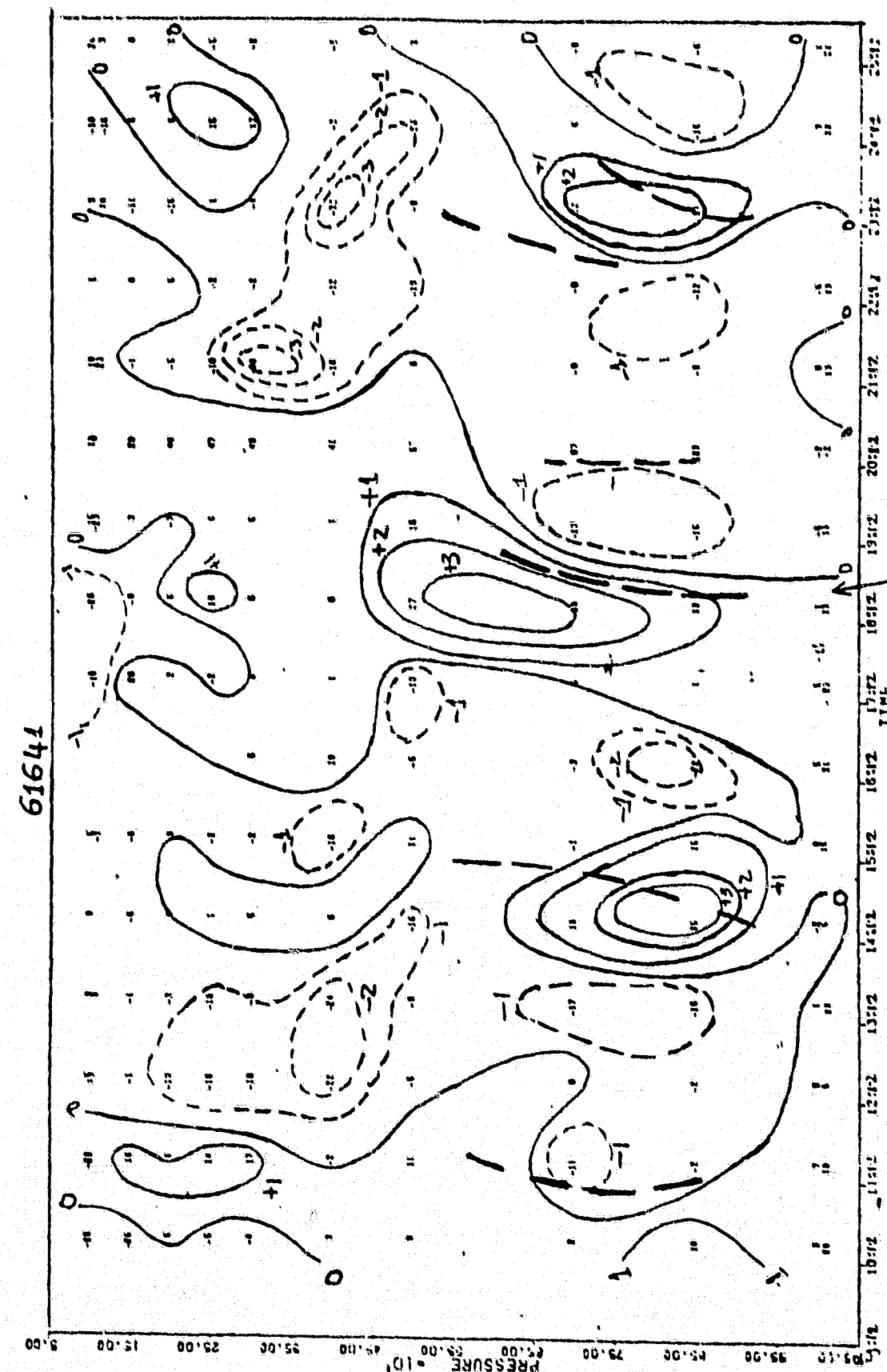

Fig. 3b. Temperature deviation time section for the DAKAR station: solid lines represente positive anormalies (1 c), dashed lines represente negative anormalies (1 c), heavy dashed lines represente the wave passages and the 16-19 July 1979 wave position is indicated by *

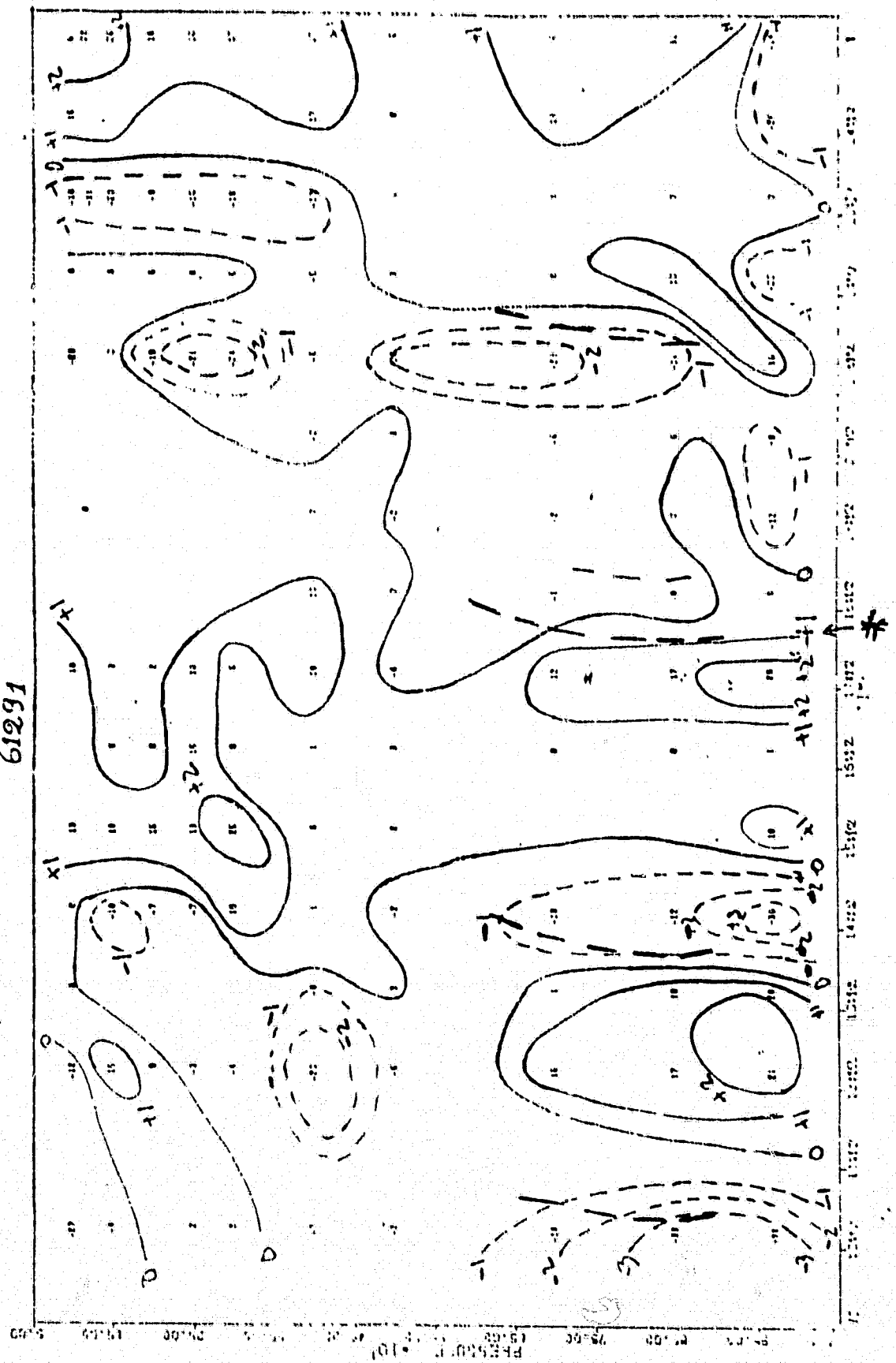

Fig. 4b. Same as Fig. 3b. except for BAMAKO station

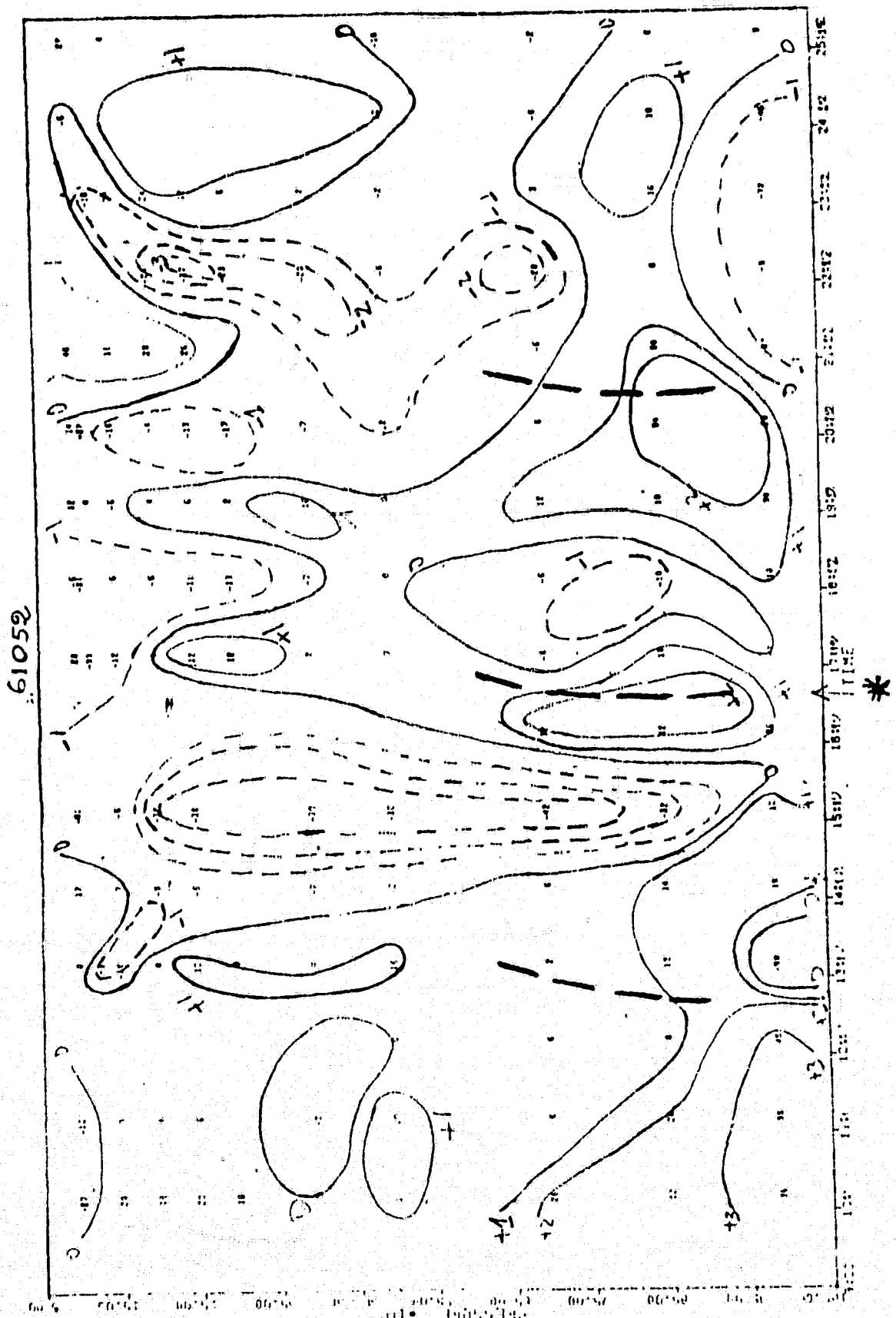

Fig. 5b. Same as Fig. 3b. except for NIAMEY station

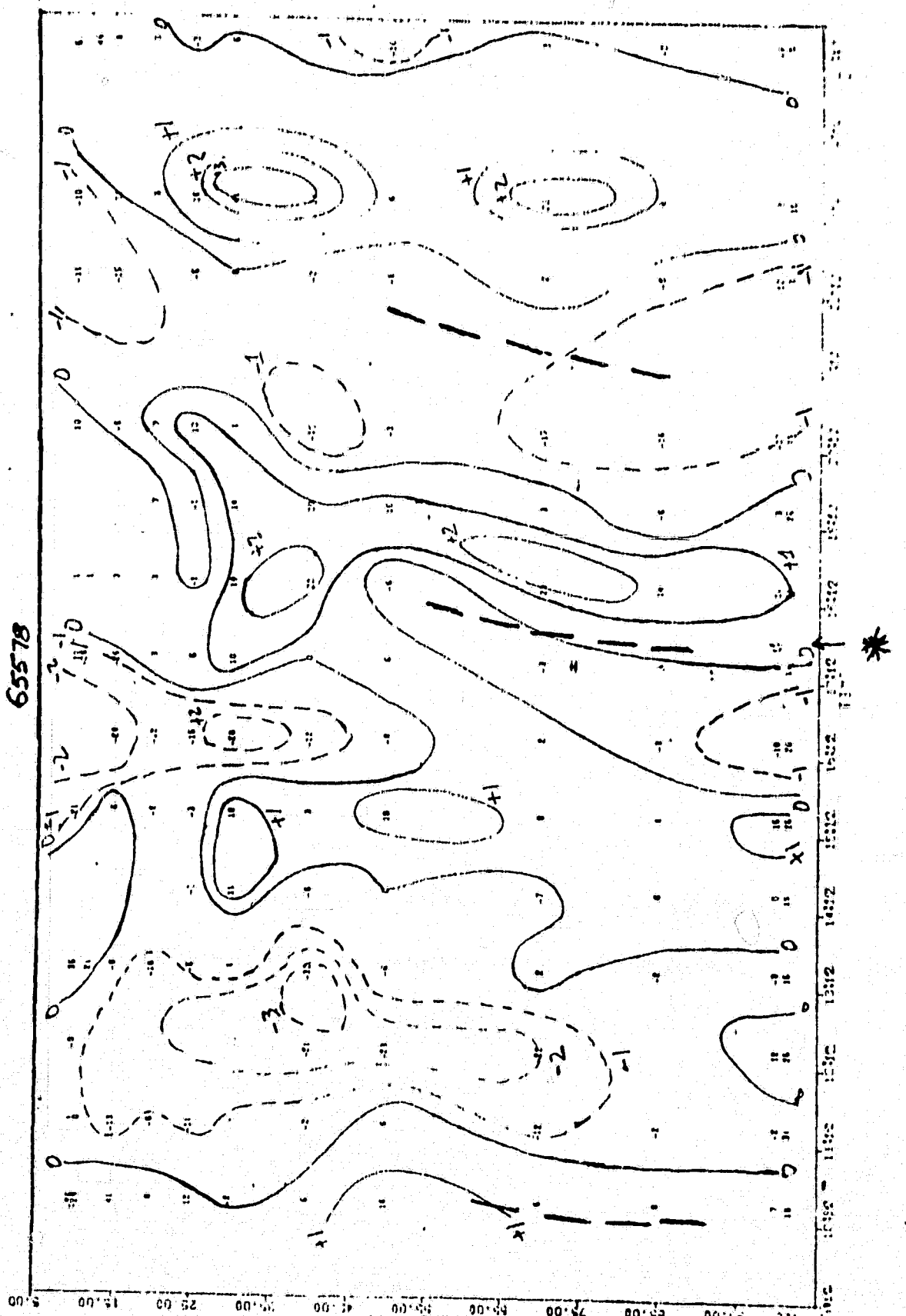

Fig. 6b. Same as Fig. 3b. except for ABIDJAN station

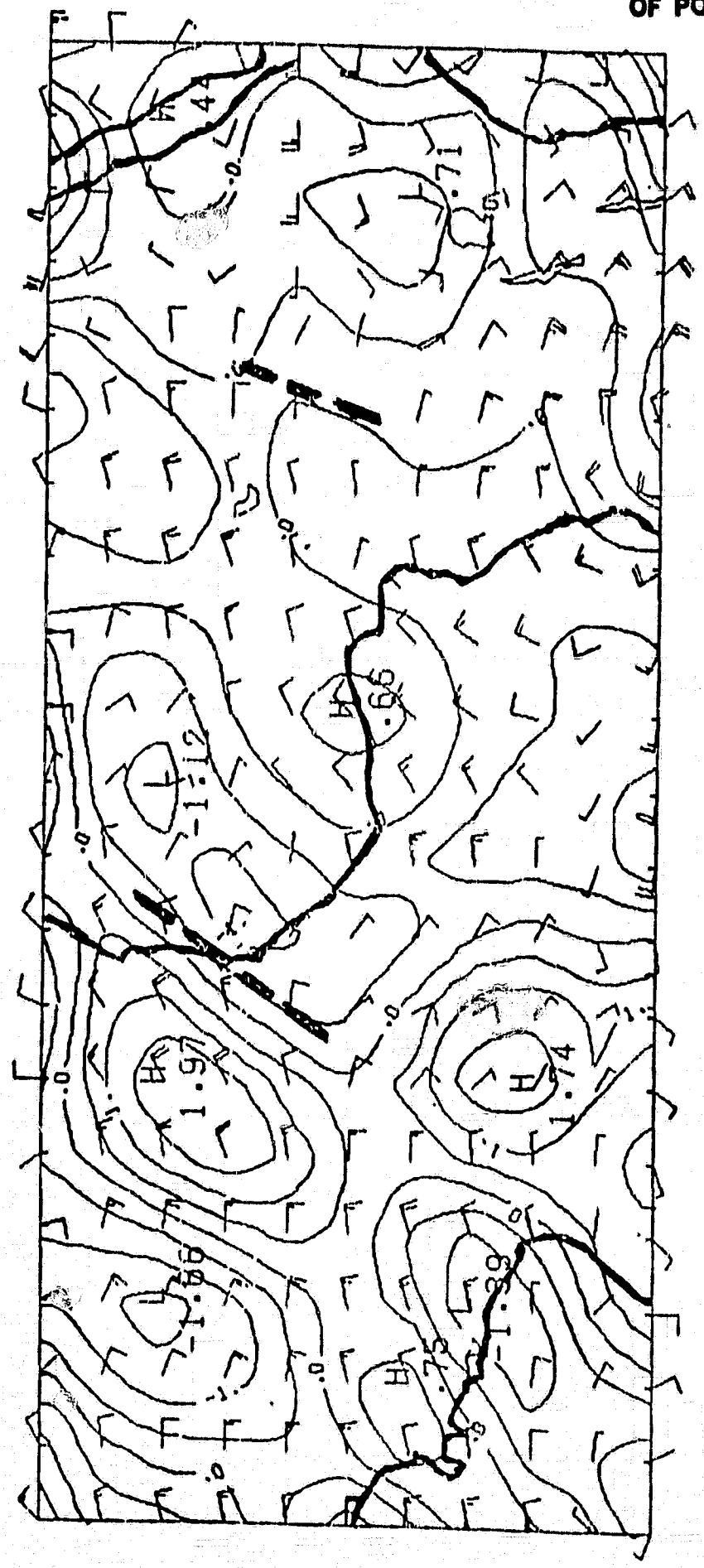

Fig. 7a. General circulation model results from Estoque et al. showing winds and temperature perturbations (solid lines) at 00 GMT, 17 July 1979.

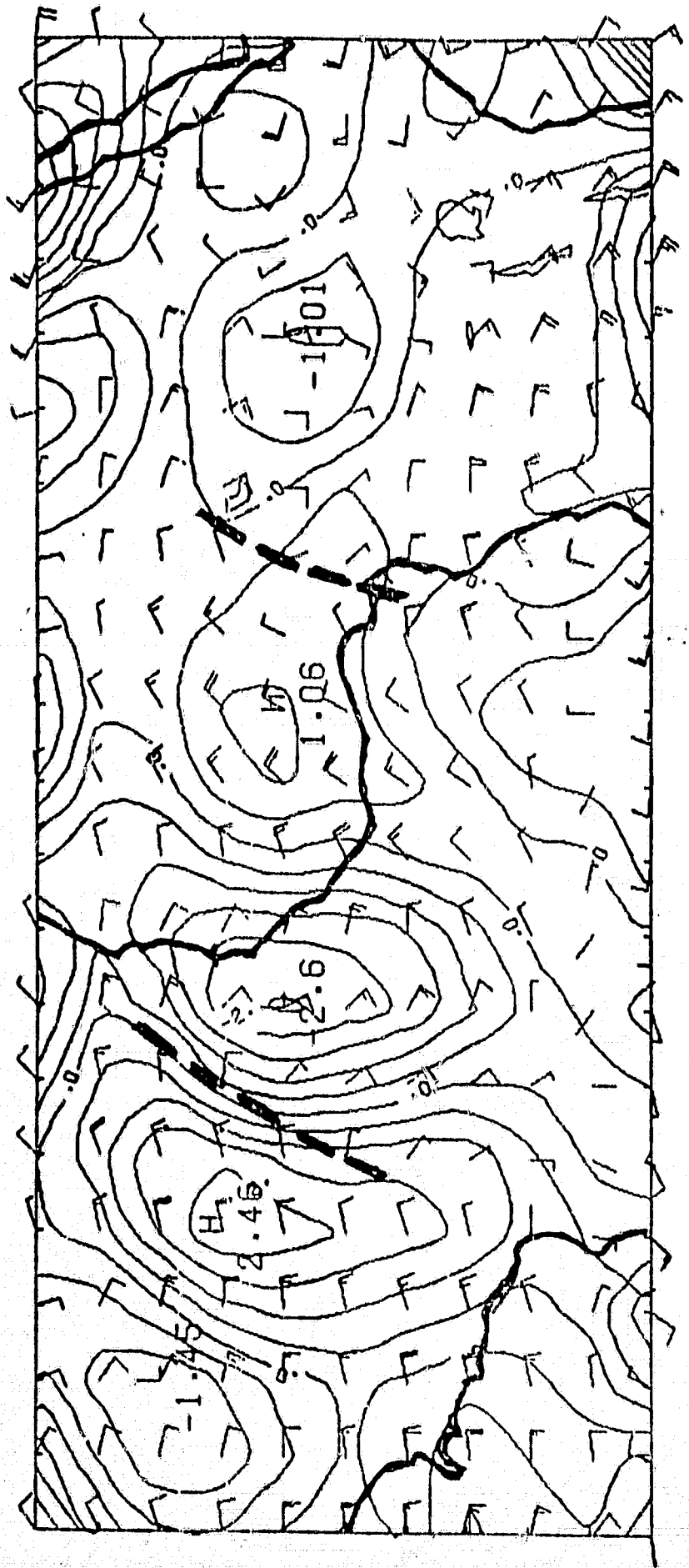

Fig. 7b. Same as Fig. 7a. except for 00 GMT, 18 July 1979

Fig. 8a. Satellite picture for 15 July at 11:55 GMT, arrow indicates the position of the wave.

Fig. 8b. Same as Fig. 8a except for 16 July at 11:55 GMT.

Fig. 8c. Same as Fig. 8a except for 17 July at 11:55 GMT.

Fig. 8d. Same as Fig. 8a except for 18 July 1979 at 11:55 GMT.

Fig. 8e. Same as Fig. 8a except for 19 July 1979 at 11:55 GMT.

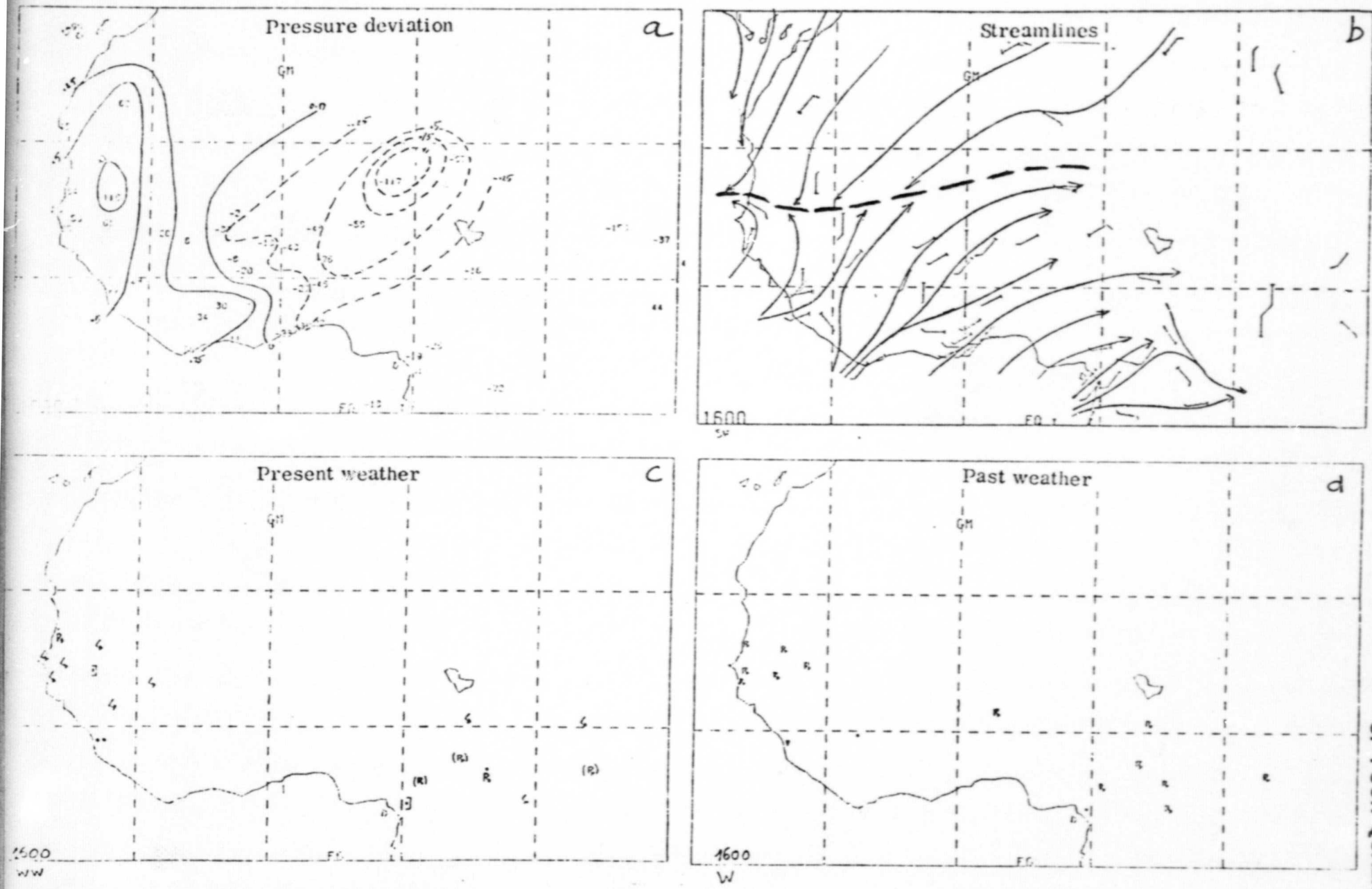

Fig. 9. Surface analyses at 00 GMT on 16 July 1979: a) pressure deviation, b) streamlines, c) present weather, d) past weather, e) cloud coverage, f) 24hr precipitation, g) 24hr temperature change, h) 24hr dew point depression change, i) 24hr pressure change, j) 6hr pressure change.

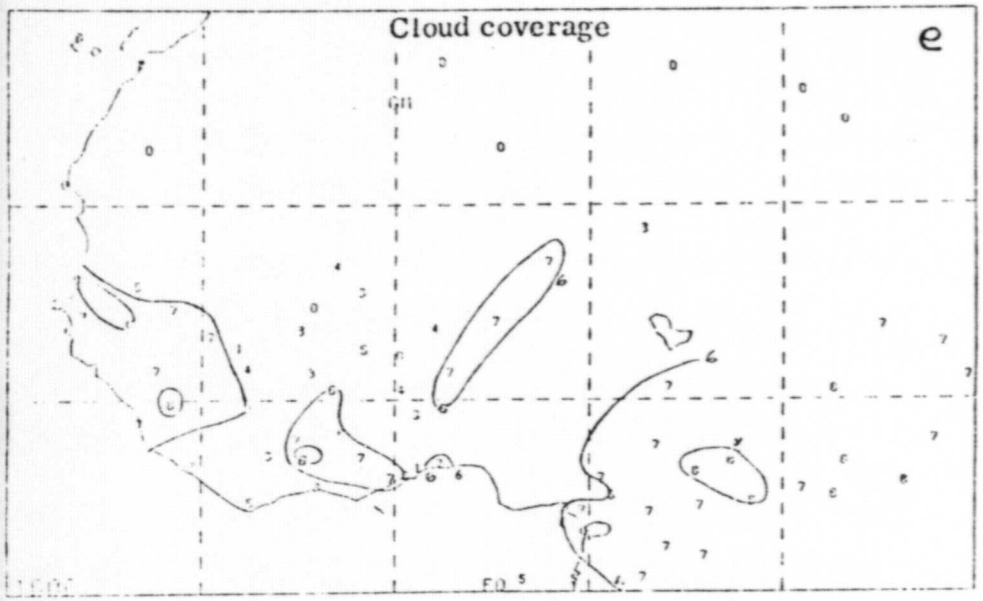

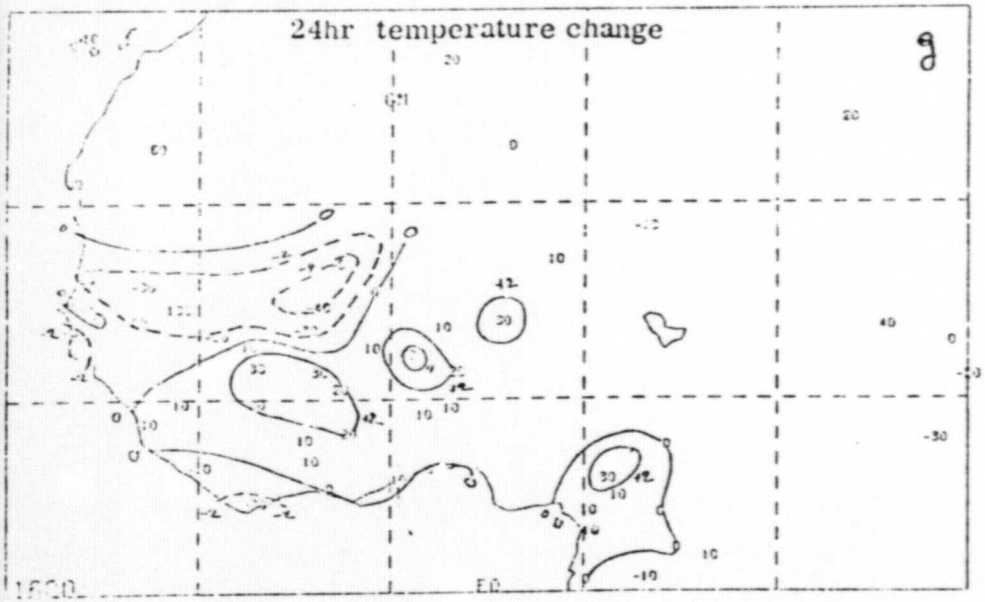

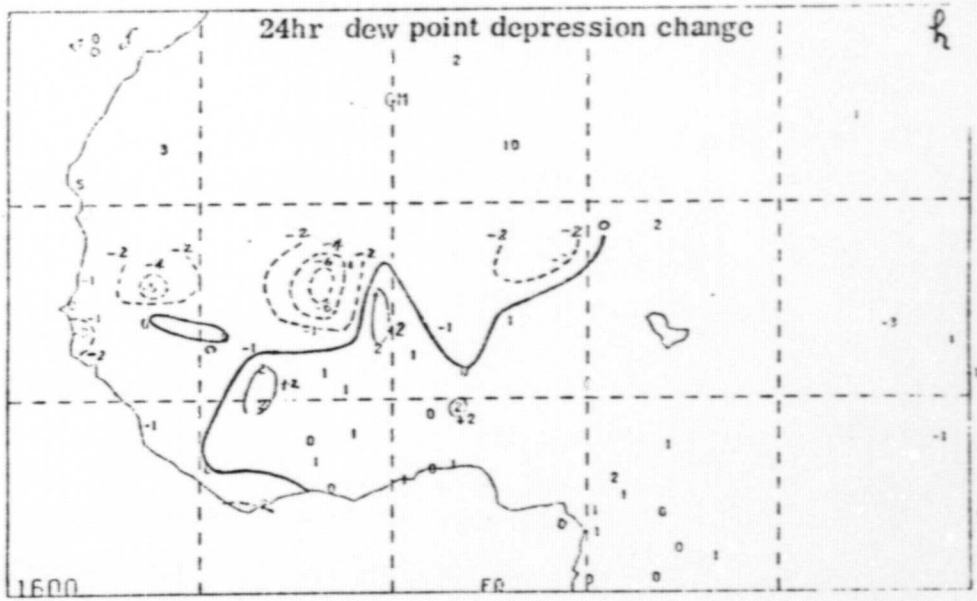

Fig. 9. continue

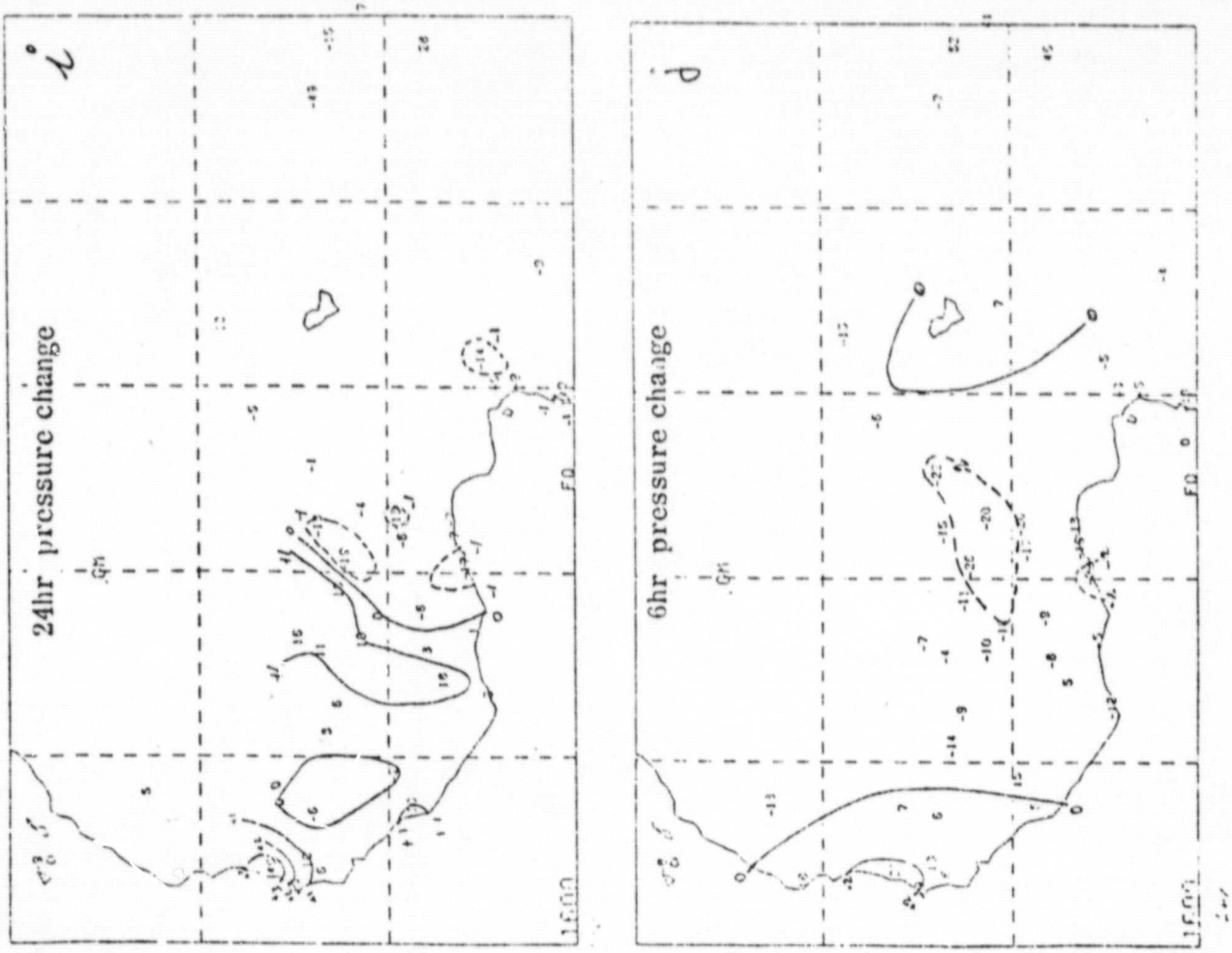

Fig. 9. continue

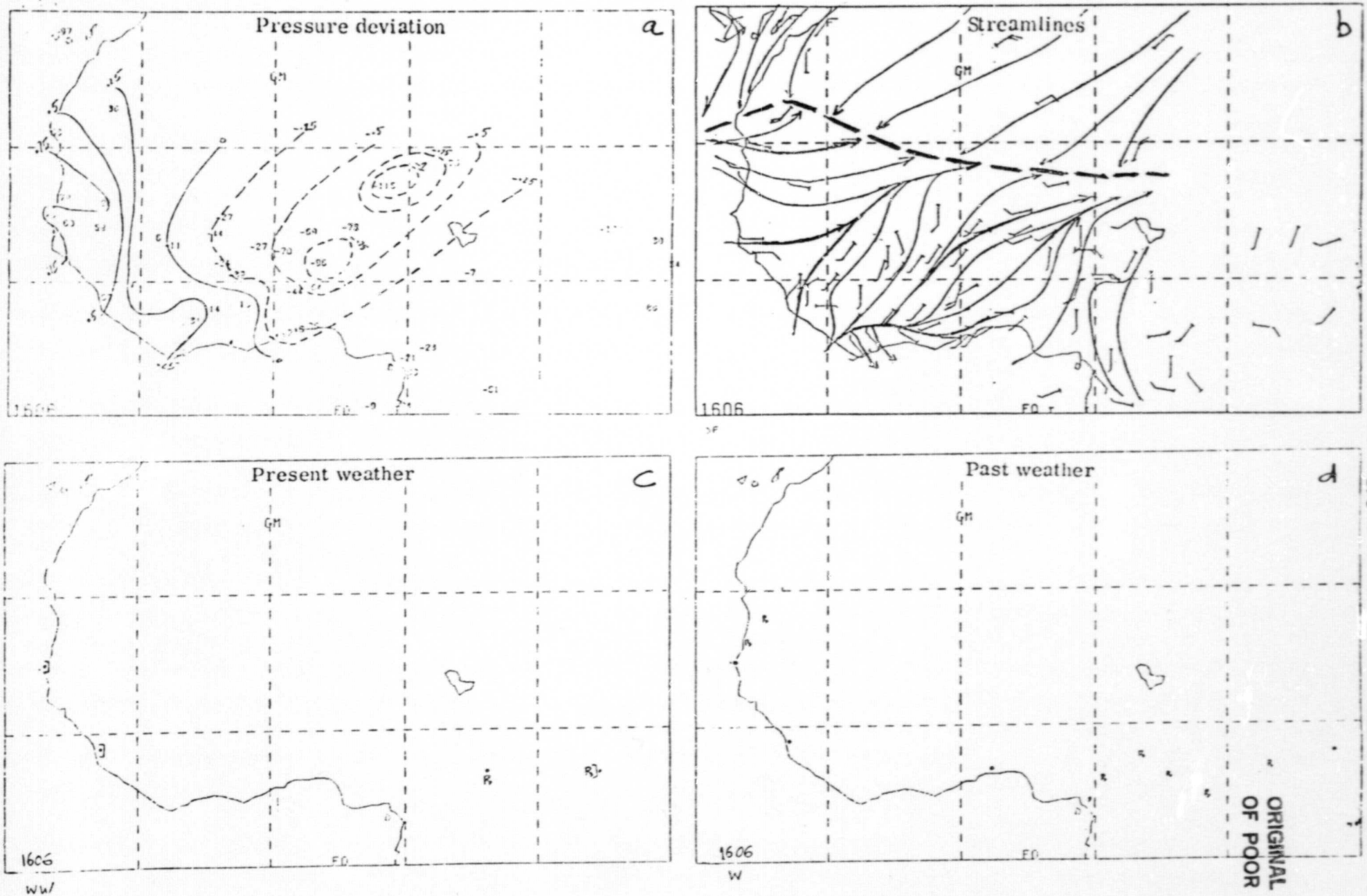

Fig. 10. Same as Fig. 9. except for 06 GMT, 16 July 1979.

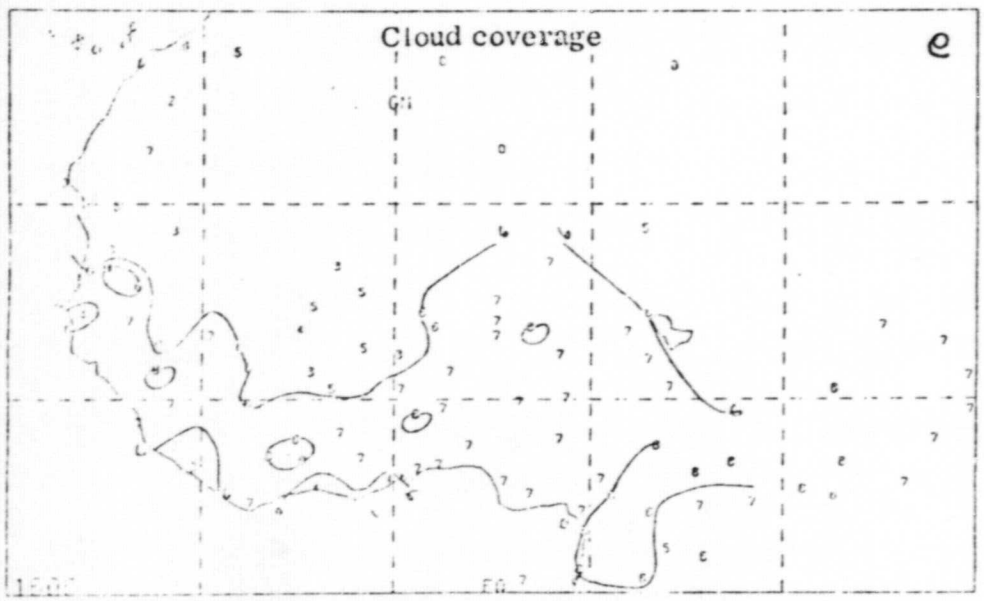

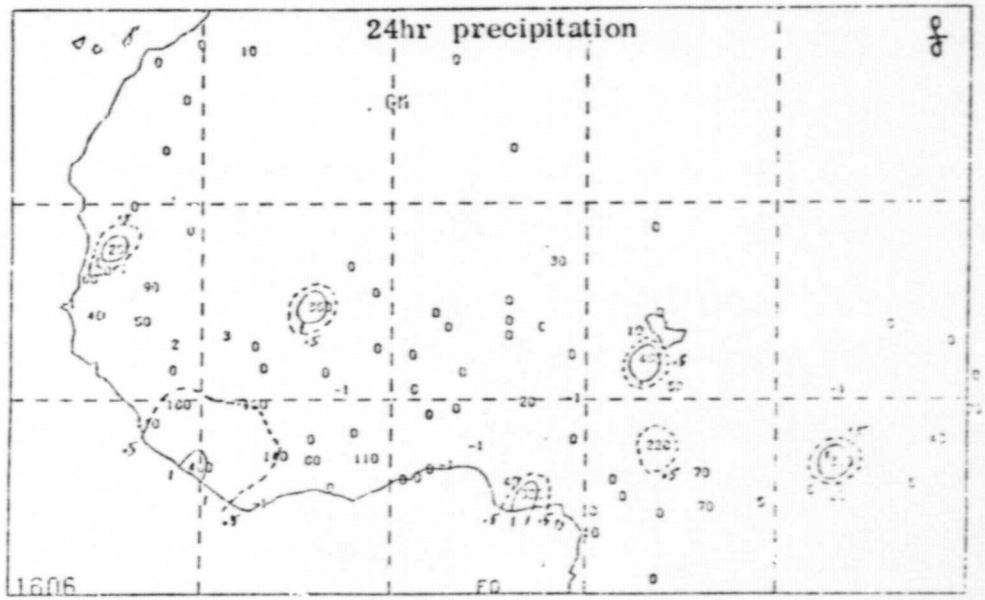

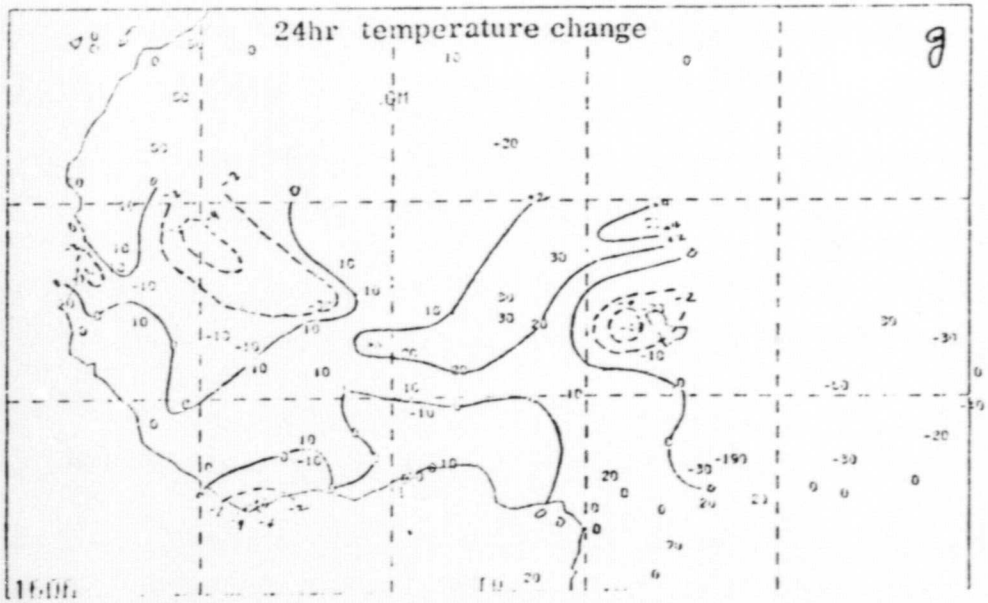

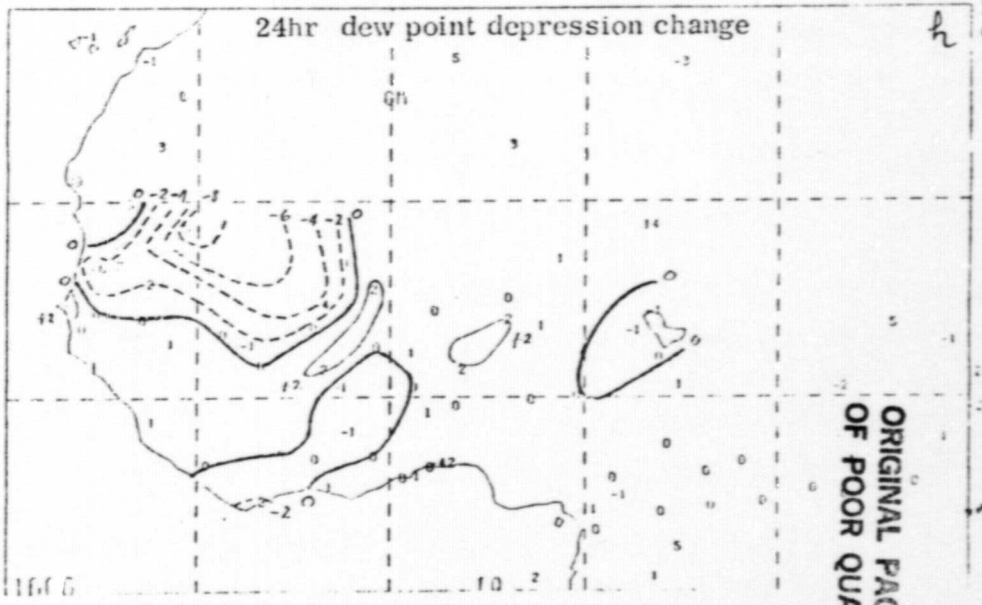

Fig. 10. continue

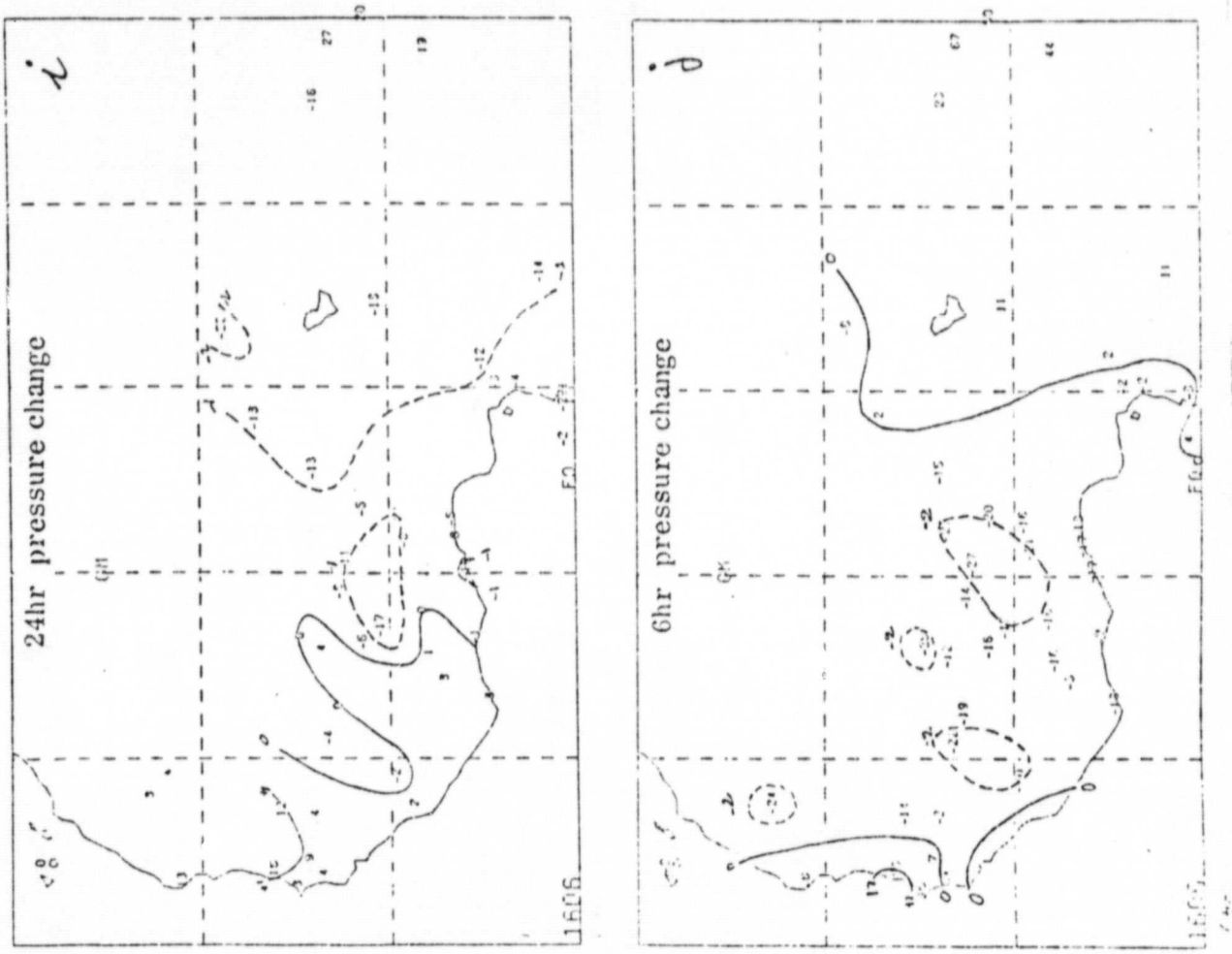

Fig. 10. continue

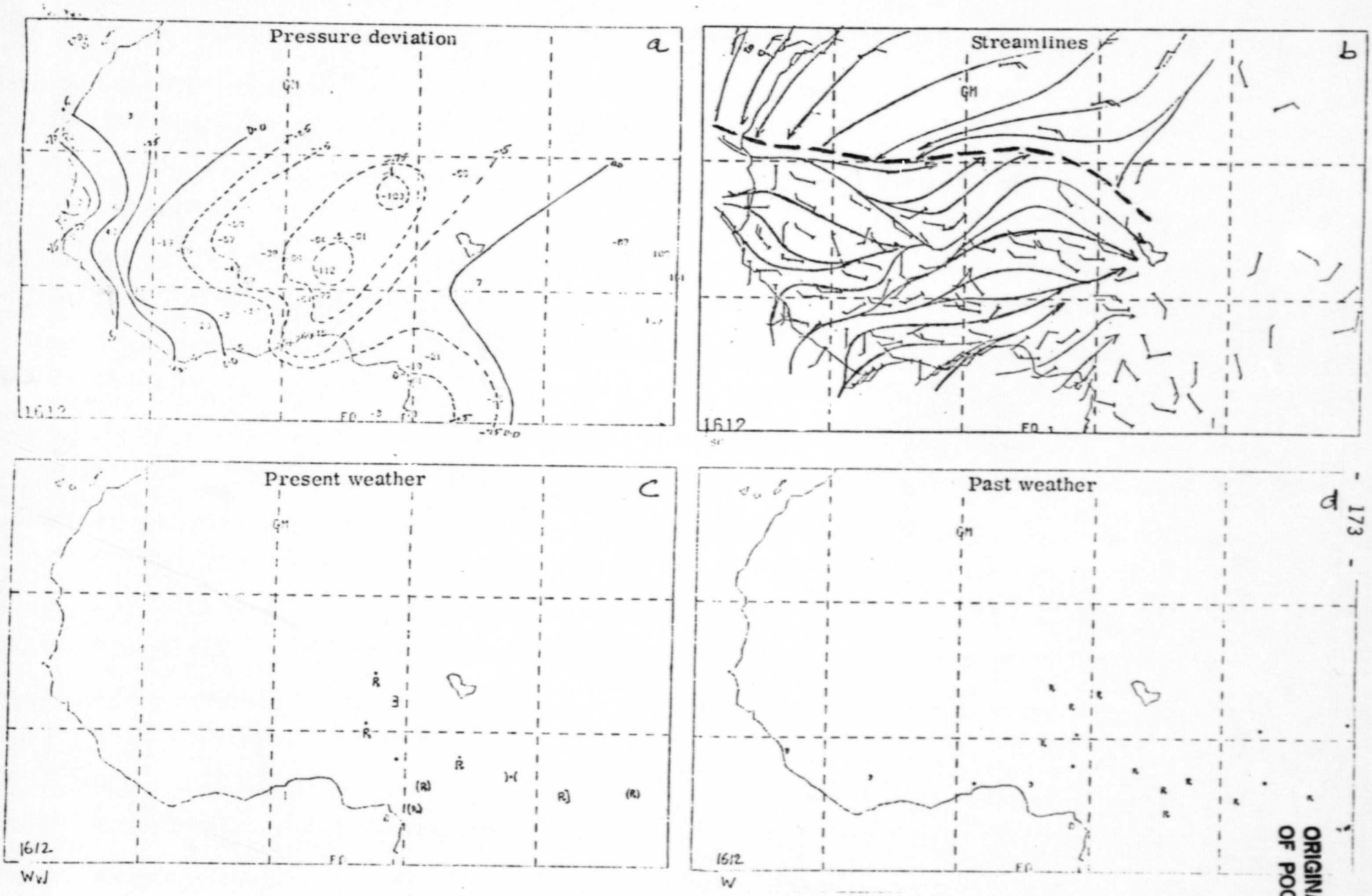

Fig. 11. Same as Fig. 9. except for 12 GMT, 16 July 1979.

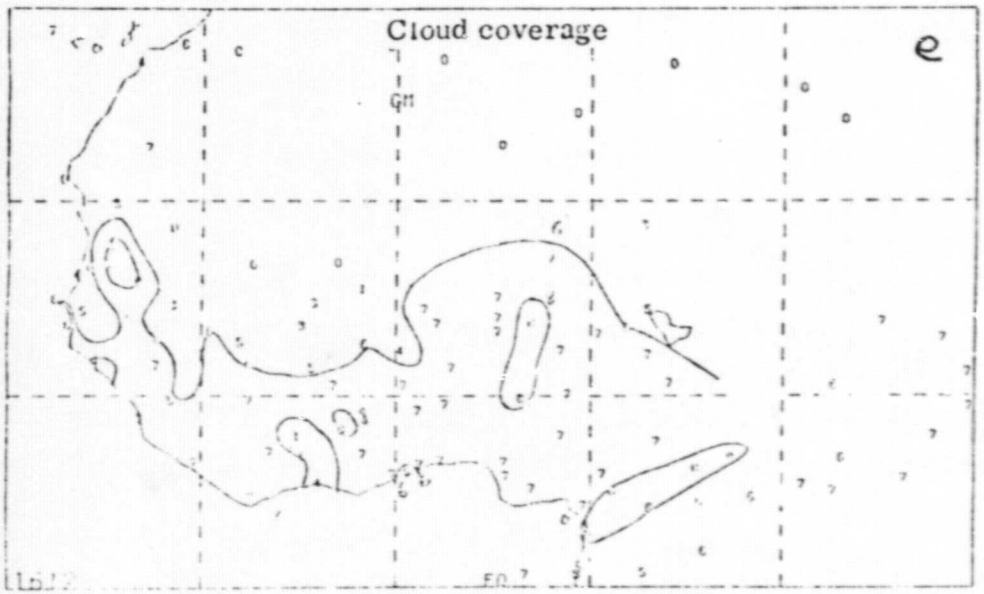

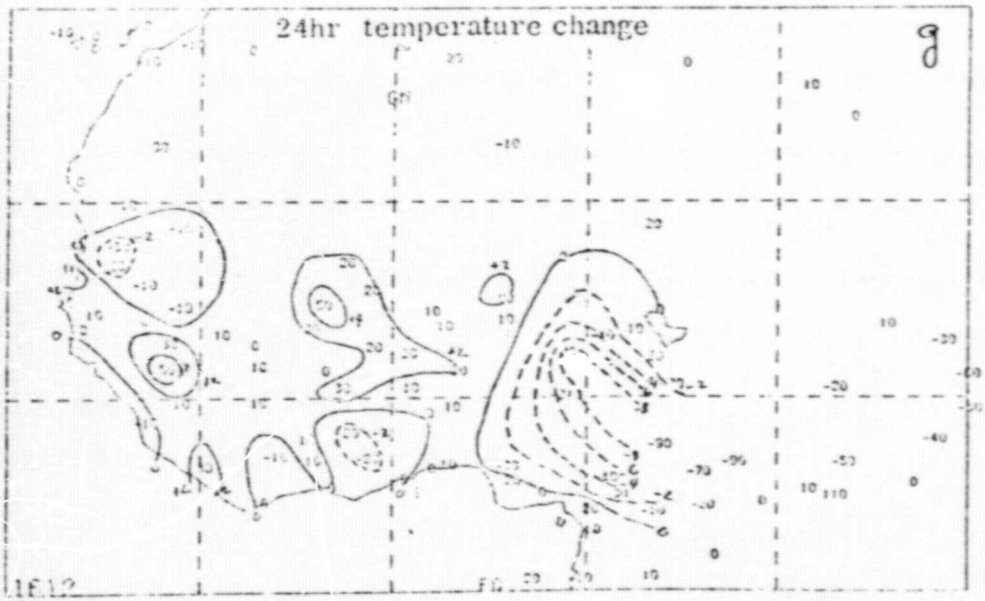

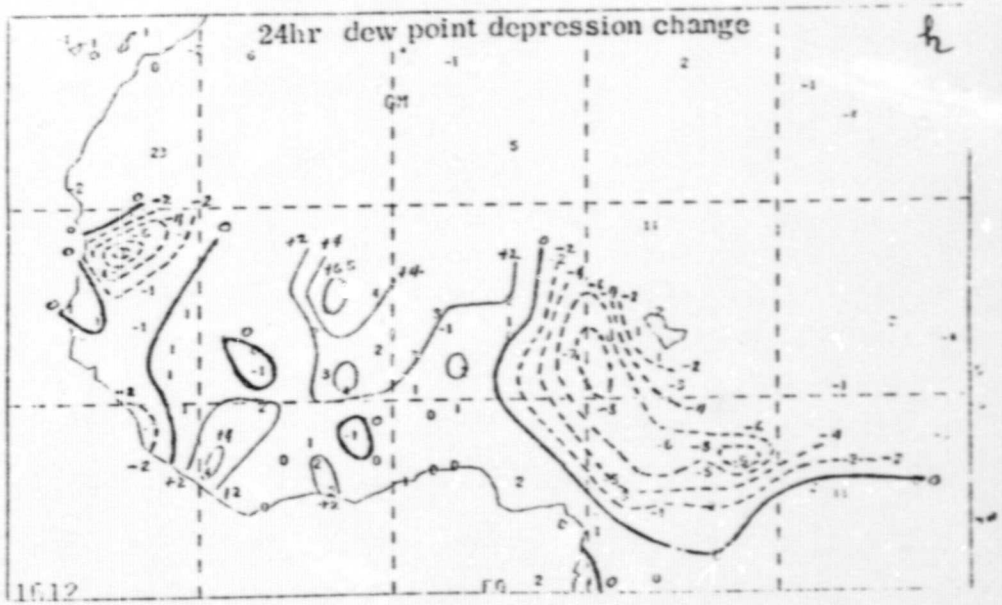

Fig. 11. continue

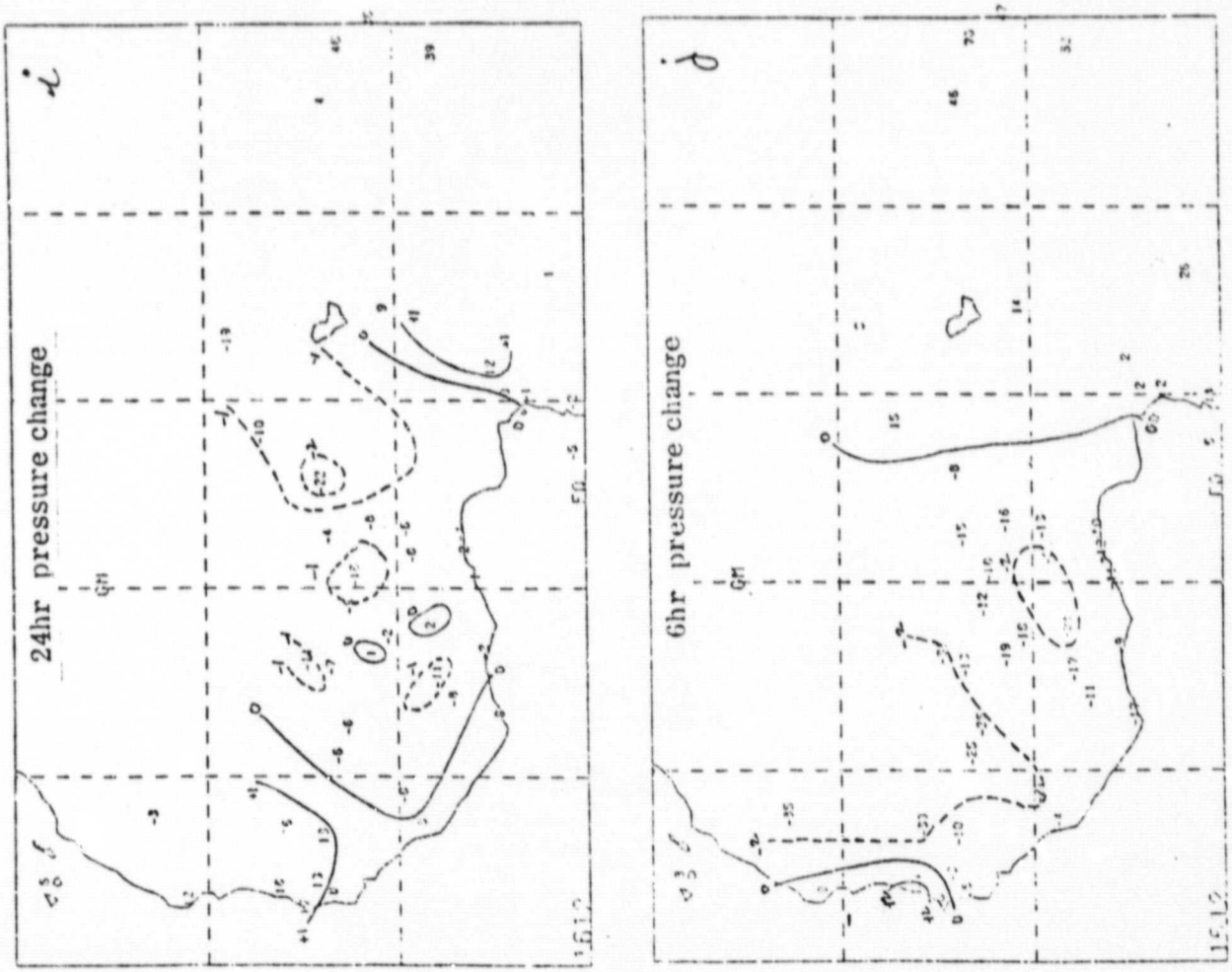

Fig. 11. continue

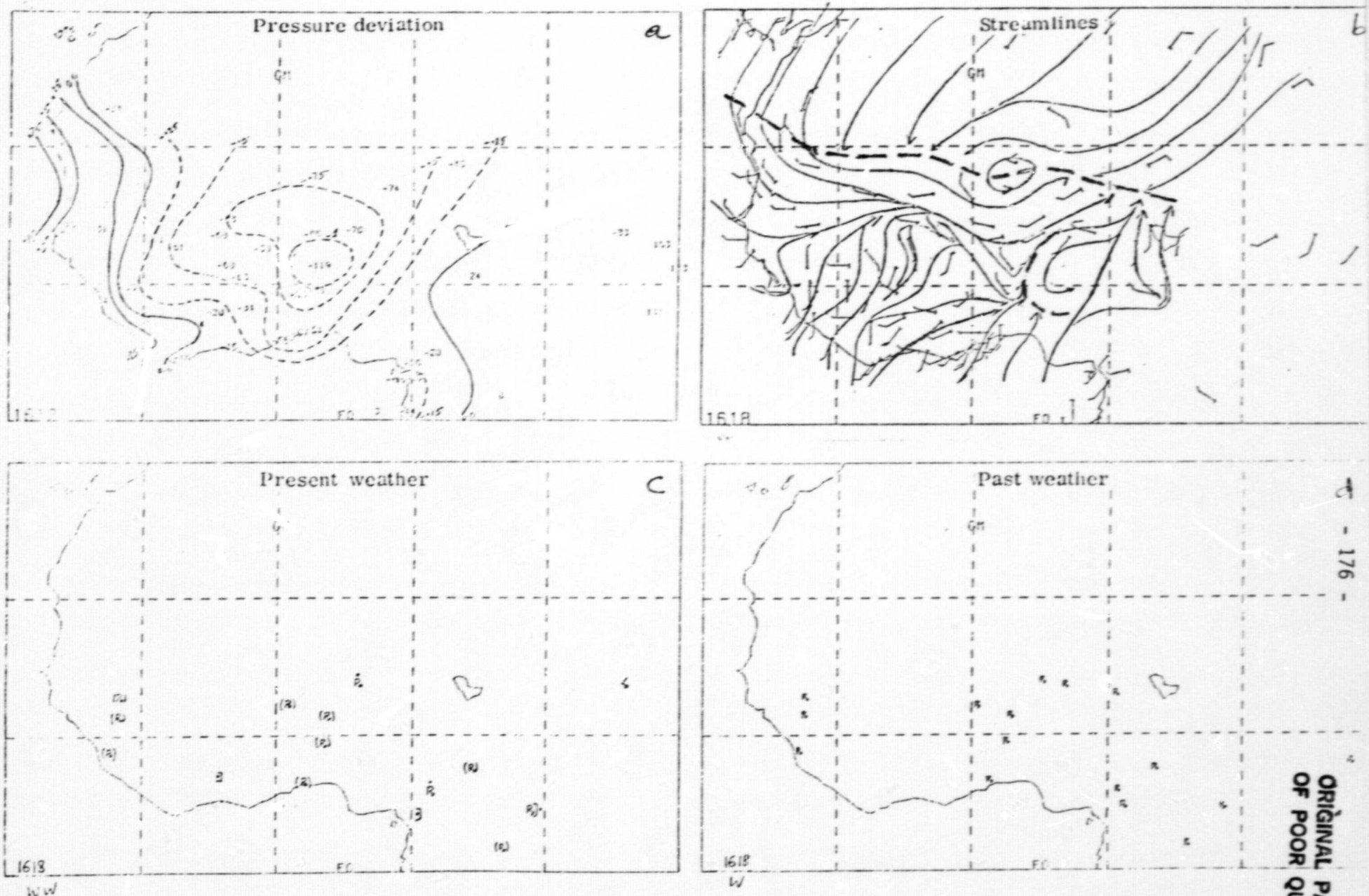

Fig. 12. Same as Fig. 9. except for 18 GMT, 16 July 1979.

Fig. 12. continue

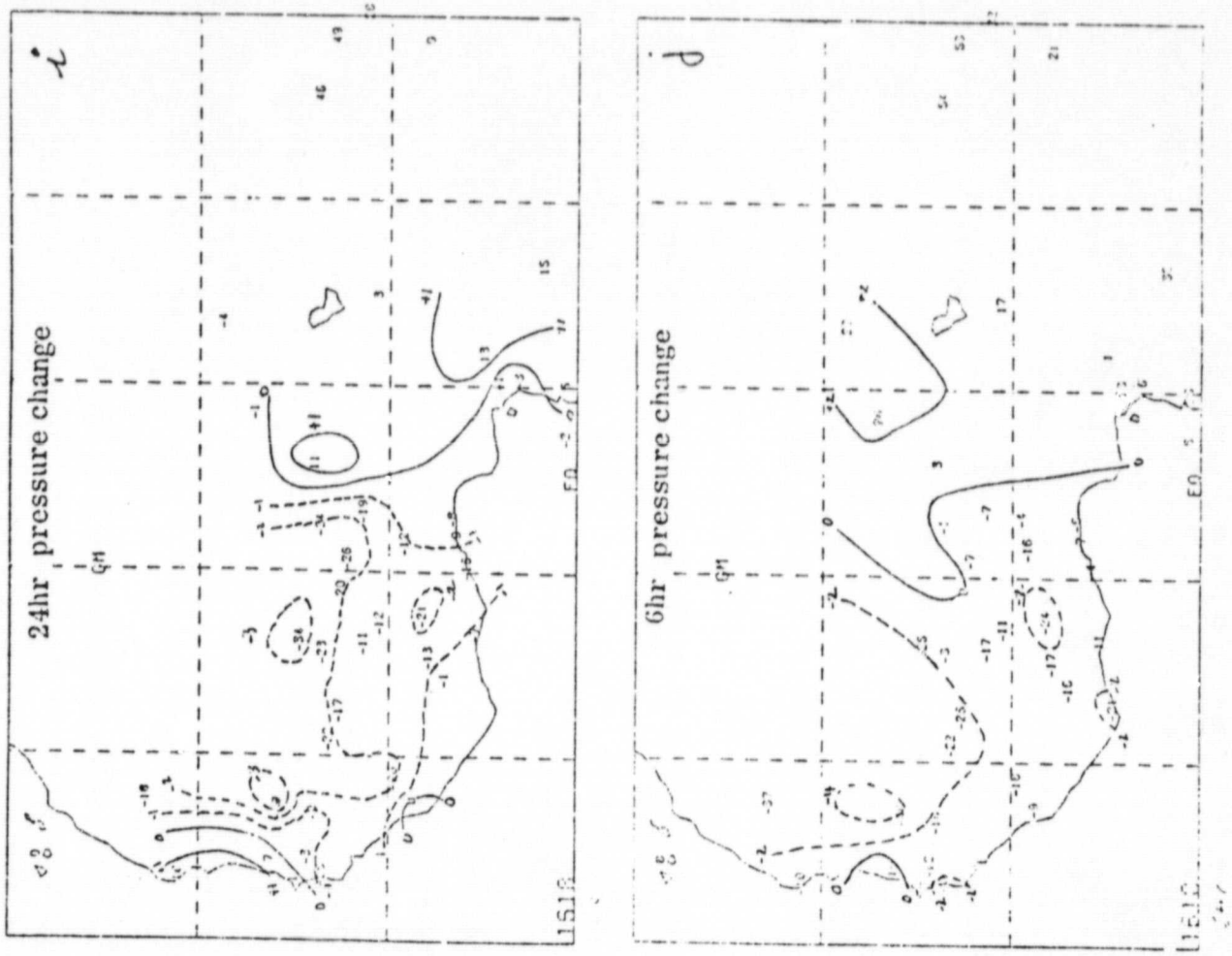

Fig. 12. continue

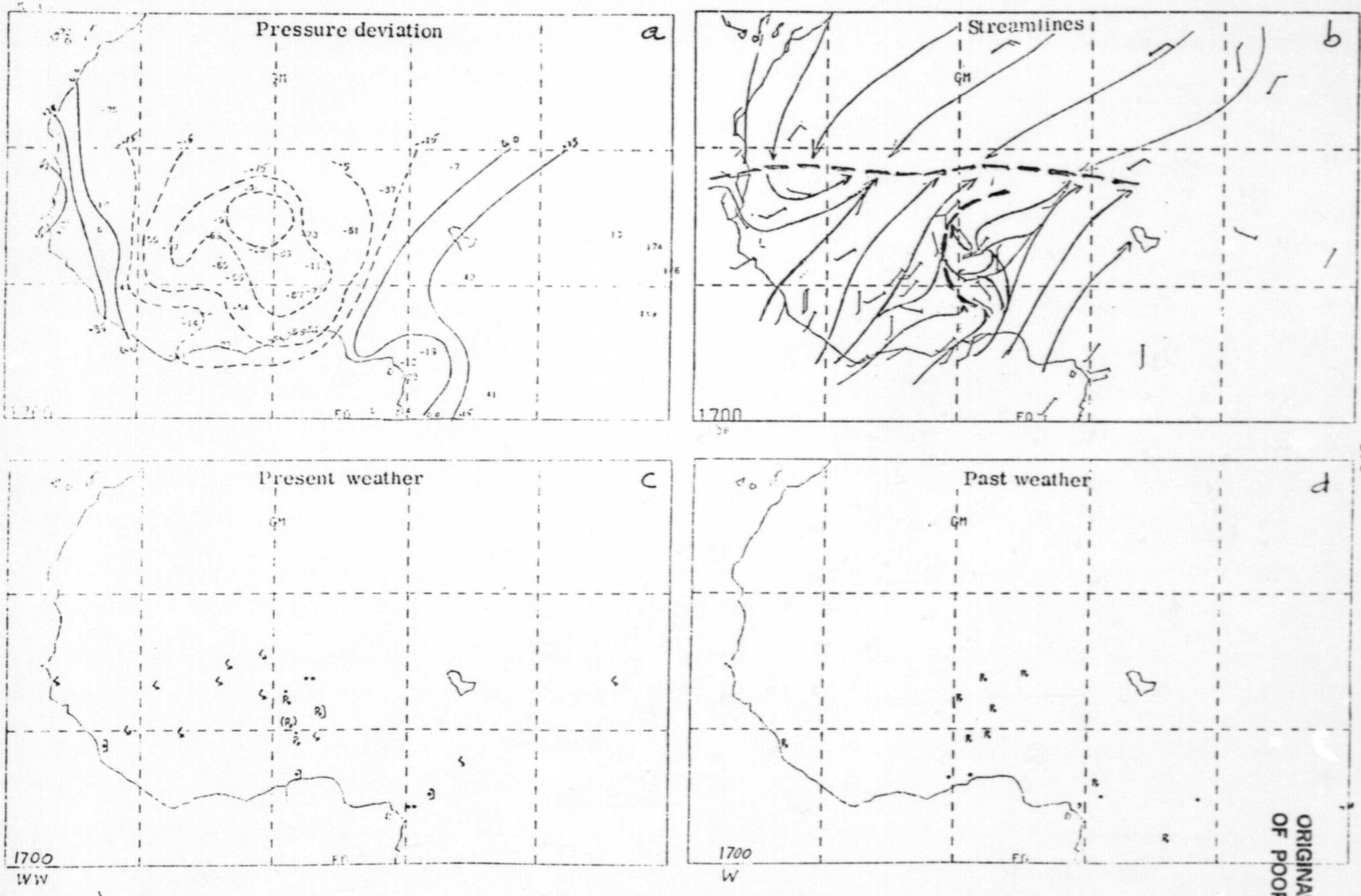

Fig. 13. Same as Fig. 9. except for 00 GMT, 17 July 1979.

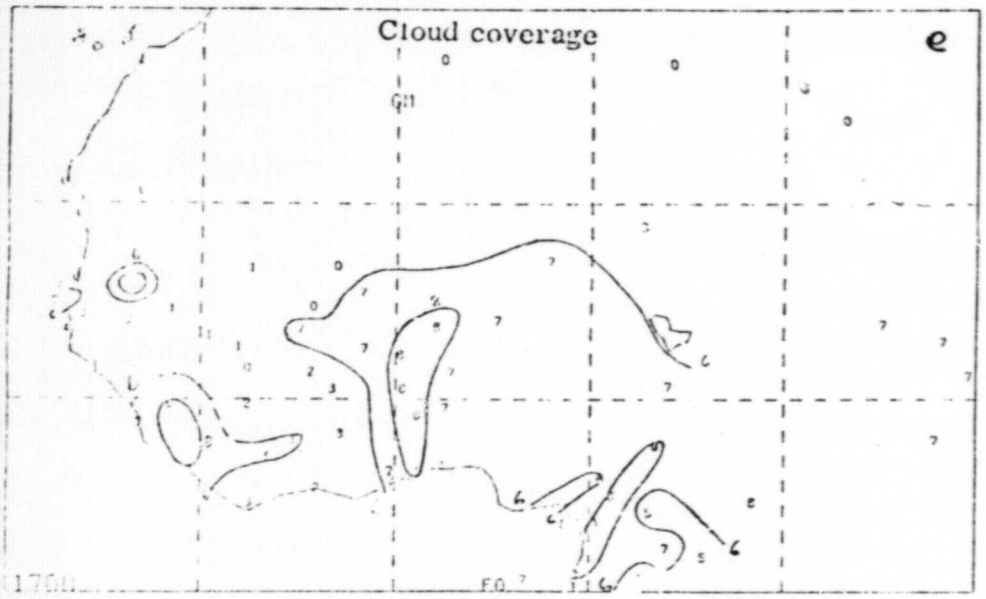

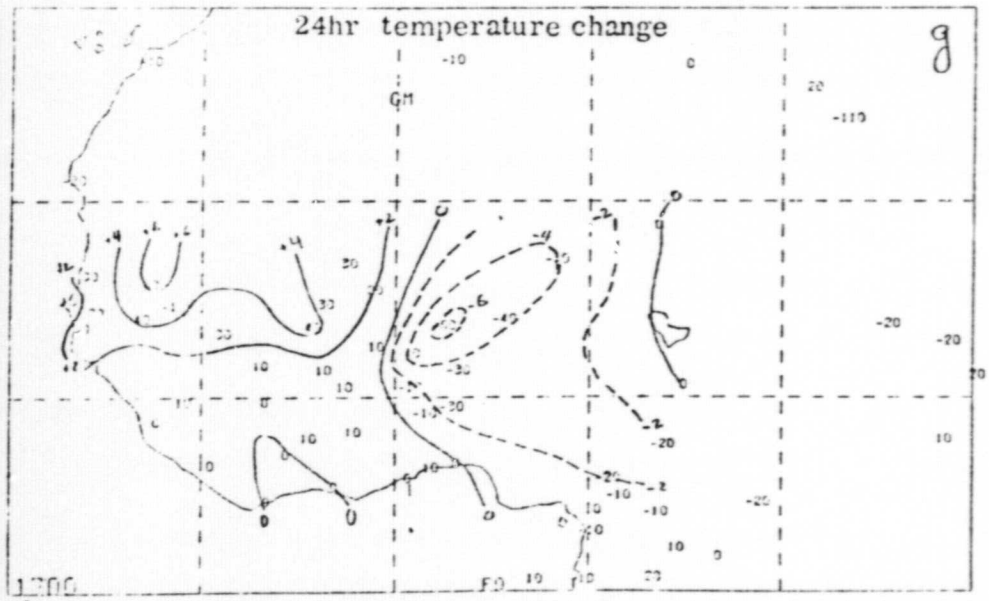

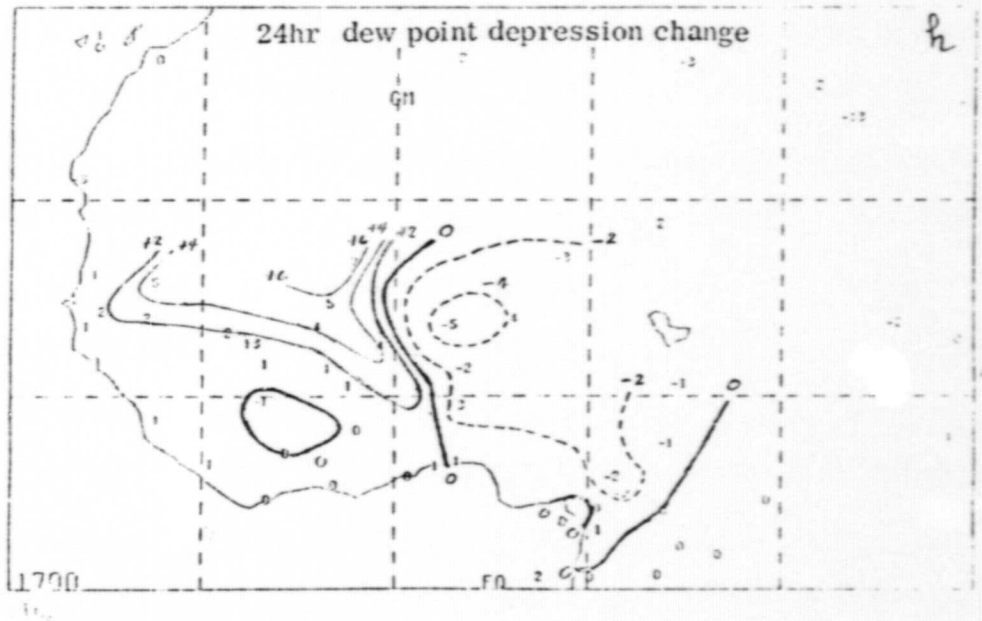

Fig. 13. continue

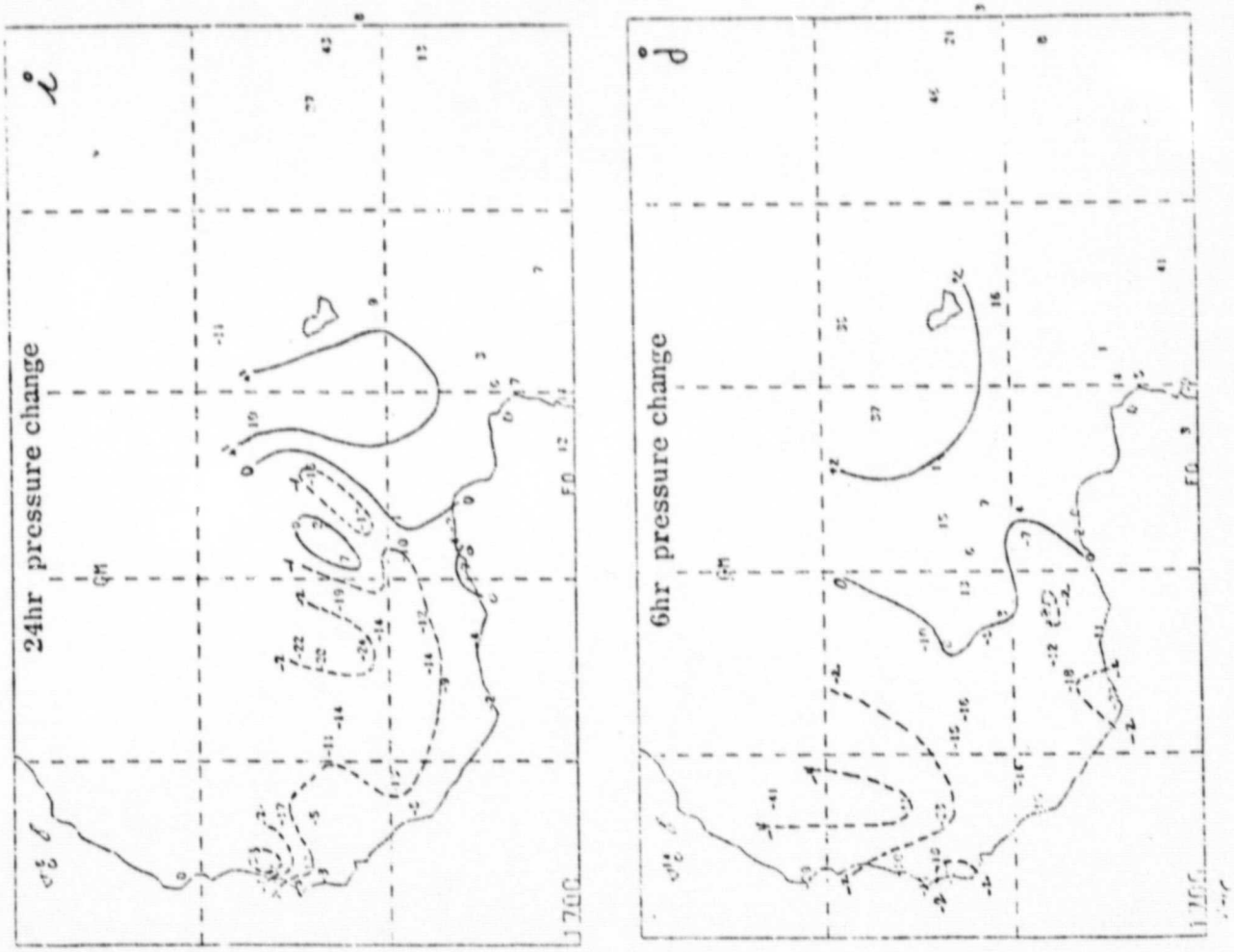

Fig. 13. continue

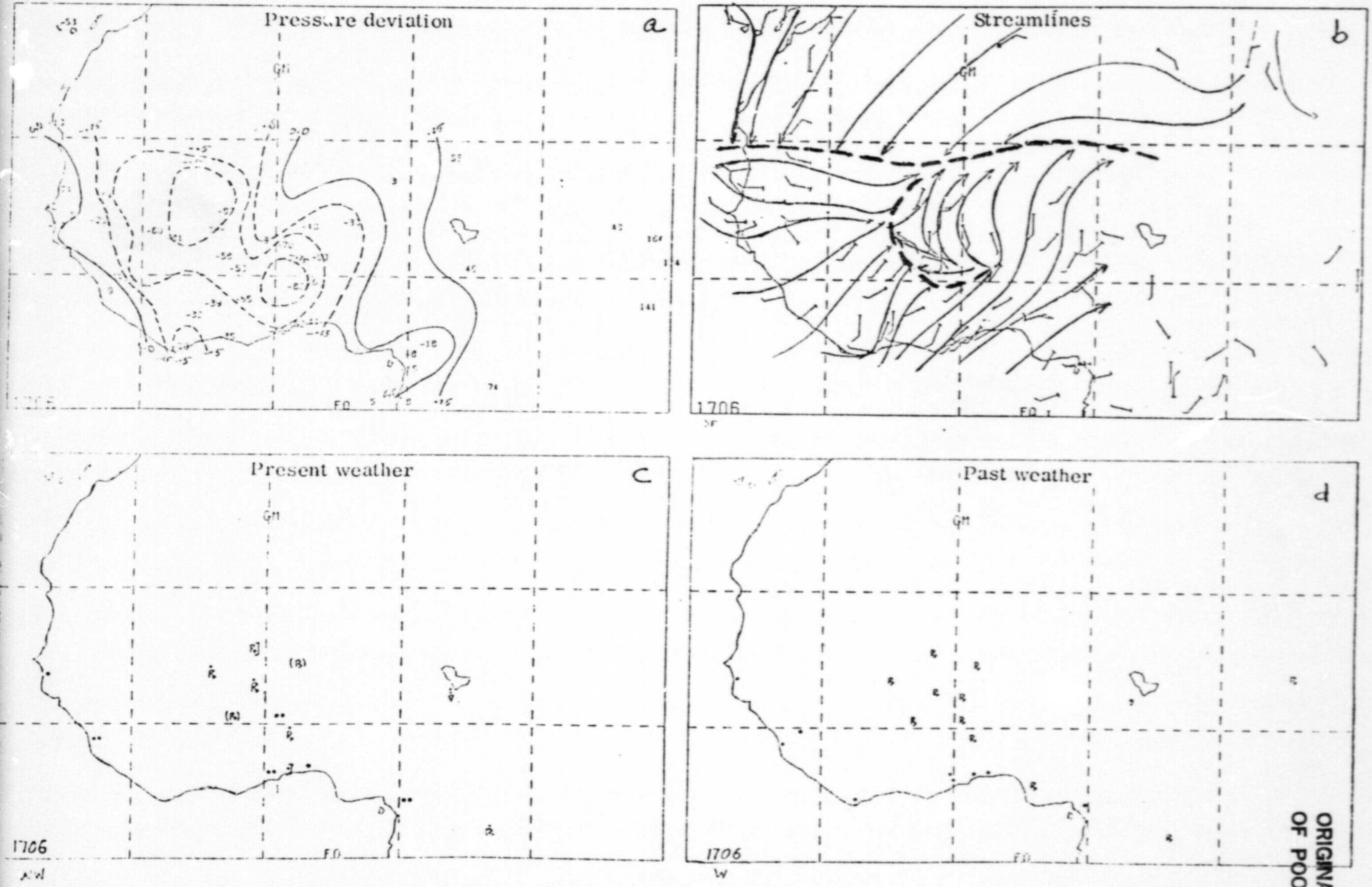

Fig. 14. Same as Fig. 9. except for 06 GMT, 17 July 1979.

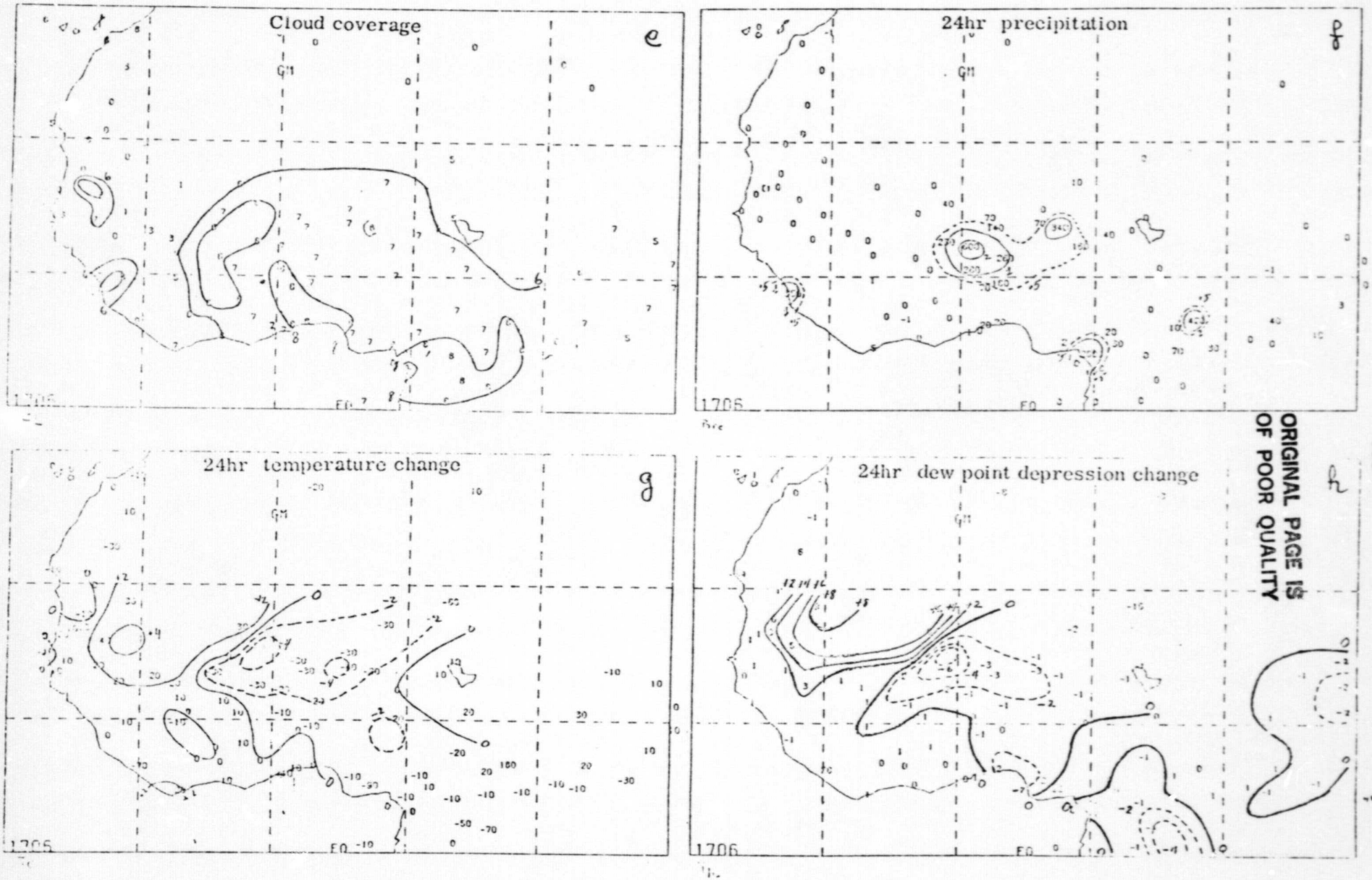

Fig. 14. continue

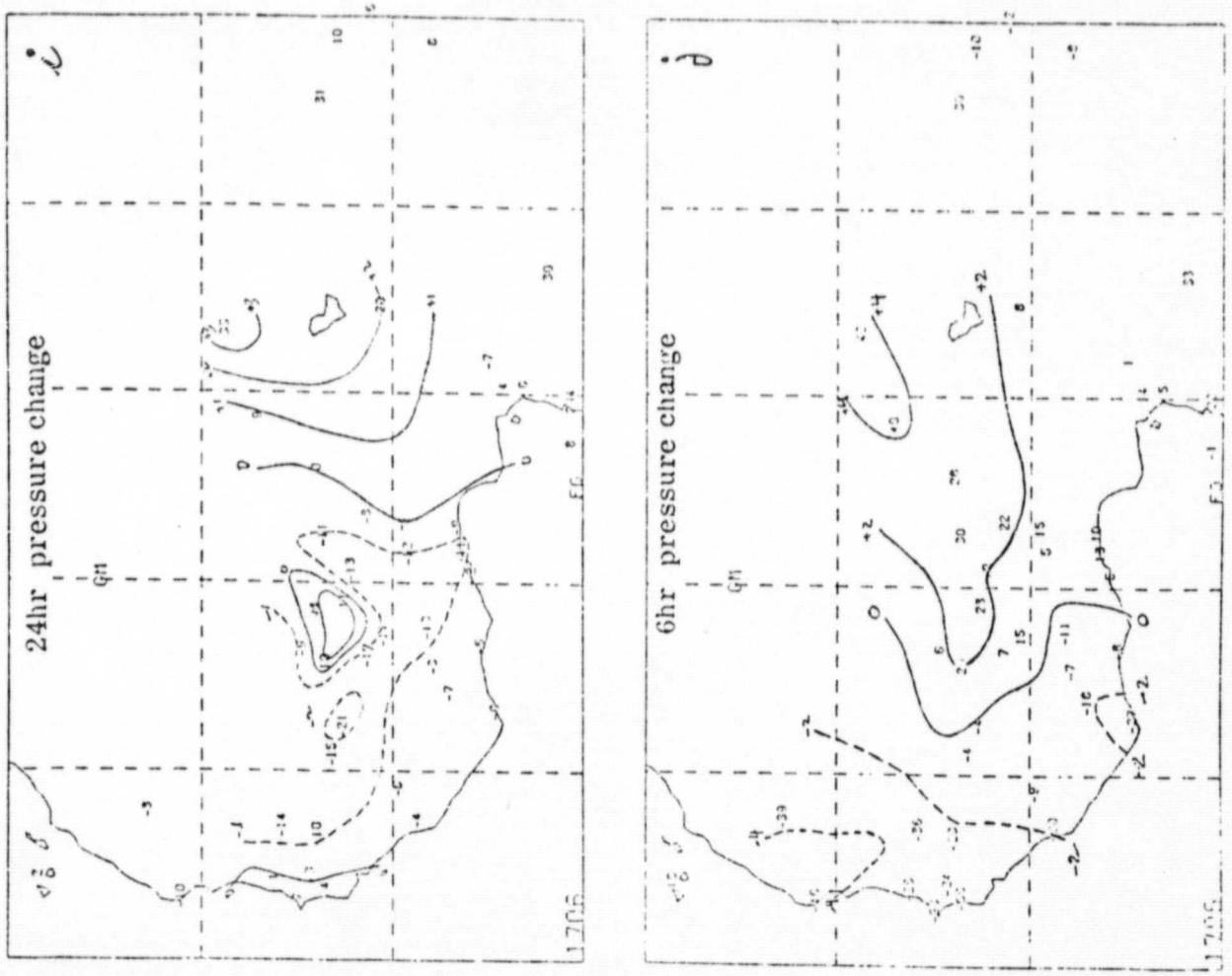

Fig. 14. continue

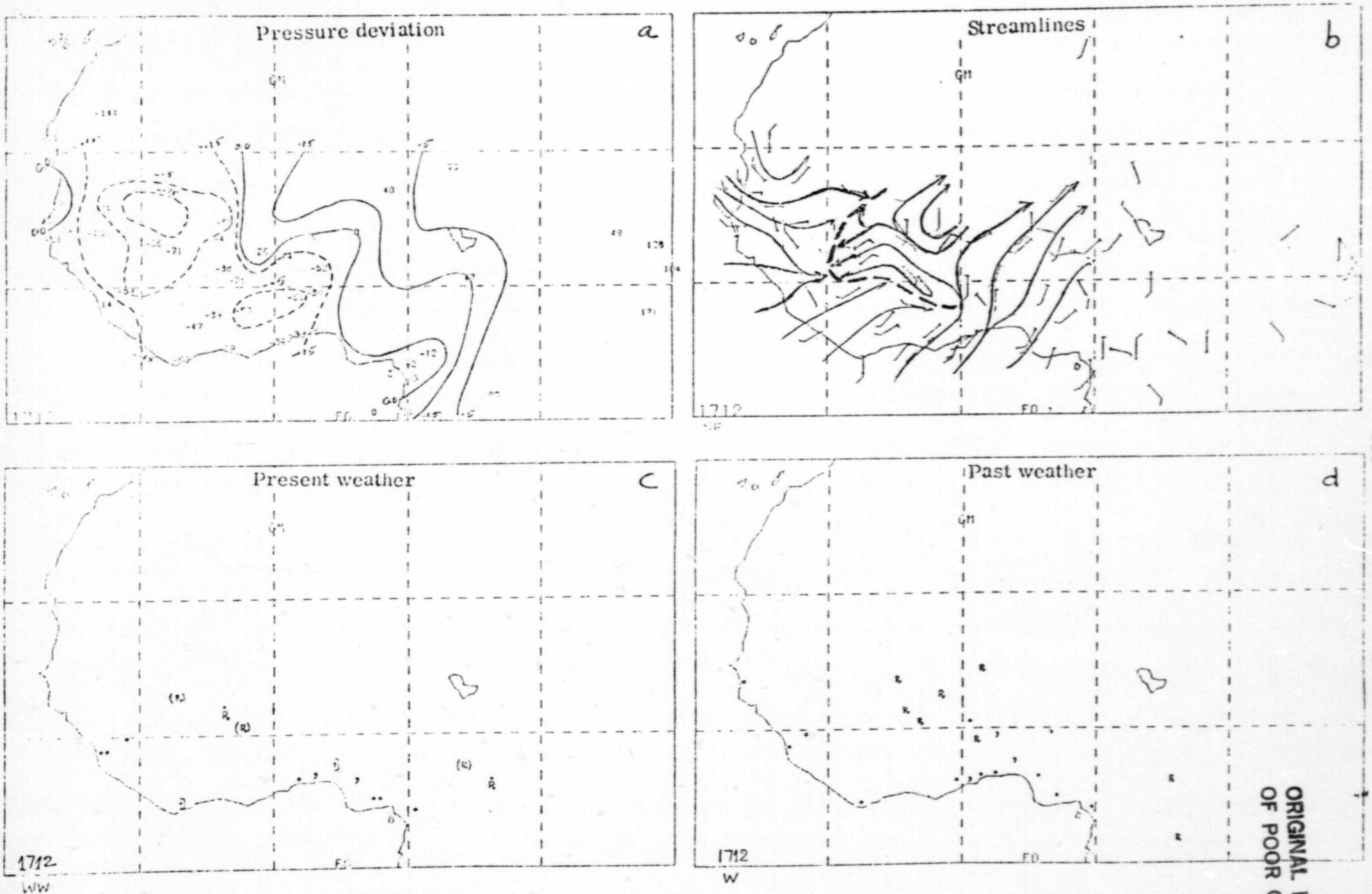

Fig. 15. Same as Fig. 9. except for 12 GMT, 17 July 1979.

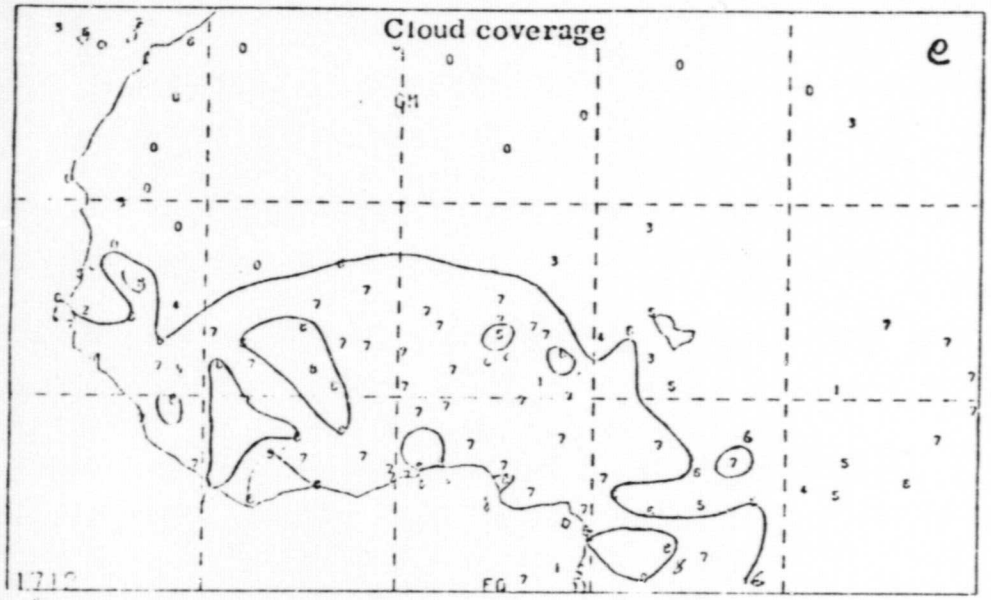

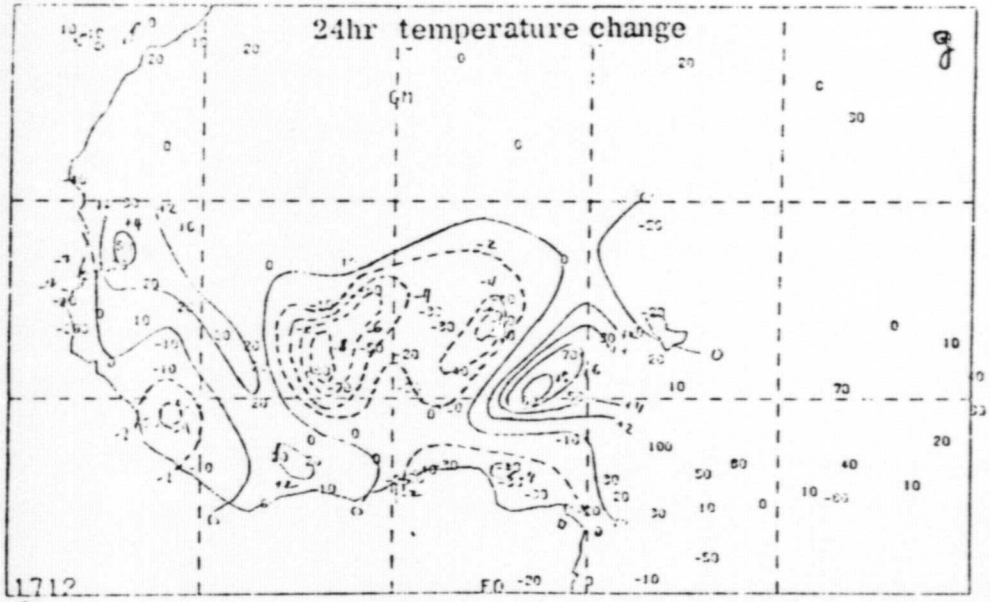

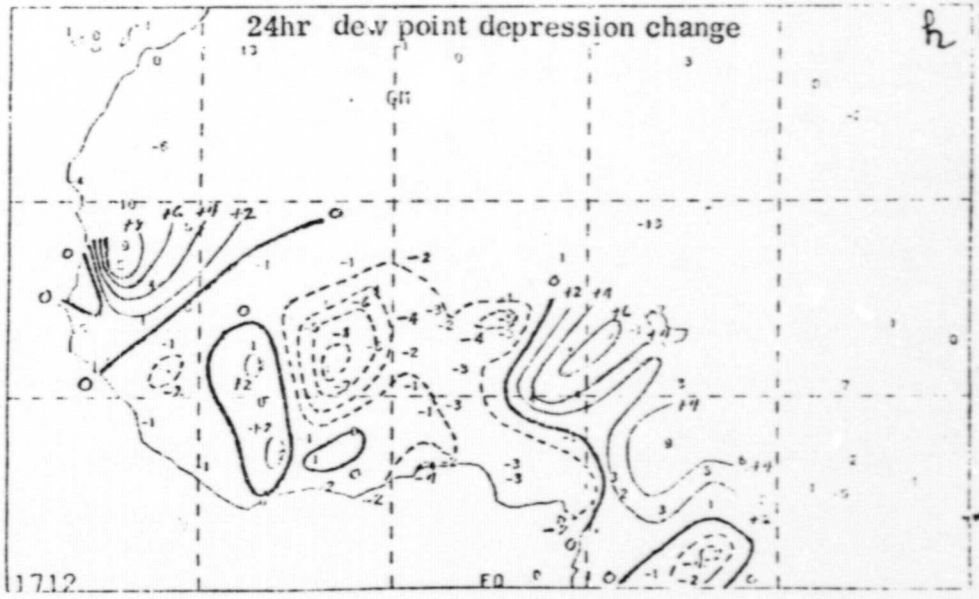

Fig. 15. continue

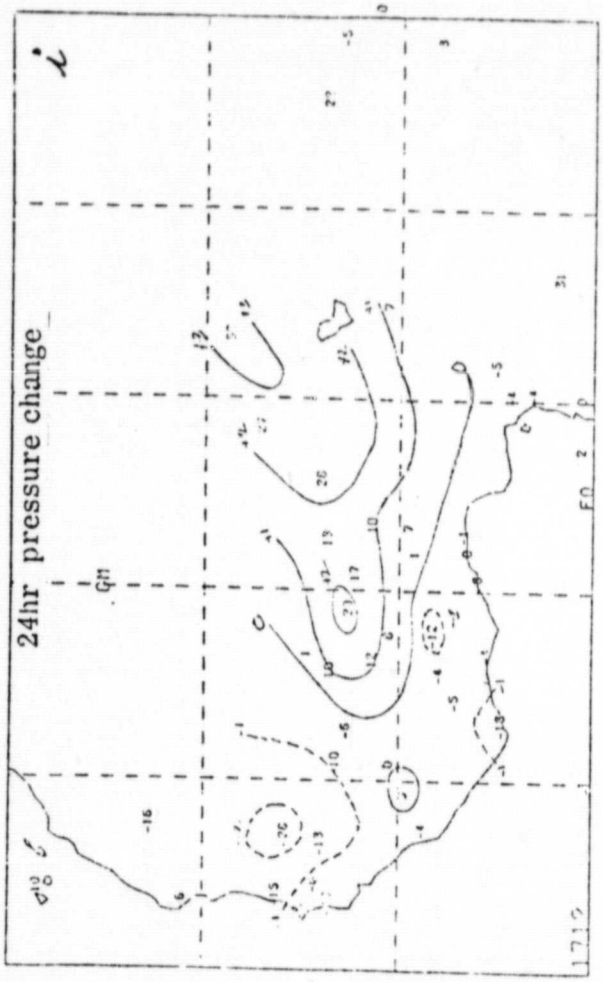

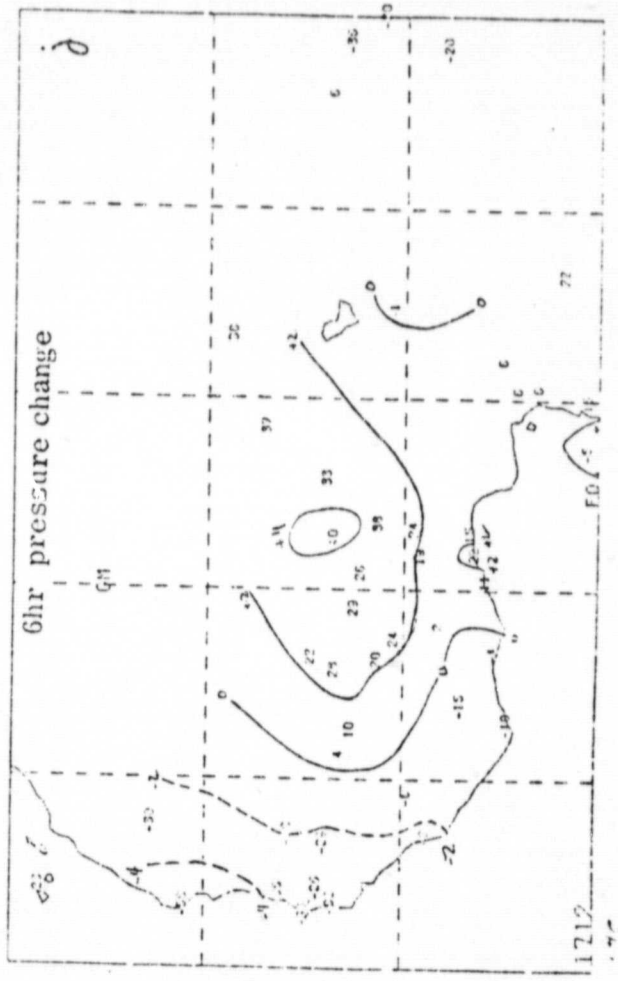

Fig. 15. continue

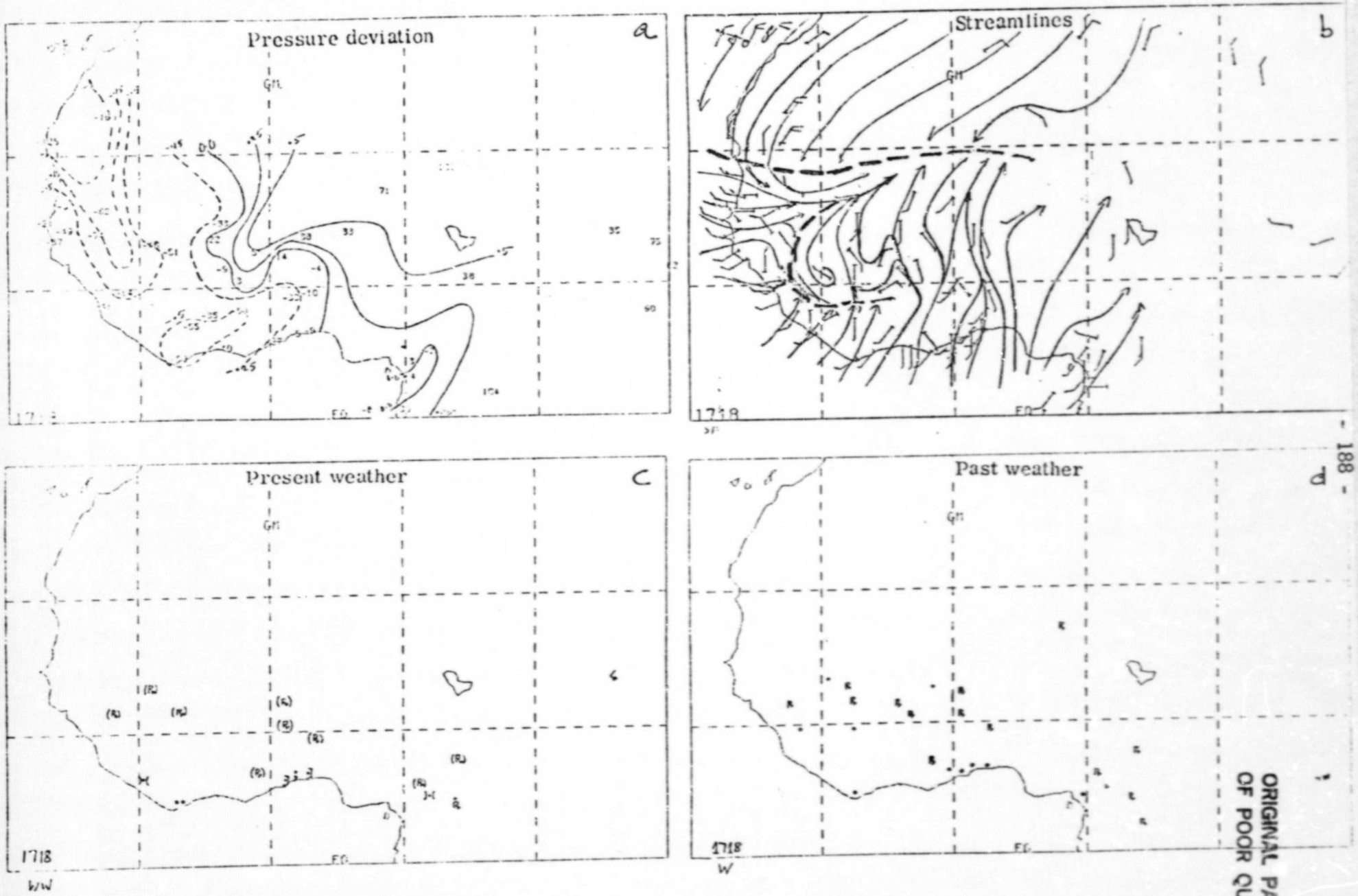

Fig. 16. Same as Fig. 9. except for 18 GMT, 17 July 1979.

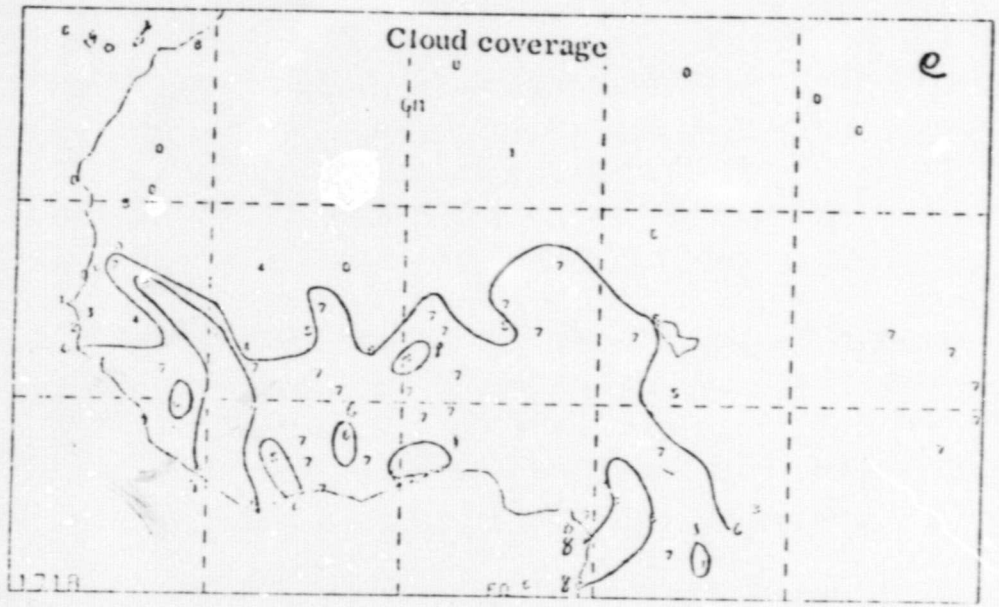

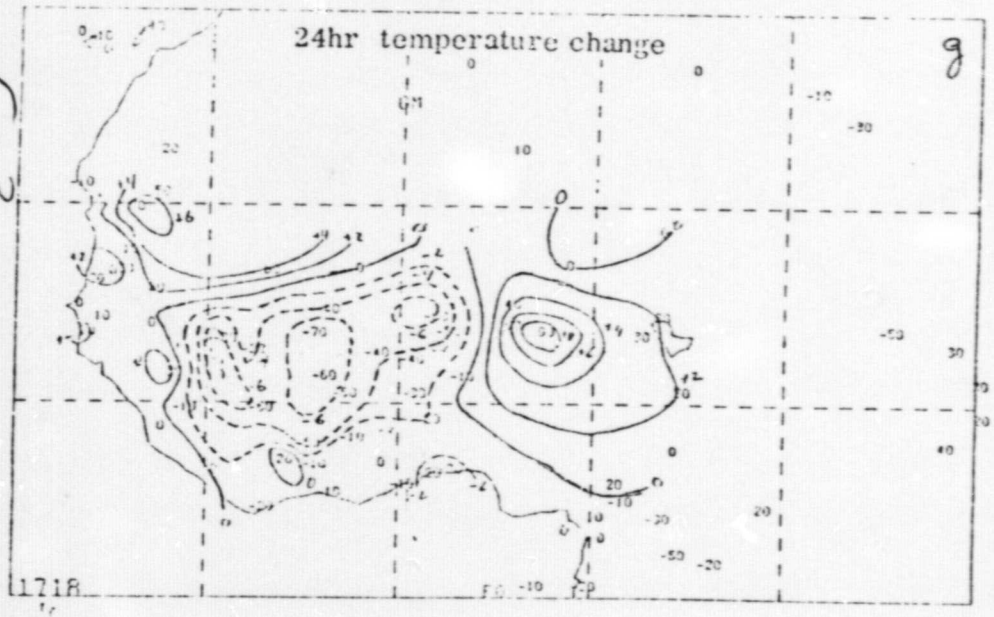

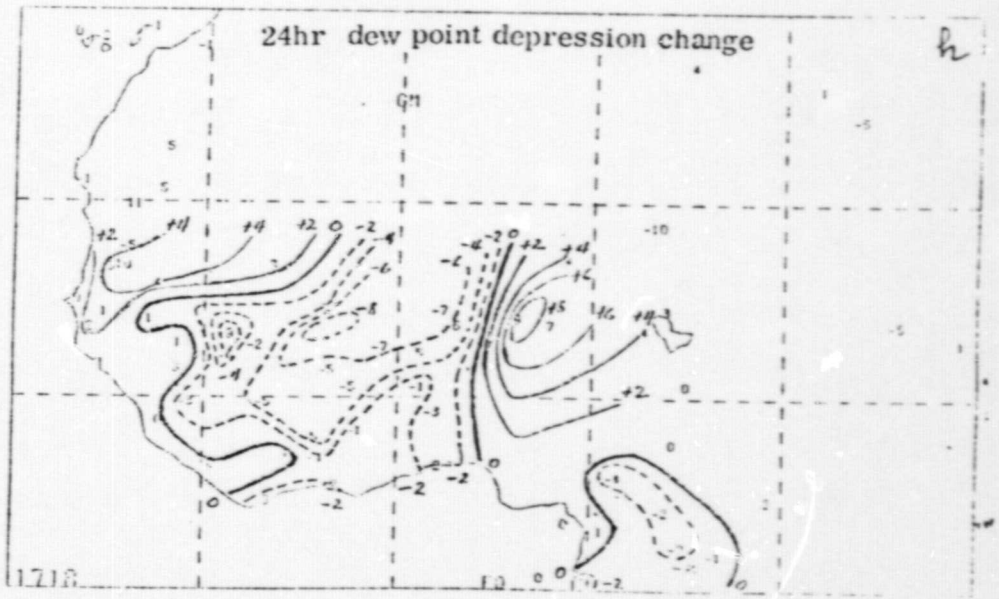

C-3

Fig. 16. continue

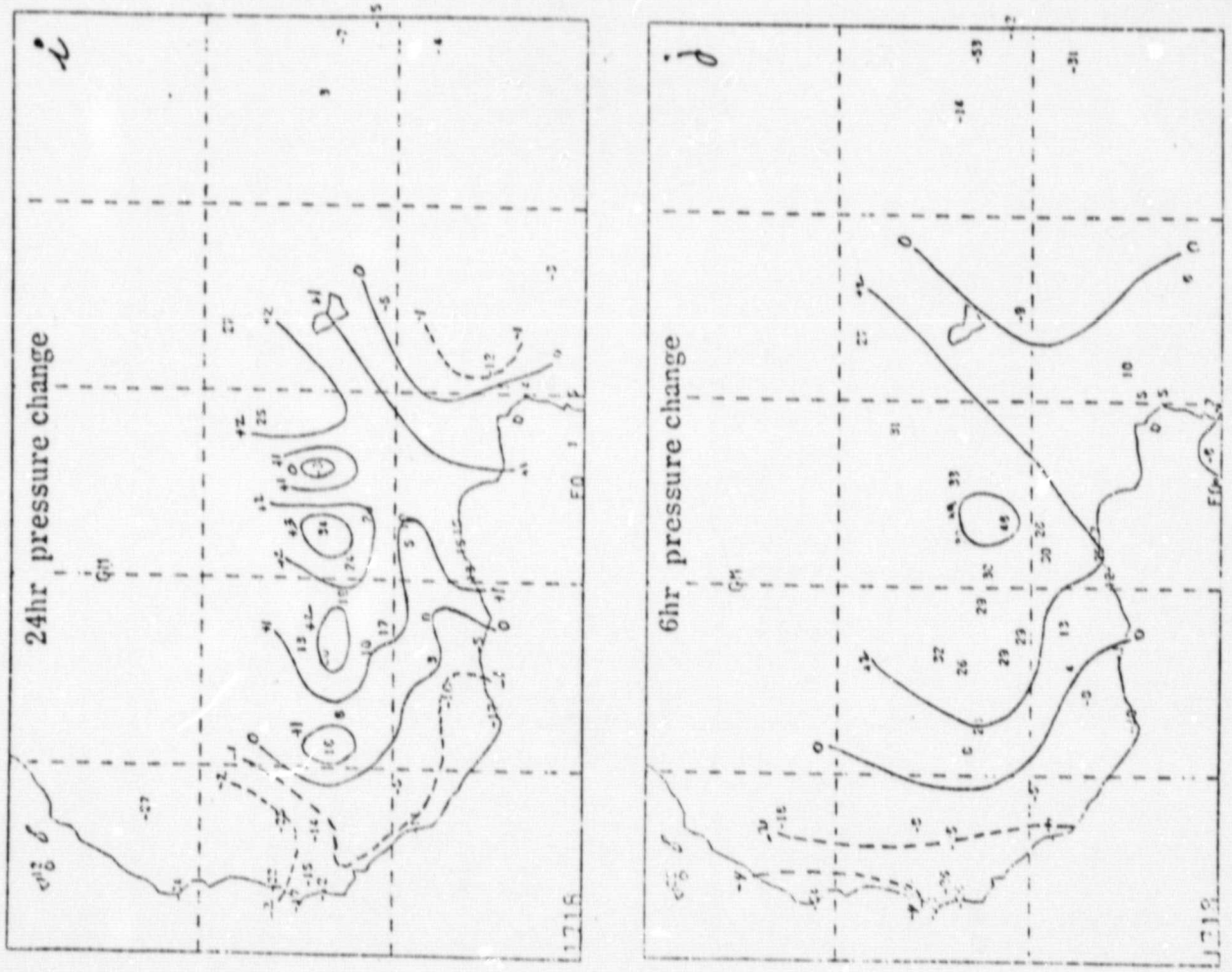

Fig. 16. continue

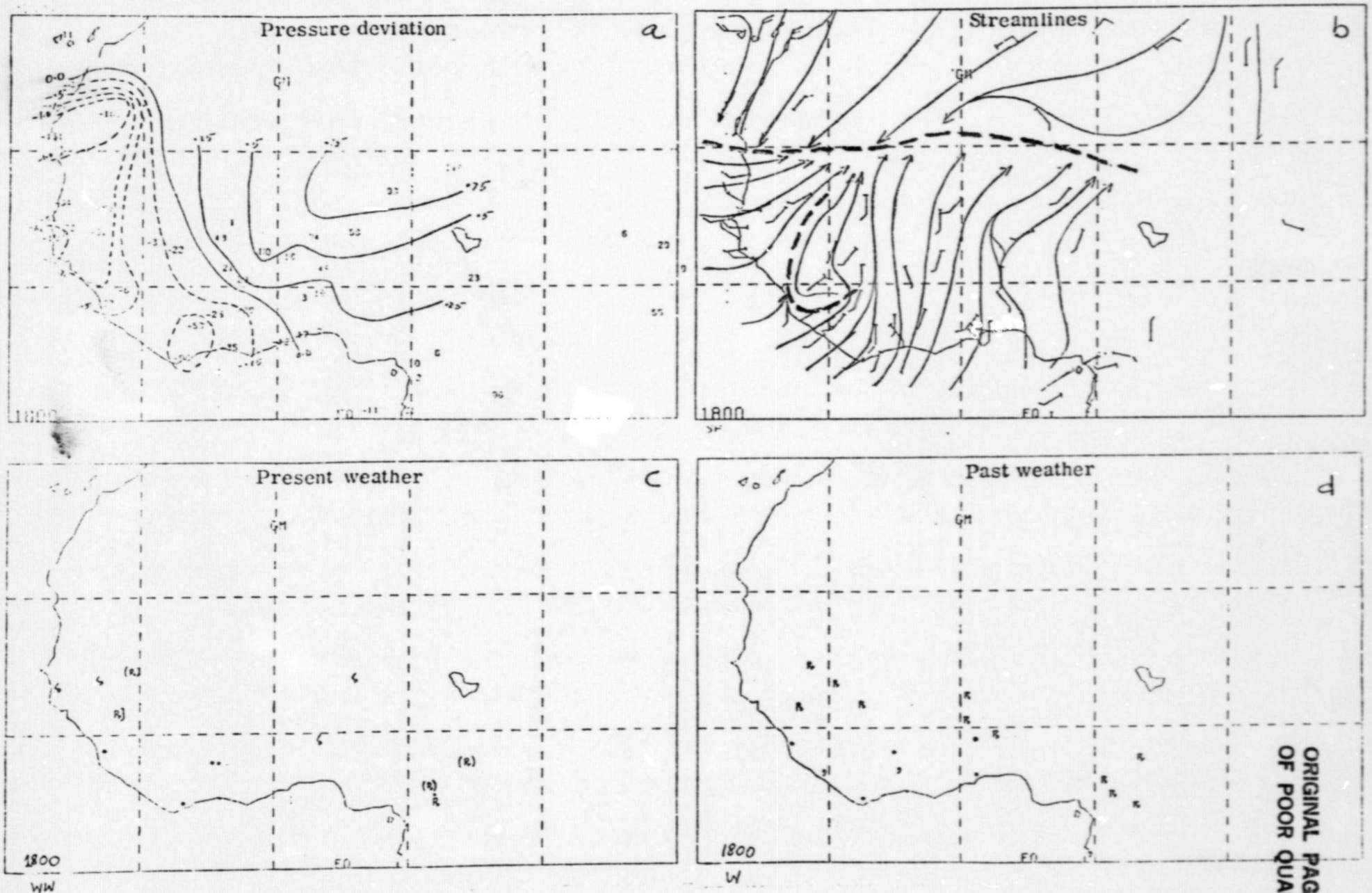

Fig. 17. Same as Fig. 9. except for 00 GMT, 18 July 1979.

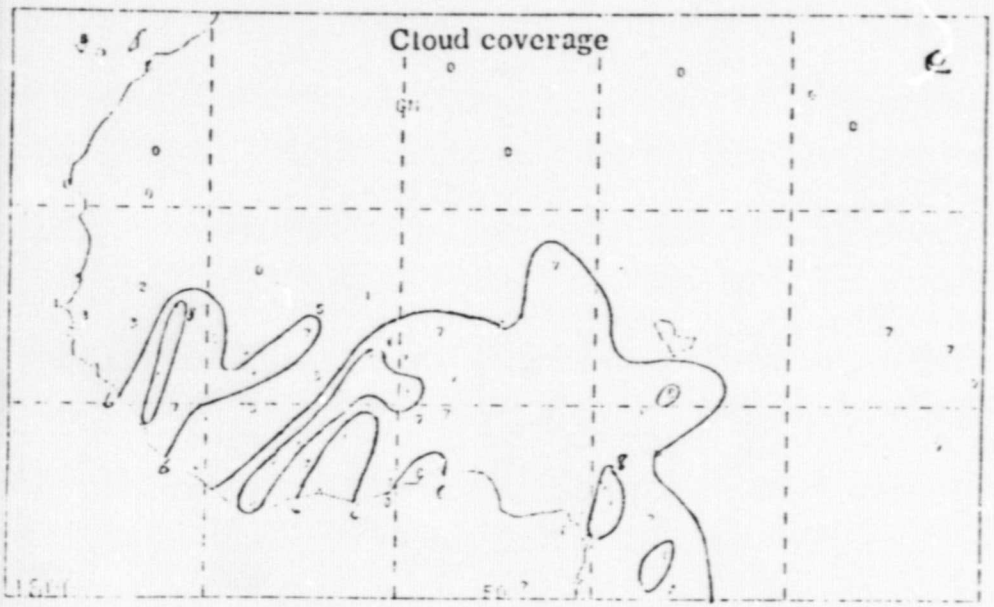

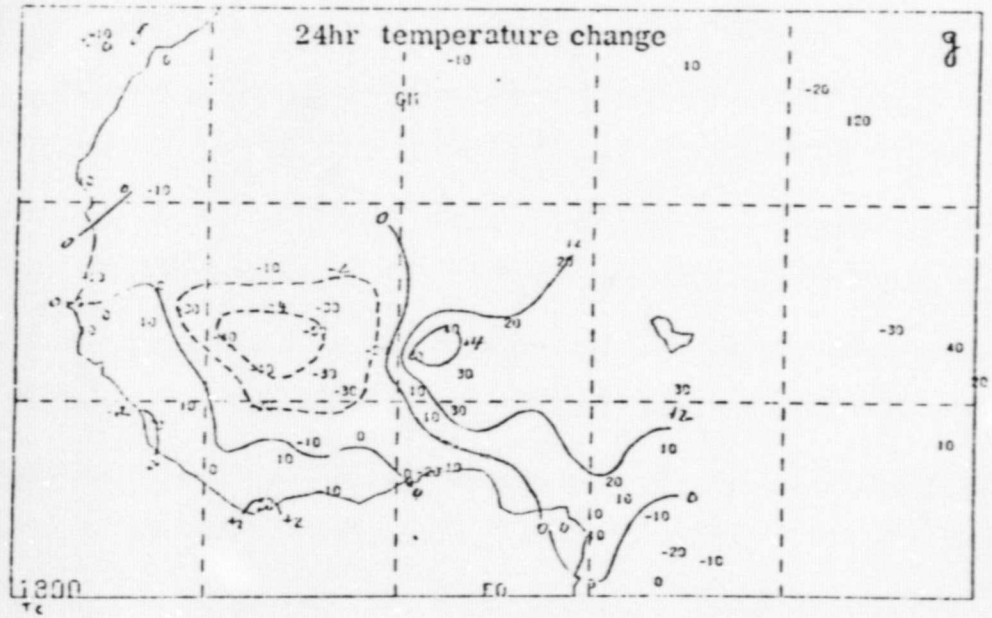

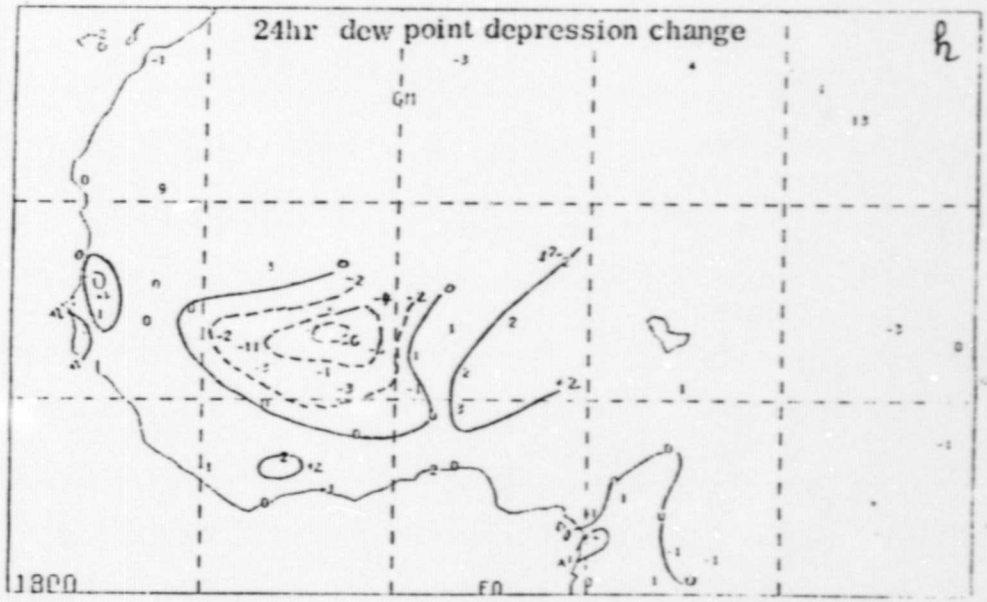

Fig. 17. continue

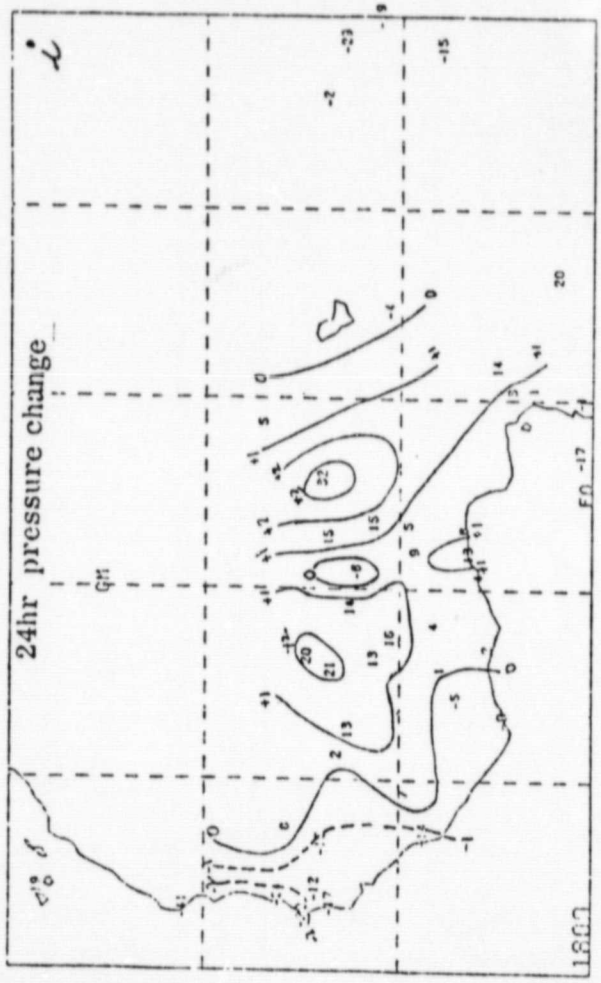

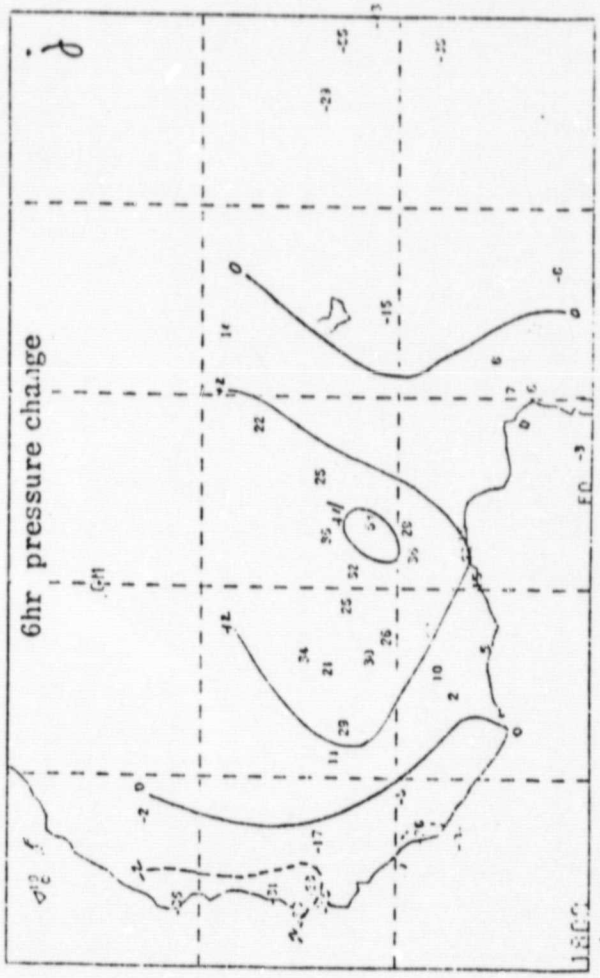

Fig. 17. continue

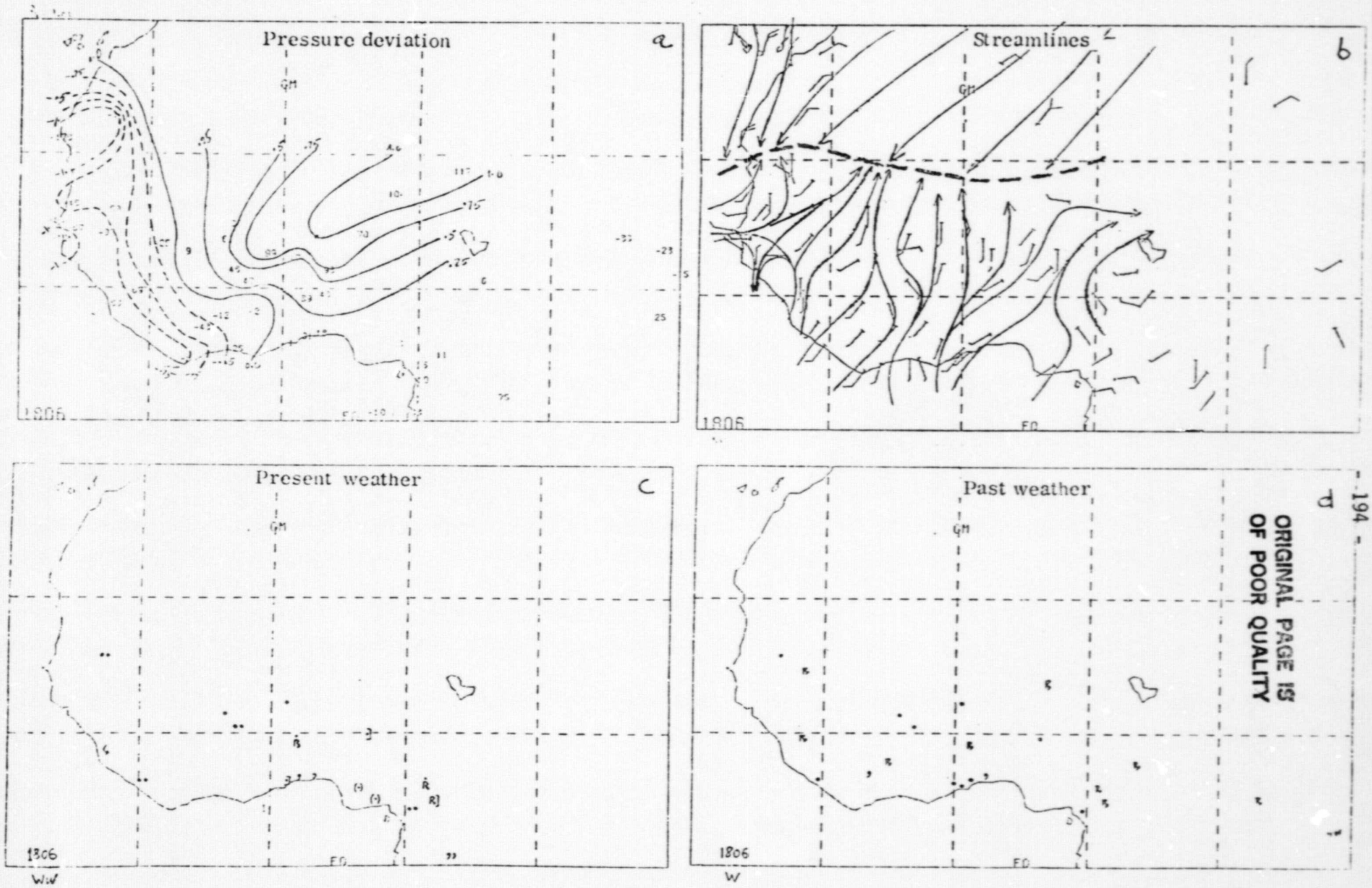

Fig. 18. Same as Fig. 9. except for 06 GMT, 18 July 1979.

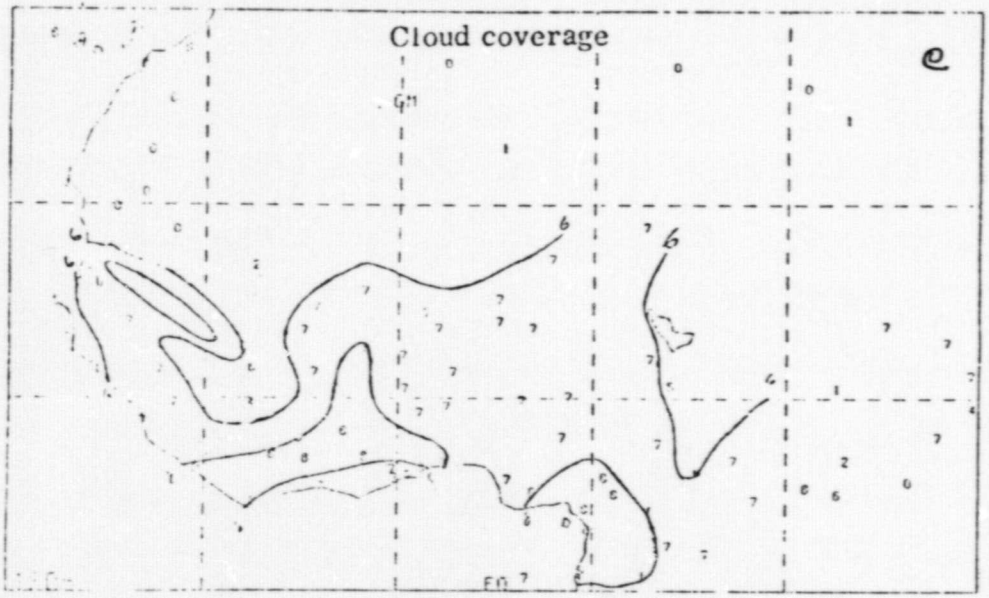

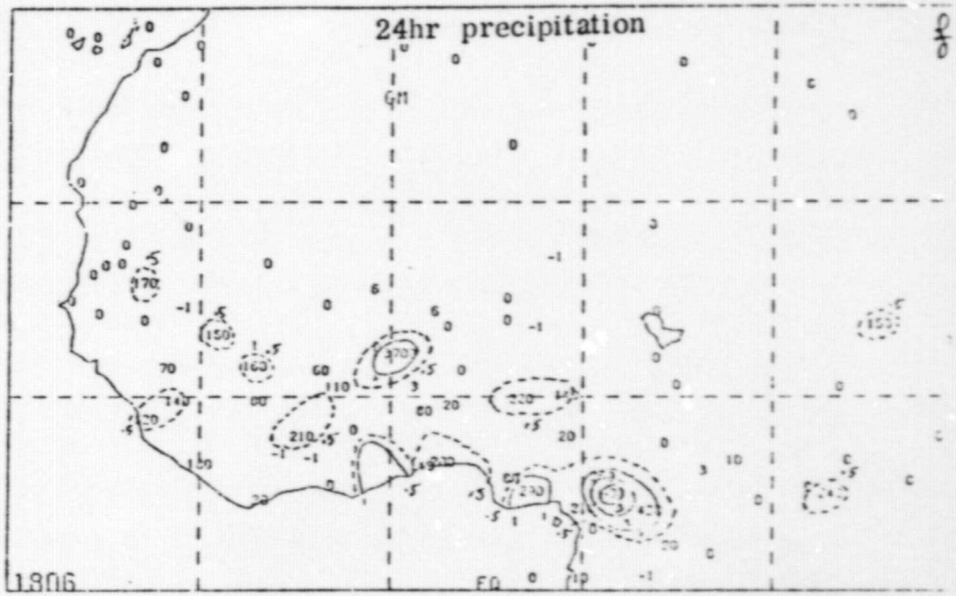

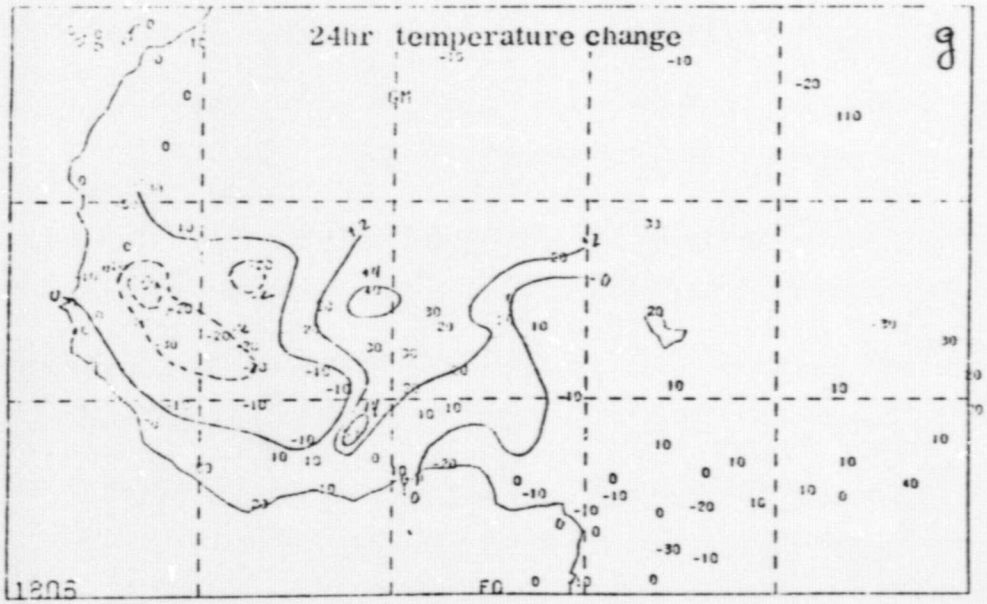

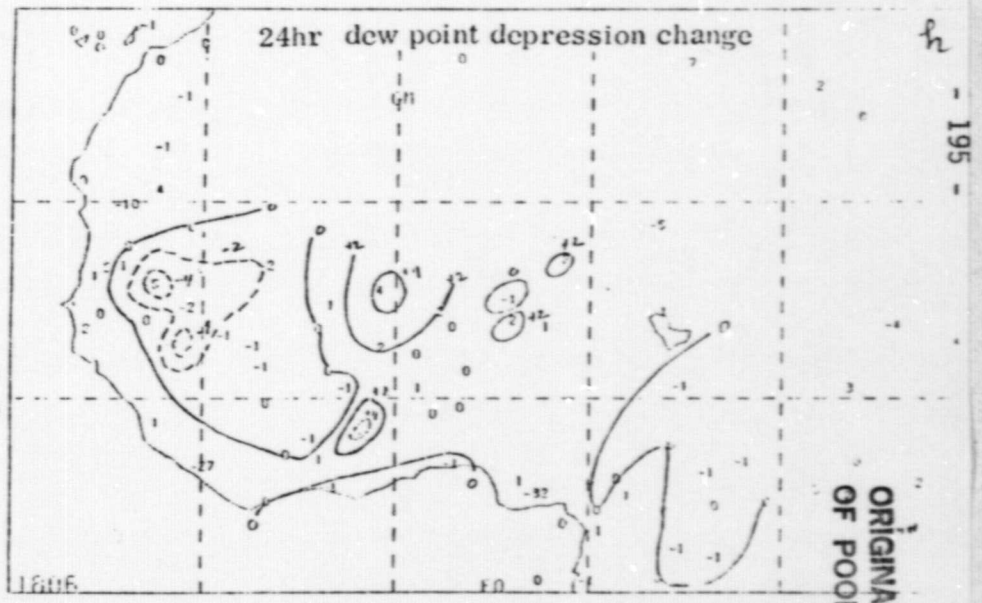

Fig. 18. continue

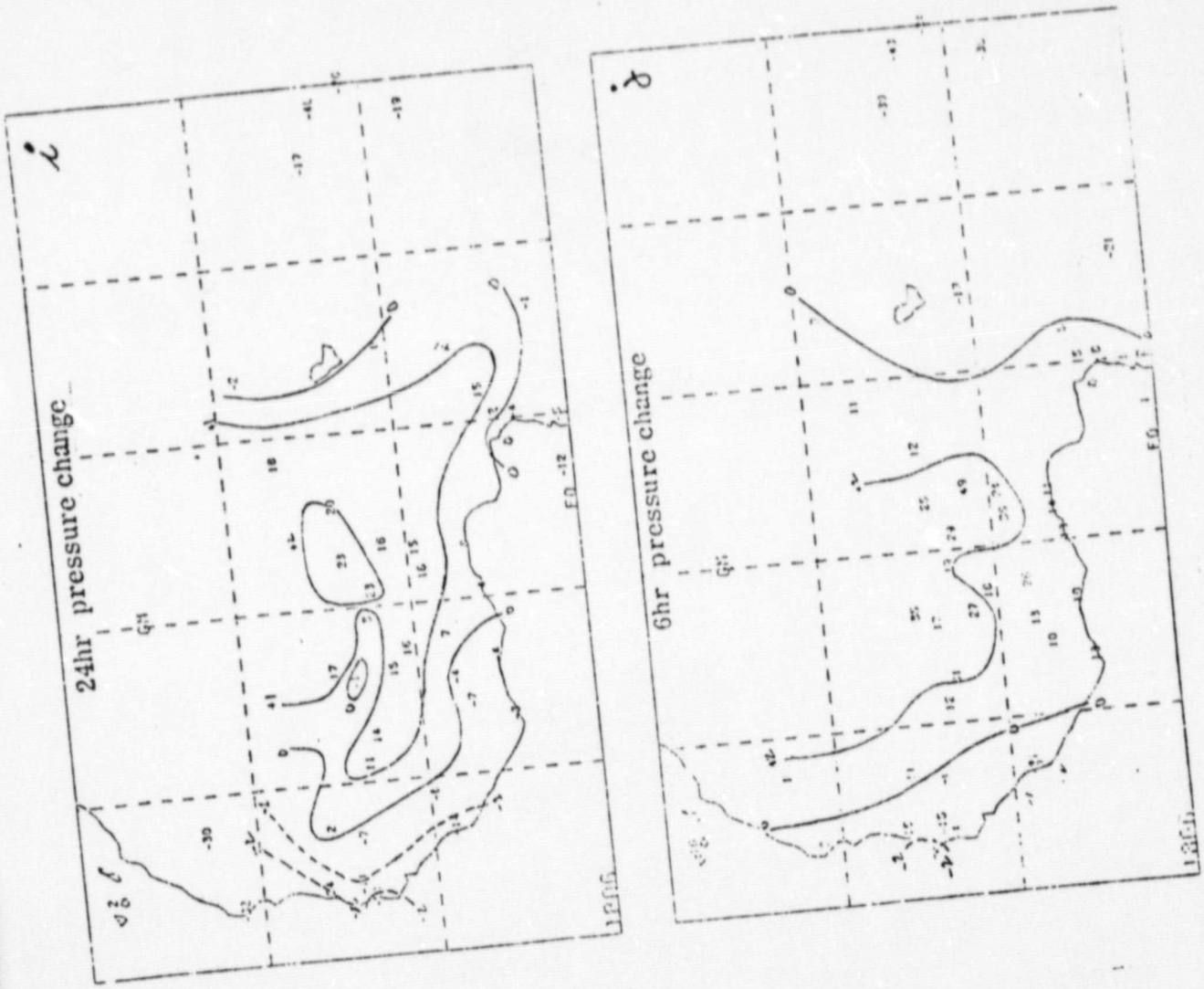

Fig. 18. continue

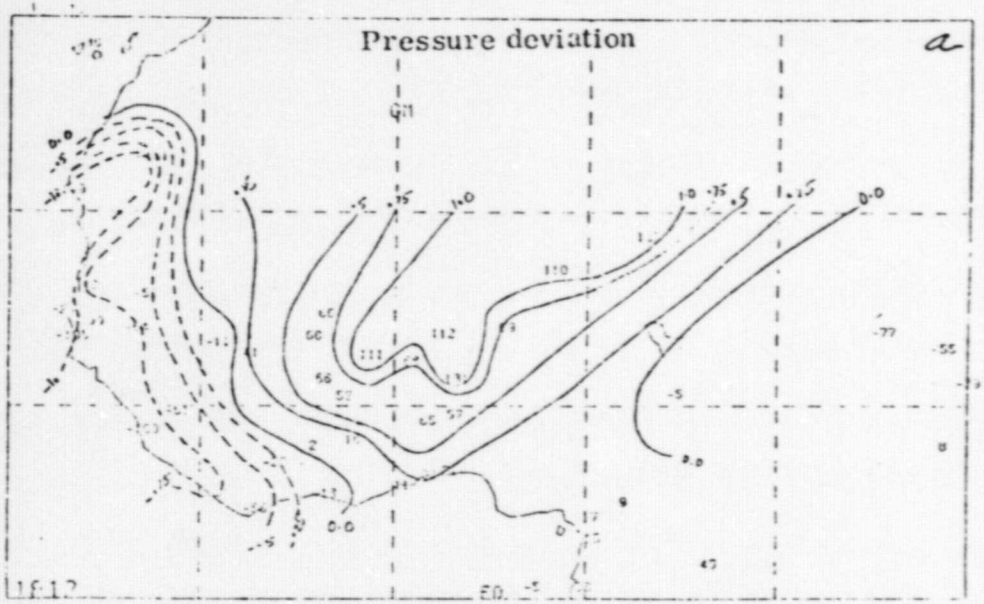

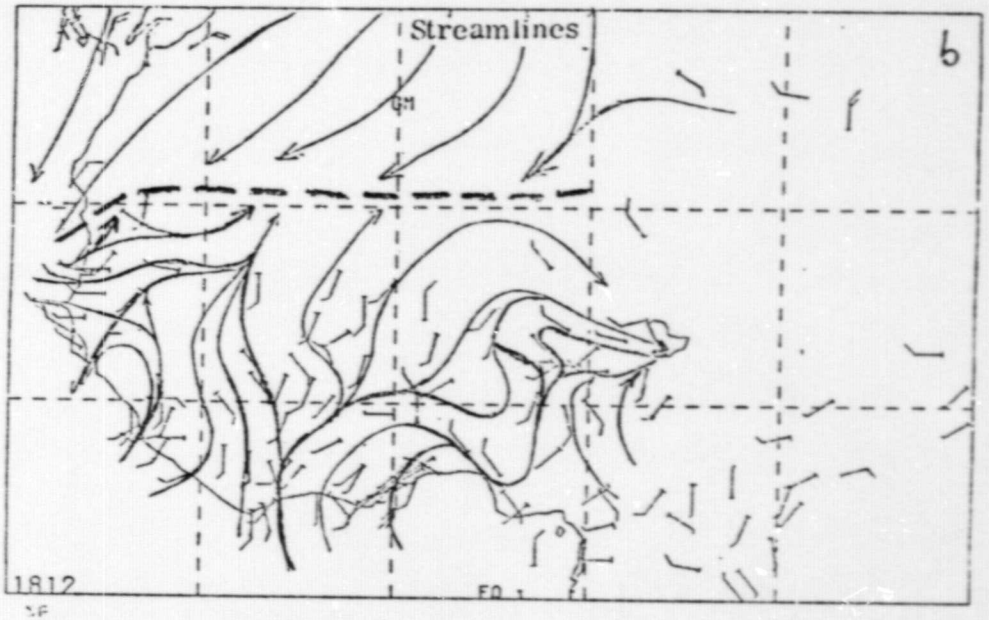

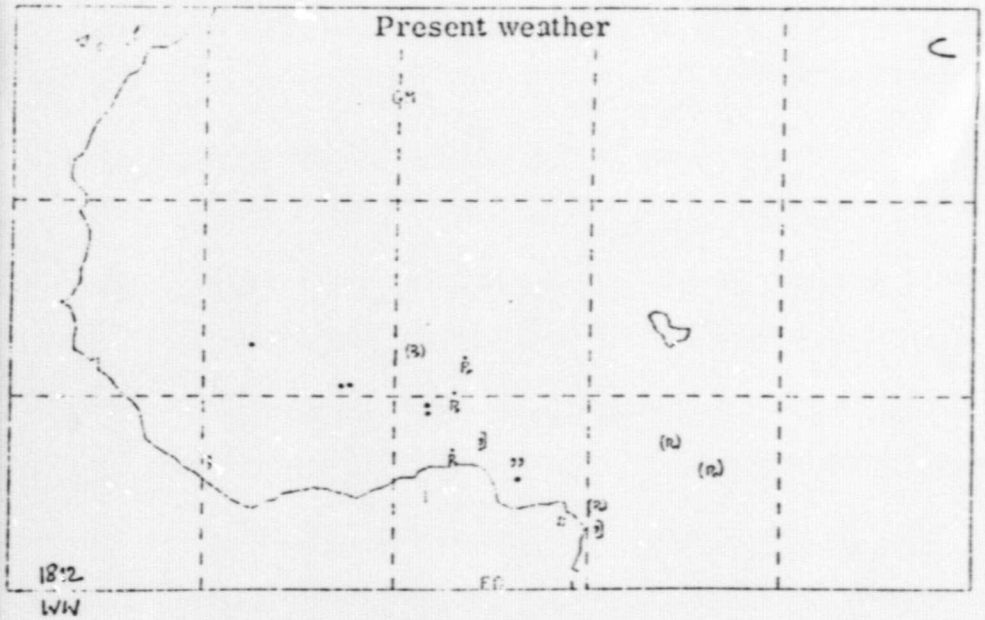

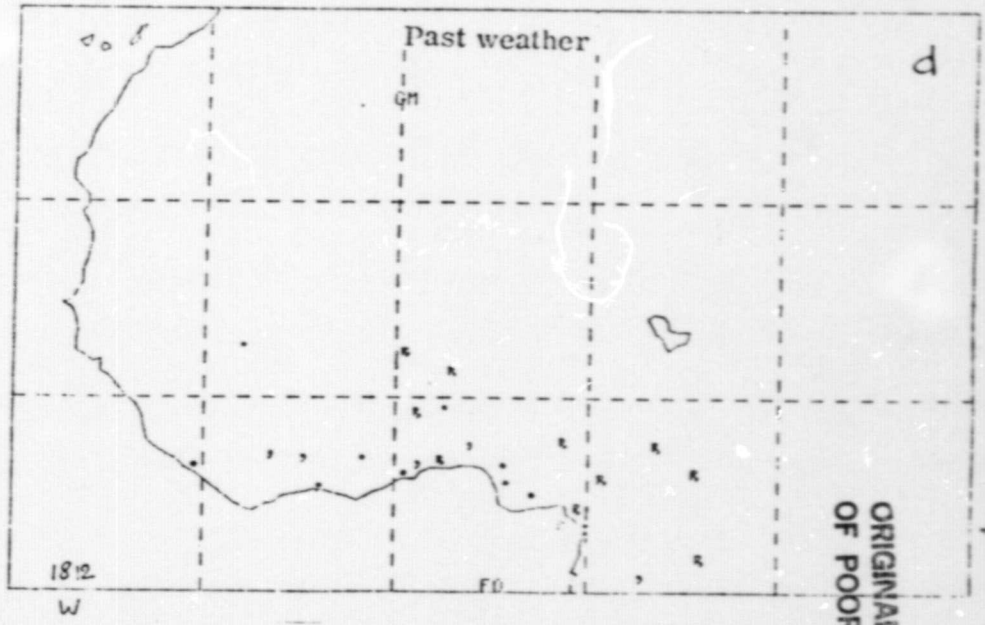

Fig. 19. Same as Fig. 9. except for 12 GMT, 18 July 1979.

Fig. 19. contimue

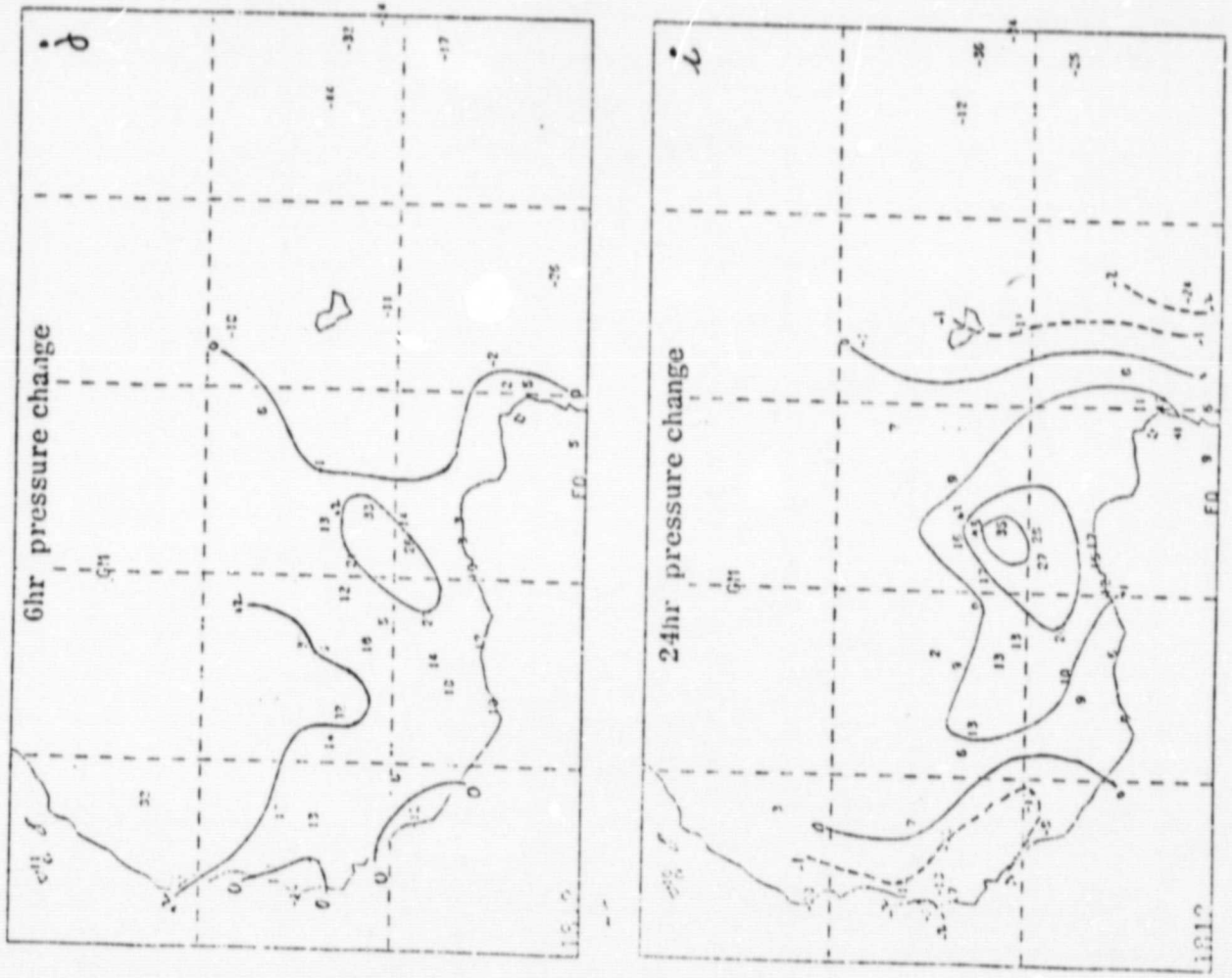

Fig. 19. continue

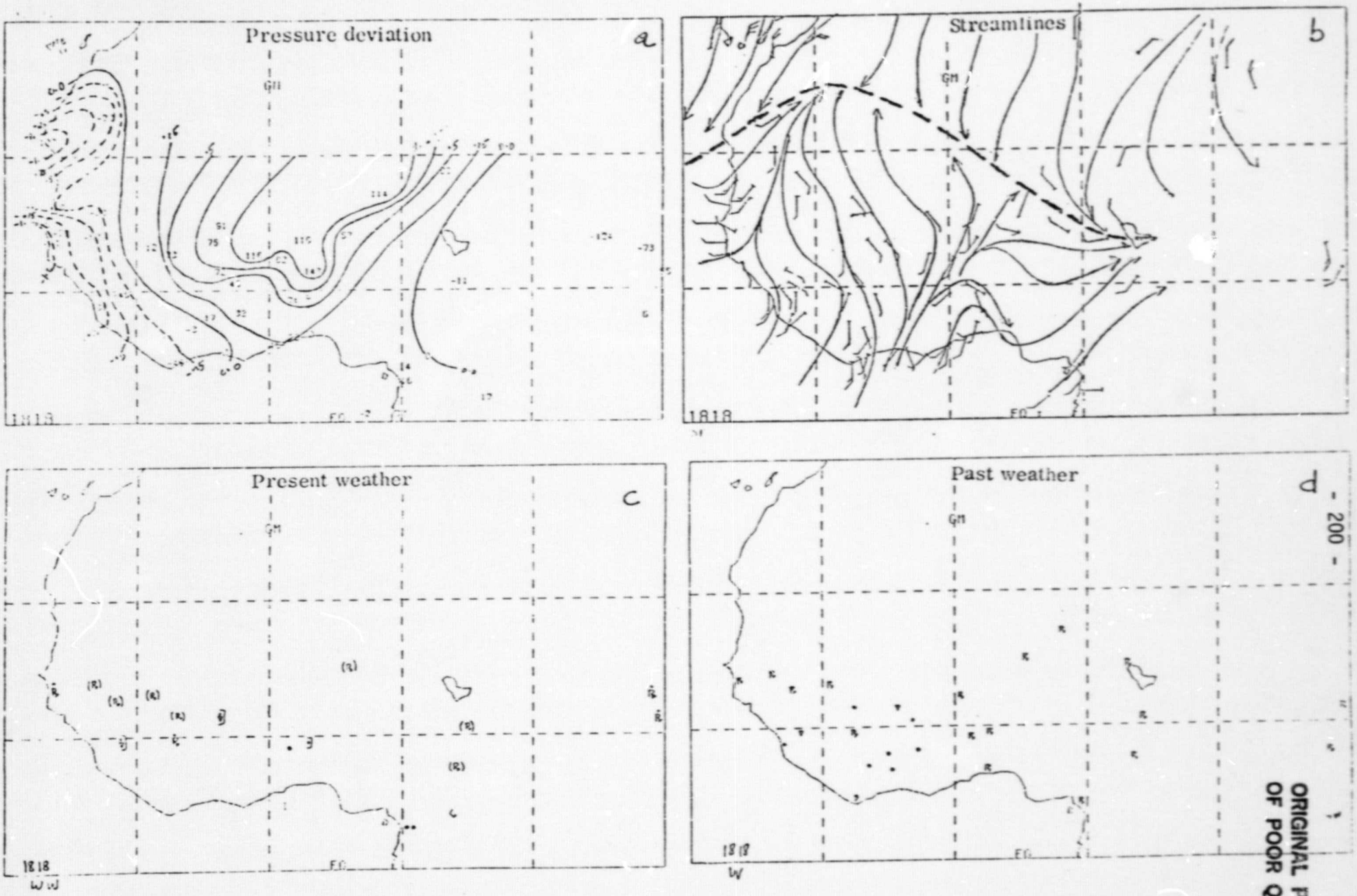

Fig. 20. Same as Fig. 9. except for 18 GMT, 18 July 1979.

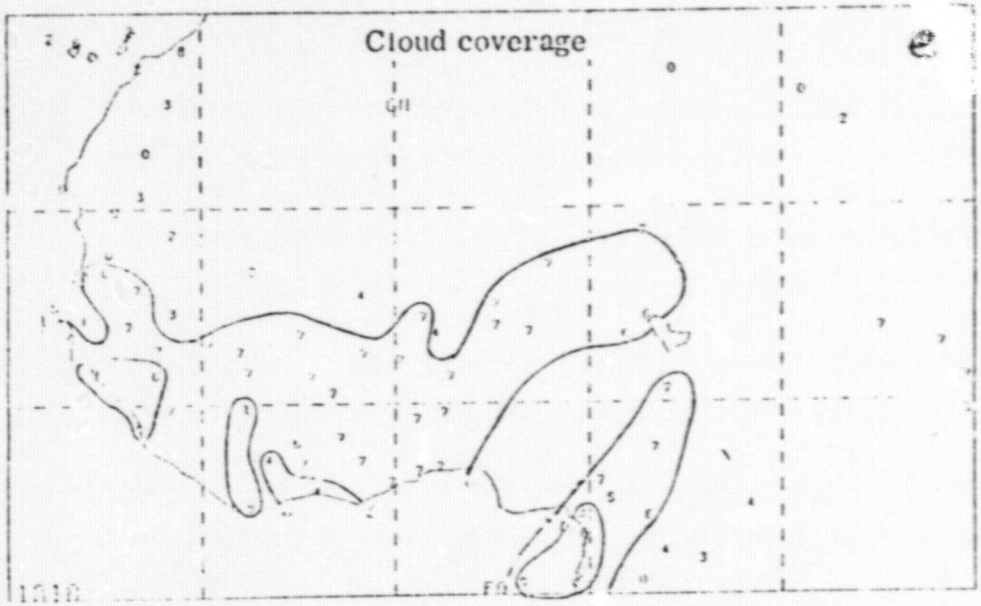

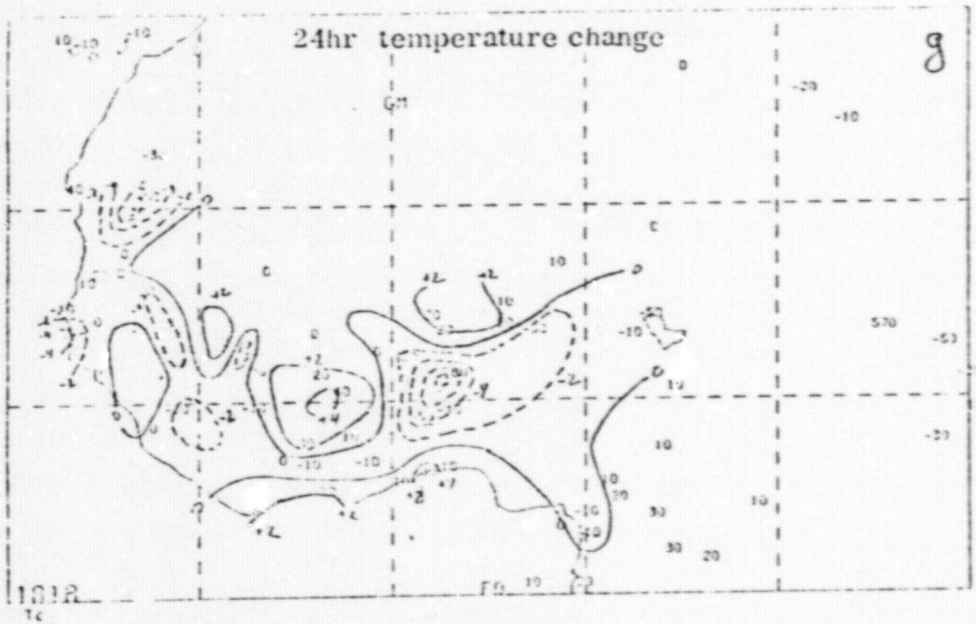

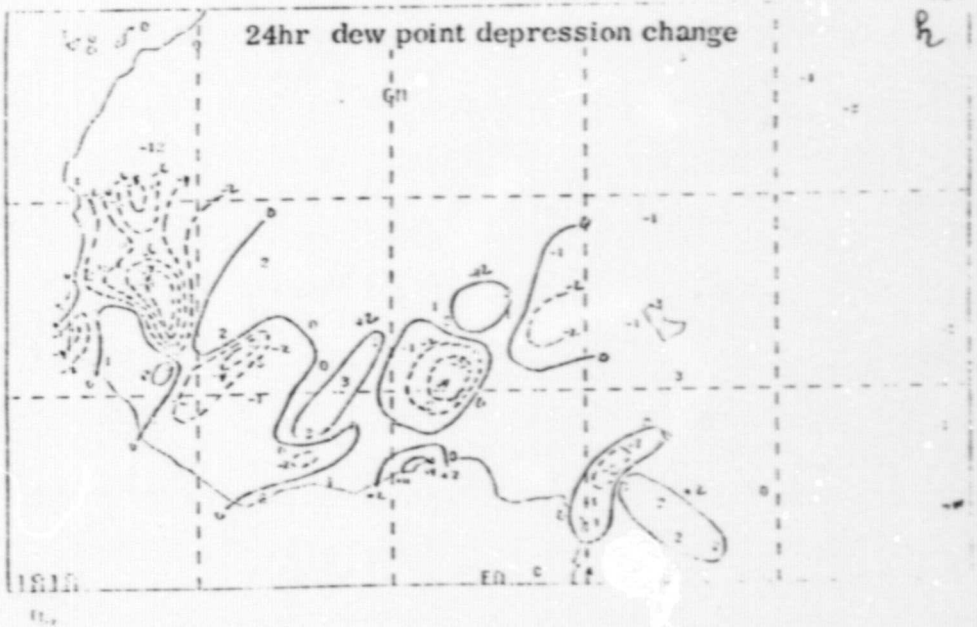

Fig. 20. continue

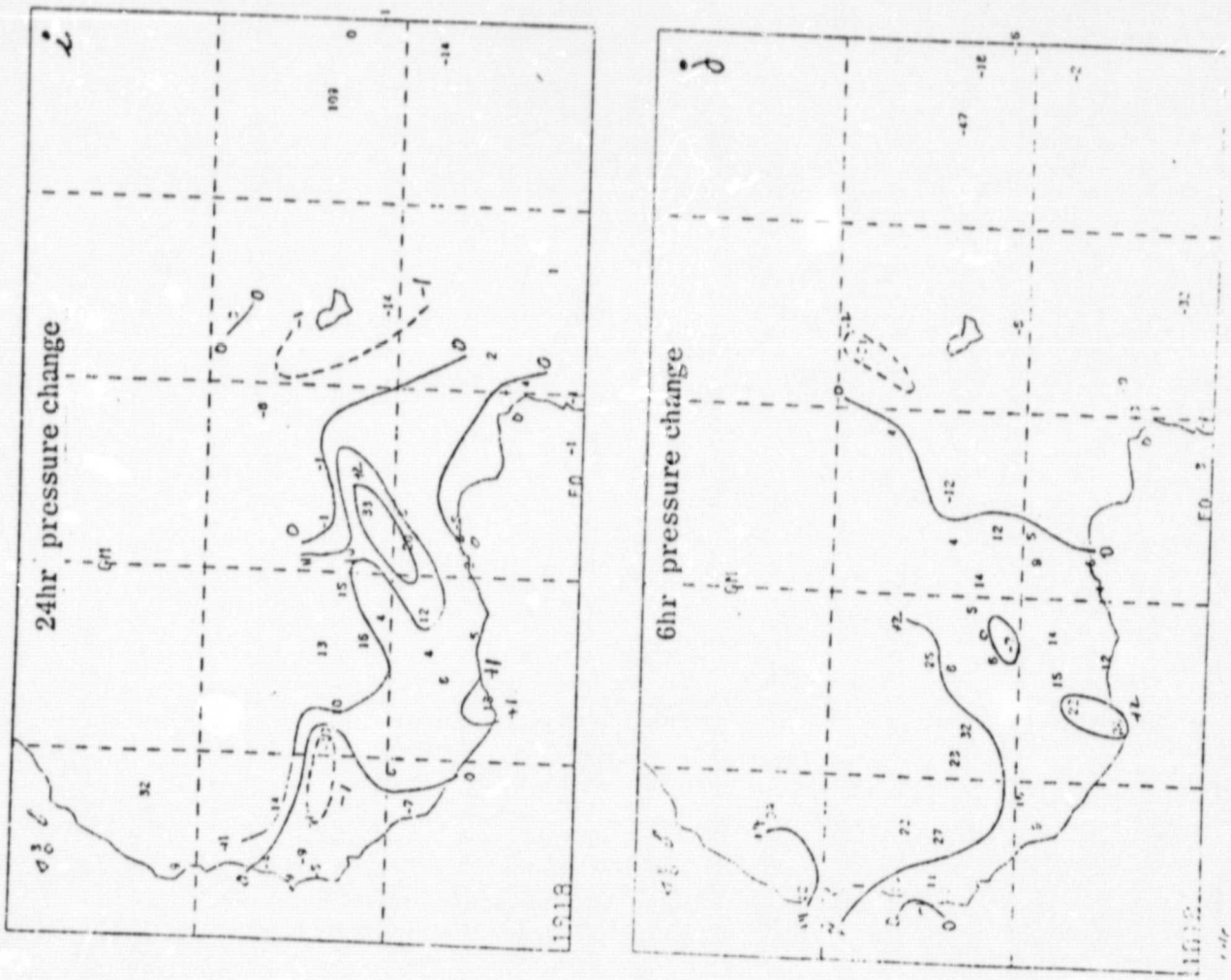

Fig. 20. continue

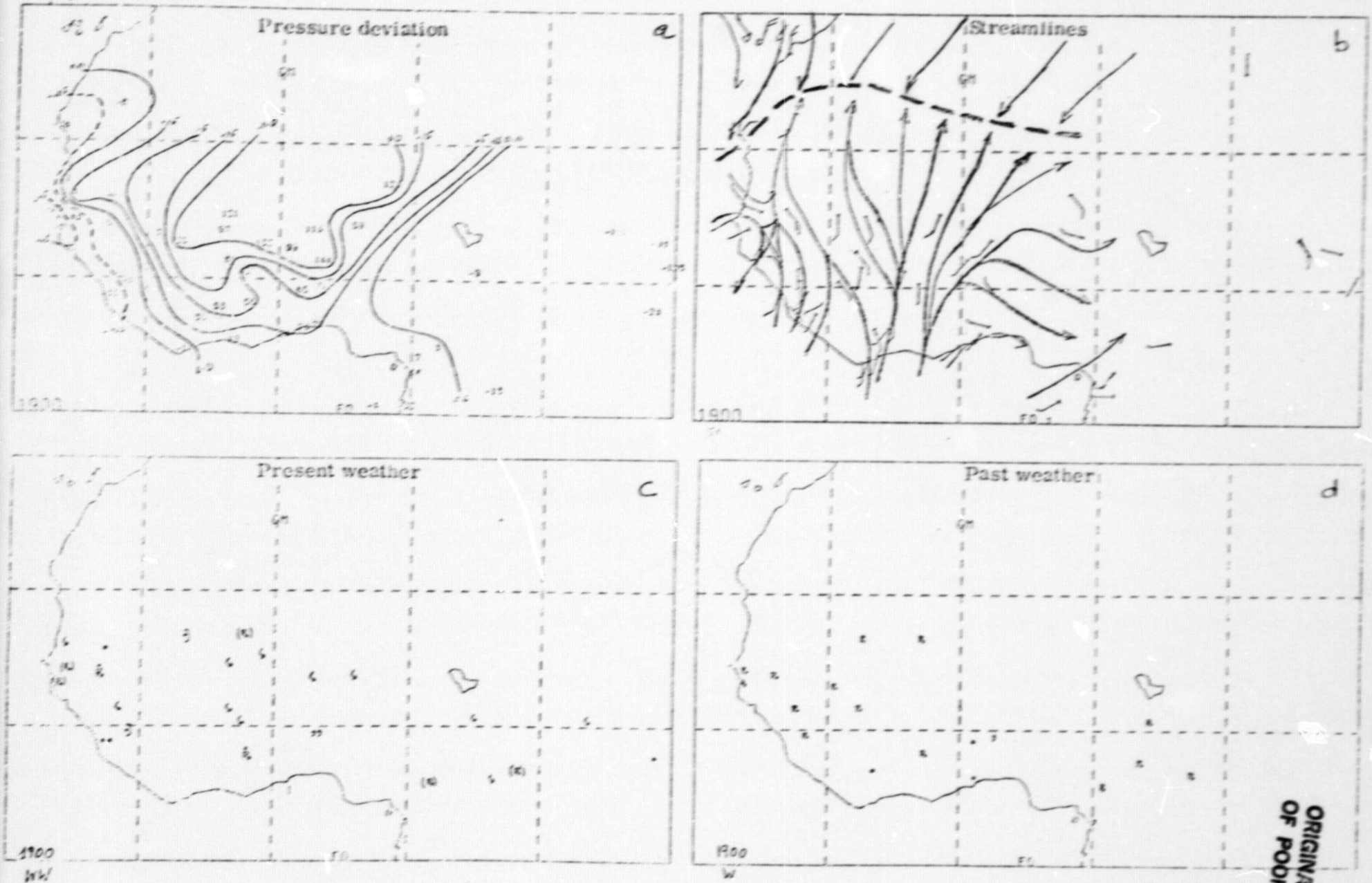

Fig. 21. Same as Fig. 9. except for 00 GMT, 19 July 1979.

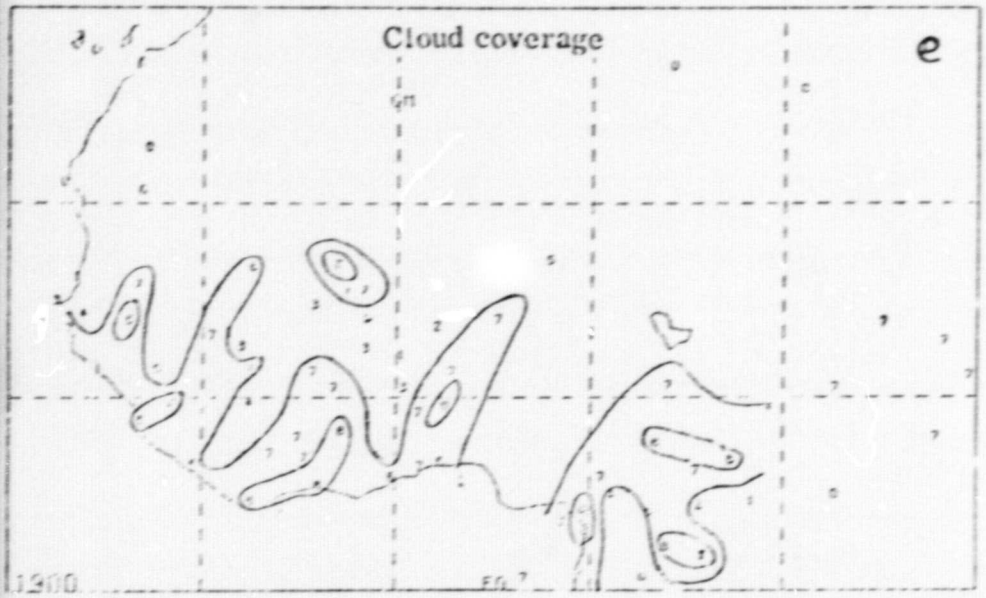

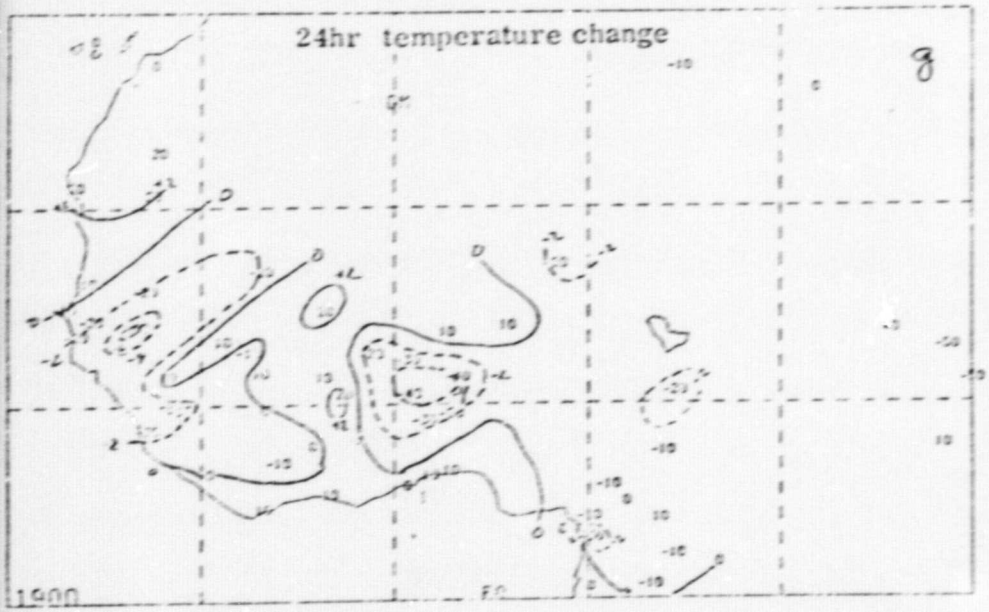

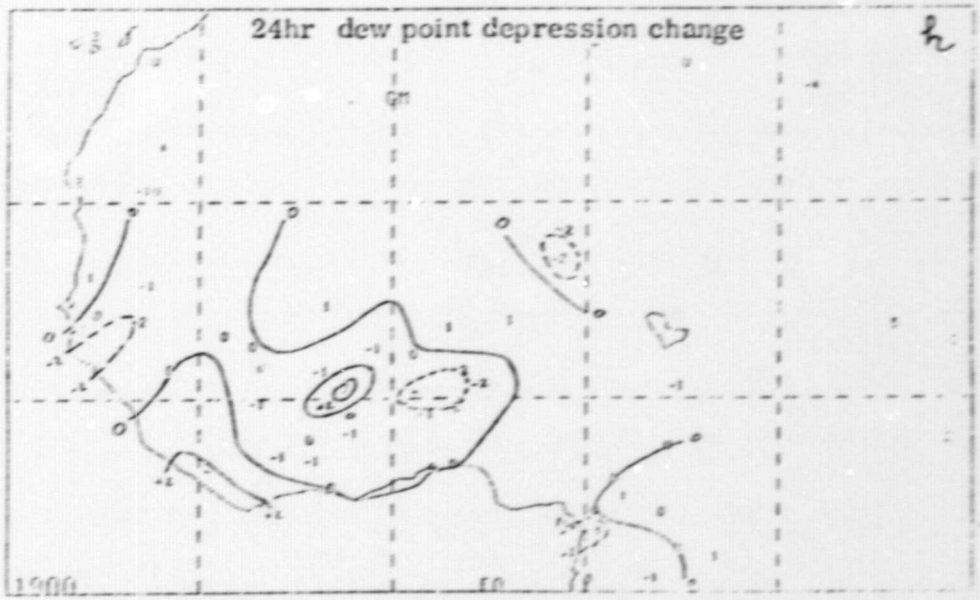

Fig. 21. continue

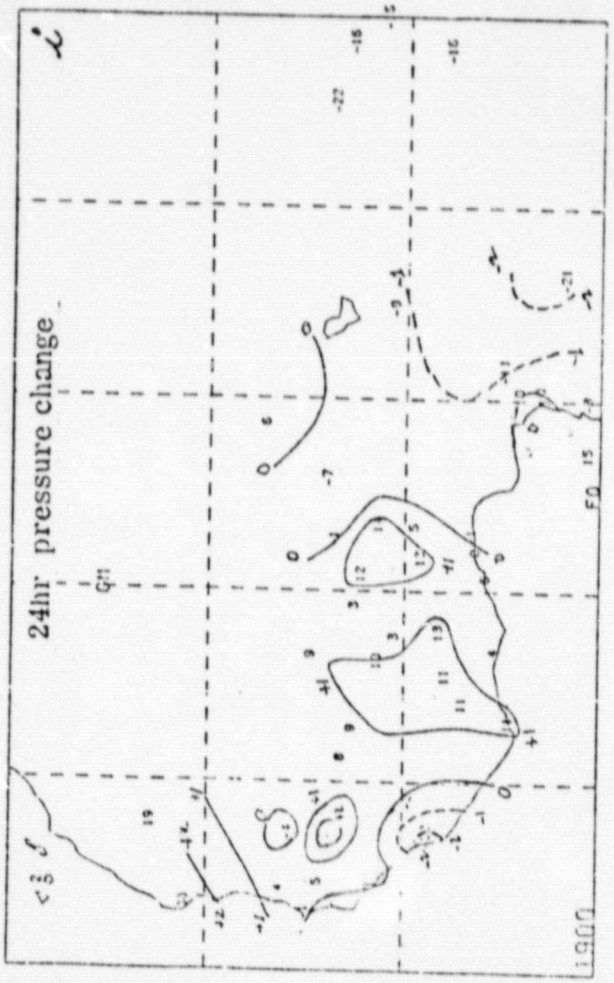

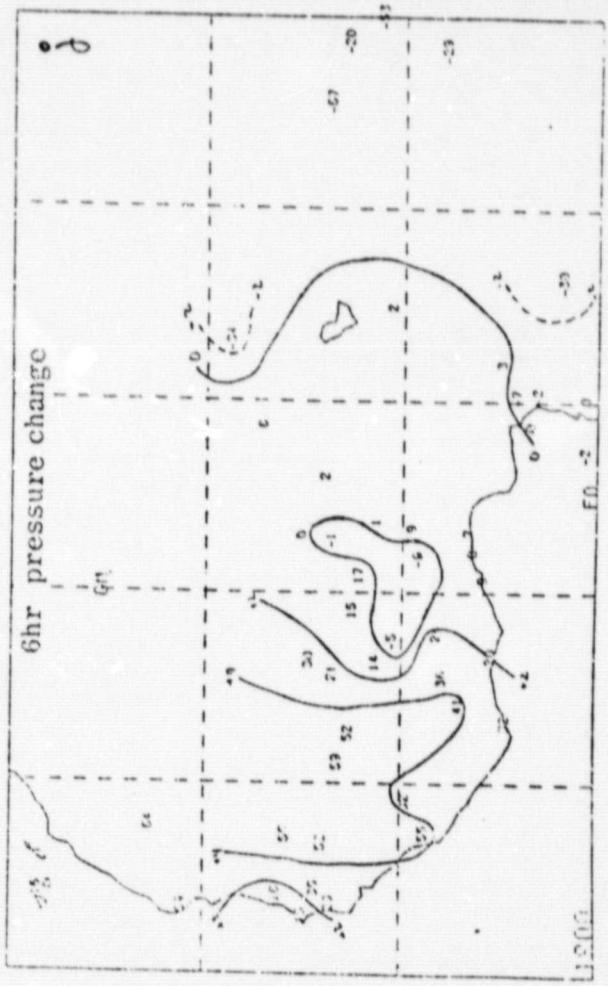

Fig. 21. continue

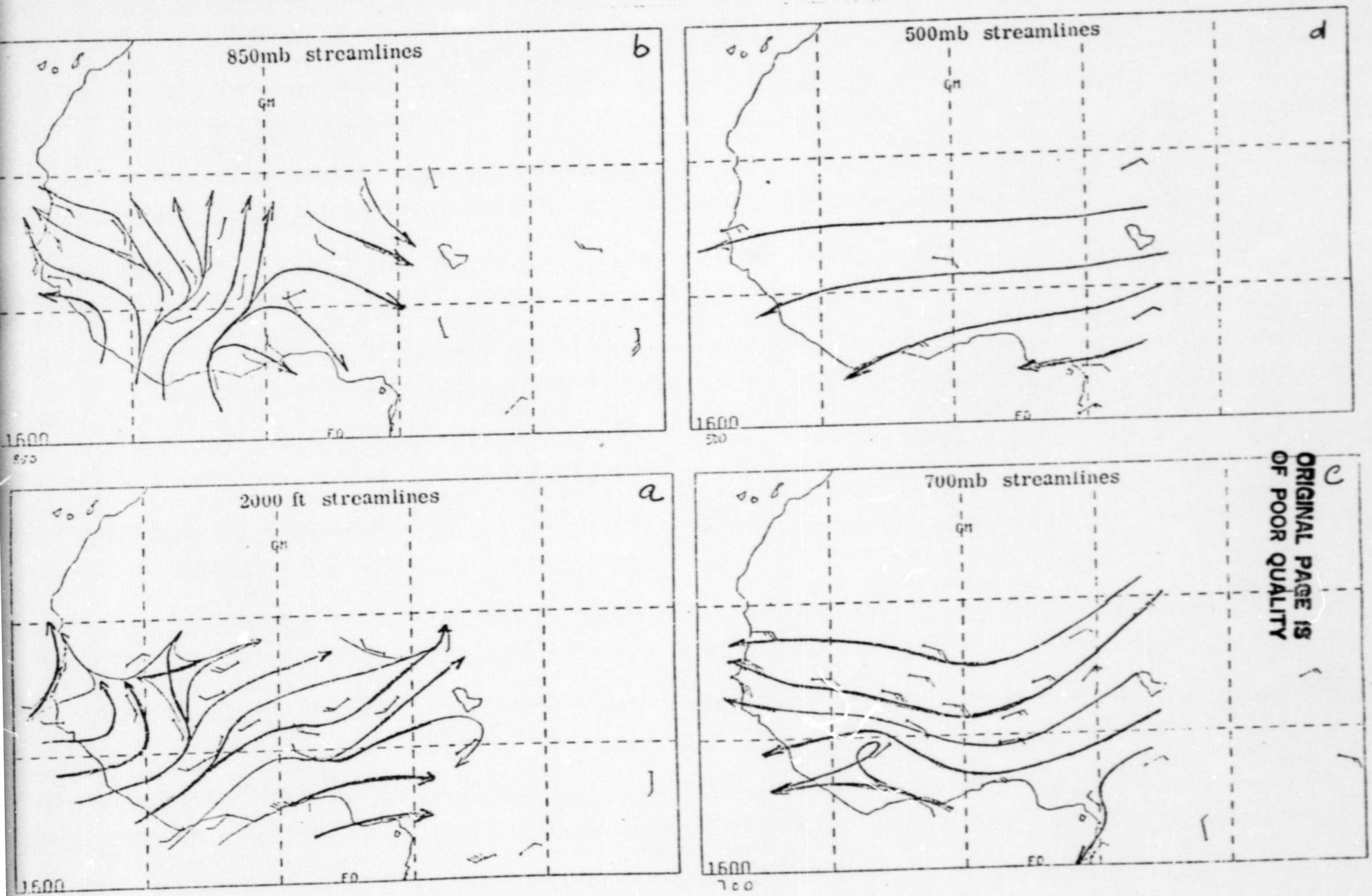

Fig. 22. Upper air streamlines: a) at 2000 ft, b) at 850mb, c) at 700mb, d) at 500mb, e) at 300mb, f) at 200mb for 00 GMT, 16 July 1979.

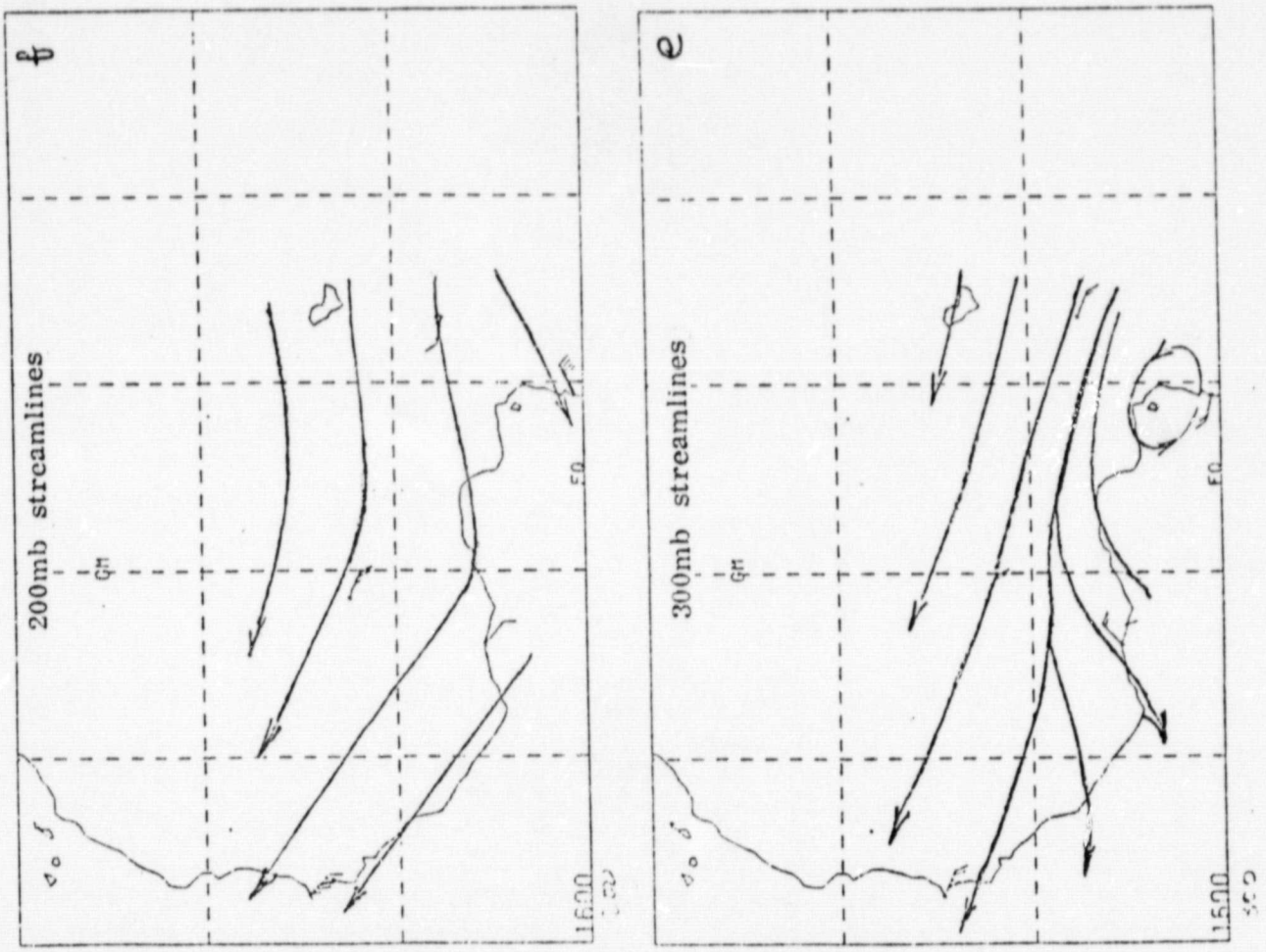

Fig. 22. continue

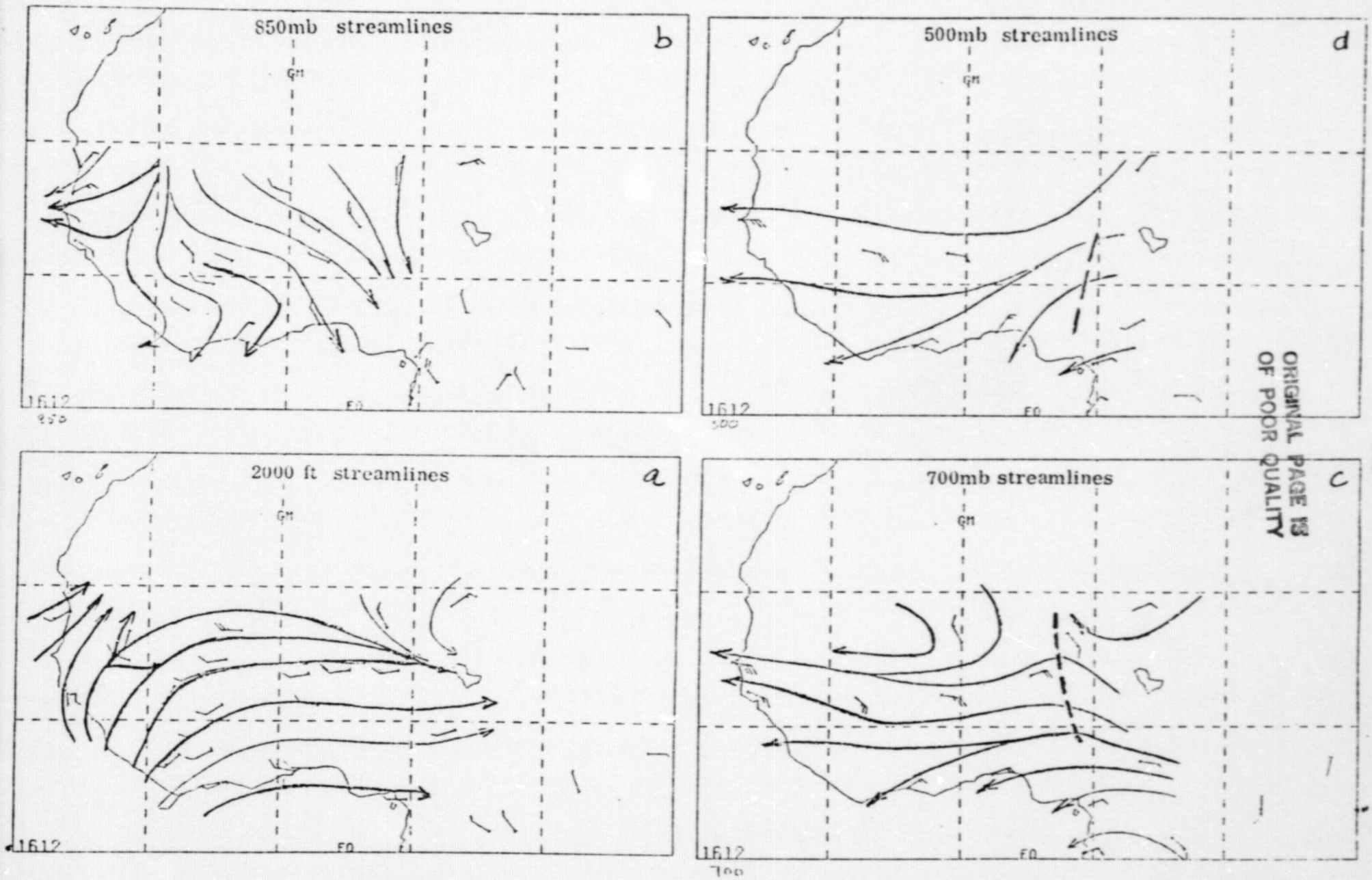

Fig. 23. Same as Fig. 22. except for 12 GMT, 16 July 1979.

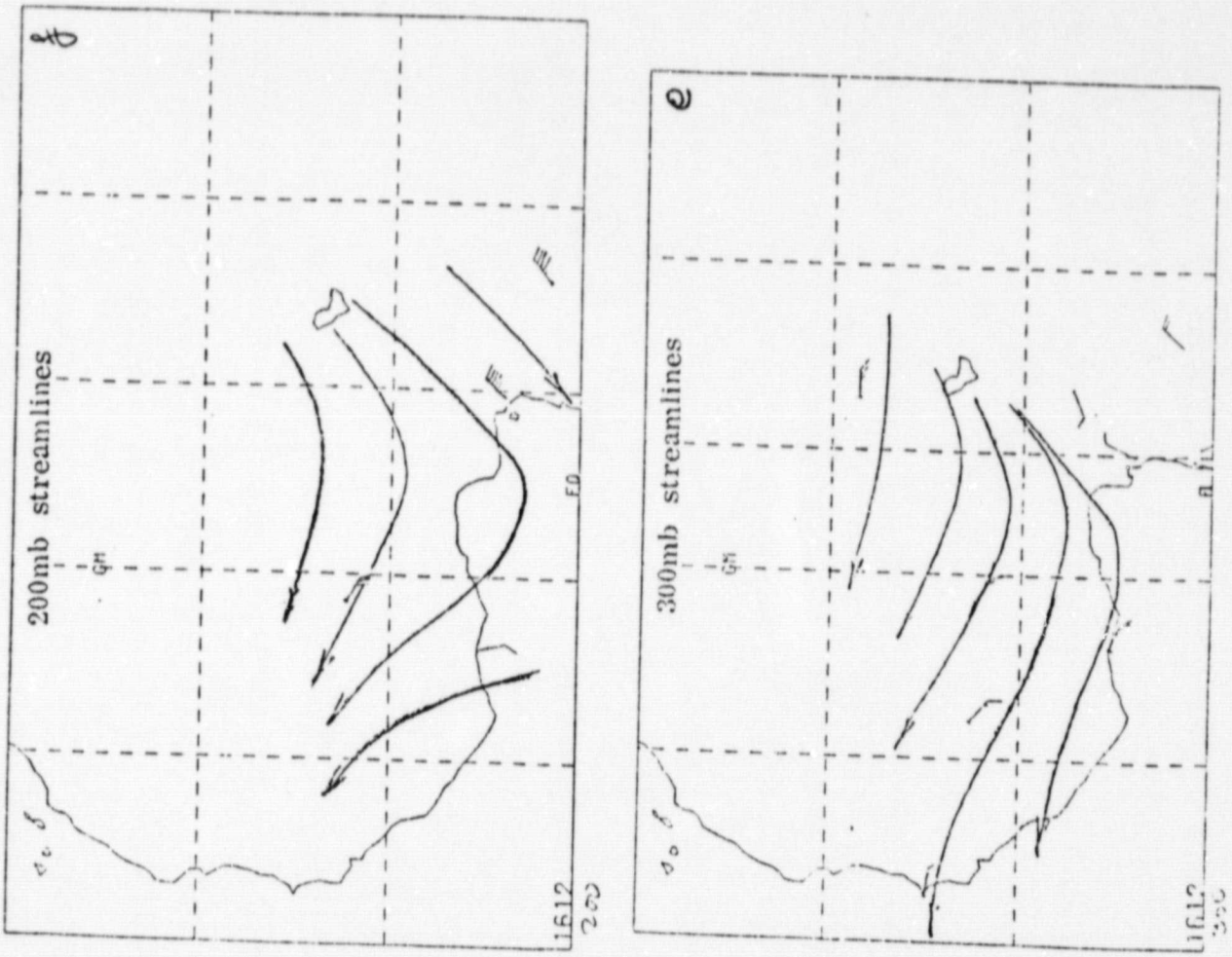

Fig. 23. continue

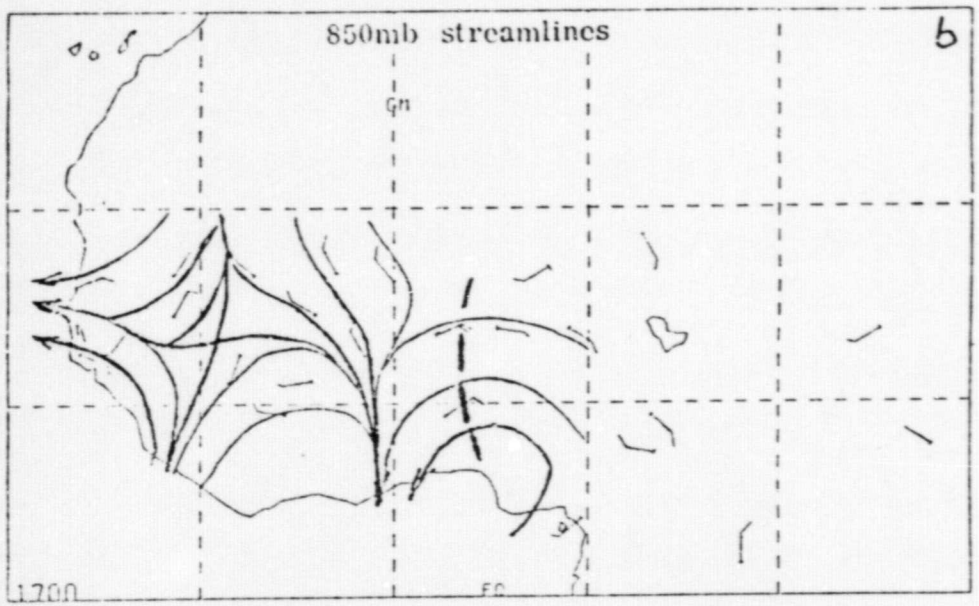

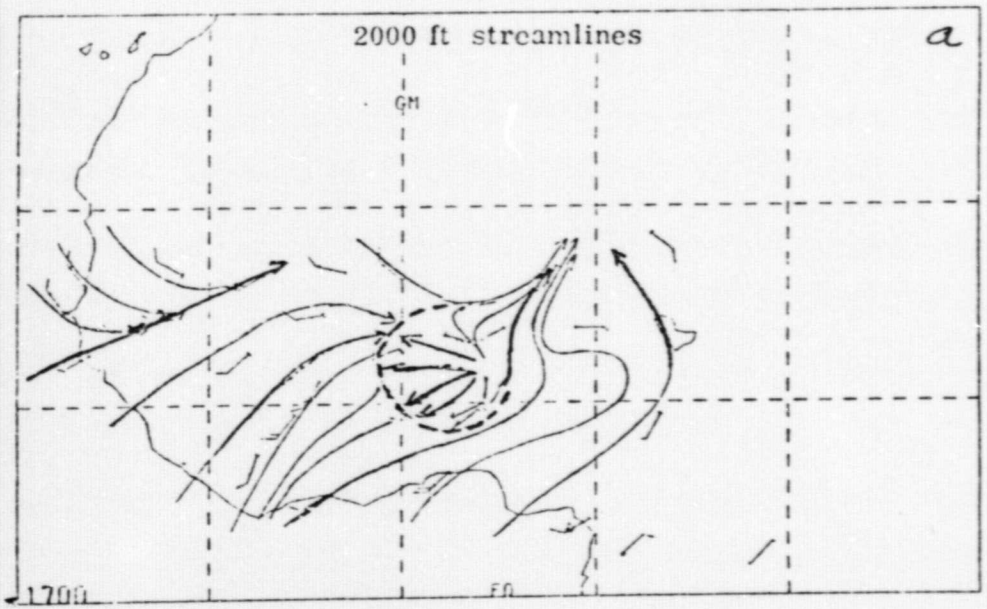

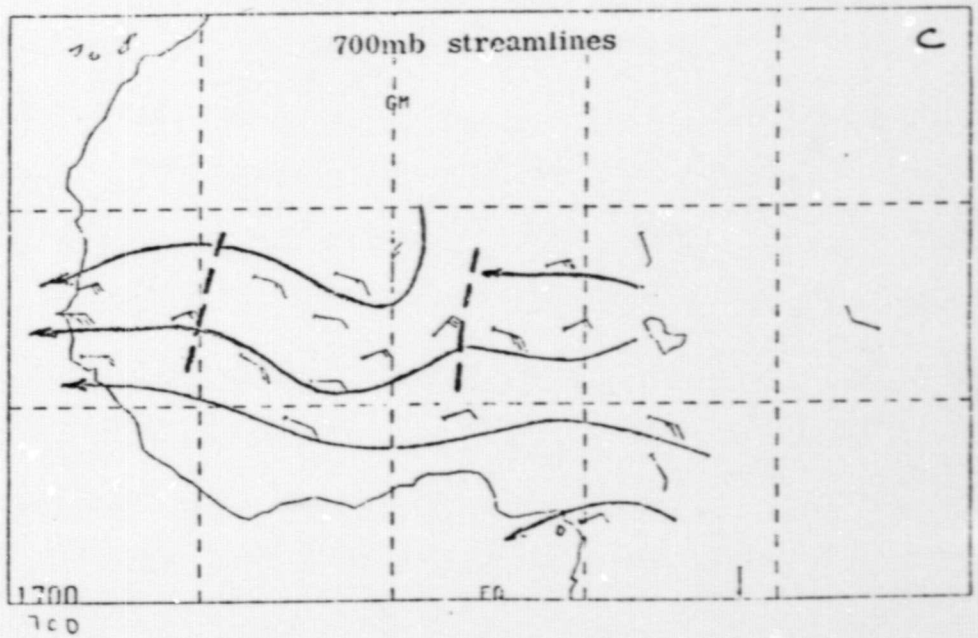

Fig. 24. Same as Fig. 22. except for 00 GMT, 17 July 1979.

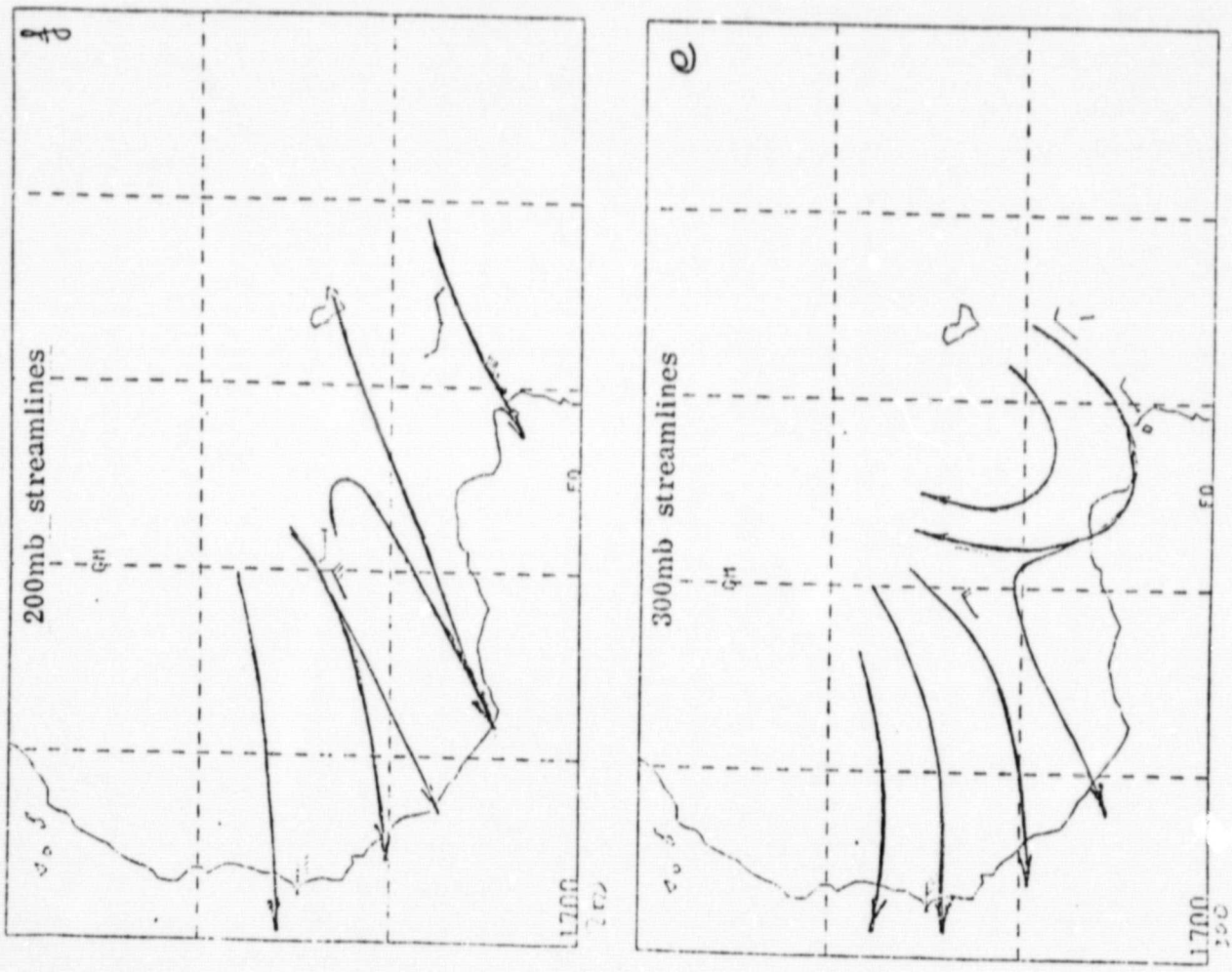

Fig. 24. continue

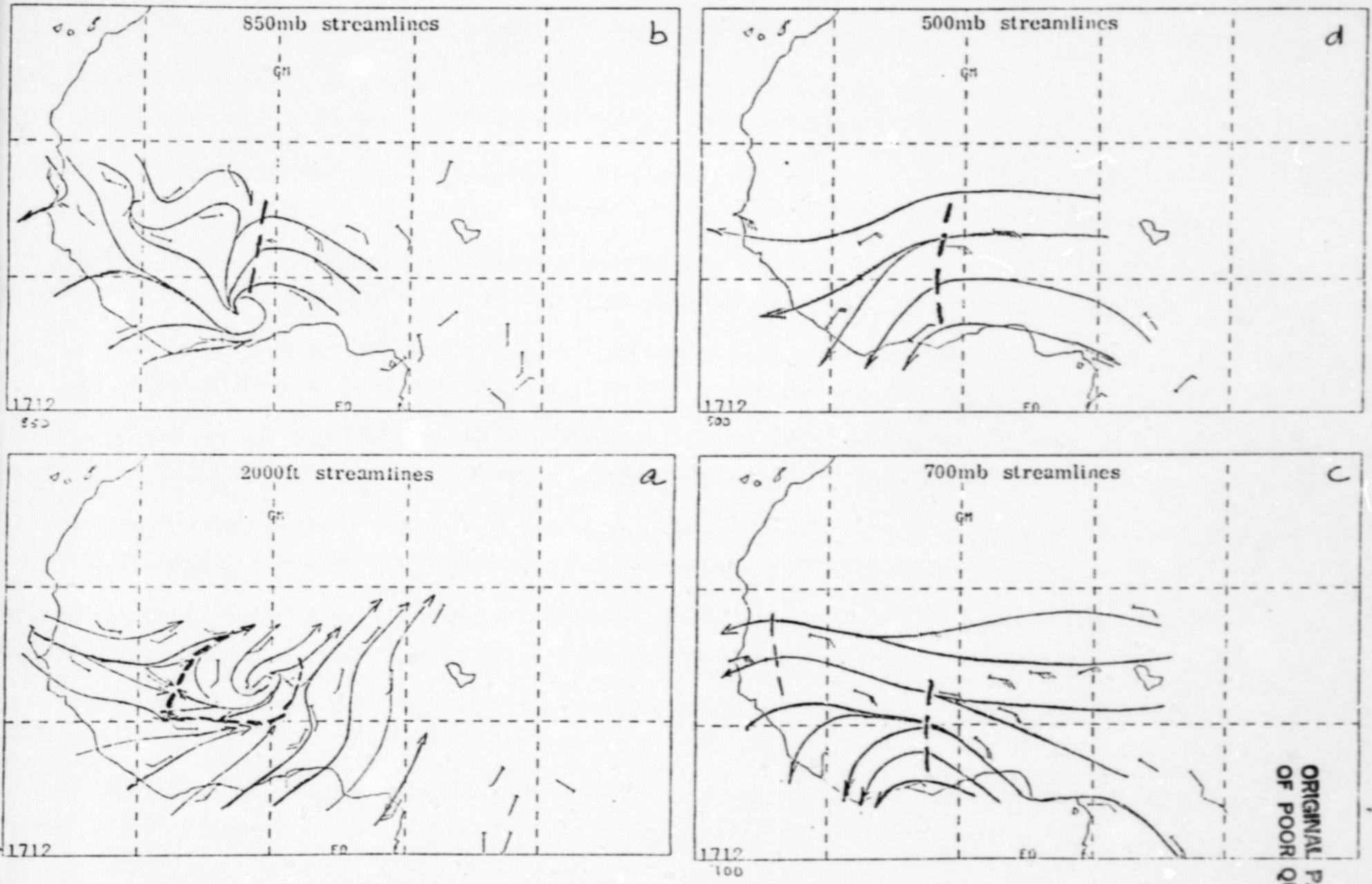

Fig. 25. Same as Fig. 22. except for 12 GMT, 17 July 1979.

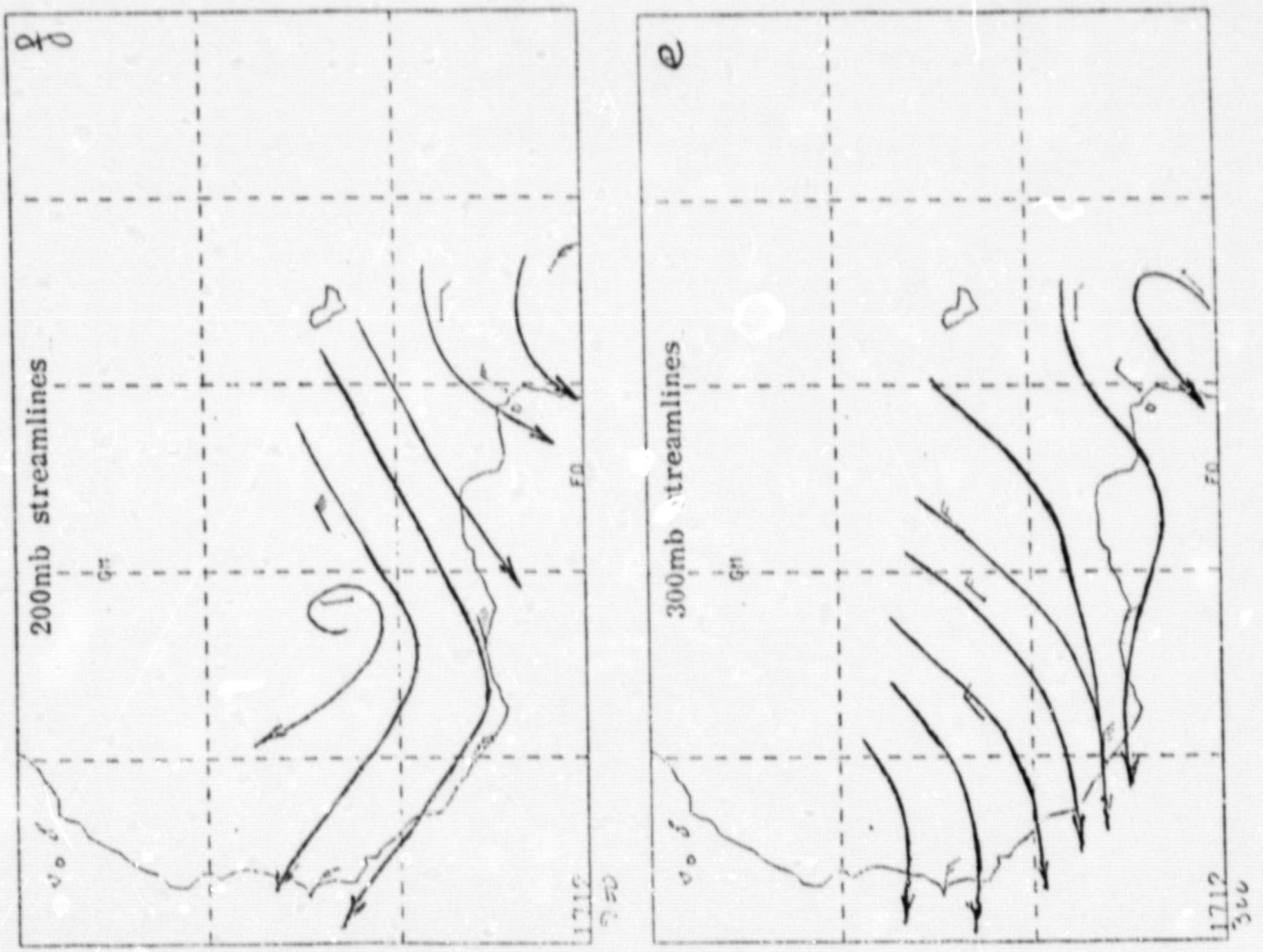

Fig. 25. continue

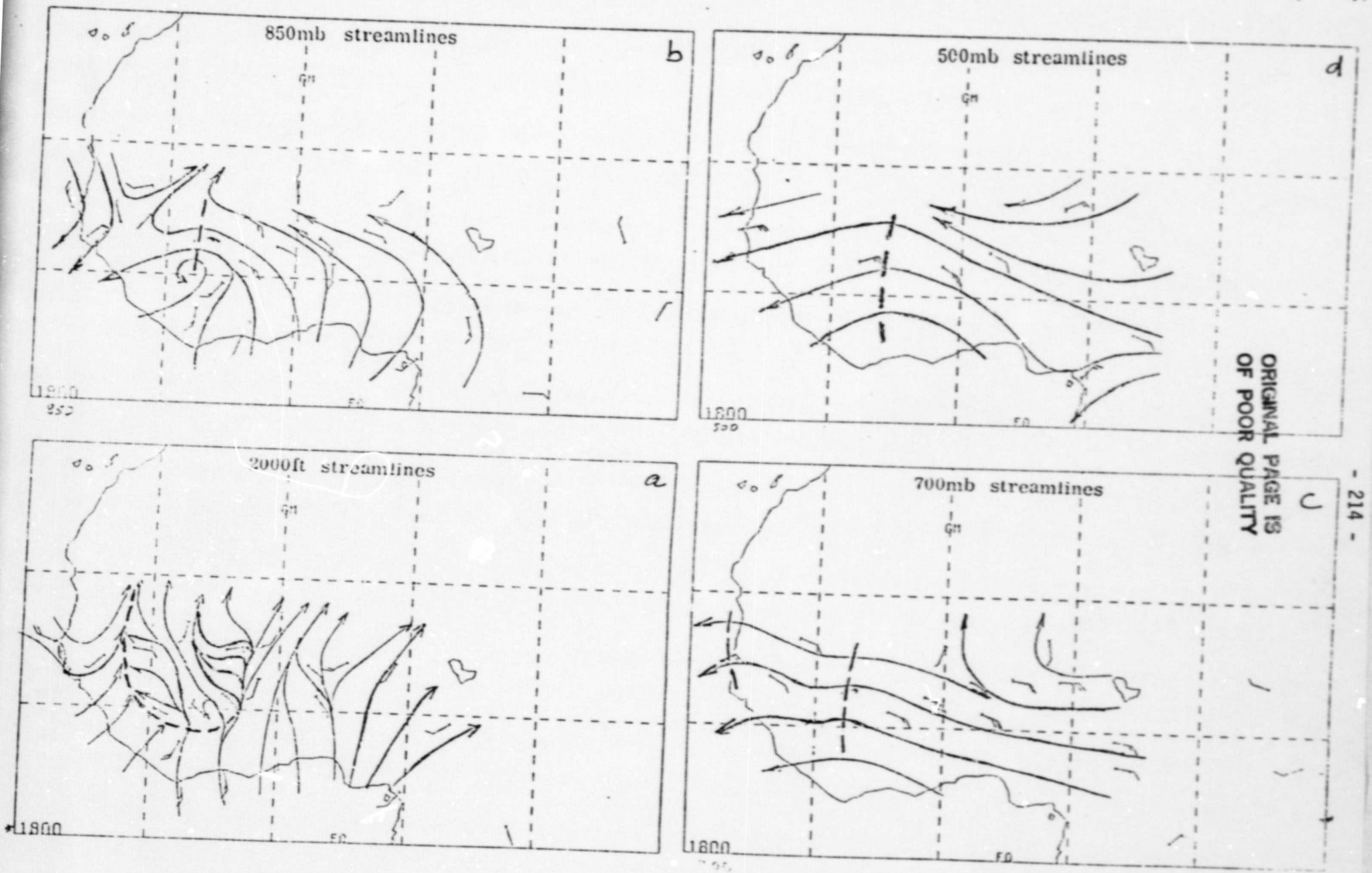

Fig. 26. Same as Fig. 22. except for 00 GMT, 18 July 1979.

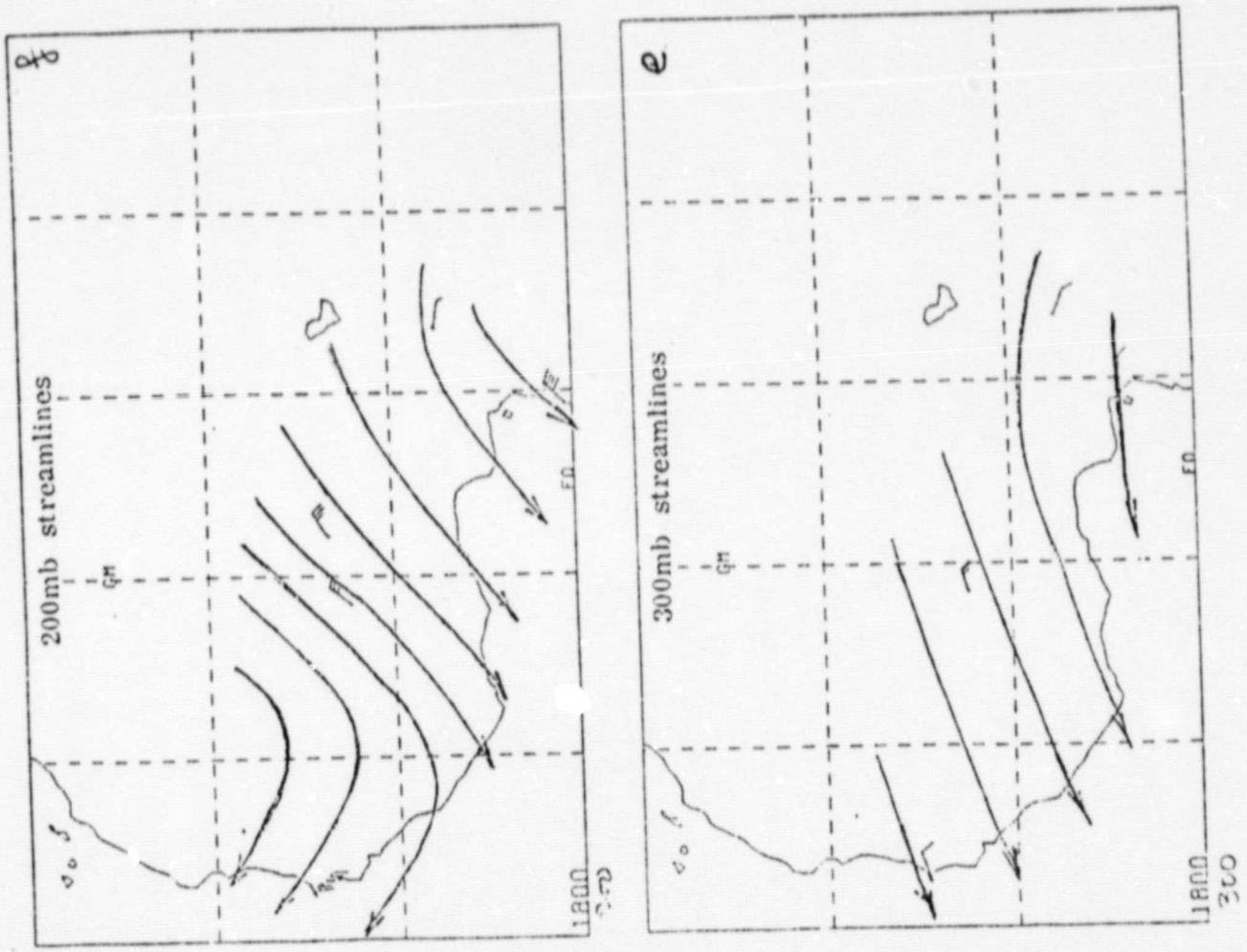

Fig. 26. continue

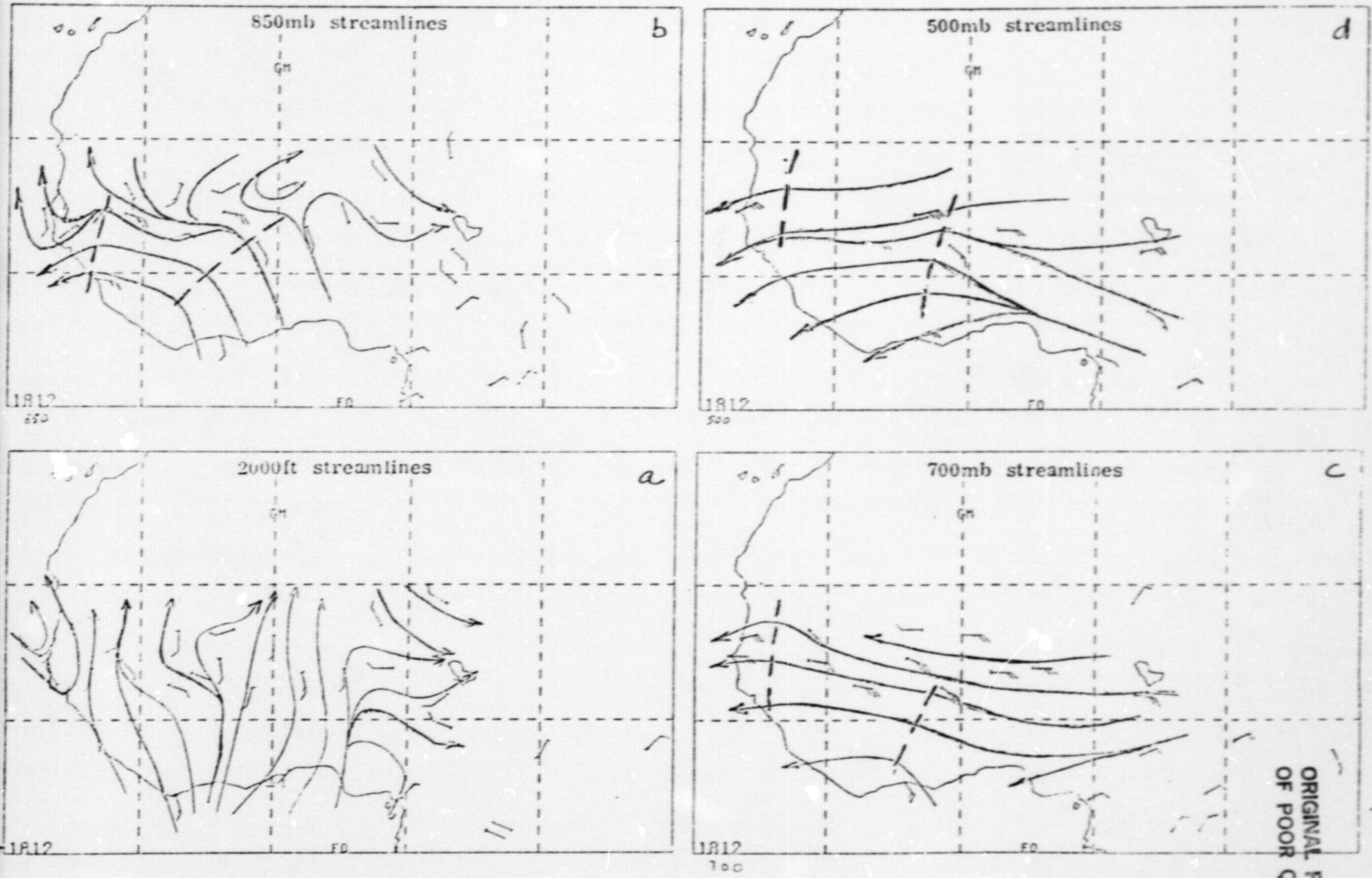

Fig. 27. Same as Fig. 22. except for 12 GMT, 18 July 1979.

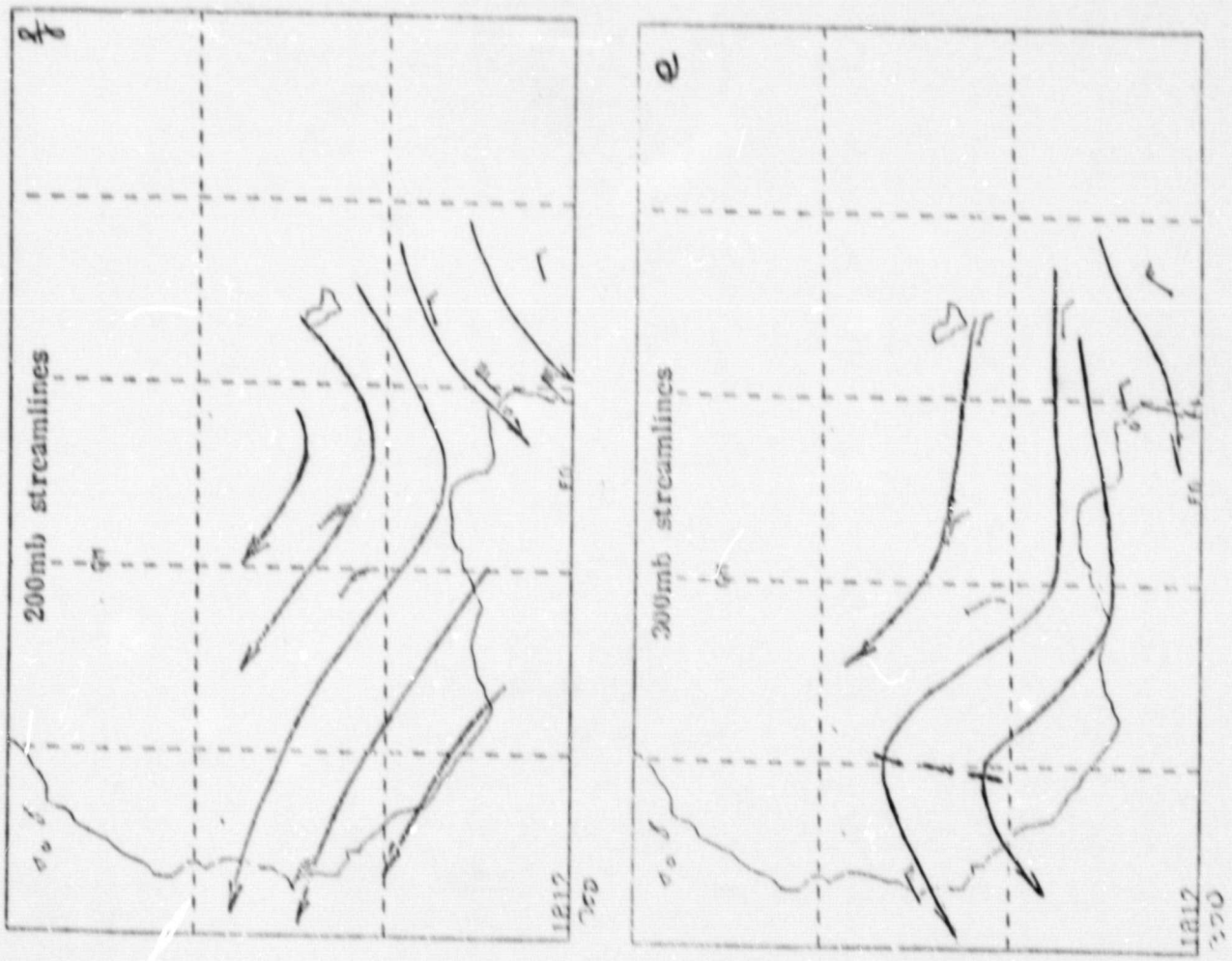

Fig. 27. continue

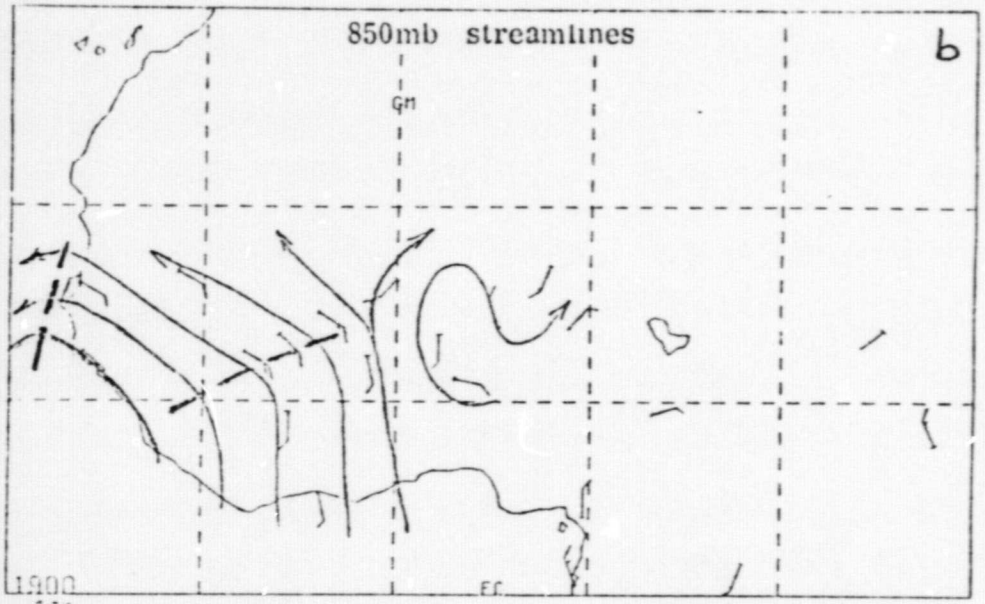

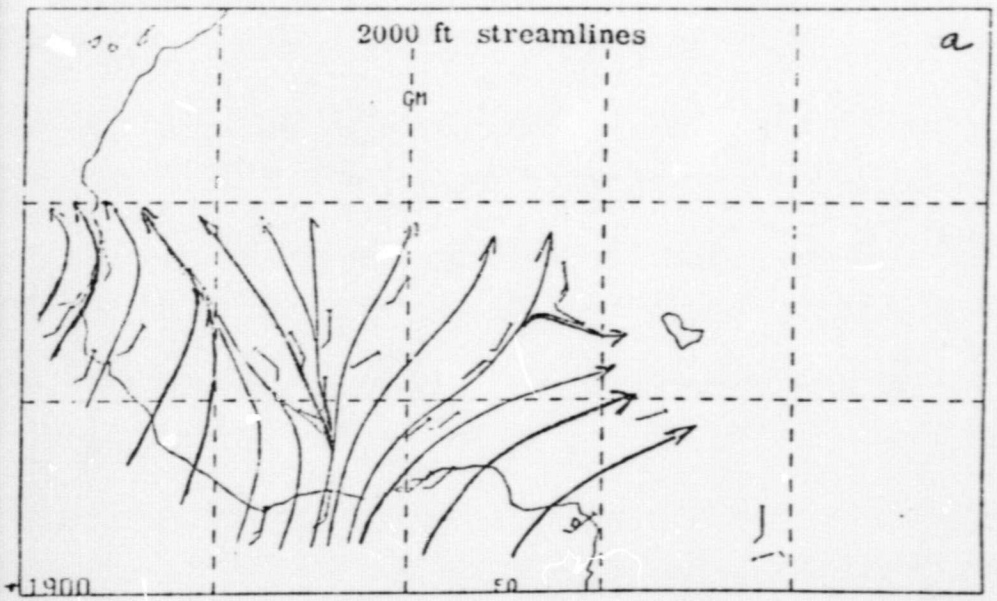

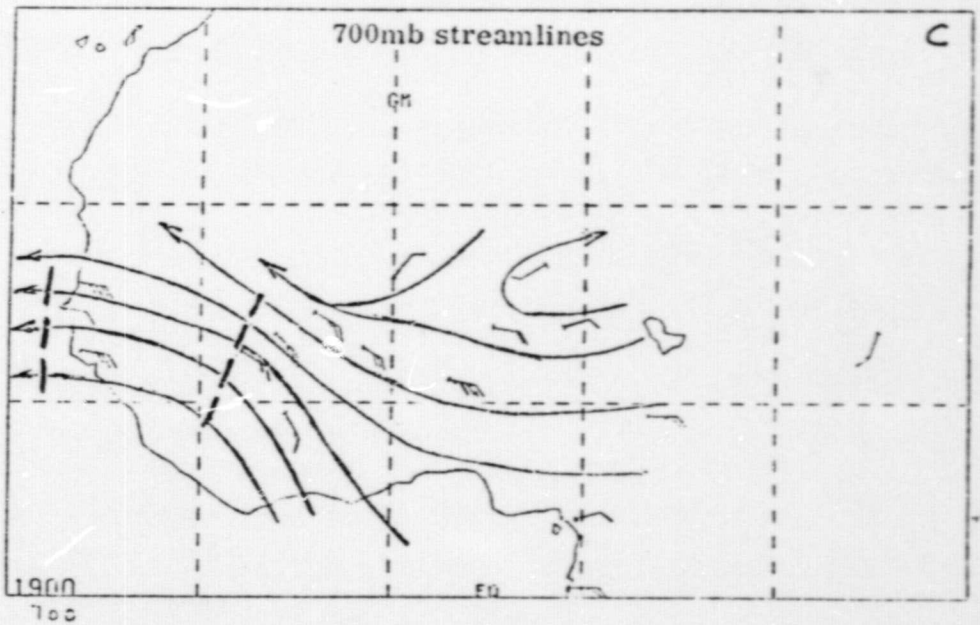

Fig. 28. Same as Fig. 22. except for 00 GMT, 19 July 1979.

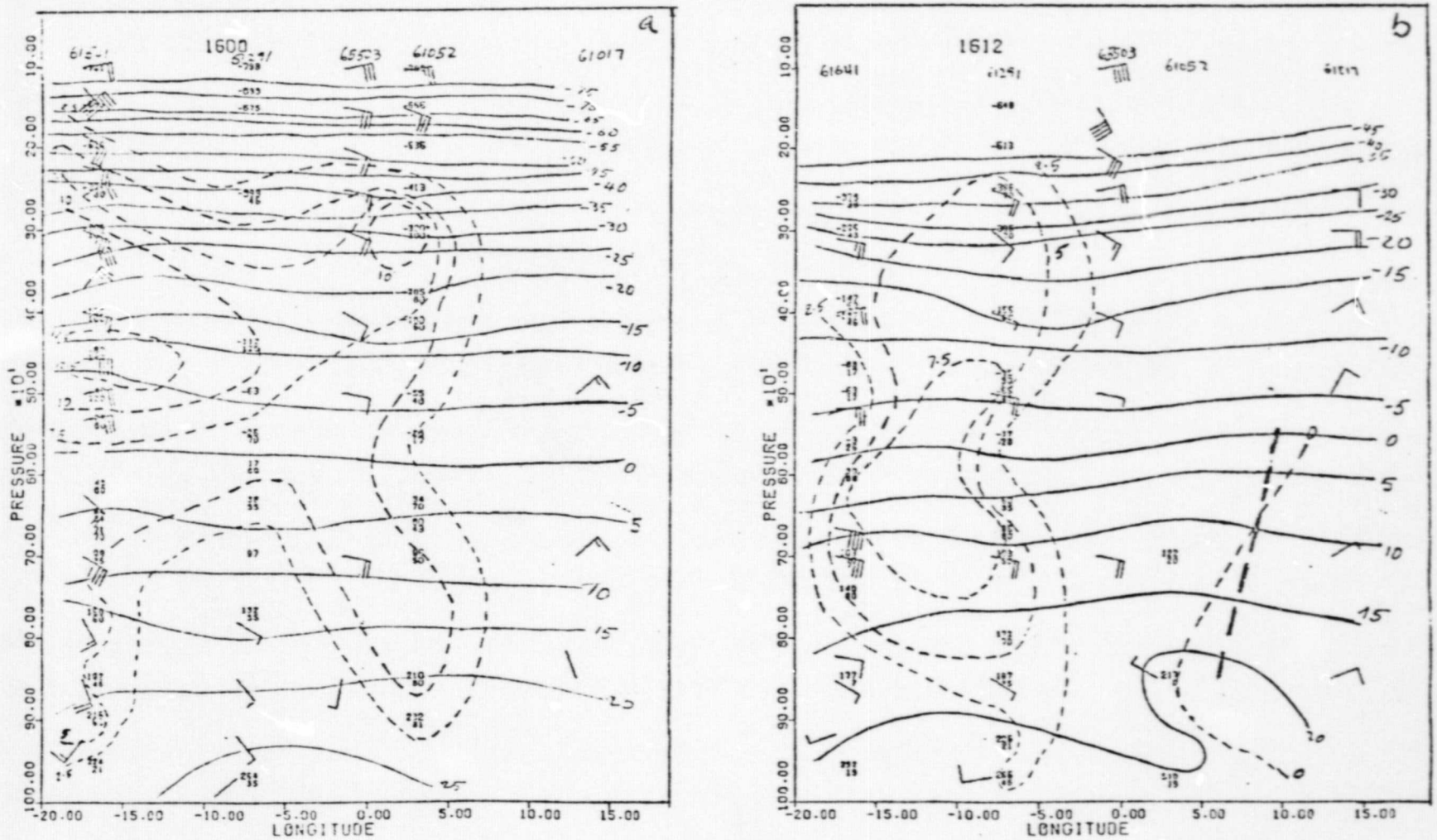

Fig. 29. Space cross section around 14N; solid lines are temperature (5 c interval), dashed lines are dew point depression (2.5 c interval) and heavy dashed line shows the wave position at: a) 00 GMT 16 July, b) 12 GMT 16 July, c) 00 GMT 17 July, d) 12 GMT 17 July, e) 00 GMT 18 July, f) 12 GMT 18 July, g) 00 GMT 19 July 1979.

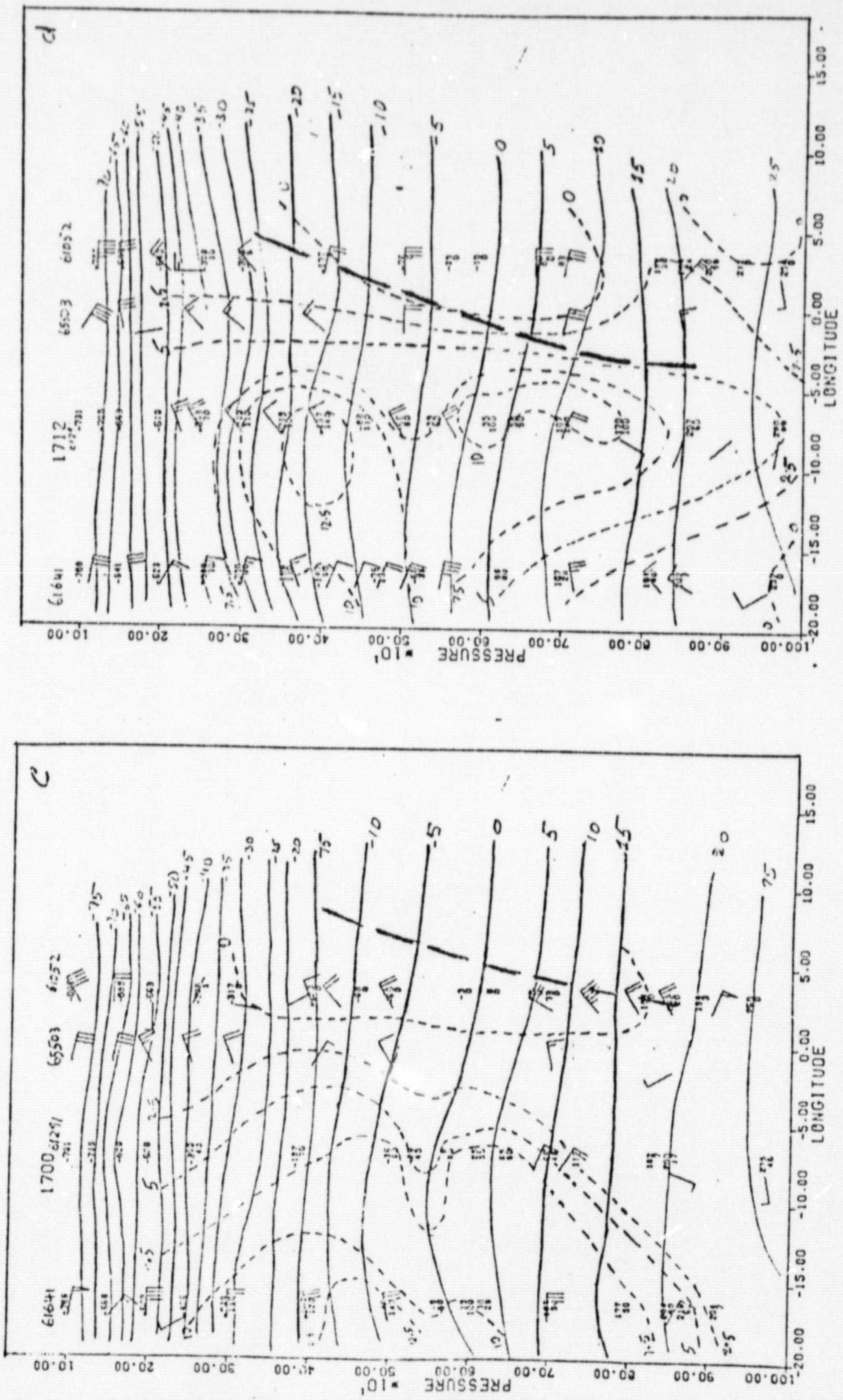

Fig. 29. continue

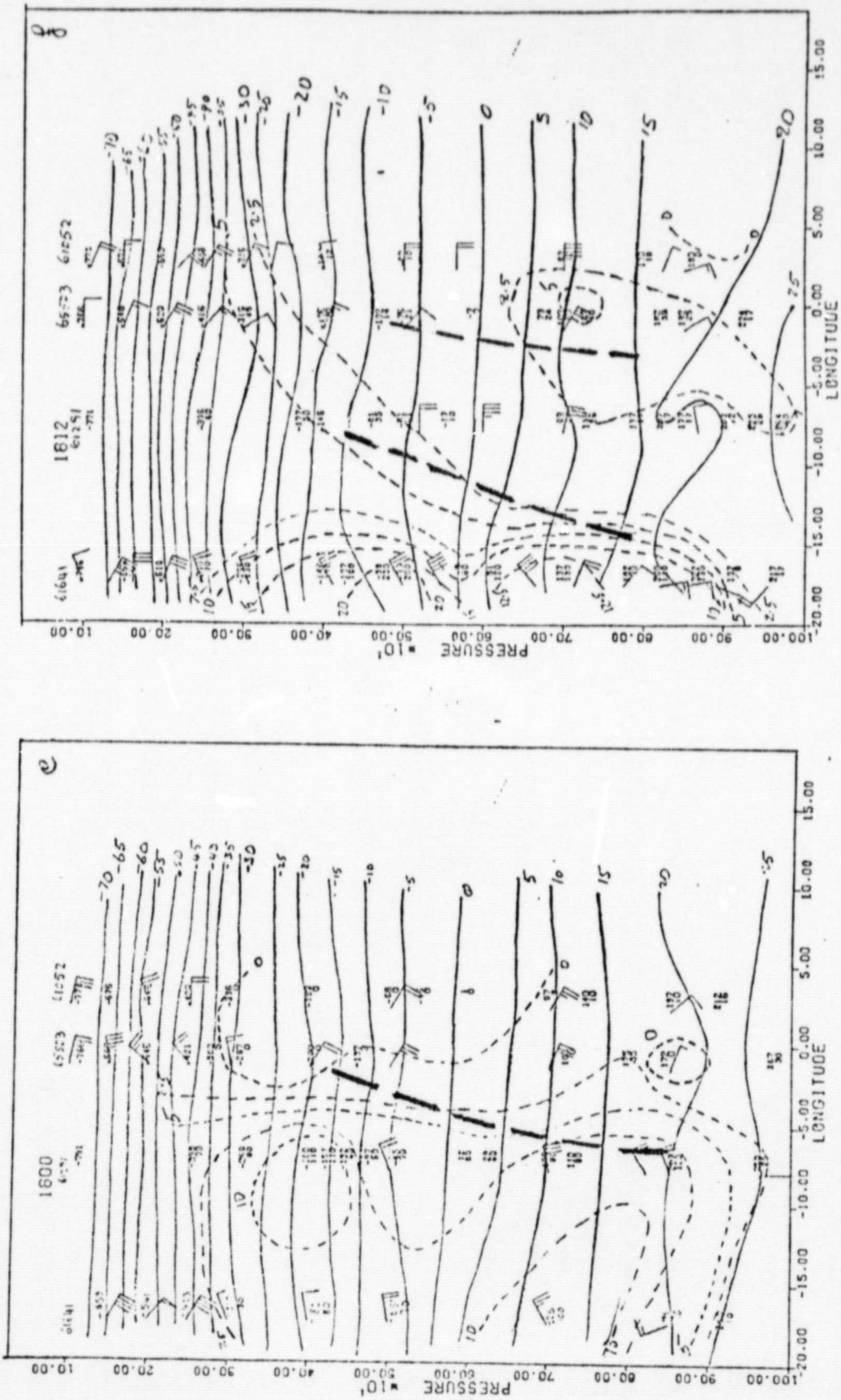

Fig. 29. continue

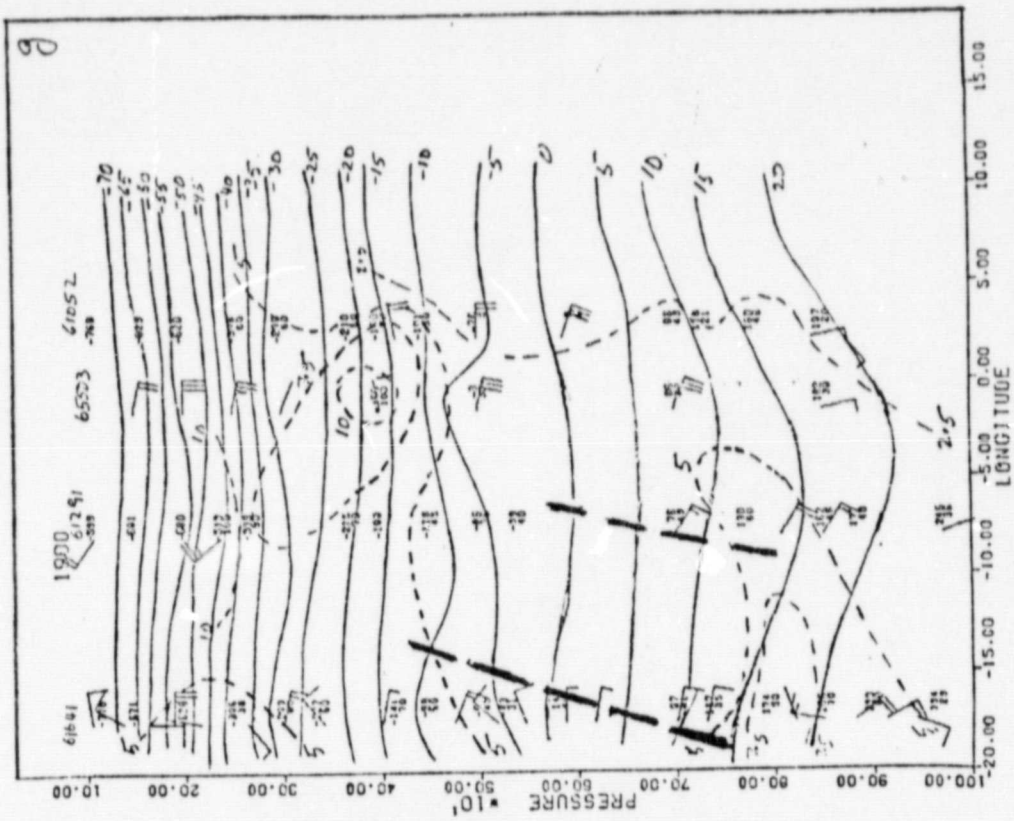

Fig. 29. continue

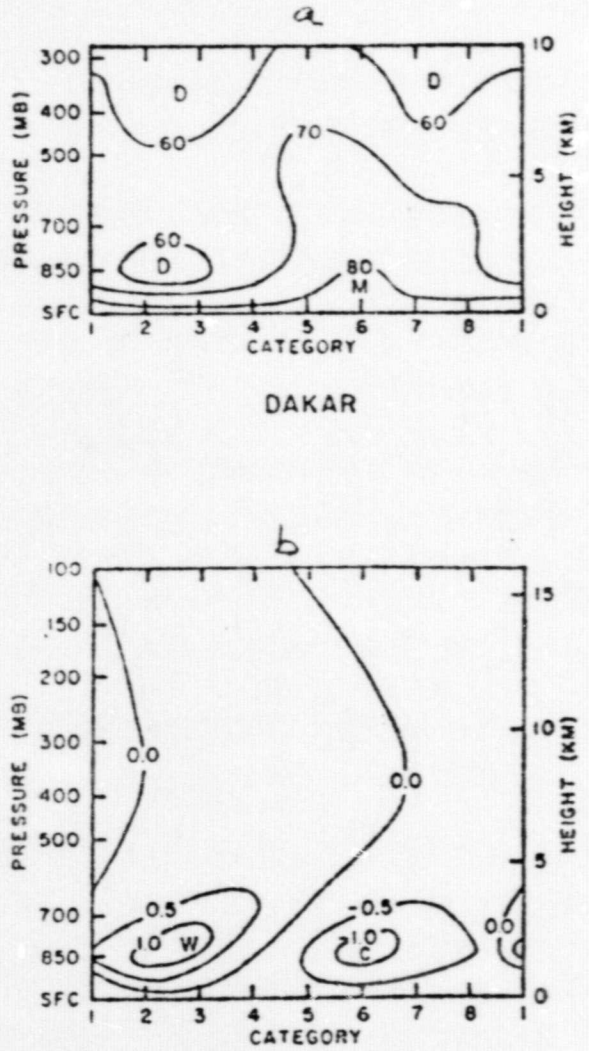

Fig. 30. Composite diagram of upper air data at DAKAR (Burpee, 1974). Category 4 represents the trough position: a) Relative humidity (percent), b) Temperature deviation.

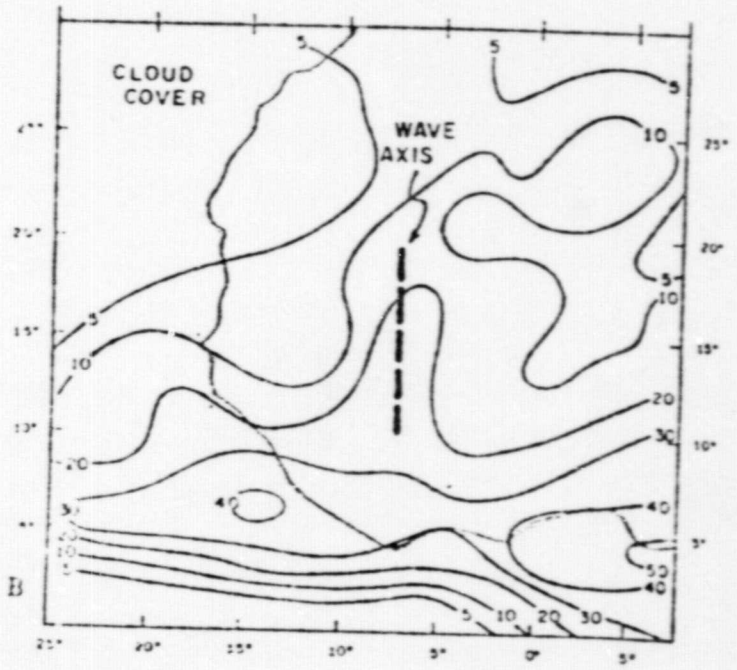

Fig. 31. Mean percentage cover of cloud, from Carlson 1969b.

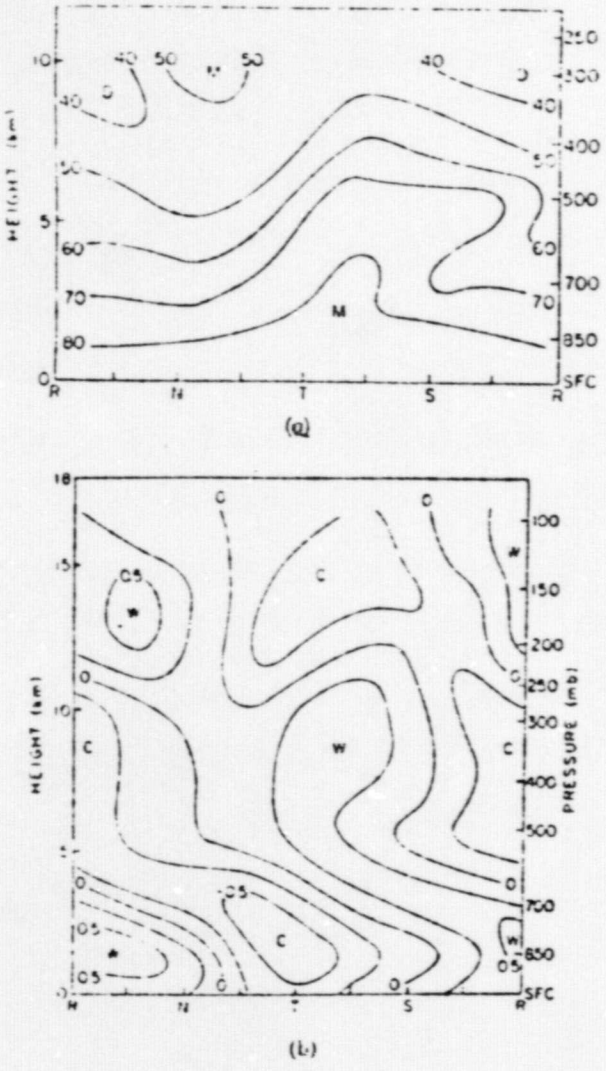

Fig. 32. Vertical cross section along 11N (Reed et al., 1977)
a) Relative humidity (percent),
b) Temperature deviation.

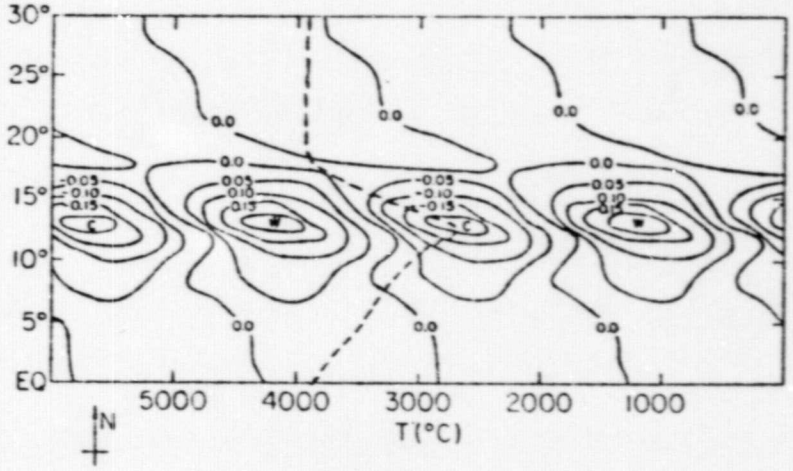

Fig. 33. Temperature perturbations at 800mb, contour interval is 0.05°c from Rennick, 1976; trough indicated by dashed line.

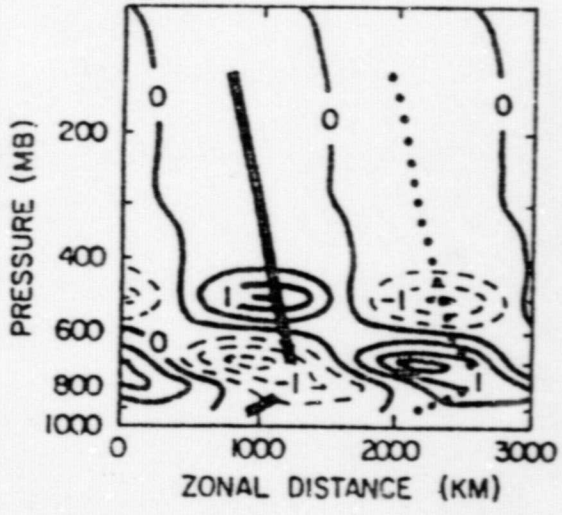

Fig. 34. Temperature perturbations at 11N contour interval is .5°c, from Mass, 1979; trough indicated by heavy line.

EPILOGUE

The principal motivation for the research project has been to get an answer to the question:

Is the GLAS General Circulation Model able to reproduce wave type synoptic disturbances in the tropics?

Our studies have definitely shown that the model is indeed able to reproduce such disturbances throughout the tropics. Furthermore, a detailed study of the characteristics of the simulated disturbances over Africa has found that their structure and their behavior are verified reasonably well by observations. Our studies have also found that, in one of the summers simulated, the disturbances are predominantly of one type, i.e. closed vortices; in another summer, the predominant disturbances are open waves. These findings are significant because they indicate that numerical prediction in the tropics is definitely achievable with primitive equation models. In particular, we mention two interesting possibilities which should be attempted in the near future:

(1) the day-to-day numerical prediction of African disturbances on an operational basis;

(2) the long range prediction (general outlook) of the general characteristics, such as type (closed vortices or open waves), intensity, frequency, of tropical disturbances over Africa and the Atlantic Ocean. The general outlook may even include an estimate of the number of hurricanes (above or below normal) and the general regions to be affected (Western Caribbean,